

THE FIBER SOCIETY



*Advancing Scientific Knowledge
Pertaining to Fibers and Fibrous Materials*



The Fiber Society 2018 Spring Conference

**Co-organized with The Society of Fiber
Science and Technology, Japan**

*Fibers and Textiles for Value Creation
in Connected Industries*

June 12–14, 2018

Conference Chair

Dr. Takeshi Kikutani

Tokyo Institute of Technology, Tokyo, Japan

Venue

*Tower Hall Funabori
Tokyo, Japan*

Program

Monday, June 11

1:00 PM–5:00 PM The Fiber Society Governing Council Meeting, Bunka-Gakuen University
3:00 PM–7:30 PM Pre-registration and Welcome Reception, Bunka-Gakuen University

Welcome Message

The fiber community of Japan is privileged and honored to hold The Fiber Society's Spring 2018 Conference at Tower Hall Funabori in Tokyo, Japan, from June 12 to 14. Customarily, The Fiber Society holds spring conferences outside of the United States and fall conferences inside the United States. This is the first Fiber Society conference in Japan. The conference is co-organized with The Society of Fiber Science and Technology, Japan. Two other organizations related to fibers and textiles, The Textile Machinery Society of Japan and The Japan Research Association for Textile End-Uses, are co-sponsoring this conference.

The Fiber Society and The Society of Fiber Science and Technology, Japan, have a certain similarity from the view point of their origins. The Fiber Society was founded in 1941 with its original name, "Industrial Fiber Society." The Society of Fiber Science and Technology, Japan, was established in 1943 when The Society of Cellulosics and The Society of Fiber Industry merged. Growth of the Societies in the early years was boosted through the development of synthetic fibers. Today, both Societies represent and support a wide range of research fields related to fibers and textiles.

We set the theme of this conference as "Fibers and Textiles for Value Creation in Connected Industries." Cooperation by people from different fields of research, from different disciplines, and from different regions of the world is essential for a world-wide, prosperous future. Continued far-reaching and wide-ranging collaboration and exchange of ideas among the people in the field of fibers and textiles, especially between The Fiber Society and The Society of Fiber Science and Technology, Japan, are essential for the creation of innovation in our field.

On behalf of the conference Organizing Committee, I welcome all delegates and wish everyone the best for an academically and professionally fruitful meeting. And I hope all delegates from abroad enjoy their stay in Japan.



A handwritten signature in black ink, appearing to read "T. Kikutani". The signature is stylized and fluid, written over a light-colored background.

Prof. Takeshi Kikutani
Conference Chair
President of the Society of Fiber Science and Technology, Japan

The Fiber Society

The Fiber Society is incorporated as a not-for-profit professional and scientific association, dedicated to the advancement of knowledge pertaining to fibers, fiber-based products, and fibrous materials. The Society comprises individuals who are chemists, physicists, engineers, and designers with interests in the field of fiber science engineering and technology.

2018 Fiber Society Officers

Jintu Fan, President, Cornell University

René Rossi, Vice-president, Empa

Janice R. Gerde, Secretary, U.S. Customs and Border Protection

Ian R. Hardin, Treasurer, University of Georgia

Governing Council

Maria José Abreu, University of Minho

Takeshi Kikutani, Tokyo Institute of Technology

Thomas Gries, RWTH Aachen University

David Hinks, North Carolina State University

Yordan Kyosev, Niederrhein University

Sergiy Minko, University of Georgia

The Society of Fiber Science and Technology, Japan (SFSTJ)

The Society of Fiber Science and Technology, Japan (SFSTJ) was founded in 1943. The SFSTJ is a great contributor to the development of textile science and industry in Japan. The activities of SFSTJ focus on the fields of fiber science and technology and broadly extend to many interdisciplinary areas. The textile industry is widely distributed across areas from basic fiber material development and application, to apparel and fashion design. The fiber industry also plays a major role in manufacturing business. Nearly 10 percent of all employees in the manufacturing industry, (over 2 million people) are engaged in this field. SFSTJ offers valuable information exchanges through gatherings with scientists and engineers, to give you new ideas and directions for your work. Furthermore, joining SFSTJ can provide you with a unique overview of the field, and this knowledge can help to drive your education, research and business activities.

Board of Directors

President: Takeshi Kikutani, Tokyo Institute of Technology

Vice-presidents: Kunio Kimura, Okayama University; Kenji Ogino, Tokyo University of Agriculture and Technology; Norimitsu Kamiyama, Teijin Frontier Co., Ltd.

Members: Hiroshi Ito, Yamagata University; Tadahisa Iwata, University of Tokyo; Asami Nakai, Gifu University; Shinichiro Sue, Fukui University; Hiroshi Urakawa, Kyoto Institute of Technology; Jun-ichi Kadokawa, Kagoshima University; Akihiro Omatsuzawa, Japan Chemical Fibers Association; Yukino Oizumi, Tokyo Metropolitan Industrial Technology Research Institute; Akira Tsuchida, Gifu University; Kaname Katsuraya, Wayo Women's University; Satoko Okubayashi, Kyoto Institute of Technology; Masatoshi Tokita, Tokyo Institute of Technology; Yoshinobu Tsujii, Kyoto University; Mari Inoue, Kobe University; Hideaki Morikawa, Shinshu University; Toshiaki Hayashi, Toyobo Co., Ltd.; Yoshitaka Aranishi, Toray Industries, Inc.; Hideaki Ikenaga, Asahi Kasei Corp.; Hiroshi Yamamoto, Mitsubishi Chemical Corp.; Jiro Tanaka, Kuraray, Co., Ltd.; Shogo Mutagami, KB Seiren, Ltd.; Kenji Kode, Unitika Ltd.; Wataru Saka, Kao Corp.; Harutaka Katsuno, Nisshinbo Textile Inc.; Tomoyuki Terao, Oji Holdings Corp.; Ken-ichi Sugimoto, Bridgestone Corp.

Statutory Auditors: Toshihiro Hirai, Shinshu University; Kaoru Suganuma, FCG Research Institute, Inc.; Hiroki Murase, Kyoritsu Women's University

Day I – Tuesday, June 12

Morning Session

9:00 Registration: 2nd Floor Foyer

	Room FS-A, 5th Floor, Small Hall
9:30	Welcome Remarks and Announcements <i>Takeshi Kikutani, Conference Chair</i> <i>Jintu Fan, President, The Fiber Society</i>
9:50	Plenary Lecture: Yoshiro Tajitsu, Kansai University <i>A New Wearable Sensor in the Shape of a Braided Cord</i> Chair: Jintu Fan, Cornell University

10:30 Break

	Room FS-A 5th Floor, Small Hall	Room FS-B 2nd Floor, Tou-Gen (桃源)
	Session: Smart Polymers, Fibers, and Textiles <i>Chair: Jonathan Chen, University of Texas-Austin</i>	Session: Fundamentals of Fiber and Textile Science, Testing, and Characterization <i>Chair: Chureerat Prahsarn, MTEC</i>
10:50	Keynote: <i>Recent Developments of Smart and Multifunctional Fibrous Materials and Clothing</i> Jintu Fan, Cornell University	Keynote: <i>Quantitative Evaluation of Odour Retention on Different Fibre Types</i> Xungai Wang, Deakin University
11:20	<i>Improved Electrical Conductivity of PUNanofiber Web Coated with SWCNT/AgNW and Exploration as Textile Sensors</i> Eugene Lee, Yonsei University	<i>Surface Functional Textile for Healthcare Application with Rechargeable Antibacterial Activity</i> Zhentan Lu, Wuhan Textile University
11:40	<i>Wearable Fiber Organic Electrochemical Transistors for Biological Sensing</i> Yuedan Wang, Wuhan Textile University	<i>Investigation of Fiber-based Influences on Bacterial Adherence</i> Klas-Moritz Kossel, RWTH Aachen University
12:00	<i>Melt-spun Conductive Elastomeric Fibers for Smart Textiles: Implications for Bio-signal Recordings</i> Ladan Eskandarian, Myant, Inc.	<i>Challenges from Wearable Technologies</i> Ning Pan, University of California-Davis
12:20	<i>Open</i>	<i>Electrostatic Spinning—Spraying for Cell-laden Hybrid Membranes Mimicking the Native Blood Barrier</i> Giuseppino Fortunato, Empa

	Room FS-C 2nd Floor, Fuku-Jyu (福寿)	Room FS-D 2nd Floor, Hei-An (平安)
	Session: Sustainable Polymer Materials/Advanced Cellulose Fibers and Textiles <i>Chair: Tadahisa Iwata, University of Tokyo</i>	Session: Dyeing and Finishing/Design and Merchandising <i>Chair: Kazumasa Hirogaki, University of Fukui</i>
10:50	Keynote: <i>Research Activities on Bio-based Fibers in Toray Industries, Inc.</i> Yoshitaka Aranishi, Toray Industries, Inc.	Keynote: <i>Developing a Natural Dyeing Method for Obtaining Turkey Red Color</i> Recep Karadag, Marmara University
11:20	<i>Cellulose Dissolution in Ionic Liquids: A Theoretical Study</i> Takuya Uto, Kagoshima University	<i>Structural Change and Guest Release from Cyclodextrin Inclusion Complex Treated at Ultra-high Pressure</i> Kenji Hisada, University of Fukui
11:40	<i>Highly Stiff Cellulose Fibers Spun from Liquid Crystalline Microcrystalline Cellulose Solutions Using DMSO as Co-solvent with an Ionic Liquid</i> Chenchen Zhu, University of Bristol	<i>Adsorption of Acid Dye on Guanidine Groups Grafted Polyacrylonitrile Fibers</i> Biao Wang, Donghua University
12:00	<i>Hierarchical Core-Sheath PPy@CNT/BC Macrofibers with High Electrochemical Performance for All-Solid-State Supercapacitors</i> Shiyan Chen, Donghua University	<i>Development of Multifunctional Surfaces for Advanced Textile Applications</i> Hatice İbili, Gaziantep University

12:20	<i>Preparation of Highly Stretchable Elastomeric Composites Reinforced with Well-defined Nanofiber Network of Bacterial Cellulose</i> Keita Sakakibara, Kyoto University	<i>Parameters Affecting the Electrospinning Process with Flame Retardant Agent</i> Bilgen Kapar, Gaziantep University
12:40–13:50	Lunch: Rooms FS-B and FS-C 13:00–13:30 Lunch Seminar, Room FS-B, Presented by Rigaku Corporation <i>3D Observation and Analysis of μm Fiber Composites by X-ray Microscopy</i> Yoshihiko Takeda, X-ray Research Laboratory, Rigaku Corporation	

Afternoon Session

	Room FS-A 5th Floor, Small Hall	
13:50	Plenary Lecture: Sanjay Rastogi, Maastricht University <i>Unprecedented Physical and Mechanical Properties of Solvent-free Processed Tapes and Films of Ultra-high Molecular Weight Polyethylene</i> Chair: Takeshi Kikutani, Tokyo Institute of Technology	

14:30 Break

	Room FS-A 5th Floor, Small Hall	Room FS-B 2nd Floor, Tou-Gen (桃源)
	Session: Smart Polymers, Fibers, and Textiles <i>Chair: Bipin Kumar, Indian Institute of Technology Deli</i>	Session: Fiber Manufacturing and Characterization <i>Chair: Thomas Gries, RWTH Aachen University</i>
14:50	<i>Acoustoelectric Conversion Properties of Electrospun Nanofiber Webs</i> Tong Lin, Deakin University	<i>Comparison of Solution Spinning Setups for PLA Monofilaments</i> Klas-Moritz Kossel, RWTH Aachen University (for Georg-Philipp Paar)
15:10	<i>Characterization of Hybrid Smart Yarns Engineered for Versatile Applications in Sportswear, Medical, and Multifunctional Textiles</i> Amir Shahzad, National Textile University	<i>Stereocomplexation of the Melt-spun Fibers of the Blends of Segmented PLLA/PDLA with a Low Optical Purity</i> Masaki Yamamoto, Kyoto Institute of Technology
15:30	<i>Application of Carbon Nanomaterial to Biodevice for Biofuel Cell with Carbon Binding, Peptide-fused Enzyme</i> Shin-ichiro Suye, University of Fukui	<i>Study on High-resolution, On-line Diameter Measurement of PET Fiber in High-speed, Melt-spinning Process</i> Young Chan Choi, Korea Institute of Industrial Technology
15:50	<i>Electro-conductivity of Staple Polyester Fibres Coated by Ag in Vacuum</i> Ivelin Rahnev, Technical University of Sofia	<i>High Modulus Nylon 66 Yarn for Tire Cord Fabric Development</i> N. Uğur Kaya, Kordsa Teknik Tekstil A.Ş.

16:10 Break

	Session: Smart Polymers, Fibers, and Textiles <i>Chair: Jintu Fan, Cornell University</i>	Session: Fiber Manufacturing and Characterization <i>Chair: Takeshi Kikutani, Tokyo Institute of Technology</i>
16:30	Keynote: <i>Carbon-based Yarn Supercapacitor for Energy Storage</i> Jonathan Y. Chen, University of Texas-Austin	Keynote: <i>Auxetic Structures from 3D Printed Hybrid Textiles</i> Thomas Gries, RWTH Aachen University
17:00	<i>Smart Textile Actuator Using Stress Memory Polymer</i> Bipin Kumar, Indian Institute of Technology Deli	<i>Properties and Applications of New, Heat-resistant Polyamide Fiber</i> Satoshi Koizumi, Kuraray Co., Ltd.
17:20	<i>Development of Superhydrophobic Energy Harvesting Textile via Plasma Treatment of Poly(vinylidene fluoride) Nanoweb</i> Beomjun Ju, Seoul National University	<i>Three-component Composite, Anti-counterfeiting Fiber Based on Cross-section Pattern</i> Ronggen Zhang, Donghua University
17:40	<i>Open</i>	<i>Open</i>

	Room FS-C 2nd Floor, Fuku-Jyu (福寿)	Room FS-D 2nd Floor, Hei-An (平安)
	Session: Sustainable Polymer Materials/Advanced Cellulose Fibers and Textiles Chair: Yutaka Kawahara, Gunma University	Session: Dyeing and Finishing/Design and Merchandising Chair: Recep Karadag, Marmara University
14:50	<i>Effects of a Biobased Filler on the Crystallization Behaviors of Poly(L-lactic acid)</i> Amit Kumar Pandey, Kyoto Institute of Technology	<i>Structural Coloration of Textile Controlling Structure of Colloidal Crystal Array on Fiber and Textile</i> Kazumasa Hirogaki, University of Fukui
15:10	<i>Forcibly Spinning of Bombyx mori Silkworm Silk Ended in Complete Failure</i> Yutaka Kawahara, Gunma University	<i>Development of a New Outdoor Sport Shirt Using a Thermal Manikin Under Different Climatic Conditions</i> Maria José Abreu, University of Minho (for André Catarino)
15:30	<i>Fabrication and Characterization of Transparent, Flexible, and Water-insoluble, Non-mulberry Silk Fibroin Films</i> Kelvin O. Moseti, Tokyo University of Agriculture and Technology	<i>Colorful Fluorine-free Superhydrophobic Polyester Fabric Developed via Disperse Dyeing Process</i> Ji-Hyun Oh, Seoul National University
15:50	<i>Structural Change and Its Effect on the Mechanical Property of Silk Induced by Tensile Deformation</i> Taiyo Yoshioka, National Agriculture and Food Research Organization	<i>Safer Hair Dyeing by Using Biobased Materials: Techniques, Dyeability, and Protection Effect</i> Hidekazu Yasunaga, Kyoto Institute of Technology
16:10 Break		
	Session: Sustainable Polymer Materials/Advanced Cellulose Fibers and Textiles Chair: Chenchen Zhu, University of Bristol	Session: Carbon Fibers and Advanced Composite Materials Chair: Dong Wang, Wuhan Textile University
16:30	Keynote: <i>High-performance, Bio-based Plastics Synthesized from Natural and Unnatural Polysaccharides</i> Tadahisa Iwata, University of Tokyo	Keynote: <i>Consideration of the Impregnation Process of Polymer Melt to Carbon Fiber Bundle by Steady-state Viscoelastic Flow Simulation</i> Shuichi Tanoue, University of Fukui
17:00	<i>Development of Thermostable Polymers from Plant-derived Aromatic Hydroxy Acids</i> Daisuke Ishii, University of Tokyo	<i>Improvements in Determination of Carbon Fibre Strength Distribution Using Automation and Statistical Data Analysis</i> Faisal Islam, MINES ParisTech
17:20	<i>Utilization of Plant Biomass as Valuable Materials via Sustainable Process</i> Kazuhiro Shikinaka, National Institute of Advanced Industrial Science and Technology	<i>Strength Reduction in Liquids and Its Application in Defect Analysis for Carbon Fibers</i> Masatoshi Shioya, Tokyo Institute of Technology
17:40	<i>Open</i>	<i>Influence of Chemical Pretreatments on Processing, Structure, and Properties of Rayon-based Carbon Fibers</i> Gajanan Bhat, University of Georgia
18:20	Buses load from Tower Hall Funabori to banquet venue (1st floor, Exhibition Hall)	
19:30	Banquet (Hotel Gajoen Tokyo; 3-minute walk from Meguro Station)	
21:30	Buses load from banquet venue for return to conference venue or major stations	

Day II – Wednesday, June 13

Morning Session

9:00 Registration

	Room FS-B 2nd Floor, Tou-Gen (桃源)	Room FS-C 2nd Floor, Fuku-Jyu (福寿)	Room FS-E 3rd Floor
	Session: Smart Polymers, Fibers, and Textiles <i>Chair: Mari Inoue, Kobe University</i>	Session: Fundamentals of Fiber and Textile Science, Testing, and Characterization <i>Chair: Sachiko Sukigara, Kyoto Institute of Technology</i>	Session: Fundamentals of Polymer Material: Synthesis, Polymerization, Characterization, and Its Physics <i>Chair: Toyoaki Hirata, University of Fukui</i>
9:20	<i>Mechanical and Electrical Properties of Graphene-coated Polyurethane Nanofiber Webs as a Strain Gauge</i> Eunji Jang, Yonsei University	<i>Effect of Vapor Permeability and Aperture of Outdoor Parka and Environmental Velocity on Evaporative Heat Transfer and Ventilation Rate Using Sweating Thermal Manikin and Tracer Gas Methods</i> Yayoi Satsumoto, Yokohama National University	<i>Syntheses and Wettability of Poly(fluoroalkyl (meth)acrylate)s with Carbamate Linker</i> Yi Liu, Guizhou Normal College
9:40	<i>Proton Conductive Polymer Nanofiber Framework: Fabrication and Application to Polymer Electrolyte Fuel Cells</i> Manabu Tanaka, Tokyo Metropolitan University	<i>Determination of Total Comfort of Sport Caps Using Wear Trials</i> Maria José Abreu, University of Minho	<i>Polymer Hybrid Membranes for CO₂ Capture</i> Shinji Kanehashi, Tokyo University of Agriculture and Technology
10:00	<i>Waterborne Fabrication of Fluoride-free, Magnetic, Superhydrophobic Fabrics</i> Sida Fu, Deakin University	<i>Evaluation Parameters for Friction Properties of Woven Fabrics by Rotational Dragging with Tactile Sensor</i> Toshiyasu Kinari, Kanazawa University	<i>Facile Fabrication of Poly(glycidyl methacrylate)-b-polystyrene Functional Nanofibers Under Shearing Field</i> Wenwen Wang, Wuhan Textile University

10:20 Break

	Session: Smart Polymers, Fibers, and Textiles <i>Chair: Christophe Daniel, Università Degli Studi di Salerno</i>	Session: Fundamentals of Fiber and Textile Science, Testing, and Characterization <i>Chair: Xungai Wang, Deakin University</i>	Session: Fundamentals of Polymer Material: Synthesis, Polymerization, Characterization, and Its Physics <i>Chair: Shinji Kanehashi, Tokyo University of Agriculture and Technology</i>
10:40	<i>Highly Air-permeable, Directional, Water-transport Cotton Fabrics</i> Hongxia Wang, Deakin University	<i>Effect of Different Processing Technique and Softener Treatments on the Surface Friction of Cotton Fabric</i> Ateeq ur Rehman, National Textile University	<i>Photonic Films of Block Copolymers Comprising a Main-chain Liquid Crystalline Central Segment Connected to Amorphous Segments at Both Ends</i> Masatoshi Tokita, Tokyo Institute of Technology
11:00	<i>Melt Spinning of Novel, Luminescent, Polypropylene-shaped Fibers</i> Chureerat Prahsarn, MTEC	<i>Optical Properties of Cashmere Fabrics</i> Sachiko Sukigara, Kyoto Institute of Technology	<i>Regularity of Spherical Microdomain Ordering in a Triblock Copolymer Ultrathin Film</i> Rasha A. H. Bayomi, Kyoto Institute of Technology
11:20	<i>Clothing Pressure of Elastic Socks: Measurement and Prediction Calculation</i> Mari Inoue, Kobe University	<i>Unique Multiple Melting Behavior of High-speed Melt Spun Polylactide Fibers</i> Midori Takasaki, Kyoto Institute of Technology	<i>Effect of Alkyl Chain Length of Fatty Acids on Adsorbed Layer Formation of the Acids and Local Viscosity at Metal/Fluid Interface</i> Toyoaki Hirata, University of Fukui

11:40	<i>Open</i>	<i>Fabrication of Gradient Structure in Melt Spun Polymer Blend Fibers</i> Long Chen, Donghua University	<i>Fully Return-to-Nature Polymer Research for Sustainability of Resources</i> Seong Hun Kim, Hanyang University
Room FS-P (1st Floor, Exhibition Hall)			
12:00–13:20	Poster Session Obligation Time: Odd Numbered 12:00–12:40; Even Numbered 12:40–13:20		
13:20–15:00	Lunch: Rooms FS-B and FS-C 13:30–14:00 Lunch Seminar, Room FS-B, Presented by JASCO Corporation <i>Investigation of Residual Stress Distribution by Laser Raman Microscopy in Fiber Materials with Various Production Conditions</i> Wataru Takarada, Toyko Institute of Technology		

Afternoon Session

	Room FS-B 2nd Floor, Tou-Gen (桃源)	Room FS-C 2nd Floor, Fuku-Jyu (福寿)	Room FS-E 3rd Floor
	Session: Smart Polymers, Fibers, and Textiles <i>Chair: Rudolf Hufenus, Empa</i>	Session: Fundamentals of Fiber and Textile Science, Testing, and Characterization <i>Chair: Konstantin Kornev, Clemson University</i>	Session: Carbon Fibers and Advanced Composite Materials <i>Chair: Gajanan Bhat, University of Georgia</i>
15:00	<i>Syndiotactic Polystyrene Fibers with Nanoporous Crystalline Phases: An Efficient Material for Sorption of Volatile Organic Pollutants</i> Christophe Daniel, Università Degli Studi di Salerno	<i>Will Polyolefin and Polytetrafluoroethylene Filaments Become the Next Generation Filter Materials?</i> Kyung-Ju Choi, Clean & Science	<i>The Effects of Interfacial Adhesion for Mechanical Properties of CFRTPs Made with Polyamide 6</i> Toshihira Irisawa, Nagoya University
15:20	<i>Optical and Mechanical Properties of PA/PET Blend Fibers for Artificial Hair with Different Major Components</i> Shunsuke Sato, Aderans Co., Ltd.	<i>Influence of Polymer Grade, Process Parameters, and Capillary Modification on the Shape Factor of Noncircular Cross-section Fibers</i> Inga Noll, RWTH Aachen University	<i>Highly Transparent PVA-co-PE Nanofiber/Epoxy Film</i> Dong Wang, Wuhan Textile University
15:40	<i>Improvement of Aerosol Oil-mist Filtration Performance Through Superoleophobic Treatment of Fibrous Filters</i> Xin Wei, Deakin University	<i>Effect of Curvature on Wetting and Dewetting of Complexly Shaped Fibers</i> Konstantin Kornev, Clemson University	<i>Ionic Liquid-based Electrolytes Containing Inorganic Nanofibers for Quasisolid Energy Devices</i> Hidetoshi Matsumoto, Tokyo Institute of Technology
16:00	<i>Anti-Tuberculosis Nanofibrous Membrane</i> Varol Intasanta, NANOTEC	<i>Numerical Simulation of Melt Spinning Process Incorporating Crystallization Characteristic of Polypropylene in Super Cooling Conditions</i> Yasuhiko Otsuki, Prime Polymer Co., Ltd.	<i>Preparation of Few-layer Graphene Using Ionic Liquid as Green Media and Its Application in Polymer Composite and Fibers</i> Ye Chen, Donghua University

16:20 Break

	Session: Smart Polymers, Fibers, and Textiles <i>Chair: Varol Intasanta, NANOTEC</i>	Session: Fundamentals of Fiber and Textile Science, Testing, and Characterization <i>Chair: Jinlian Hu, Hong Kong Polytechnic</i>	Session: Carbon Fibers and Advanced Composite Materials <i>Chair: Shuichi Tanoue, University of Fukui</i>
16:40	<i>Multifunctional Liquid-core Fibers</i> Rudolf Hufenus, Empa	<i>Smart and Safe Chemical Protective Clothing</i> Eugenija Strazdiene, Vilnius University of Applied Science	<i>On the Development of Sustainable Composites Reinforced with High-performance Regenerated Cellulose Fibers</i> Chenchen Zhu, University of Bristol (for Anastasia Koutsomitopoulou)
17:00	<i>Irradiated Hydrogel Fibers Responsive to Moisture</i> Bin Fei, Hong Kong Polytechnic University	<i>Washing and Wearing Processes Effects on Soldiers Uniforms: Friction Sound Characterization</i> Floriane Leclinche, Université de Haute-Alsace	<i>Inducing the Crystallization in Cotton Cellulose Ion Gel Films for Enhanced Mechanical Properties</i> Muhammad Abdul Haq, Kagoshima University
17:20	<i>Preparation and Thermo-responsive Properties of Temperature-Sensitive-Gel(TSG)/Polymer Functional Films</i> Jin Gong, Yamagata University	<i>Blocked</i>	<i>Antibacterial Nano-crystalline Cellulose modified with N-halamine/Quaternary Ammonium Salts</i> Xuehong Ren, Jiangnan University
17:40	<i>Open</i>	<i>Blocked</i>	<i>Hydrogel Surface Functionalization of Cotton to Improve Wound Dressing Applicability</i> Maria José Abreu, University of Minho (for Graça Soares)
Room FS-D (2nd Floor, Hei-An)			
18:30	SFSTJ Annual Meeting and Social Gathering with The Fiber Society		

Day III – Thursday, June 14

9:00 Registration

	Room FS-B 2nd Floor, Tou-Gen (桃源)	Room FS-F 2nd Floor, Hou-Rai (蓬莱)	Room FS-E 3rd Floor
	Session: Fiber Manufacturing and Characterization <i>Chair: Caroline Schauer, Drexel University</i>	Session: Fundamentals of Fiber and Textile Science, Testing, and Characterization <i>Chair: Guowen Song, Iowa State University</i>	Session: Fundamentals of Polymer Material: Synthesis, Polymerization, Characterization, and Its Physics <i>Chair: Dominique Adolphe, ENSISA</i>
9:20	Keynote: Can Fibers Lead the 4th Industrial Revolution? Moon W. Suh, North Carolina State University	Keynote: Fundamentals for Memory Fibers and Their Potential Jinlian Hu, Hong Kong Polytechnic University	Keynote: Continuous Supernanofibers for the Next Generation Tough Structural Composites Yuris Dzenis, University of Nebraska-Lincoln
9:50	<i>Yarn and Fabric Performances in a Modified Ring Spinning System</i> Rong Yin, Hong Kong Polytechnic University	<i>Fabric Drape Model Considering Shear and Bending</i> Liu Yang, Shinshu University	<i>Derivation of Statistical Principle: Explaining the Heating Rate Dependence of Degradation Temperature of Ziegler-Natta Poly(styrene)</i> Masatomo Minagawa, NPO, Dream-Create-Laboratories
10:10	<i>Fabric Defect Detection and Classification by Applying Convolutional Neural Networks</i> Maximilian Kemper, RWTH Aachen University	<i>Effect of Drying Temperature on Shrinkage Ratio of Knitted Clothing</i> Yurika Hashimoto, Shinshu University	<i>Preparation and Characterization of Modified Polyesters with Flame Retardancy and Anti-droplet Properties by Copolymerization</i> Peng Ji, Donghua University

10:30	<i>Electrospinning vs. Centrifugally Spinning—Processing and Applications</i> Xiangwu Zhang, North Carolina State University	<i>Evaluation of Nanoscale Structure and Mechanical Properties of Fibers Using FIB-notch Techniques</i> Taylor Stockdale, University of Nebraska-Lincoln	<i>Dye Decomposition and Cr (VI) Reduction Under Visible Light by a Cellulose Acetate Fiber Cross-linked with Amorphous TiO₂</i> Hanako Asai, University of Fukui
-------	---	---	---

10:50 Break

	Session: Fiber Manufacturing and Characterization <i>Chair: Moon Suh, North Carolina State University</i>	Session: Fundamentals of Fiber and Textile Science, Testing, and Characterization <i>Chair: Laurence Schacher, ENSISA</i>	Session: Fundamentals of Polymer Material: Synthesis, Polymerization, Characterization, and Its Physics <i>Chair: Yuris Dzenis, University of Nebraska-Lincoln</i>
11:10	<i>Control of Structure and Mechanical Behavior of Continuous Nanofibers Through Addition of Small Amounts of Nano-inclusions</i> Dimitry Papkov, University of Nebraska-Lincoln	<i>A Novel Approach to Evaluate Thermal Protective Performance of Clothing Subjected to Stretching Forces</i> Guowen Song, Iowa State University	<i>Isothermal Crystallization Experiments for Poly(L-lactic acid) Containing a Liquid-type Nucleation Agent by Small- and Wide-angle X-ray Scattering</i> Thi Ngoc Diep Pham, Kyoto Institute of Technology
11:30	<i>Polymer Nanofiber-based Filter Media with Tailored Three-dimensional Structure High-efficient Air Filtration Through Suspension Drying Techniques</i> Ke Liu, Wuhan Textile University	<i>Testing Method for the Evaluation of Flammability of Meta-aramid Blended Yarns</i> Jie Feng, Hong Kong Polytechnic University	<i>Microspheres with Dimple Morphology of Poly(p-oxyferuloyl) Prepared by Reaction-induced Phase Separation</i> Hironori Atarashi, Okayama University
11:50	<i>Electrospinning PAN of Increasing Isotacticity</i> Caroline L. Schauer, Drexel University	<i>Beyond Fibers and Ropes: Best Practices</i> Rafael Chou, Samson Rope Technologies	<i>Measuring the Interfacial Tension of Polymer Melts: A Modified Fiber Retraction Method</i> Yurong Yan, South China University of Technology
12:10	<i>Blocked</i>	<i>Online Appearance Inspection System of DTY Packages</i> Fei Li, Donghua University	<i>Preparation of Poly(1,4-phenylene terephthalamide) from Poly(ethylene terephthalate) by Means of Reaction-induced Crystallization</i> Kunio Kimura, Okayama University

Room FS-F (2nd Floor, Hou-Rai)

12:30 **Poster Award Ceremony and Closing Remarks**

12:50 **Conference Concludes**

Poster Session

Wednesday, June 13 — Room FS-P, Exhibition Hall, First Floor

Fundamentals of Polymer Materials: Synthesis, Polymerization, Characterization, and Its Physics

Chao-Hung Cheng	<i>Ultra Small-angle X-ray Scattering Analysis of Block Copolymer-grafted Silica Nanoparticle Hybrid Films Under Mechanical Deformation</i>
Soroush Mehdizadeh	<i>Effect of Spacer Geometry on Reverse Electrodialysis (RED) Resistance</i>
Chung Hee Park	<i>Electric Heating Performance and Superhydrophobicity of Cotton Fabric In-situ Polymerized with Pyrrole Using Binary Oxidants</i>
Masahiro Yasukawa	<i>Performance and Efficiency Comparison Between Pressure-retarded Osmosis and Reverse Electrodialysis</i>
Mitsuru Higa	<i>Characterization of Charge Mosaic Membranes Prepared by Ion-track Graft Polymerization</i>

- Saeko Harada *Characterization of Cation-exchange Membranes Prepared by Ion-track Graft Polymerization*
- Tsuyoshi Saito *Preparation and Characterization of PVA-based Charge Mosaic Membranes Prepared by Polymer Coating (for Yuriko Kakihana)*

Fundamentals of Fiber and Textile Science, Testing, and Characterization

- Fumiya Sakakibara *Polymer Alloy of Polybutylene Terephthalate and Polyrotaxane and Its Physical Properties*
- Maria José Abreu *Sensory Evaluation of Female Jeans Using the CALM Scale to Assess Total Comfort*
- Maximilian Kemper *Industry 4.0 and the Future of Textile Production in High-wage Countries*
- Hyewon Kim *Fabric Movement and Washing Performance in the New Front-loading Washer with Built-in Pulsator*
- Klas-Moritz Kossel *Textile Production Theory for Digital Applications in Fiber Production and Processing (for Daniel Buecher)*
- Tsuyoshi Chiba *Analysis of Tactile Sensation of Synthetic Leather Using Logistic Regression Analysis*
- Tao Hua *Structure Analysis of a Colorful Woven Fabric Based on Colored Weft Yarn Mixing*
- Masaki Tanaka *Cleaning Liquid of Dilute Emulsion System Containing Fatty Alcohol for Removing Non-polar Oil from Fabrics*
- Yosuke Taniguchi *New Method for Estimating Synergic Effect or Offsetting Effect in Removal Process of Soils and Dyes from Fabrics*
- Seung Woo Han *Preparation and Characterization of Kapok Nonwoven for Oil-separation Filter*
- Mariko Sato *Study of Comfort of Japanese Traditional Uniforms: Shinto Priest Costumes*
- Davaajav Narantogtokh *Relationship Between Fabric Surface Texture and Friction Using Tri-axial Force Plate*
- Maika Tamari *Evaluation of Performance Such as Hygroscopic Exothermic Property and Heat of Vaporization of Clothing Materials*
- Noriko Fukuda *Effect of Wearing Cloche Hat on Comfort Sensation of Young Women Mountain Walking in Summer in Shiga Highlands*
- Ayumi Takemoto *Effect of Homologous Modeling of Three-dimensional Human Body Shape Data on Body Types Analysis*
- Maria José Abreu *Preparation and Characterization of Gelatin/Arabic Gum Microcapsules Containing Methyl Salicylate Deposited onto a Cotton Fabric (for André Catarino)*

Fiber Manufacturing and Characterization

- Nanjanporn Roungpaisan *Crystalline Structure in High-speed Melt Spun Fibers of Blend of Poly(L-lactic acid) and Poly(D-lactic acid)*
- Yi-Min Lin *Separation of Oil-in-Water Emulsions Stabilized by Different Types of Surfactants Using Electrospun Fiber Membranes*
- Seung Jin Lee *Preparation and Characterization of High-tenacity PTFE Filament Using Melt Spinning Process*
- Tomoki Tokuda *Structure and Properties of Poly(ethylene terephthalate) Fiber Webs Prepared Through Laser-heated Electrospinning and Biaxial Stretching Processes*
- Moo Sung Kim *Preparation of Amorphous Super-engineering Plastic Fibers by Melt-spinning*

Dongwoo Go	<i>PET Fiber Formation Through Continuous Cold Drawing Process with Infusion of Organic Solvent</i>
Eunjin Park	<i>Computational Fluid Dynamics Analysis on Capillary Flow Through Cross-section Profiled Fibers</i>
Tong Cheng	<i>Preparation and Characterization of PSA/Cellulose Alloy Fibers with N-methylmorpholine-N-oxide Monohydrate as Solvent</i>
Youjung Song	<i>Polyurethane Nanofibrous Membranes Prepared via Suspension Electrospinning</i>
Hyung Joo An	<i>Preparation of Islands (High Molecular Weight PET) in the Sea (PP)-type Bicomponent Fibers by Using High-speed Melt Spinning</i>
Jiaxiong Zou	<i>The Impact of Pre-orientation on the Crystallization of Poly(ethylene terephthalate) Fiber During Uniaxial Tension</i>
Masato Masuda	<i>Innovative Conjugate Spinning Technology NANODESIGN[®]</i>

Dyeing and Finishing : Design and Merchandising

Chi-wai Kan	<i>Dyeing Wool Fibre in a Lower Temperature Condition</i>
Dejun Feng	<i>Preparation of Colored Antibacterial Functional Acrylic Fibers by Gel Adsorption Method</i>
Manami Fukumura	<i>A Consciousness Survey on Kurashiki Canvas and Design Proposal</i>

Smart Polymers, Fibers, and Textiles

Takashi Kurose	<i>Fabrication of High-resolution Conductive Patterns on the Thermal Imprinted Polyetherimide Film by Capillary Flow of Conductive Ink</i>
Do-Kun Kim	<i>Fabrication of Piezoelectric PLLA/BaTiO₃ Filaments for Smart Sensors and Their Applications</i>
Hyun-Jung Choi	<i>Electrical Percolation Behavior of Carbon Black/Polymer Composites</i>

Sustainable Polymer Materials : Advanced Cellulose Fibers and Textiles

Yutaka Kawahara	<i>Influence of Electrolyte on the Self-organization of Liquid Silk</i>
Meguru Yokoyama	<i>Fabrication and Characterization of Anti-yellowing Silk with TiO₂ Coating on Zirconium Phosphate Undercoat</i>
Chikako Nakazawa	<i>Construction of a Cell Adhesive Silk Fibroin Material by Mixing with Peptides</i>
Natsuki Shirai	<i>Characteristics of the Cellulose Nanofiber Coatings on TEMPO-treated Fabrics</i>
Yoko Okahisa	<i>Production of Cellulose Nanofibers from Oil Palm Residue</i>
Kosuke Iriyama	<i>Preparation of Porous Cellulose Acetate-Titanium Dioxide Composite Fiber and Its Characterization</i>

Carbon Fibers and Advanced Composite Materials

Lingli Deng	<i>Design and Characterization of Micro- and Nano-hybrid Mats with High-filtration Efficiency</i>
Inga Noll	<i>Reactive Fibers for Air Filtration in Wastewater Treatment Plants</i>
Mònica Ardanuy	<i>Influence of Non-cellulosic Components Removal on the Wet-Dry Cycling Durability of Flax Textile-reinforced Cement Composites</i>

Local Organizing Committee

Takeshi Kikutani, Tokyo Institute of Technology, Conference Chair
Toshihiro Hirai, Shinshu University
Mari Inoue, Kobe University
Kaname Katsuraya, Wayo Women's University
Yutaka Kawahara, Gunma University
Masaaki Minagawa, NPO, Dream-Create-Laboratories
Hiroto Nonomura, SFSTJ
Satoko Okubayashi, Kyoto Institute of Technology
Keita Sakakibara, Kyoto University
Mariko Sato, Bunka Gakuen University
Masatoshi Shioya, Tokyo Institute of Technology
Sachiko Sukigara, Kyoto Institute of Technology
Wataru Takarada, Tokyo Institute of Technology
Shuichi Tanoue, Fukui University
Masatoshi Tokita, Tokyo Institute of Technology
Megumi Yamamoto, SFSTJ
Taiyo Yoshioka, National Agriculture and Food Research Organization

Plenary Speakers

A New Wearable Sensor in the Shape of a Braided Cord

YoshiroTajitsu

Faculty of Science and Engineering, Kansai University, Japan

kenji_imoto@imonet.jp

A new piezoelectric sensor was developed in the shape of a Japanese traditional braided cord known as a “Kumihimo,” by weaving piezoelectric poly-*l*-lactic acid (PLLA) fibers (piezoelectric PLLA braided cord). We then developed a system for measuring pulse waves with a Wi-Fi communication system using a piezoelectric PLLA braided cord with decorative knots.

Functional glasses and wristwatches have already been commercialized as wearable devices are already out in the market. However, the wearers feel unnatural when these devices are used. This unnatural feeling has contributed to the stagnant wearable device market. The ideal wearable device must be worn comfortably and stably. To achieve this, we attempted to realize a functional apparel (e-textiles) [1,2]. In this study, we have developed a wearable sensor in the shape of a Japanese traditional braiding cord, known as a Kumihimo, by weaving piezoelectric poly-*l*-lactic acid (PLLA) fibers, as shown in Fig. 1 [2,3].

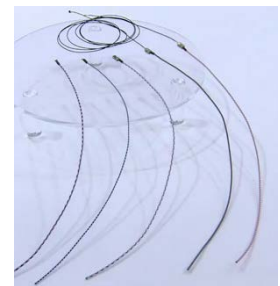


Fig. 1. New piezoelectric sensor (piezoelectric PLLA braided cord).

Pulse sensing by piezoelectric braided cord tied in decorative knot

The important finding in our study is that the intersection on the knot of the braided cord limits the direction of the motion of the cord and the number of contact points propagating the external force because of the constraint condition caused by the cord crossing itself at contact points in the decorative knot [3]. The motion of some types of decorative knots under applied stress was obtained by a finite element method on the basis of the structure symmetry of the decorative knot. On the basis of the simulation results, we developed the following system for detecting pulse waves. The kiccho decorative knot, which reacts only to the small motion of the human pulse without reacting to the direction of the large motion of the shoulder and neck, was used as a choker worn around the neck, as shown in Fig. 2 [3]. Figure 2 shows a demonstration of detecting a pulse wave by a choker braided by a piezoelectric braided cord. The signal due to the pulse wave detected by the choker sensor is sent to a smart phone through a Wi-Fi communication system. A clear signal was accurately observed. In other words, small motion can be detected without being disturbed by the large motion caused by the piezoelectric braided cord, without using a PC and complex and expensive electrical circuits.

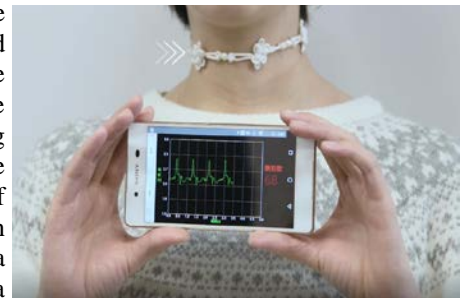


Fig. 2. Pulse wave signal detected by a choker braided by a piezoelectric PLLA braided cord.

REFERENCES

- [1] Carpi, F., Smela, E. *Biomedical Applications of Electroactive Polymer Actuators*. London: Wiley, 2009.
- [2] Tajitsu, Y. *Ferroelectrics*, 515:1, 2017: 44-58.
- [3] Tajitsu, Y. *IEEE Transactions on Dielectrics and Electrical Insulation*. (In press)

ACKNOWLEDGMENT

We thank Teijin Co. Ltd., Japan, for kindly supplying the piezoelectric braided cords. This work was also supported in part by Grants-in-Aid for Scientific Research (Nos. 24655108 and 15K13714) from the Ministry of Education, Culture, Sports, Science and Technology of Japan.

Unprecedented Physical and Mechanical Properties of Solvent-free Processed Tapes and Films of Ultra-high Molecular Weight Polyethylene

Sanjay Rastogi

Aachen Maastricht Institute for Bio-based Materials
Maastricht University
Geleen, The Netherlands

sanjay.rastogi@maastrichtuniversity.nl

Ultra-High Molecular Weight Polyethylene (UHMWPE) having molar mass greater than a million g/mol is an engineering polymer that is used for societal demanding applications including Water (membranes for filtration), Energy (membranes for battery separators), Security (body protection), and Health (prostheses). The polymer when processed into uniaxial or biaxial drawn objects provides unprecedented mechanical properties making it to be the strongest man-made fibers or tapes or films. Because of the high melt viscosity, conversion of the intractable polymer into fibers or films often requires use of toxic solvents that are required to disengage entangled chains prior to processing. Making use of advances in polymer chemistry, physics and processing the paper aims to address the viable solvent free processing route of the intractable polymer into tapes (having oriented fibers along the draw direction) or films. The ease in processing, combined with enhanced mechanical properties, makes the adopted route sustainable while overcoming restrictions on the usage of solvents. The solvent free, uniaxially drawn tapes are found to have high thermal conductivity (approaching aluminum) in an insulator. The combination of unique physical and mechanical properties makes the solvent free processed tapes equivalent to natural diamond. The paper aims to link fundamentals of polymer science to technology development.

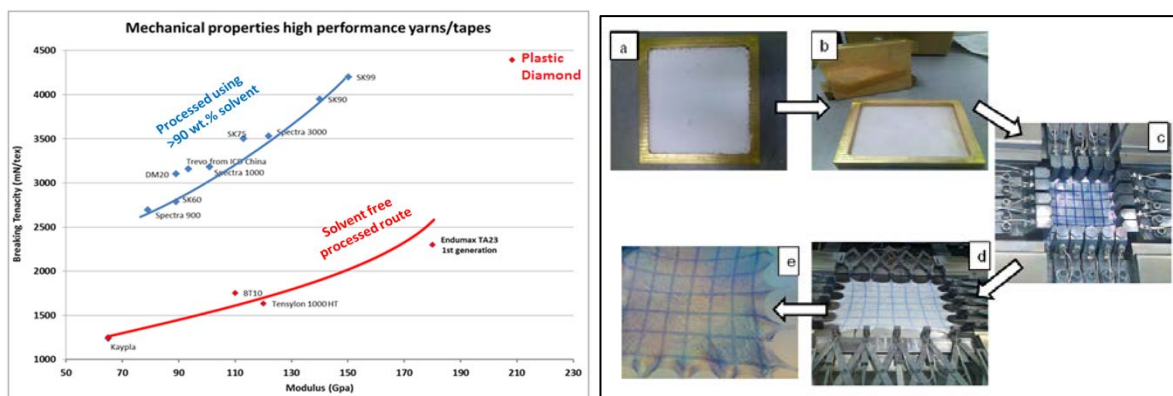


Figure on the left compares tensile strength and tensile modulus of the solution (gel) processed UHMWPE fibers with the commercially available solid-state (solvent free) processed tapes. The paper addresses route to achieve physical and mechanical properties equivalent to *plastic* diamond i.e. solvent free processed tapes having tensile strength and tensile modulus higher than the solution spun fibers. Figure on the right shows biaxial stretching of UHMWPE, free of solvent - making them the strongest man-made tapes and films.

ACKNOWLEDGMENT The author extends thanks to PhDs and post-docs who contributed over years in the development of the project. Financial support from Loughborough University (UK), Max-Planck Institute for Polymer Science, Teijin Aramid, Borealis AG and the Dutch Polymer Institute is gratefully acknowledged.

Smart Polymers, Fibers, and Textiles

Recent Developments of Smart and Multifunctional Fibrous Materials and Clothing

Jintu Fan

Department of Fiber Science & Apparel Design
Cornell University

jf456@cornell.edu

Wearable technology and smart clothing are poised to revolutionize our living environment. However, further development of the field is very much dependent on the accuracy and reliability of wearable sensing technologies, the ability of wearable actuators to respond the changes of human conditions and environment, the seamless integration of sensors, actuators, energy storage devices and communication devices in fashionable products without compromising comfort, appearance, and easy-care. In this presentation, I will share recent developments in smart and multi-functional fibrous materials and clothing at Cornell including directional flow fabric, superhydrophilic wrinkle-free fabric, fluoro-free oil repellent finish, moisture responsive fabric with stomata-like pores, breathable piezoelectric membrane, and air-moving thermoregulatory clothing, and discuss the functionality and remaining challenges of these state-of-the-art technologies.

Improved Electrical Conductivity of PU Nanofiber Web Coated with SWCNT/AgNW and Exploration as Textile Sensors

Eugene Lee, Eunji Jang, Gilsoo Cho

Department of Clothing and Textiles, Yonsei University, Seoul, Korea

gscho@yonsei.ac.kr; imujin@yonsei.ac.kr

The purpose of this paper is to (1) find out the most appropriate coating methods by using SWCNT, (2) measure the electrical conductivity changes as the amount of SWCNT, (3) investigate the effect of the amount of AgNW on electrical conductivity, (4) study how heat and time combination (21 °C, 24 h and 50 °C, 24 h) and ethyl alcohol (untreatment and treatment) affect the electrical conductivity, and (5) verify whether the specimens are coated with the conductive materials successfully by characterizing the surface and chemical properties. Single-walled carbon nanotubes dispersed in water (SWCNTs, 1wt%) and silver nanowires dispersed in water (AgNW, 1wt%) were used in this study. Electrical conductivity was induced to the polyurethane nanofiber web by a dip-coating process utilizing SWCNT/AgNW solution. The sheet electrical resistance of the specimens was evaluated. FE-SEM (Field-emission scanning electron microscopy) was used to analyze surface property. HR-XRD (High resolution X-ray diffraction), Raman spectra, and FT-IR (Fourier transform infrared spectroscopy) analyses were conducted. The result showed that the sheet electrical resistance of the specimens coated with SWCNT decreased as the amounts of SWCNT increased. However, as the amounts of AgNW increased, the resistance of the specimens coated with SWCNT/AgNW increased. After heat treatment, the electrical resistance substantially decreased, as well as after ethanol treatment. As a result of the surface property, SWCNT/AgNW formed an electrical network and densely covered on the surface of the nanofibers. And, according to the result of chemical properties, SWCNT/AgNW was uniformly and successfully coated on the nanofiber web after heat treatment.

ACKNOWLEDGMENT

This research was supported by the National Research Foundation of Korea (NRF) funded by the Ministry of Education, Science and Technology (No. NRF-2016R1A2B4014668) and the Brain Korea 21 Plus Project of Dept. of Clothing and Textiles, Yonsei University in 2018. This research was partially supported by the Graduate School of Yonsei University Research Scholarship Grants in 2018.

Wearable Fiber Organic Electrochemical Transistors for Biological Sensing

Yuedan Wang, Xing Qing, Quan Zhou, Yang Zhang, Dong Wang

College of Materials Science and Engineering, Wuhan Textile University, Wuhan, China

wydan2015@163.com

Wearable electronic devices that can be comfortably and three-dimensional integrated with human body have attracted great attention in recent years. With the fast development of electronic industry, the population using smart sensors were dramatically increased for the application in real time monitoring personal health conditions and environmental changes. It is indispensable to develop the high response and flexible sensor for promising application. Organic thin film transistors are often used as an amplifier to improve sensitivity. Among them, fiber organic electrochemical transistors is endowed with superior property and dramatically flexibility to apply for sensor application¹⁻². In this study, the novel wearable fiber organic electrochemical transistors (FECTs) based on graphene, nanofiber and polypyrrole have been prepared, the chemical structure, surface morphology, mechanical property and conductivity were investigated by SEM, IR, Instron and so on. Moreover, the electrical properties of FECTs have also been characterized. The transistors showed high on/off ratio of 10^2 , fast switch speed, and long cycling stability. The biological sensor based on the fiber organic electrochemical transistors have also been investigated, it exhibited high sensitivity, outstanding selectivity and fast response time. In addition, the device presented a good reproducibility. Specifically, the biosensors have been successfully used for sensing glucose and dopamine levels in real sample analysis, indicating that the devices are promising for in real-time detection of bio-markers in human body. In addition, the textiles were constructed by the coated monofilaments using the weaving machine. It can be woven into fabric for wearable E-textiles. All the results indicate that the novel fiber transistors pave the way for portable and wearable electronics devices, which has a promising future for healthcare and biological application.

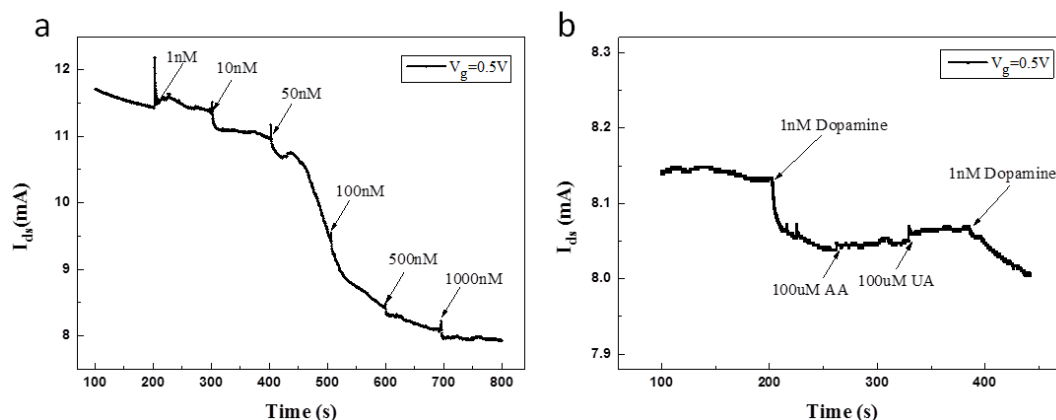


Figure 1. The sensitivity (a) and selectivity (b) of PPy/NFs/PA6 biosensors based on fiber organic electrochemical transistors.

REFERENCES

- [1] Cicoira, F., Sessolo, M., Yaghmazadeh, O., DeFranco, J.A., Yang, S.Y., Malliaras, G.G. "Influence of Device Geometry on Sensor Characteristics of Planar Organic Electrochemical Transistors." *Advanced Materials*, 22, 2012: 1012.
- [2] Lin, P., Yan, F., Yu, J., Chan, H.L., Yang, M. "The Application of Organic Electrochemical Transistors in Cell-Based Biosensors." *Advanced Materials*, 22, 2012: 3655.

ACKNOWLEDGMENT

This work was financially supported by the National Natural Science Foundation of China (51503157, 51473129).

Melt-spun Conductive Elastomeric Fibers for Smart Textiles: Implications for Bio-signal Recordings

Ladan Eskandarian¹, Milad Alizadeh Meghrazzi^{1,2}, Mohammadreza Naeimirad³ and Milad Lankarany^{1,4}

¹Myant, Inc., Toronto, ON, Canada; ²IBBME, University of Toronto, Toronto, ON, Canada; ³Department of Materials and Textile Engineering, Razi University, Kermanshah, Iran; ⁴The Hospital for Sick Children (SickKids), Toronto, ON, Canada

ladan.eskandarian@myant.ca

Conductive stretchable fibers can be used in various contexts for the development of e-textiles. In this work, we demonstrated a method to extrude carbon-loaded thermoplastic elastomers (TPEs) into conductive fibers. The resulting fibers display resistance values of $5 \text{ K}\Omega\cdot\text{cm}^{-2}$, demonstrating that the high conductivity of TPEs is not lost when transferred to textile fibers. These conductive elastomeric fibers were used to knit electromyography (EMG) and electrocardiography (ECG) sensors directly in textiles.

Melt-spinning trials were conducted on carbon black-filled thermoplastic elastomer (ESD C 2800 B-45A) purchased from RTP, MN, USA using FET pilot plant (equipped with an extruder by L/D of 4, draw-line, water bath quench and various heated draw and relaxation zones) to produce ultra-stretchable monofilament. Melt-spun fibers were evaluated for physical, morphological and electrical characterizations.

Draw ratio and quenching process of the extruded filament are important factors that affect the stretchability and conductivity achieved. On the other hand, the decrease in diameter of the filament will result in a decrease in conductivity and tensile strength, and therefore it is important to optimize the fiber diameter during the melt spinning process. Thus, our present study aims at: (1) establishing how the above-mentioned factors influence the quality of the fiber and how it correlates with the resulting conductivity; and (2) explore the suitability of our extruded conductive TPE fibers for knitting, weaving or embroidery of smart textiles.

Some qualitative experiments were performed to emulate the conditions that the fiber may encounter during usage and handling. The fiber was initially stretched up to 300% and the resistance was found to increase by two orders of magnitude, but the fiber did not lose its electrical conductivity. The resistance recovered to its initial pre-stretched value upon returning the fibers back to a non-stressed state.

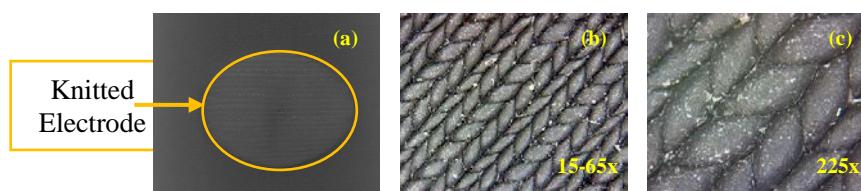


Figure 1. Regular and microscopic pictures of knitted electrode with conductive TPE fibers: (a) knitted EMG/ECG sensor electrodes; (b) 15-65x magnification; (c) 225x magnification.

The textile EMG/ECG is recorded from arm/chest by EMG/ECG Olimex embedded in Arduino Uno for five subjects. The recorded EMG/ECG signals and their filtered signals ($[0.8 - 200]$ Hz for EMG and $[0.8-40]$ Hz for ECG) are shown in Figures 2. The quality of recorded EMG/ECG signals by textile knitted DRY-Electrodes was comparable with that obtained by gel electrodes.

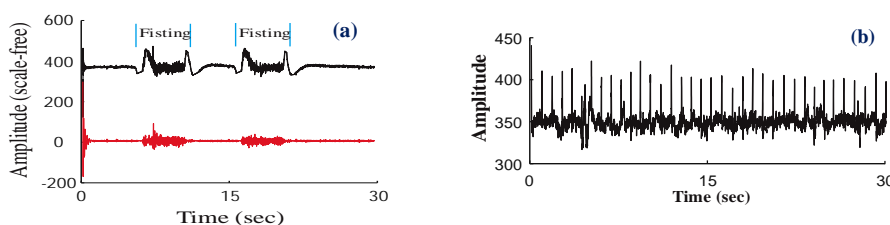


Figure 2. (a) Recorded EMG signals from arm: solid black line shows EMG signals and solid red line shows their high-pass filtered signals (0.8-200 Hz); (b) recorded ECG signals from chest.

Acoustoelectric Conversion Properties of Electrospun Nanofiber Webs

Jian Fang, Chenhong Lang, Hao Shao, Tong Lin

Institute for Frontier Materials, Deakin University, Geelong, Australia

tong.lin@deakin.edu.au

Electrospinning offers a simple but efficient approach to directly produce piezoelectric nanofibers. The high electric field and intensive fiber stretching during electrospinning contribute to high β crystal phase content and oriented electric dipoles within electrospun nanofibers. These unique features enable randomly orientated nanofiber webs to have strong mechanical-to-electric conversion ability. Here, we report the sound-to-electrify conversion properties of electrospun piezoelectric nanofiber webs. The electrospun nanofiber webs were assembled into a device to test the acoustoelectric conversion performances. The energy conversion capability was found to be dependent on nanofiber dimension, β phase content within nanofiber, fiber orientation, polymer type, sound source, and device structure. The piezoelectric nanofiber webs can be used either as sound sensor and energy generator. When used for sensing sounds (see the device, nanofiber morphology and voltage output in Figure 1), the device showed five times higher sensitivity than its piezoelectric film counterpart. A nanofiber energy generator can generate 14.5 V and 28.5 μ A electrical outputs, which are sufficient to run 27 commercial LEDs without using energy accumulation unit.

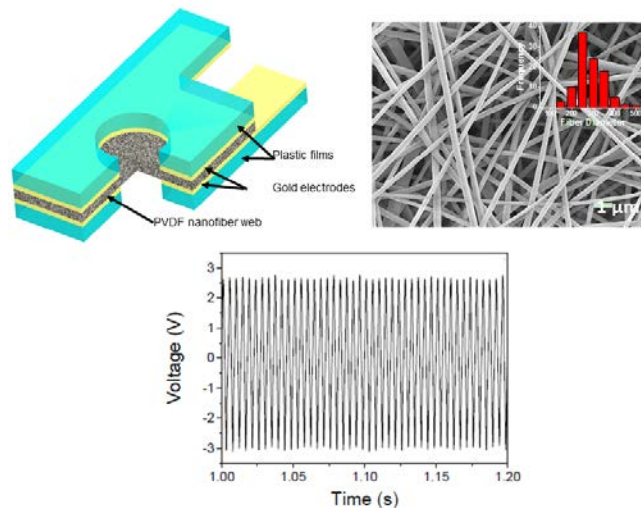


Figure 1. Nanofiber device for conversion of acoustic waves into electricity (left up), morphology of the nanofibers under SEM and their diameter distribution histogram (right up), and voltage output of the device under sound.

Characterization of Hybrid Smart Yarns Engineered for Versatile Applications in Sportswear, Medical, and Multifunctional Textiles

Amir Shahzad, Abher Rasheed, Zulfiqar Ali, Bilal Qadir

National Textile University

amir_textilian@hotmail.com; bilal_ntu81@hotmail.com

In sportswear, textile-based smart wearable systems are used for vital sign and performance monitoring. Similarly, in medical textiles, such kind of wearable monitoring systems are also suitable to detect and respond quickly to any abnormal symptoms in the bed rest patients. The piezoresistive behavior of smart textiles is commonly employed in the fabrication of such wearable monitoring systems. Furthermore, textiles for the comfort, antistatic, antibacterial and heating characteristics are also needed somewhere in medical textiles for healthcare and hygiene purpose. The primary focus of this research is to develop a cost-effective, durable and easy processable piezoresistive hybrid smart yarn with multifunctional characteristics. For this purpose, hybrid yarns, composed of polyester and stainless steel fibers (PS) are produced using conventional ring spinning process. Yarn samples produced with PS 80:20 ratio, at three levels of twist factor, represented by PS-1, PS-2, and PS-3 respectively are given in Table I along with their linear density, tensile, and linear electrical resistance (LER) values.

Table I: Physical, tensile, and electrical properties of yarns measured.

Yarn Sample	Twist Factor (TF)	Linear density (tex)	Tenacity (cN/tex)	Elongation %	LER ($\Omega/10$ cm yarn)
PS-1	2200	57.79	24.41	9.11	136.26
PS-2	2678	57.82	25.51	9.52	104.86
PS-3	3175	59.18	26.09	9.94	93.80

The results given in the table prove that by increasing level of twist in a smart hybrid yarn, both electrical resistance and mechanical properties are improved significantly. The heating characteristics of yarn were also investigated and it is found that at increasing levels of applied voltage and combination of yarn elements, the temperature of yarn is also increased. In order to evaluate the multifunctional characteristics of yarn, it is fabricated into a knitted fabric. This stretchable piece of knitted fabric is found to possess the novel features of the piezoresistive strain sensor, a pressure sensor as multilayers structure of the knitted fabric, interactive style with touchscreen devices as a functional glove and good antibacterial potential for healthcare and hygiene applications in medical textiles. Another piece of smart yarns was also engineered using a combination of viscose and stainless steel fiber which responds quickly to change in moisture content by changing its LER value. Such yarn can be used to develop monitoring of wound exudate and pressure ulcers.

KEYWORDS: Smart Yarn, Hybrid, Multifunctional, Stainless steel, linear electrical resistance.

Application of Carbon Nanomaterial to Biodevice for Biofuel Cell with Carbon Binding, Peptide-fused Enzyme

Shin-ichiro Suye^{1,2,3}, Aina Tonooka¹, Hiroaki Sakamoto^{1,3}, Takenori Satomura^{2,3}

¹Department of Frontier Fiber Technology and Science, University of Fukui, Japan

²Department of Applied Chemistry and Biotechnology, University of Fukui, Japan

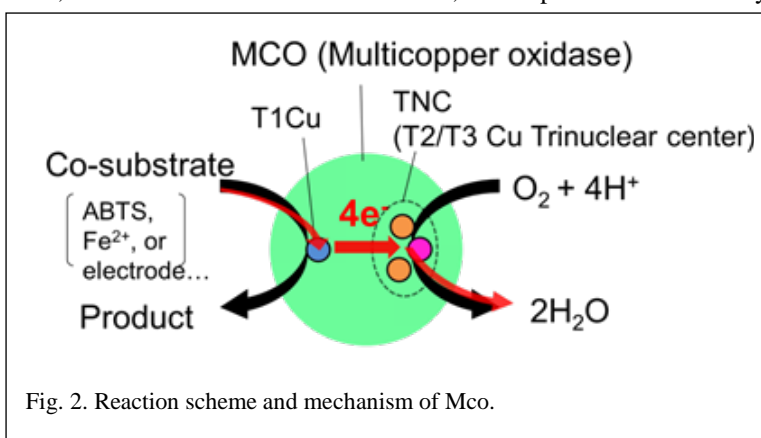
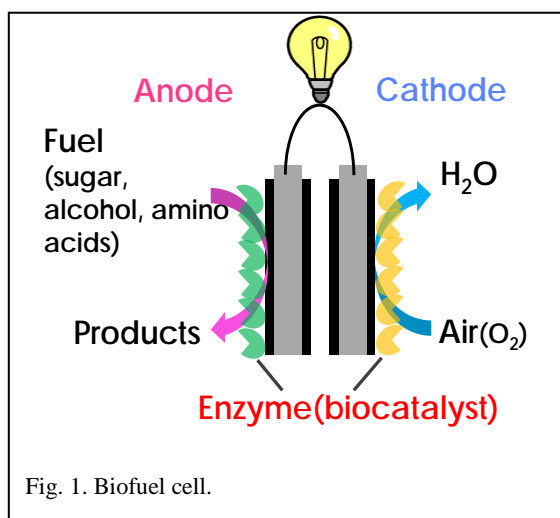
³Life Science Innovation Center, University of Fukui, Japan

suyeb10@u-fukui.ac.jp

INTRODUCTION

Biofuel cells (BFCs) generate electric energy from biochemical substances using enzyme as device catalysts. Power density of BFCs depends on many factors, such as mass transfer, catalytic reaction, electron transfer, and amount of electroactive enzyme. To improve current density of BFC electrodes, carbon nanomaterials are useful as electrode. Carbon nanomaterials have great advantages for electrode material, high chemical stability, high conductivity, and low costs. Carbon nanomaterials such as carbon nanotubes, graphene and Ketjen black (KB) are remarkable to improve the performance on the biodevices. High orientation of enzyme on the device is also important for high current density. The optimal position of redox and catalytic site in enzyme on device can significantly facilitate the associated electrocatalytic reaction. A short distance between redox site and electrode has been shown to lead to fast electron transfer, producing high current density in device. Meanwhile, the catalytic site should be located on the side of device facing away from the electrode surface. This would allow substrate as fuel molecule to easily approach the catalytic site, enhance the substrate diffusion rate, and improve current density.

To link target of enzyme and carbon surface, specific bond is essential. In the present study, we focused on carbon nanotube binding peptide (CBP) with affinity binding with carbon nanotube surface. We coordinated multicopper oxidase from *Pyrobaculum aerophilum* (McoP) fused CBP that get short distance between T1 Cu site of McoP and carbon surface when McoP fused CBP combine to CNT. CBP fused at C terminal of McoP was expressed genetically. Enzymes immobilization via CBP is expected to contribute easier construction of electrode with high performance on cathode.



EXPERIMENTS

Materials and Apparatus

Yeast extract and tryptone were obtained from nacalai tesque (Kyoto, Japan). Single walled carbon nanotube (SWCNT) and grassy carbon electrode (GCE) were purchased from Sigma-ALDRICH Co., Ltd. (Missouri, USA) and BAS (Tokyo, Japan). Coomassie (Bradford) Protein Assay Kit was from Thermo Fisher SCIENTIFIC (Massachusetts, USA). All other reagents were purchased from Wako (Osaka, Japan). The water passed through a Milli-Q water purification system was used for purification enzyme. In electrochemical measurement, SP waster purified using MILLIPORE was used.

Expression and Purification of McoP-CBP

McoP fused CBP (McoP-CBP) was expressed in *Escherichia coli* (BL21-Codon-Plus (DE3)-RIPL), as same previously described expression of McoP [1]. CBP sequence was used LLADTTHHRPWT found using phage display method [2]. At first, we got PAE1888-CBP fragment coded McoP-CBP using PCR with primer including CBP sequence and PAE1888 as template. Then linearized pET11a vector was ligated with PAE1888-CBP fragment to construct pET1888-CBP expression plasmid vector using in-fusion cloning. pET1888-CBP was used for transformation of strain, and LB medium was used for cells cultivation. McoP-CBP was purified from a crude extract to obtain a high-purity enzyme through a three-step process using heat treatment (80°C, 10 min), anion-exchange chromatography and gel filtration chromatography. The molecular weight, purity and enzyme activity were determined as previously described. To compare, McoP (WT) was prepared using same expression and purification methods.

Preparation of McoP-CBP/SWCNT Complex

SWCNT was dispersed in 2M HCH and placed over night for purification. Then SWCNT washed enough water and 10 mM Tris-HCl buffer (pH 7.2). Purified SWCNT 1 mg and 1mg/ml McoP-CBP solution 1 ml were mixed in tube. Further this mixture sonicated for 3 h to bind CBP with CNT. Then McoP-CBP/SWCNT complex was rinsed using buffer to remove unbound McoP-CBP. This rinsed buffer containing McoP-CBP was quantified protein to estimate binding McoP-CBP in complex using Coomassie (Bradford) Protein Assay Kit. WT/SWCNT complex was prepared through same processes. Activities of complexes were measured using same condition for enzyme solution.

Preparation of McoP-CBP/SWCNT Complex Immobilized Electrode

To construct the cathode, McoP-CBP was immobilized on GCE. GCE was polished using microparticle and operated electrochemical treatment in 50 mM H₂SO₄. A 10 µl of 1mg-SWCNT/ml McoP-CBP/SWCNT complex was casted on cleaned GCE and dried for 3h at room temperature. Then 0.5 % nafion solution was coated on complex and dried for 3h at room temperature to get McoP-CBP/SWCNT/GCE. And WT complex immobilized electrode also prepared.

Electrochemical Experiments

Cyclic voltammetry (CV) was operated using a three-electrode cell on an ALS electrochemical analyzer system (Model 1205B, BAS Inc., Tokyo, Japan). The working, counter and reference electrodes were the enzyme-immobilized electrode, platinum mesh and Ag/AgCl electrode, respectively. All potential values reported below are with respect to the Ag/AgCl reference electrode. The CV measurements were recorded at 10 mV/s. Glycine-HCl buffer (50 mM, pH 3.0) saturated O₂ or N₂ in the absence of mediator at 50°C.

RESULTS AND DISCUSSION

Amount of immobilized protein in complex and activity

At first, amount of immobilized protein on the complex and activity were investigated. Enzyme activity of McoP-CBP and WT were 1.9 units/mg and 2.2 units/mg, respectively. Immobilized protein amount on McoP-CBP/SWCNT and WT/SWCNT complex were also similar (ca. 1.00 mg/mg-CNT). However, activity of McoP-CBP/SWCNT and WT/SWCNT were 0.88 units/mg-CNT and 1.27 units/mg-CNT, respectively. McoP-CBP/SWCNT showed lower activity compared with WT/SWCNT. CBP was introduced C-terminal located near T1 Cu of McoP. It indicates that McoP-CBP is binding to SWCNT surface via CBP with high orientation

coordinating short distance between T1 Cu and SWCNT surface. ABTS of substrate is hard to access to T1 Cu as active site because T1 Cu was closed carbon nanotube surface at McoP-CBP/SWCNT.

Electrochemical Characterization of McoP-CBP/SWCNT Immobilized Cathode

Then the electrochemical characterization of McoP-CBP/SWCNT immobilized on the cathode was investigated using CV at 50°C. Oxygen reduction current of McoP-CBP/SWCNT/GCE appeared at +0.30 V. McoP immobilized on the electrode via CBP reveals that electron transfer from electrode to T1 Cu is easier than electrode random adsorption of WT. At +0.1 V, large reduction wave based on the oxygen reduction was shown by non-oriented immobilized enzyme. It implies that McoP CBP/SWCNT/GCE contained non-oriented enzyme absorbing on SWCNT.

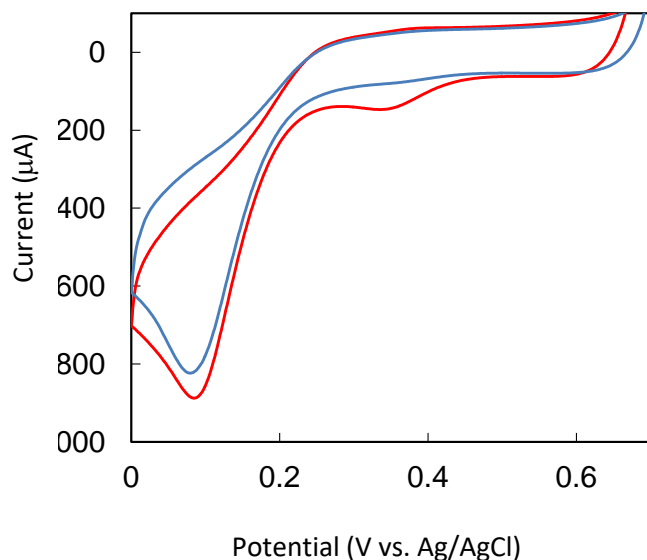


Fig. 3. CVgrams of McoP/SWCNT complexes immobilized GCE.

REFERENCES

- 1) H. Sakuraba, K. Koga, K. Yoneda, Y. Kashima, T. Ohshima. *Acta Cryst.*, F67, 2011: 753. 2014, Doi : 10.4172
- 2) Z. Su, T. Leung, J., et al. "Conformational selectivity of peptides for single-walled carbon nanotubes." *J. Phys. Chem. B Lett.*, 110, 2006: 23623-27.
- 3) A. Koto, S. Taniya, H. Sakamoto, T. Satomura, H. Sakuraba, T. Ohshima, S. Suye. *J. Biosens. Bioelectron.*, 5, 1000148.

Electro-conductivity of Staple Polyester Fibers Coated by Ag in Vacuum

Hristo Hadjiev², Ivelin Rahnev¹, Philip Philippov³

¹College of Sliven (TUS); ²Faculty of Engineering and Pedagogy of Sliven (TUS);

³Technical University of Sofia, Bulgaria

irahnev@tu-sofia.bg

INTRODUCTION

The essence of this experimental work comprises the application of a silver (Ag) coating on staple polyester fibres in vacuum environment by means of ion beam sputtering. The method for the deposition of thin film coatings in a vacuum environment is physical. The characteristic feature of this method is the very good adhesion towards the substrate, uniformity, and density of the deposited films with minimal internal tensions, the possibility to deposit very thin films even several nanometres, good reproducibility of the films, and others. Subject of this article is the experimental planning and the consecutive implementation of the variants, and the electric resistance of the fibres coated by thin film of Ag. The method of the deposition of thin film coatings in a vacuum environment is physical. The characteristic feature of this method is the very good adhesion towards the substrate, uniformity, and density of the deposited films with minimal internal tensions, the possibility to deposit very thin layers even several nanometres, good reproducibility of the films, and others.

EXPERIMENTAL WORK DESCRIPTION

Ion plasma sputtering is carried out in specially designed for this purpose vacuum recipient. In this specific case, the vacuum chamber (1) is made of thick-walled stainless steel with a volume of 510cm³, figure 1. The evacuation of the vacuum chamber is done with shutter primary pump Leybold (7) for medium vacuum to 1 x 10⁻³ mbar and Turbo-molecular vacuum pump Pfeiffer for high and very high vacuum to 1 x 10⁻⁷ mbar. The chosen method of ion beam sputtering in a vacuum is characterizing by low temperature deposition of thin layers. Substrate (6) used in the present work is staple polyester with finesse of 3.3 dtex and 64 mm average length. In this experiment, like a substance for the sputtering, the target (5) is made of silver (Ag 99.999). The conductivity test of the silver-coated fibres is realising by a central composite rotatable experiment (D plans) with two factors: target voltage - U_t and exposure time - τ_e . The target voltage (3) of the sputtering varies from 2 to 5 kV. The exposure time varies from 20 to 120 min. At each variant of the deposition of a thin film of Ag on the surface of the fibres the tension of the ion beam sputtering and the exposition time were changed. At increasing of the operating pressure more than 6 x 10⁻³ mbar this leads to a reduction in the rate of sputtering of the target, a reduction of the adhesion layer, distortion of the homogeneity of the thin film during the construction of the crystal lattice of the film coating.

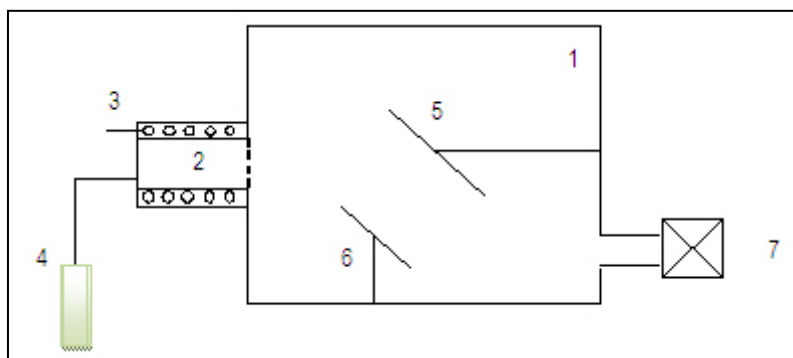


Figure 1. Vacuum chamber of ion beam sputtering.

The extreme range of response of the studied process can be described by conducting a 3-level experiment, an ECCR2 (D-plans), based on the full factory. This is the most suitable experiment to investigate objects in the textile industry. The mathematical model of ECCR2 is an equation of the type:

$$y_R = b_0 + \sum b_i x_i + \sum b_{ij} x_i x_j + \sum b_{ii} x_i^2$$

Table 1. ECCR2 values of the factors levels.

	Variants								
Factor 1, X1	-	+	-	+	-1,4142	1,4142	0	0	0
Factor 2, X2	-	-	+	+	0	0	-1,4142	1,4142	0
Tension [kV]	2,44	4,56	2,44	4,56	2,00	5,00	3,50	3,50	3,50
Time [min]	35,00	35,00	105,00	105,00	70,00	70,00	20,00	120,00	70,00
No variant	1	2	3	4	5	6	7	8	9*5

MEASUREMENT EQUIPMENT

The investigation of the chemical composition of the coated fibres is carrying out by means of EDX analysis with apparatus JEOL 6390 and INCA Oxford. The measurement of the electrical conductivity of the wrapped fibres is carrying out by means of a digital ohmmeter. The device for measuring the electrical resistance of the silver coated fibers is shown in Figure 2.

After the statistical processing of the laboratory results and by the regression coefficients, the variation in fibre electrical resistance and the relative atomic weight of the deposited silver are visualised in Figure 2.



Figure 2. Electric resistance measuring device.

EXPERIMENTAL RESULTS

The morphology of the polyester fibers coated by silver thin film is shown on the REM photograph of figure 3. The relative distribution of the atomic mass of carbon (C), oxygen (O) and silver (Ag) in the fibrous mass of the substrate is shown in the spectrogram of Figure 3.

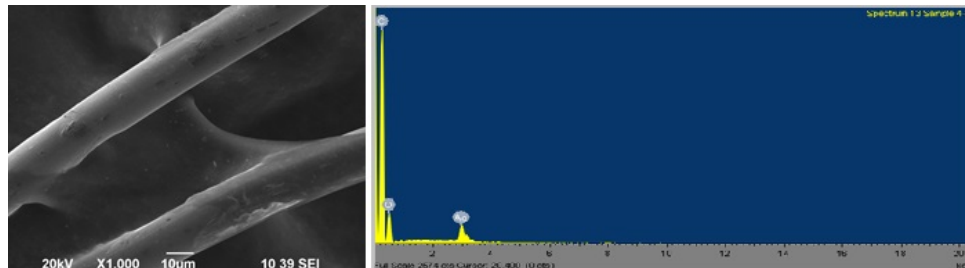


Figure 3. REM and EDX spectrogram of the polyester fibers coated by argen thin film.

In order to evaluate the variation of the electric resistance, or the electro-conductivity of the thin film, an experimental plan was designed. The processing of the experimental results and the statistical treatment carried out allowed the calculation of the regression coefficients of the target polynomial. Results of the metrology tests are given in the table.

Table 2. Regression coefficients of the tested properties.

property	coefficients of regression						freedom level	Ficher criterium
	b0	b1	b2	b12	b11	b22		
Ag/glass, nm	138,3300	101,9500	159,0200	11,1100	106,1100	115,0000	9	6,25
Ag-Pes, %	12,6100	0,7997	5,3747	-1,4267	2,1889	2,6111	5	33,19
Rabs-Pes, kOm	3,1667	-0,7774	-1,0131	0,5556	-0,5278	-0,0833	5	4,41

Figure 4 illustrates the effects of ion beam voltage and exposure time on the fraction of the silver ions in the fibrous mass and the electro conductivity of the polyester fibers coated by silver.

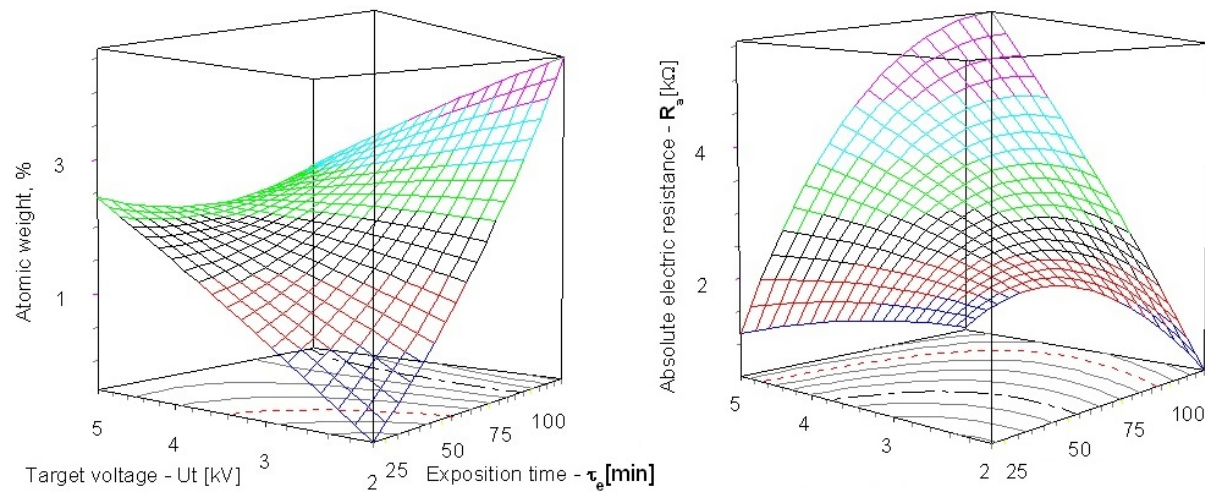


Figure 4. Response surfaces of the silver (Ag) relative mass weight and the absolute electric resistance of the coated fibers.

CONCLUSION, ANALYSIS, AND DISCUSSION

The advantage of ECCR2 consists in the design of a 3D graph of the functional change of the studied parameters. The simultaneous presentation of both experimental surfaces directs the conclusions in two main directions. The relative increase of silver atoms reduces the electrical resistance of the coated fibres. The exposure time has a pronounced and predominant almost linear nature, whereas the impact of the target voltage has a smooth and parabolic character. In this case, the duration of exposure has a predominantly and principally linear character. The figure shows that increasing the deposition time of the thin layer of silver, then the electrical resistance of the coated fibers decreases. At the same time, the target voltage has a parabolic effect on the conductivity of the thin film. This requires additional experimental work and in-depth research into this technological factor. In any case, the positive relationship between the technological factors and the increased electrical conductivity of the coated polyester fibers is obvious. This is a testimony of increasing the thickness of the thin layer of silver. The modified fibres can be incorporated into a spinning mixture and by their electrical conductivity to obtain fabrics with screen protection against electromagnetic irradiation.

- [1] Philippov Philipp, Rahnev I. R., Slavova V. "Integral perspective of the textiles and the hybrid microelectronic element." *General Textile Conference Sofia'14 Proceedings*, Vol. 1, ISBN 978-954-91951-2-5, Edition STU of TCL, 2014: 103-20.
- [2] Philipov Philipp., Rahnev I. R., Hadjiev Hr.. "Hybrid microelectronic technology in textile techniques with the aim of realizing smart textiles." *ISSE 15*, ISBN 978-963-313-177-0, Paper A20, 2015.
- [3] Andonova, Snezhina. "A study of correlation dependence between the criteria optimization of the humidity and yhermal process." *Journal Tekstil i Obleklo*, Vol. 6, ISSN 1310-912X, 2017: 144-48.
- [4] Rahnev Ivelin. "Virtual migration in the spinning fibrous sheaf." *Proceedings 16th World Textile Conference Autex 2016*, 677(082) (0.034.2), Ljubljana, Slovenia, 2016, ISBN 978-961-6900-17-1

ACKNOWLEDGMENT: Authors thank E. Mirogljo EAD-Sliven for their support and collaboration.

Carbon-based Yarn Supercapacitor for Energy Storage

Yuxiang Huang^{1,2}, Jonathan Y. Chen¹, Guangjie Zhao²

¹The University of Texas at Austin, Austin, TX, USA; ²Beijing Forestry University, Beijing, China

jychen2@austin.utexas.edu

INTRODUCTION

Yarn supercapacitors are developed as a new yarn product potential for energy storage needed in wearable electronic devices. Much attention has been drawn to the development of electrode materials from carbon nanomaterials, but high cost and uncertain potential health impact of these nanomaterials remain to be a challenge. This paper presents a new yarn supercapacitor made of carbon fiber (CF) and activated carbon fiber (ACF). Two complex yarn structures for yarn supercapacitor fabrication are studied and their electrochemical properties are assessed. Potential applications of the yarn supercapacitor in end-use markets are discussed.

METHOD

The CF material used was a commercial grade PAN-based filament. The ACF material was produced from liquefied wood biomass. These fiber materials were used for construction of two complex yarn structures. The first structure was CF filament loaded with ground ACF. The second one was CF filament wrapped with ACF fiber bundle. Two kinds of yarn electrodes were formed by coating a thin layer of PVA-based electrolyte gel onto the surface of each complex yarn. A yarn supercapacitor was composed of a pair of yarn electrode twisted together (Fig. 1). Electrochemical properties of the yarn supercapacitors, in terms of cyclic voltammetry (CV), galvanostatic charge/discharge (GC), and electrical impedance spectroscopy (EIS), were measured and analyzed.

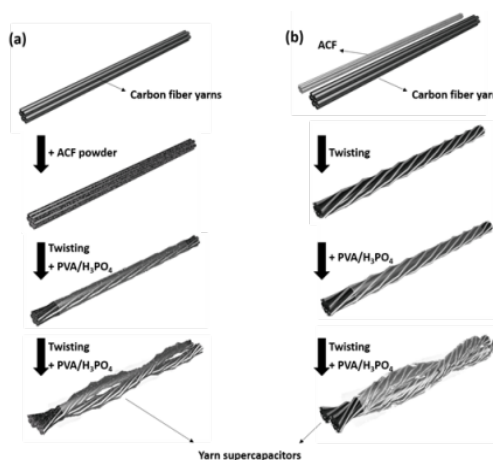


Fig. 1. Yarn supercapacitor structure

RESULTS AND CONCLUSION

From the CV test it was revealed that the ACF-particle loaded yarn electrode had a higher capacitive performance than the ACF-fiber wrapped yarn electrode (Fig. 2). Upon different yarn bending deformation from arbitrary bending to crumpling, the yarn supercapacitor kept high capacitance retention in a range of 83-97% (Fig. 3), showing an excellent mechanical reliability. The EIS measurement result indicated that the ACF-particle loaded yarn electrode also had a higher linear slope (better ion diffusion) and lower equivalent serial internal resistance (ESR) than the ACF-fiber wrapped yarn electrode (Fig. 4), suggesting a faster electron transfer. In summary, because of low ACF strength, direct wrapping and twisting of fibrous ACF with CF filament was not a feasible way for fabricating yarn supercapacitors. In contrast, the yarn supercapacitor fabricated by CF deposited with ACF powder exhibited a high specific length capacitance of 43 mF cm^{-1} .

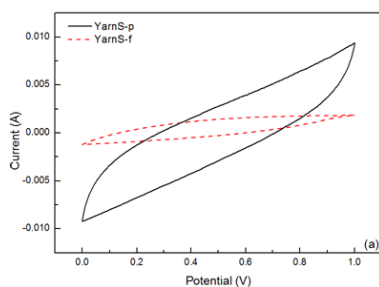


Fig. 2. CV curves

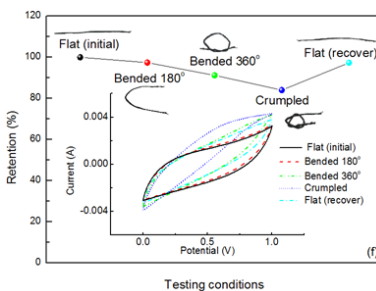


Fig. 3. Capacitance vs. bending

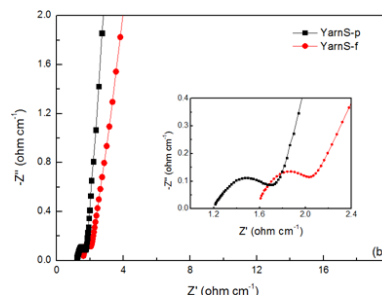


Fig. 4. EIS Nyquist plots

Smart Textile Actuator Using Stress Memory Polymer

Bipin Kumar

Department of Textile Technology, Indian Institute of Technology Delhi, India

bipin@textile.iitd.ac.in

Since their inception, textiles have been important in human history and significantly impacted the economic development and global trade. Although they are more popular as clothing serving two main attributes - aesthetics and protection. However, with the rapidly changing needs of consumers over a few decades, textiles are becoming smarter, generating creative and novel solutions for many engineering and medical problems. In this research, a new intelligent function, i.e. stress control, in the textile will be introduced. This novel function of stress control allows programming and storing the internal stress in the structure of textile, and also enabling it to retrieve the stored stress reversibly with an external stimulus such as heat (Figure 1a & 1b). The paper addresses the fundamentals of stress control and the related mechanism using a viscoelastic model consists of spring and dashpot elements. As an example of the potential application, the stress control in textile can be used for smart medical

compression treatment to allow pressure control with massaging effect for an efficient treatment of compression therapy used in chronic venous disorders (Figure 1c & 1d). It is anticipated that the research into stress control in textiles will grow in multiple dimensions as a result of their promising potential in many stress controlling applications such as pressure garments, bandages, massage devices, 3D mattress, sensors/actuators, etc.

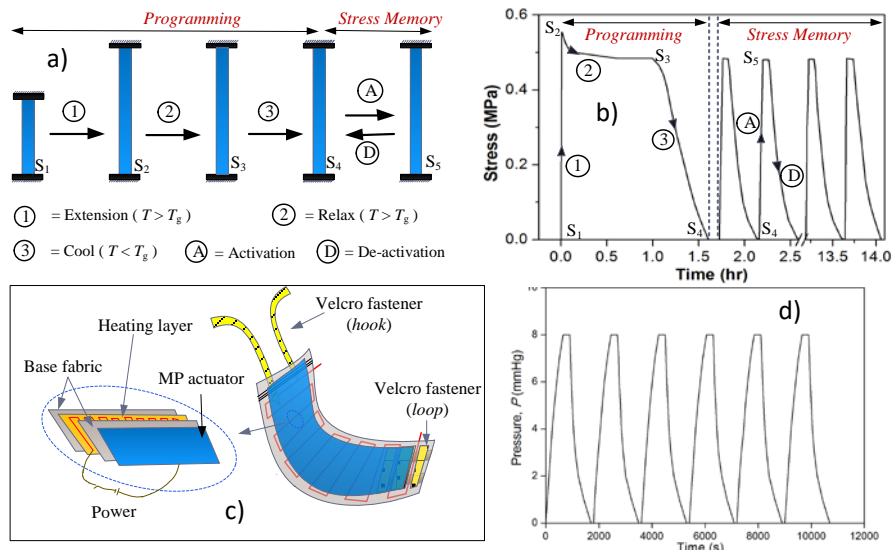


Figure 1: a) Stress memory programming method; b) Result of stress variation over time by controlling temperature; c) A bandage prototype; d) Result of dynamic pressure control

REFERENCES

1. Narayana, H., Hu, J., Kumar, B., Shang, S., Han, J., Liu, P., Lin, T., Ji, F.L., Zhu, Y. "Stress-memory polymeric filaments for advanced compression therapy." *Journal of Materials Chemistry B*, 5 (10), 2017: 1905-16.
2. Kumar, B., Hu, J., Pan, N., Narayana, H. "Investigation and designing of an orthopaedics device using stress memory actuator for smart compression." *Materials and Design*, 97, 2016: 222-29.
3. Kumar, B., Hu, J., Pan, N. "Smart medical stocking using memory polymer for chronic venous disorders." *Biomaterials*, 75, 2016: 174-81.

ACKNOWLEDGMENT

The author acknowledges the financial support received from the Department of Science & Technology (DST), India (Project Code: MI01567).

Development of Superhydrophobic Energy Harvesting Textile via Plasma Treatment of Poly(vinylidene fluoride) Nanoweb

Beomjun Ju¹, Changsang Yun², Chung Hee Park¹

¹Department of Textiles, Merchandising and Fashion Design, Seoul National University, Korea

²Department of Fashion Industry, Ewha Womans University, Korea

junghee@snu.ac.kr; zoon1405@snu.ac.kr

The wearable devices are shifting from accessory type to clothing type, and technologies for flexible battery are required for them. Since piezoelectric properties are easily damaged by the exposure to the liquids, it would be desirable for the piezoelectric textiles to have self-cleaning property by having superhydrophobic surface. Therefore, the purpose of this study is to develop superhydrophobic energy harvesting textiles prepared by poly(vinylidene fluoride)(PVDF) nanowebbs for wearable devices, and to suggest the optimum condition with respect to the piezoelectricity and surface hydrophobicity as well.

Electrospinning, plasma etching and water immersion were carried out to fabricate piezoelectric and superhydrophobic textiles for energy harvesting. The piezoelectricity and wettability were also analyzed by measuring the voltage output, water contact angle and water shedding angle. The chemical composition and crystallinity were also analyzed by XPS and XRD spectrum. Finally, to estimate the feasibility as a smart wearable system, the functional durability and breathability were examined.

Superhydrophobicity of PVDF nanoweb was successfully achieved by plasma etching and water immersion, showing water contact angle of 170° and water shedding angle of 4.7°. In addition, the superhydrophobic PVDF nanoweb exhibited excellent bouncing behavior of water droplets and repellency to various liquids as shown in Fig. 1 (a). Piezoelectric properties were enhanced after plasma etching and water immersion. The output voltage reached out 2.0V in PVDF film and 1.3V in electrospun PVDF nanoweb, but the newly developed superhydrophobic PVDF nanoweb showed improved piezoelectric performance as 1.5V as shown in Fig. 1 (b). Compared with the piezoelectric PVDF film, the superhydrophobic PVDF nanoweb showed much higher air permeability and water vapor transmission rate-which can be high potentials for smart clothing.

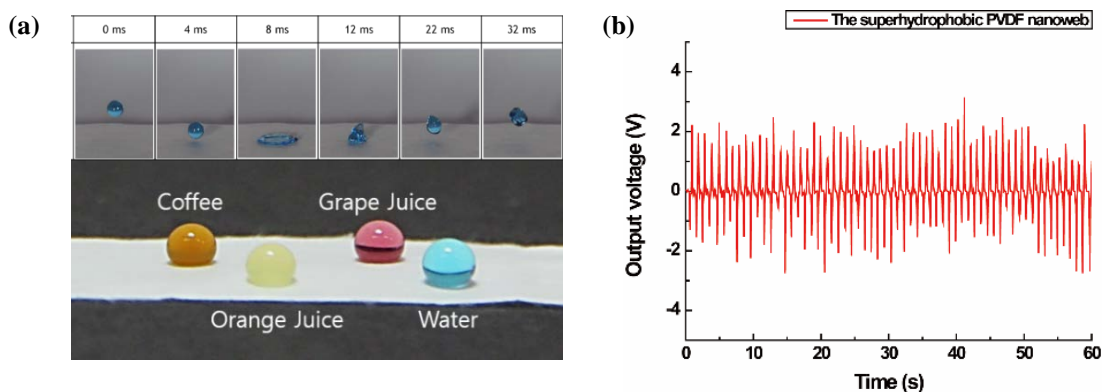


Fig. 1. (a) Bouncing behavior of water droplets and repellency to various liquids of the superhydrophobic PVDF nanoweb, (b) Output voltage results of the superhydrophobic PVDF nanoweb.

ACKNOWLEDGMENT

This work was supported by the National Research Foundation of Korea (NRF) grant funded by the Korea government (Ministry of Science and ICT) (No. 2016M3A7B4910940, No. 2015R1A2A2A03002760).

Mechanical and Electrical Properties of Graphene-coated Polyurethane Nanofiber Webs as a Strain Gauge

Eunji Jang, Eugene Lee, Gilsoo Cho

Department of Clothing and Textiles, Yonsei University, Seoul, South Korea

gscho@yonsei.ac.kr; j.eunji@yonsei.ac.kr

The objectives of this study are to (1) fabricate electronic textiles based on polyurethane nanofiber webs by graphene coating, (2) investigate the surface characteristics and evaluate tensile strength of the specimens, (3) measure the weight of the specimens before and after graphene coating to find out the amount of graphene on the polyurethane nanofiber webs, (4) measure the electrical resistance according to the graphene coating conditions and (5) observe the change of an electrical resistance value when the physical strain performed the specimen. The polyurethane nanofiber webs based electronic textiles were fabricated by coating process utilizing the aqueous dispersed non-oxidized graphene (2.0 wt%). The cross section polisher and the FE-SEM were used to analyze the surface difference of the specimens according to graphene coating. A tensile strength was evaluated using the universal material tester to examine the mechanical properties of the specimens before and after the graphene coating. The polyurethane nanofiber webs have partly irregularities in their structure due to their manufacturing process, hence three specimens were randomly selected and tensile properties were measured to obtain more objective data. An electronic balance was used to figure out the graphene contents, the weight of untreated polyurethane nanofiber webs and the graphene coated specimens were measured. The linear resistance was measured using a RCL meter in order to evaluate the electrical properties of the specimens. To verify potential of the graphene coated polyurethane nanofiber webs as a strain gauge, the process of stretching and recovering the specimens to 10% of its original length was repeated five times and the change in the electrical resistance value was observed. The results revealed that the graphene coated polyurethane nanofiber webs have a slight increase in electrical resistance by five repeated measurements, but no significant difference from the initial resistance value. This present work aimed to fabricate of electronic textiles based on polyurethane nanofiber webs by graphene coating and to evaluate of the mechanical properties and electrical performance to confirm that it is applicable to textile based strain sensor.

ACKNOWLEDGMENT

This research was supported by Basic Science Research Program through the National Research Foundation of Korea (NRF) funded by the Ministry of Education, Science and Technology (No. NRF-2016R1A2B4014668) and the Brain Korea 21 Plus Project of Dept. of Clothing and Textiles, Yonsei University in 2018.

Proton Conductive Polymer Nanofiber Framework: Fabrication and Application to Polymer Electrolyte Fuel Cells

Manabu Tanaka^{1,2}, Hiroyoshi Kawakami^{1,2}

¹Department of Applied Chemistry for Environment; ²Research Center for Hydrogen Energy-based Society (ReHES), Tokyo Metropolitan University, Tokyo, Japan

tanaka-manabu@tmu.ac.jp

Polymer electrolyte fuel cells (PEFCs) have attracted considerable attention because of their environmental friendliness and high energy conversion efficiency to realize the hydrogen energy-based society. Polymer electrolyte membrane (PEM) is one of the key components in PEFCs, and PEMs with higher-performances, including excellent proton conductivity, gas barrier property, and membrane stability, are desired for future PEFC application. Here we present our recent work on PEMs based on our proposed new concept “Nanofiber Framework (NfF).” Polymer nanofibers have been extensively studied because of their unique properties and wide applications. We have fabricated a series of proton conductive polymer nanofibers by an electrospinning method and revealed their distinguished proton conductive characteristics.^{1,2} Then, novel PEMs based on the proton conductive NfFs were prepared by combining these proton conductive nanofibers and polymer electrolytes, which filled void space among the nanofibers. For example, an NfF composite membrane composed of phytic acid-doped polybenzimidazole nanofibers and a typical PEM, Nafion[®], showed higher proton conductivity, lower gas permeability, and better membrane stability than the recast-Nafion membrane without nanofibers. The fuel cell performance by the NfF composite membrane, which enables ultra-thin membranes with their thickness less than 5 μm , was superior to that by the recast-Nafion membrane, especially at low relative humidity.³ Such NfF-based high-performance PEM will be accomplished not only by the acid-doped nanofibers but also by other proton conductive polymer nanofibers (e.g., sulfonated polyimide nanofibers).^{4,5} These ion conductive nanofibers have high potentials for applying novel materials in PEFCs and other energy-related applications.

REFERENCES

1. M. Tanaka. *Polymer Journal*, 48, 2016: 51-58.
2. R. Takemori, G. Ito, M. Tanaka, H. Kawakami. *RSC Advances*, 4, 2014: 20005-09.
3. M. Tanaka, Y. Takeda, T. Wakiya, Y. Wakamoto, K. Harigaya, T. Ito, T. Tarao, H. Kawakami. *Journal of Power Sources*, 342, 2017: 125-34.
4. T. Makinouchi, M. Tanaka, H. Kawakami. *Journal of Membrane Science*, 530, 2017: 65-72.
5. G. Ito, M. Tanaka, H. Kawakami. *Solid State Ionics*, 317C, 2018: 244-55.

ACKNOWLEDGMENT

This work is partially supported by a grant (No. P10001) from NEDO, a grant (Platform for Technology and Industry) from Tokyo Metropolitan Government, and JSPS KAKENHI (Grant Number 26410225)

Waterborne Fabrication of Fluoride-free, Magnetic, Superhydrophobic Fabrics

Sida Fu, Hua Zhou, Hongxia Wang, Tong Lin

Institute for Frontier Materials, Deakin University, Geelong, Australia

hong.wang@deakin.edu.au; sidaf@deakin.edu.au

INTRODUCTION

In recent decades, superhydrophobic surfaces have shown wide applications [1-3], and they can be fabricated by forming a nano-/microstructure with low surface energy on substrates. Most of the wet-chemical coating systems have to be prepared in organic solvents (e.g. ethanol, acetone, dimethylformamide, dichloromethane or tetrahydrofuran), which not only have high cost but also are impractical due to the potential safety and environmental issue. Apart from organic solvents, fluorinated chemicals, particularly for those containing perfluoroalkyls more than eight carbon-chain length, are widely concerned because of the potential bioaccumulation and high price [4-6]. Therefore, development of fluoride-free materials for superhydrophobic treatment is highly desirable.

Superhydrophobic porous materials with an oleophilic surface have potential applications in recovery of oil from water. When a superhydrophobic-oleophilic surface contacts with the oil polluted water, water is repelled, while oil spreads on the surface [7]. Recently, magnetic property was reported to combine with superhydrophobicity to be used in oil absorption. The introduction of magnetic responsiveness can simplify the recovery of the oil absorber as well as reduce the oil leakage from the absorber when collecting with mechanical equipment. However, limited report is available on how durable of the magnetic, superhydrophobic materials in oil recovery.

Herein, a magnetic superhydrophobic fabric was prepared using waterborne, fluorine-free coating solutions. The coating treatments are free of organic solvents and fluoride, hence environmentally friendly. The superhydrophobic and magnetic coating is durable enough to withstand at least 50 washing cycles and 500 Martindale abrasions cycles. In addition, the polydopamine (PDA) pre-coating plays a significant role in improving the adhesion of hydrophobic Fe_3O_4 nanoparticles on fabric. The coated fabric is superoleophilic with oil contact angle (CA) of 0° . The coated fabric can float naturally on the surface of oil polluted water, and it can be positioned to approach oil under magnetic actuation.

RESULTS AND DISCUSSION

In this study, durable superhydrophobic fabrics with magnetic property and oil absorption capability have been prepared through waterborne, fluoride-free coatings. As shown in Figure 1a, the fabric was pre-treated with a thin layer of PDA followed by applying hydrophobic Fe_3O_4 nanoparticles on the fabric surface. After coating with PDA/ Fe_3O_4 /HDTMS, a rough surface morphology was obtained (Figure 1b). The TEM image of fiber cross-section showed the thicknesses of PDA and HDTMS/ Fe_3O_4 coatings were about 80 nm and 20 nm, respectively (Figure 1c). The coated fabrics showed superhydrophobicity and superoleophilicity with water CA of 156° and oil CA of 0° (Figure 1d). The magnetic properties of the synthetic Fe_3O_4 nanoparticles were examined. Figure 1e shows the ZFC-FC curves of the Fe_3O_4 nanoparticles. The blocking temperature was 220 K. As shown in Figure 1f, a typical superparamagnetic characteristic curves with no hysteresis appearing after removal of the applied magnetic field. The saturation magnetization is 50.81 emu/g at 5 T and 300 K.

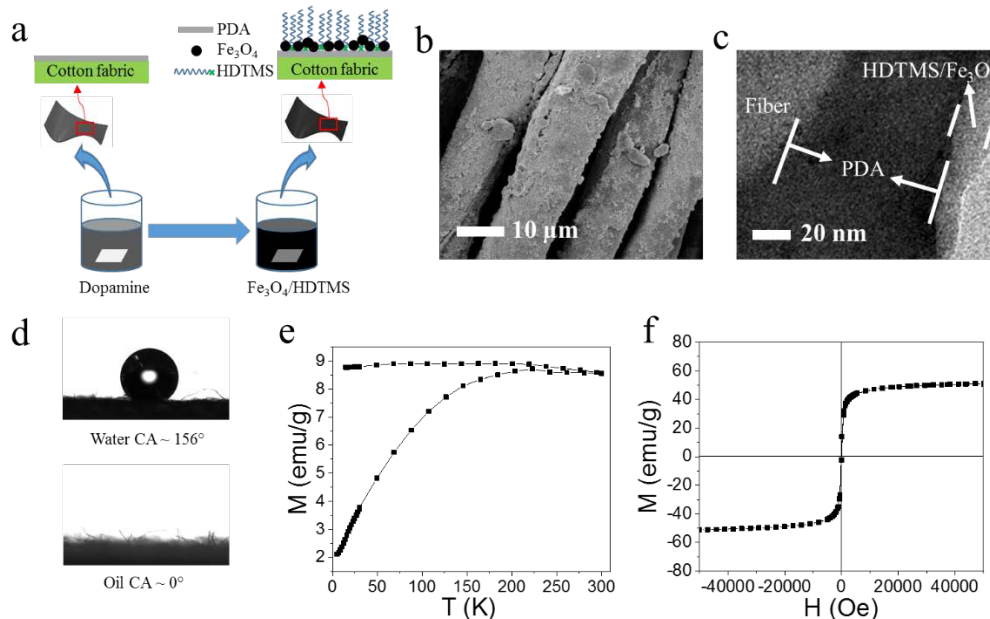


Figure 1. a) Schematic illustration of the preparation procedure for superhydrophobic magnetic cotton fabric; b) SEM image of PDA/Fe₃O₄/HDTMS coated cotton fibers; c) TEM image of cross-section of the coating thickness; d) Water CA and oil CA of the coated fabric; e) Zero field cooled-field cooled (ZFC-FC) curves measured with the field of 100 Oe; (f) Magnetization curve measured at 300 K.

Washing and abrasion durability were evaluated according to AATCC 61-2006 and ASTM D4966 standards. Figure 2a shows that the CA of the coated fabric decreased slightly with increasing the laundry cycles. After 50 washing cycles, the fabric still maintained superhydrophobicity. The CA is 152° and SA is 26°. After 100 cycles of washing, the fabric had a CA of 142°, and a SA of 39.4°. The abrasion durability was tested according to the Martindale method. As shown in Figure 2b, after 500 cycles of abrasion, CA only changed from 156° to 152°. Further increasing the abrasion cycles to 3000, CA decreased to 103°. To investigate the role of PDA in the surface coating, Fe₃O₄/HDTMS coating was applied on the fabric without pre-coating with PDA. Figure 2c&d show that the fabric lost the superhydrophobicity after 10 washing cycles and 100 abrasion cycles.

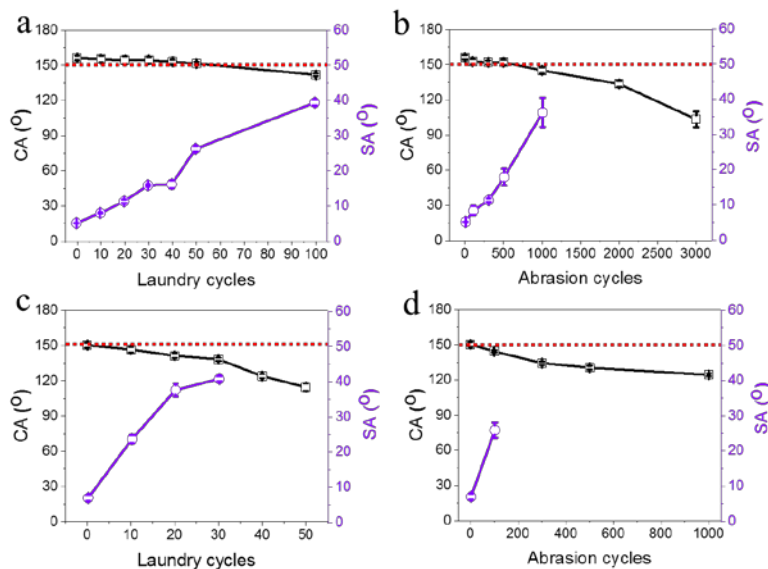


Figure 2. CA and SA of coated cotton fabrics change with a) laundry cycles and b) abrasion cycles. CA and SA of cotton fabrics without PDA coating change with c) laundry cycles and d) abrasion cycles.

Porous materials with a superhydrophobic and superoleophilic surface offer applications in recovery oil from water. When the materials were combined with magnetic property, they can be moved under magnetic actuation. As shown in Figure 3, a piece of our superhydrophobic fabric was used to recover hexadecane in water. Upon placing the coated fabric in water, the fabric naturally floated on water surface without sinking. The fabric can be moved to approach the oil contaminated area by a magnetic bar. Once hexadecane attached to the fabric, they were absorbed into the fabric matrix. Then the fabric can be picked up by the magnetic bar, and the water surface is almost clean.

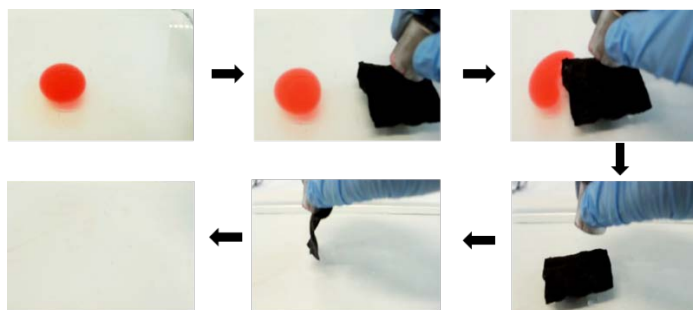


Figure 3. Recovery of hexadecane in water using superhydrophobic cotton fabric under magnetic field (hexadecane 1 ml, fabric 5 cm * 5 cm).

CONCLUSION

We have prepared a magnetic, superhydrophobic fabric using a two-step coating treatment. A thin layer of PDA was applied onto the fabric substrate, followed by applying hydrophobic Fe_3O_4 nanoparticles on the surface. The coated fabric showed a CA of 156° and a SA of 5° . The coated fabric was superoleophilic. This allows the coated fabric to be used in oil recovery. It was found that the presence of PDA pre-coating significantly enhanced the adhesion of hydrophobic Fe_3O_4 nanoparticles on fabric surface. In addition, the magnetic feature enables the coated fabric to approach oil under the actuation of a magnetic field. This magnet-responsive superhydrophobic fibrous material may be useful for oil recovery and water purification.

REFERENCES

- [1] T. T. Isimjan, T. Wang, S. Rohani. "A novel method to prepare superhydrophobic, UV resistance and anti-corrosion steel surface." *Chemical Engineering Journal*, 210, 2012: 182-87.
- [2] A. R. Siddiqui, R. Maurya, K. Balani. "Superhydrophobic self-floating carbon nanofiber coating for efficient gravity-directed oil/water separation." *Journal of Materials Chemistry A*, 2017.
- [3] B. Bhushan, Y. C. Jung. "Natural and biomimetic artificial surfaces for superhydrophobicity, self-cleaning, low adhesion, and drag reduction." *Progress in Materials Science*, 56, 2011: 1-108.
- [4] J. P. Giesy, K. Kannan. "Perfluorochemical surfactants in the environment." *ACS Publications*, 2002.
- [5] K. Kannan, L. Tao, E. Sinclair, S. D. Pastva, D. J. Jude, J. P. Giesy. "Perfluorinated compounds in aquatic organisms at various trophic levels in a Great Lakes food chain." *Archives of Environmental Contamination and Toxicology*, 48, 2005: 559-66.
- [6] N. Kudo, N. Bandai, E. Suzuki, M. Katakura, Y. Kawashima. "Induction by perfluorinated fatty acids with different carbon chain length of peroxisomal β -oxidation in the liver of rats." *Chemico-Biological Interactions*, 124, 2000: 119-32.
- [7] C. H. Lee, B. Tiwari, D. Zhang, Y. K. Yap. "Water purification: oil–water separation by nanotechnology and environmental concerns." *Environmental Science: Nano*, 2017: 514-25.

ACKNOWLEDGMENT

Funding support from Australian Research Council through a Discovery Project (DP150100406), Alfred Deakin Postdoctoral Fellowship (to H. Z), and Institute for Frontier Materials (IFM) Research Excellence Grants scheme 2018 is acknowledged.

Highly Air-permeable, Directional, Water-transport Cotton Fabrics

Hongxia Wang, Hua Zhou, Tong Lin

Institute for Frontier Materials, Deakin University, Geelong, Australia

hong.wang@deakin.edu.au

INTRODUCTION

Fabrics with directional water transport ability across the thickness have received much attention owing to the smart moisture management capability useful for sportswear, workwear, health/aged cares, and defense. Two main strategies have been developed to preparing directional water transport fabrics: (1) creating a hydrophobicity-to-hydrophilicity gradient through fabric thickness, and (2) combining a layer of hydrophobic fibers with a layer of hydrophilic fibers^[1-3].

Peoples tend to sweat heavily when doing intensive exercise, staying in high temperature environment, or under psychological stress. During these courses, proactively removal of moisture from body surface can eliminate wet feel and discomfort clicking, accelerate moisture evaporation and reduce surface temperature, which will not only improve wear comfort but also maintain the superior competitive competence. However, most of the directional water transport fabrics reported have a continuous hydrophilic fibrous layer. Once the hydrophilic layer is fully wetted, air permeability reduces largely due to pore blockage with liquid water. How to maintain high air permeability for wetted fabrics has little been reported.

In our recent study, we found that a cotton fabric after being treated by a two-step electro spray process shows directional water transport feature and stable air permeability to withstand fabric wetting. A commercial perfluoroalkyl acrylate was used as coating material. During the first step electro spray, a through-thickness superhydrophobic pattern array was formed on the cotton fabric. After another step of electro spray, directional water-transport property was introduced to the non-patterned areas. The existence of superhydrophobic pattern not only allows the fabric to maintain a high air-permeability, it also leads to 89% increase in one-way moisture transport index. When the fabric was fully wetted, it showed just 1.8% reduction in air permeability. Such a novel approach may be useful for development of next generation moisture management fabrics for various applications.

RESULTS AND DISCUSSION

Figure 1a illustrates the procedure for fabric treatment. A modified electro spraying setup consisting of a needle nozzle, an air jacket for accelerating spraying, a syringe pump, and a drum collector was employed. A piece of cotton fabric was mounted onto the drum collector. The cotton fabric has a superhydrophilic surface with water contact angle (WCA) 0°. During electro spraying, the nozzle atomized the coating solution into tiny liquid droplets which deposited on the cotton fabric because of the static attraction. A two-step electro spray was performed, to form a coating pattern in the first step and single side hydrophobic treatment in the second.

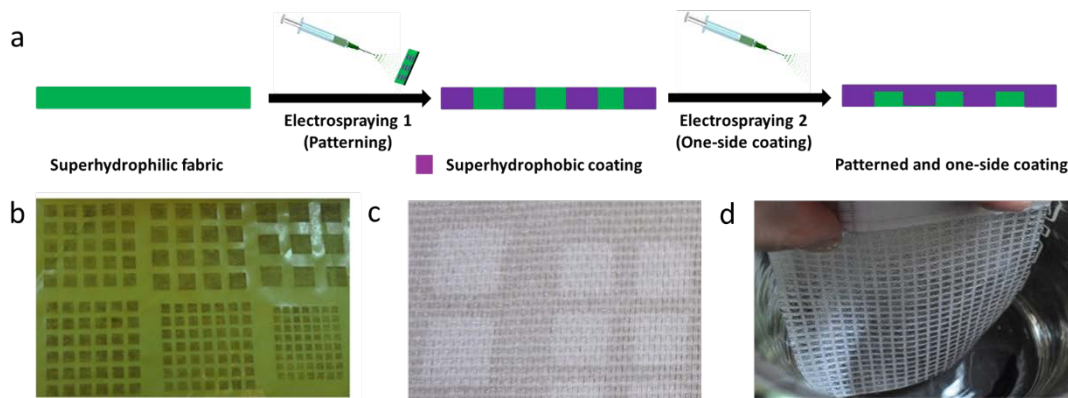


Figure 1. a) Illustration of procedure for electro spray treatment of cotton fabric, b) Screen mask with square patterns, c) patterned cotton fabric in wet state, d) patterned fabric in water (cotton fabric with 50% of superhydrophobic pattern).

To form a coating pattern on the fabric, a screening printing screen was employed as a shade mask. Figure 1b shows a photo of the screen mask with a square pattern array. During electrospraying, the screen mask was brought to cover the cotton fabric on the collector. Coating solution in the form of tiny droplets can reach the fabric only through the open areas, whereas the areas where a plastic film covered block liquid penetration. As a result, the coating solution deposited selectively on the cotton fabric forming a coating pattern. Cotton fabric is naturally hydrophilic with a contact angle of 0° . After electrospraying, the coated areas showed superhydrophobicity with a water contact angle as high as 165° . In contrast, the uncoated areas still kept the hydrophilicity.

In dry state, the fabric after pattern treatment showed the same appearance to the untreated one, because of the transparency of the coating. To observe coating pattern, the fabric was wetted with water and only the non-coated areas were wetted, showing a contrast to the patterned areas. Figure 1c shows a photo of the patterned cotton fabric in wet state. The non-wetted areas (i.e. coated) showed an exactly the same geometry to the open areas of the screen. To further observe the patterned fabric, we immersed the fabric in water. As expected, the patterned areas are still non-wettable showing a mirror surface because of the air bubbles trapped in the areas (Figure 1d).

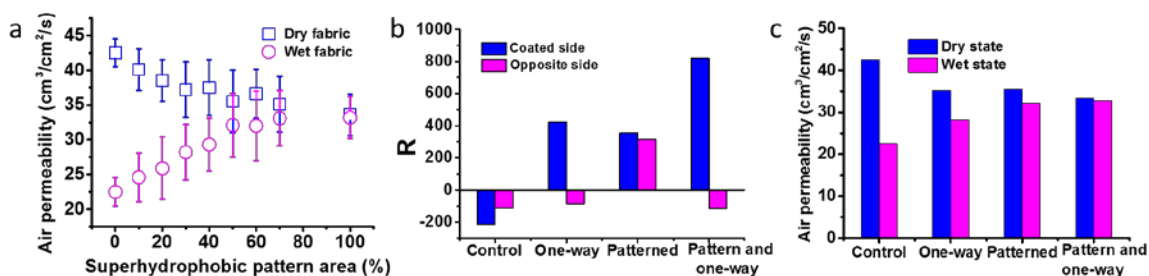


Figure 2. a) Effect of superhydrophobic pattern on air permeability in dry and wet states, b) accumulative one-way transport capacity index (R) of cotton fabrics, c) air permeability of control fabrics in dry and wet states.

Figure 2a shows the dependency of fabric air permeability on the superhydrophobic pattern area. The superhydrophobic pattern portion showed an effect on the air permeability of the fabric. At dry state, when the pattern portion increased from 0 to 50%, the air permeability showed a decrease from 42 to 36 cm³/cm²/s. Further increasing the portion from 50% to 100% led to a very small change in the air permeability. When the fabric was fully-wetted with water, the cotton fabric without non-wetting pattern showed a considerable decrease in air-permeability (to 22 cm³/cm²/s). As expected, the presence of non-wetting pattern maintained the air permeability at a higher value. When the pattern portion changed from 0 to 50%, the air-permeability of the fully-wetted fabric sample increased from 22 to 32 cm³/cm²/s. The little change in the air permeability when superhydrophobic portion increase from 50% to 100% is preassembly originated from the impermeable grid structure formed by wetted fabric area. The finer grid shows smaller resistance to air flow. The superhydrophobic pattern portion of 50% was optimal because fabric at such a patterning condition showed small difference in air permeability between dry (36 cm³/cm²/s) and fully-wetted state (32 cm³/cm²/s). Therefore, the superhydrophobic pattern portion of 50% was chosen for the further experiments.

The 50% patterned fabric was further treated by electrospraying a coating solution just on one side of the fabric. In our previous study^[4], we have elucidated that one side electrospraying of hydrophobic coating can make cotton fabric have different moisture management abilities, such as bidirectional water transport, directional water transport, and non-transport, depending on the treatment depth. In this study, we only controlled the coating to the depth (depth 34 μ m) that allowed the fabric to have a directional water transport property. Similarly, the second electrospray treatment showed little effect on fiber morphology and porous structure, except for the wettability of the non-patterned area on one fabric side.

MMT was used to measure the accumulative one-way transport capacity index (R) of the fabrics^[5, 6]. Figure 2b shows the measurement results. For the untreated cotton fabric, the R value is a negative around -214% to -110% on the two sides. For the cotton fabric with a superhydrophobic pattern (pattern portion 50%), the R value was around 300% and there was a very little difference between the two fabric sides. For the directional water transport fabric without pattern (i.e. just treated with one side electrospraying), the R values for the sprayed and

non-sprayed side were 422% and -85%, respectively. It was interesting to note that the fabric with superhydrophobic pattern (50%) and one-side spraying treatment had increased R value, over 800%, the 2nd sprayed side, where the opposite side had an R value of -115%.

A positive R value suggests that water can penetrate easily across the fabric and spread on the opposite side. The higher R value indicates more water being transported across the fabric, which is more favorable to remove sweat off the body surface and evaporate on the out layer surface. The negative R value indicates water accumulation on the feeding surface, creating wet feel to the wearer and slowing down moisture evaporation. Therefore, the higher R value suggests more comfort to wear.

In comparison with the one-side sprayed fabric (non-patterned) which also showed directional water transport ability, the one with both superhydrophobic pattern and one side spraying showed higher R value. This indicates that the superhydrophobic pattern facilitates directional water transport. This can be presumably explained by the enhanced capillary effect because of the superhydrophobic patterns, which confines water transport just in the non-coated hydrophilic matrix. The enhanced capillary effect was also observed on the patterned cotton fabric (without one side spraying treatment). Even if without one side electrospray treatment, the cotton fabric with superhydrophobic pattern showed much improved R value than the control fabric.

Figure 2c the effect of superhydrophobic pattern and one-side spraying treatment on air permeability of cotton fabrics. In dry state, the patterned and directional water transport fabric showed lower air-permeability compared with the control cotton fabric. In fully-wetted condition, all sprayed fabrics showed much higher air permeability than the control one. For the electrosprayed fabrics, the one with both one side spray and superhydrophobic pattern showed highest air permeability, followed by the superhydrophobically patterned and one side sprayed treated. The reason for the superhydrophobically patterned fabric showing higher air-permeability than the one-side electrosprayed fabric in wet state is because the through thickness non-wettable channels in the patterned areas which allow air penetration freely through the fabric. The superhydrophobic pattern and one side electrospray led to lower air permeability ($33.3 \text{ cm}^3/\text{cm}^2/\text{s}$) than other sprayed fabric, but the air permeability in the wetted state was $32.7 \text{ cm}^3/\text{cm}^2/\text{s}$, just 1.8% reduction. This can be presumably attributed to the one side electrosprayed areas are only partially wetted, having low flow resistance than the full-thickness wetted matrix.

CONCLUSION

We have demonstrated that cotton fabrics after a two-step electrospraying treatment can have a highly permeable directional water-transport function. The superhydrophobic patterns function to maintain high air permeability and meanwhile enhance the one-way transport capability. In comparison with the non-patterned directional water transport fabric, the one with superhydrophobic patterns has 1.89 times higher accumulative one-way transport capacity index, whereas the air-permeability at the fully wetted state was a very little decrease. Such a two-step electrospray may be useful for development of high performance moisture management textiles for various applications.

REFERENCES

- [1] J. Wu, N. Wang, L. Wang, H. Dong, Y. Zhao, L. Jiang. *Soft Matter.*, 8, 2012: 5996.
- [2] H. Wang, H. Zhou, H. Niu, J. Zhang, Y. Du, T. Lin. *Adv. Mater. Interfaces*, 2, 2015: 1400506.
- [3] H. Wang, J. Ding, L. Dai, X. Wang, T. Lin. *J. Mater. Chem.*, 20, 2010: 7938.
- [4] H. Wang, H. Wang, X. Wang, X. Wang, T. Lin, T. Lin. *J. Nanosci. Nanotechnol.*, 13, 2013: 839.
- [5] Y. Li, W. Xu, K. W. Yeung, Y.-l. Kwok. Google Patents, 2002.
- [6] L. Zhou, X. Feng, Y. Du, Y. Li. *Text. Res. J.*, 77, 2007: 951.

ACKNOWLEDGMENT

Funding support from Australian CRDC (Cotton Research Development Corporation) is acknowledged.

Melt Spinning of Novel, Luminescent, Polypropylene-shaped Fibers

Chureerat Praharn¹, Thanasat Sooksrimuang¹, Somboon Sahasithiwat¹, Nanjaporn Rongpaisan²,
Siriporn Kamtonwong¹, Waraporn Panchan¹, Wattana Klinsukhon¹, Natthaphop Suwannamek¹

¹National Metal and Materials Technology Center, Pathumthani, Thailand

²Rajamangala University of Technology Thanyaburi, Pathumthani, Thailand

chureerp@mtec.or.th

Many studies have been conducted on fabrication of various polymers/inorganic luminescent substances nanofiber web, using electrospinning. Very few, however, were conducted on organic luminescent substance/polymer nano-composite and its fiber formation *via* melt spinning. Organic photoluminescent substances, which contain molecular conjugation, can be activated by light and emit visible light. The characteristic of emitted light depends on the structure of molecule, and the substituents on the core molecule also play crucial role on its optical as well as thermal properties.

In this work, synthesis of novel organic luminescent substance (3,12-bis(dibutylamine)-7,8-dicyano-5,6,9,10-tetrahydrohelicene; M123), as well as fabrication of luminescent polypropylene (PP/M123) fibers having different cross-sectional shapes (circular, hollow triangular, flat, star, and W) *via* melt spinning were reported. The structure of M123 was specifically designed to contain 4 butyl groups in order to enable its homogeneous mixing with hydrophobic polypropylene matrix. Results from rheological measurement showed that melt viscosities of PP and PP/M123 at different shear rates (10-10,000 s⁻¹) were almost identical. This ensured that addition of M123 did not alter the PP melt flow through complex spinneret orifices during fiber spinning. In fiber spinning, the prepared PP/M123 resins were melt extruded through a 10-hole spinneret at spinning temperature 210°C, throughput 0.52 g/hole/min, and take up speeds of zero (free fall), 300, and 500 m/min. The quenching air temperature was 20°C, with flow speed of 0.38-0.4 m/s. Despite complex nozzle shapes, the PP/M123 fibers were continuously spun without fiber breakage, and possessed smooth surfaces. DSC characterization on PP/M123 fibers also confirmed homogeneity of M123 and PP matrix as the melting temperatures and crystallinities of PP/M123 fibers were comparable to those of PP fibers. This study demonstrated that, by employing organic luminescent M123, the processes of additive preparation and additive/polymer compounding were simplified, and a small amount of luminescent substance as 0.05% wt. could be used to yield effective luminescence. The PP/M123 fibers exhibited yellowish green color under normal light and emitted bright green light under ultraviolet (UV) light.

ACKNOWLEDGMENT

This work was supported by the National Metal and Materials Technology Center, National Science and Technology Development Agency (NSTDA), Thailand.

Clothing Pressure of Elastic Socks: Measurement and Prediction Calculation

Mari Inoue, Terumi Yoshida
Kobe University, Hyogo, Japan

inouema@kobe-u.ac.jp

In this study, we evaluated the clothing pressure of elastic socks. The purpose of this study is to be clear the effects of the tensile property of elastic socks and the compression property of the cylinder model on the clothing pressure. The clothing pressure was measured experimentally on the cylinders with different compression properties as the model body. As the results, it was found that the high coefficient correlation and the predicted ability.

MEASUREMENT OF CLOTHING PRESSURE AND THE PREDICTION CALCULATION

Clothing pressure of socks (knitted fabrics) was estimated by two methods in this study. At first, the pressure between the cylinder and the knitted fabric was measured by the air pack sensor, and it was the experimental pressure. Next, the pressure on the cylinder was predicted on the basis of the relationship between tensile property of knitted fabric and the curvature of the cylinder by using the equation reported by Kirk and Ibrahim.

Two kinds of knitted fabric for socks, which were termed as specimen S for standard socks and specimen E for elastic socks, were used as test specimen. Specimen S and E were composed of 100% nylon and 80% nylon/20% polyurethane, individually. The tensile properties of the knitted fabrics were tested by a biaxial tensile tester (Kato Tech Co.), in which strain speed was 0.4%/sec. In this measurement, sample was cut into strips, and test strip samples with 70mm x 70mm were prepared. The clothing pressure was calculated by the following equation:

$$P = F_1/R_1 + F_2/R_2 \quad \dots(1)$$

where R_1 and R_2 are radius of curvature along warp and course direction extended by the tensile loads of F_1 and F_2 , respectively. P is the pressure.

Experimental clothing pressure was measured by the air-packing method (AMI Co. Ltd.). Air volume of 1 ml was poured into an air pack with 20 mm diameter or an I-type air pack. The air pack was connected to a pressure transducer by a silicon tube. The output data were recorded through the amplifier and the values were adopted as the average by the measurements repeated more than three times. The air pack was attached on the surface of the cylinder or three types of mat stuck on the cylinder. The compression properties of the three types of mat (compression energy $WC(N/m^2)$; 0.172 (mat2), 0.476 (mat3), 1.385(mat4)) were used. Mat was used to imitate the different softness or stiffness of the human skin.

RESULTS AND DISCUSSION

The relationship between experimental pressure measured by I-type air pack and calculated pressure was shown in Fig. 1. It was found the high coefficient correlation and the predicted ability, and it was little difference between three types of mats. As the results, it was found the high coefficient correlation between experimental data and calculated though the calculated pressure was smaller than experimental pressure measured by both of air pack types. The pressure measured by circular air pack type was closer to calculated pressure than I types.

ACKNOWLEDGMENT

This study was supported by JSPS KAKENHI Grant Numbers 17H01954.

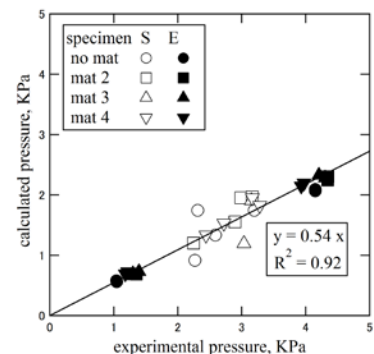


Fig. 1. Relationship between experimental and calculated pressure.

Syndiotactic Polystyrene Fibers with Nanoporous Crystalline Phases: An Efficient Material for Sorption of Volatile Organic Pollutants

Christophe Daniel, Gaetano Guerra

Dipartimento di Chimica e Biologia, Università Degli Studi di Salerno,
Via Giovanni Paolo II, Fisciano (SA), Italy

cdaniel@unisa.it

Syndiotactic polystyrene (s-PS) is a commercially available thermoplastic stereoregular polymer produced by Idemitsu (trade name of Xarec) presenting a very complex polymorphic behaviour. In particular it is capable to form two nanoporous crystalline phases named δ and ε which have been thoroughly described in literature. Both crystalline forms correspond to a packing of polymer chains in the helical $s(2/1)2$ conformation but the δ form is characterized by a monoclinic unit cell with empty space organized as isolated cavities with a maximum dimension of nearly 8.1 Å and a volume of c.a. 115 Å³ while the ε form has an orthorhombic unit cell with empty space organized as channels with a diameter of c.a 5 Å (see Figure 1).

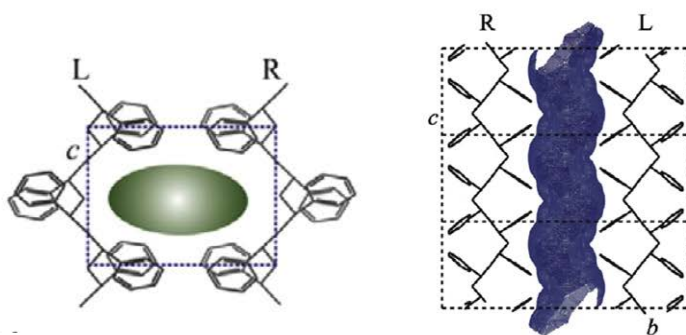


Figure 1. Lateral views of the s-PS monoclinic δ (left) and orthorhombic ε (right) nanoporous crystalline forms.

Both crystalline nanoporous frameworks rapidly absorb volatile organic molecules (VOCs), even if present in traces in air or water and hence are promising for applications in chemical separations and molecular sensorics. It is well established that the sorption capacity of VOC in nanoporous s-PS materials depends on the amount of nanopores and thus increases with the degree of crystallinity but it is nearly independent of the nature of the sample (film, powder, aerogel,...). However the VOC sorption kinetics strongly depends on the nature of the sample and for example films present a low sorption kinetics while fine powders are characterized by fast sorption kinetics.

In this contribution, it will be shown that s-PS nanoporous fibers with diameter between 3 and 20 μm obtained by standard melt processes such as melt spinning or melt blowing followed by solvent sorption-desorption treatment can be easily prepared. The influence of the solvent treatment and fiber diameter on the crystalline structure, morphology and sorption properties of the nanoporous fibers will be shown and discussed. In particular it will be shown that s-PS nanoporous fibers are characterized by high sorption capacity and fast sorption kinetics of VOC both from air and water.

The sorption properties, the manageable morphology as well as the simple preparation procedure which can be easily scaled up for large scale production make nanoporous s-PS fibers particularly suitable as filter sorption medium to remove traces of pollutants from water and moist air.

Optical and Mechanical Properties of PA/PET Blend Fibers for Artificial Hair with Different Major Components

Shunsuke Sato¹, Yuki Kato¹, Masatoshi Seki¹, Fumitaka Sugawara¹, Yutaka Shirakashi¹, Takeshi Kikutani²

¹Product Planning Development Department, Aderans Co., Ltd., Tokyo, Japan

²Department of Materials Science and Engineering, Tokyo Institute of Technology, Tokyo, Japan

shunsuke.sato@aderans.com

Polyamides and polyesters are generally used for preparing artificial hair for wigs of daily use. The artificial hair needs to exhibit gloss like human hair. For this purpose, various technologies have been developed to introduce roughness on the fiber surface. Recently, we have reported that the fibers with surface roughness can be produced by extruding a blend of polyamide 6 (PA6) and poly(ethylene terephthalate) (PET) with PET as a minor component at a temperature lower than the melting temperature of PET. Along with incorporating gloss like human hair, artificial hair needs to have sufficiently high mechanical properties. For this purpose, fibers need to be drawn to a certain level, however drawing leads to the deterioration of surface roughness.

With the aim of improving the mechanical properties of polyamide/polyester blend fibers for artificial hair, aromatic-aliphatic co-polyamide (MXD6) was also used as a polyamide component, and the melt spinning of fibers of the blends of PA6/PET, PA6/MXD6/PET and MXD6/PET were performed maintaining the PET composition at 20 %. The as-spun fibers were subjected to the in-line drawing process of various draw ratios to improve mechanical properties.

SEM photographs of the three types of drawn fibers prepared from the as-spun fibers obtained with the extrusion temperature of 240 °C are shown in Fig.1. It can be seen that the degree of surface roughness was improved with the increase of MXD6 composition from 0 to 80 %. Tensile properties of the prepared fibers are shown in Fig.2. The fibers with MXD6 as the major component showed the highest tensile modulus, whereas the fibers with PA6 as the major component exhibited the highest tenacity and knot strength. The fibers with the blend of PA6/MXD6 as the polyamide component showed the lowest mechanical properties. These results suggested the possibility of improving both surface roughness and mechanical properties by introducing MXD6 as the polyamide component.

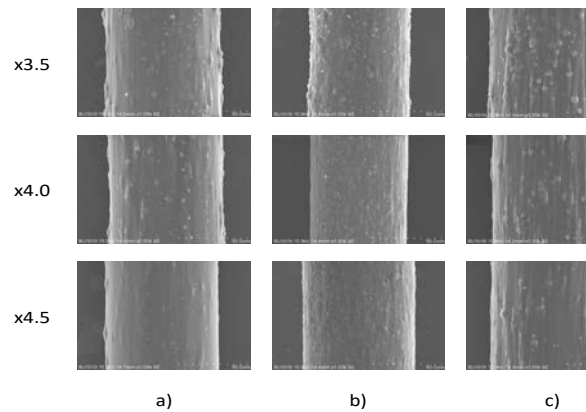


Fig. 1. Scanning electron micrographs of fibers of PA6/PET, PA6/MXD6/PET and MXD6/PET. Extrusion temperature was 240°C. a) PA6/PET = 80/20; b) PA6/MXD6/PET = 40/40/20; c) MXD6/PET = 80/20.

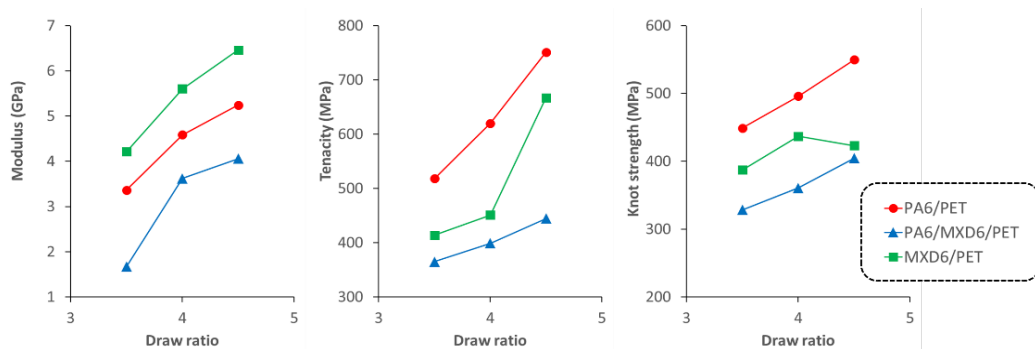


Fig.2. Tensile properties of the drawn fibers prepared from as-spun fibers obtained with the extrusion temperature 240°C.

Improvement of Aerosol Oil-mist Filtration Performance Through Superoleophobic Treatment of Fibrous Filters

Xin Wei, Hua Zhou, Tong Lin, Hongxia Wang

Institute for Frontier Materials, Deakin University, Geelong, Australia

hong.wang@deakin.edu.au; ubi@deakin.edu.au

INTRODUCTION

Aerosol oil-mists are formed by various mechanisms including lubrication, thermal, vibration, friction, rotation and high-speed gas transmission.^[1] They can cause serious issues, for instance, corrosion, erosion, wear, leakage, clogging, contamination in machinery and extra energy consumption.^[2] Elimination of oil mists from air or particular gas is a prerequisite process for a number of application areas including aerospace, automotive, engineering and manufacturing, electronics, food and beverage, medical, mining, pharmaceuticals, energy generation, everyday life and many more.^[3]

Fibrous materials are predominately used for making oil-mist filters owing to the small pore size, 3D surface texture, good flexibility, large surface area, ease of functionalization, and mass production capability. Besides filter material, fibrous structure and drainage layer, surface property shows great influences on oil mist filtration performance according to different droplet capture mechanisms. However, existing studies were all focused on filters with ordinary wettability, such as oleophobicity and oleophilicity.^[4-5] Since recent papers demonstrated that super non-wettable surfaces with have largely different oil repellency to ordinary non-wettable surface, superoleophobicity has attract significant attention both in research and industry. Superoleophobicity is referred to surfaces with a contact angle greater than 150° for oils.^[6] However, the effect of superoleophobicity on aerosol mist filtration properties of fibrous filters has not been reported in research literature.

In our recent study, we found that when a durable superoleophobic filter was achieved by dip coating the glass fiber nonwoven substrate in perfluoroalkyl acrylic copolymer (PFAP) water solution, the filtration performance was largely enhanced. The coated filter showed a significantly increased filtration efficiency and quality factor for small oil-mists, but the pressure drop only had a very little increase, benefit from the “bounce-collide-drain” mechanism of superoleophobic surfaces.

APPROACH

A commercial glass-fiber nonwoven filter material was used as a model. A perfluoroalkyl acrylic copolymer (PFAP) water solution (5 wt.%) was applied onto the fibrous filter through a dip-coating method followed with curing process at 150° for 1 hour. The filters were tested under a purposed built apparatus use di-ethyl-hexyl-sebacate (DEHS) to generate aerosol oil mists. The air flux was stabilized at 127.2 L/min and driven by a vacuum pump. Both filtration performance for small (0.01 – 0.8 μm) and large (0.5 – 20 μm) oil mists were collected at pseudo-steady state.

RESULTS AND DISCUSSIONS

Figure 1a illustrates the coating procedure of achieving superoleophobic surfaces based on glass fiber nonwoven mats. As shown in Figure 1b, after coating treatment, the orange-dyed olive oil (10 μl) shown spherical shapes with contact angle (CA) of 159° on treated glass fiber nonwovens. A series of oil fluids with different surface tension values was used to examine the dependency of CA on surface tension (Figure 1c). It is clearly indicated that the coated fabric has a CA greater than 150° to the liquid with a surface tension above 32 mN/m. This treated fibrous filter shows not only superoleophobicity but also superhydrophobicity, a typical characteristic of superamphiphobicity. The wettability of untreated (marked as “control” in figures) glass fiber nonwoven was also examined. It had an oil CA of 32.8°, and oil droplet could stay on fabric surface for about 5 seconds. Figure 1d shows the SEM images of the fibrous filter before and after coating treatment. The glass fibers orientated randomly in the fibrous structure. After coating treatment, the fibers looked very similar to the uncoated ones with a uniform coating layer.

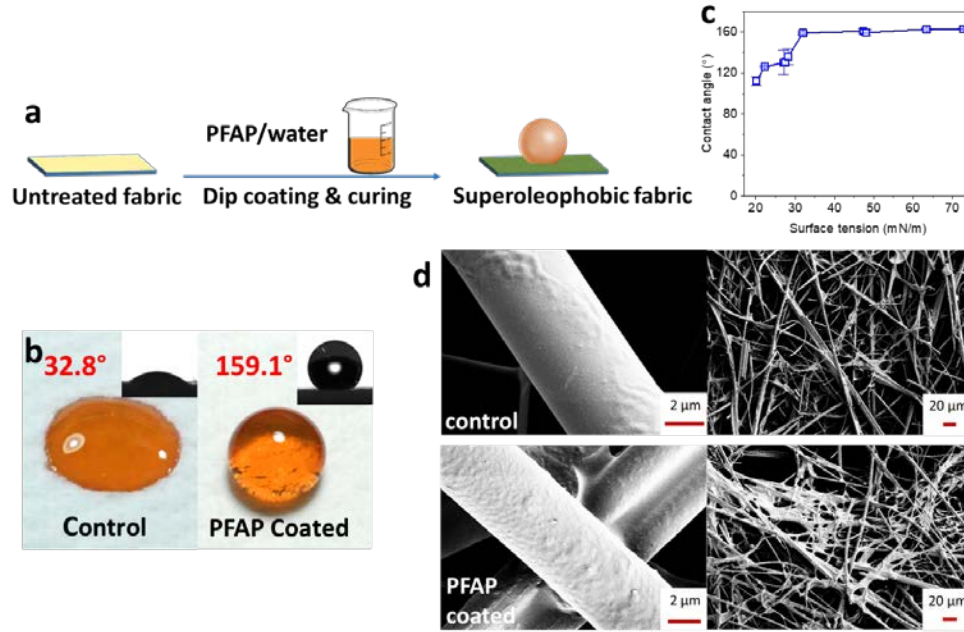


Figure 1. (a) Illustration of the procedure of superoleophobic treatment of fibrous filters. (b) Photo of oil droplets (orange-dyed olive oil) on untreated and PFAP treated fibrous filters. (c) Effect of liquid surface tension on the contact angle of the PFAP treated fibrous filter. (d) SEM images of untreated and PFAP treated fibrous filters.

Both single and multilayer fibrous filters were tested to study the influences of surface wettability and filter thickness on filtration performance (Figure 2). This equipment has been stated to have high accuracy and sufficient reliability for aerosol mist filtration test. Figure 2a shows the dependency of pressure drop on filter thickness. The superoleophobic filter showed a pressure drop of 7.3 kPa, which is slightly higher when compared to the untreated filter (6.9 kPa). A linear relationship between pressure drop and filter thicknesses was observed, which is similar to the trend on the uncoated filter. Furthermore, there is an attractive finding that the superoleophobic filter with a thickness of 1.12 mm had a pressure drop of 8.3 kPa, which is much lower than that of the untreated fibrous filter with a thickness of 2.80 mm (10.1 kPa). The lower pressure drop indicates lower air flow resistance, therefore lower energy cost for gas transport.

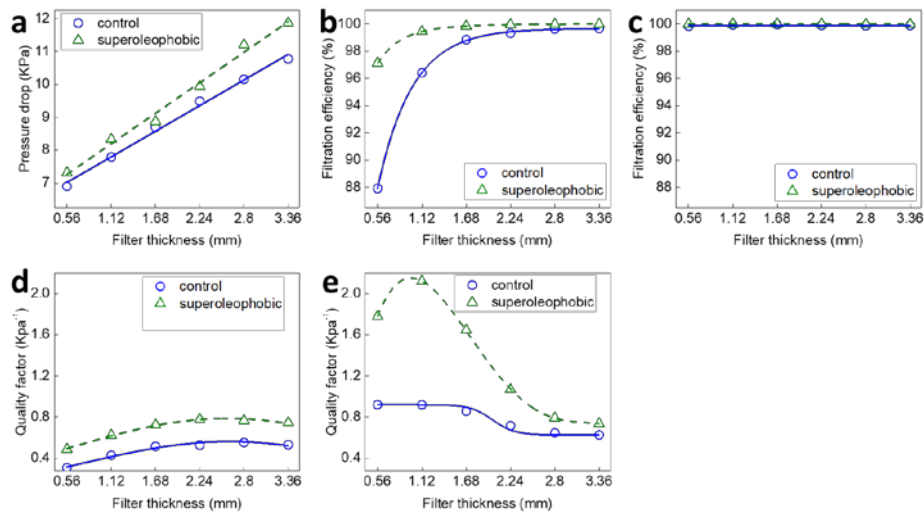


Figure 2. (a) Effect of surface wettability on the pressure drop of fibrous filters. (b-c) Effect of filter thickness on the filtration efficiency of fibrous filters for (b) small oil mists (size 0.01–0.8 mm) and (c) large oil mists (size 0.5–20 mm). (d-e) Effect of filter thickness on the quality factor of fibrous filters for the filtration of (d) small oil mists and (e) large oil mists.

In figure 2b&c, for the PFAP treated single layer filter, the filtration efficiency for small oil mists was as high as 97.12%, increased by 10% when compared to the untreated fibrous filter (87.91%) of the same thickness. This cannot be achieved by untreated filter even if the thickness is 2.5 times thicker. When the filter thickness was 1.12 mm, the efficiency for large oil mists reached almost 100%. Quality factor is applied to evaluate the filtration performance in combination of efficiency and pressure drop. The superoleophobic filter at thickness 2.24 mm showed the highest quality factor for small mists (0.777 kPa^{-1}), about 1.5 times greater than the untreated ones. When using superoleophobic filter for large oil mists, the maximum quality factor (2.120 kPa^{-1}) appear at the thickness of 1.12 mm, which is twofold higher than the untreated one. With further increasing the filter thickness, a little increase on filtration efficiency and negative effect on quality factor for large oil mists occurred. These results revealed that superoleophobic filter at 1.12 mm thickness has the best filtration property.

The mechanism for improvement of oil mist filtration by superoleophobic coating was proposed in Figure 3a&b based on the experimental results. When oil mists pass through a fibrous filter, oil mist attachment is affected by fiber surface wettability. Oil droplets tend to spread along oleophilic fibers and accumulate in the intersection region. After that, the collected oils move through the matrix barrier driven by the forces of gravity and airflow. As shown in figure 3a, they finally dispose off the filter through two main routes: draining away from in the desired paths, or re-entraining in downstream flow and results in reduction of efficiency. In our study, filters with superoleophobicity have high repellency to oil. As small oil mists reach the filter surface at a certain speed, they are easily bounce back and force like elastic balls. During this stage, small mists may collide with each other or the later arriving ones and become larger, until they are too heavy to bounce. Lastly, the large droplets will leave the fiber along the direction with minimized energy. Therefore, superoleophobic filters show large improvement in filtration performance. Therefore, superoleophobicity shows a significant effect on oil mist attachment, accumulation, transport, and disposal of fibrous filters.

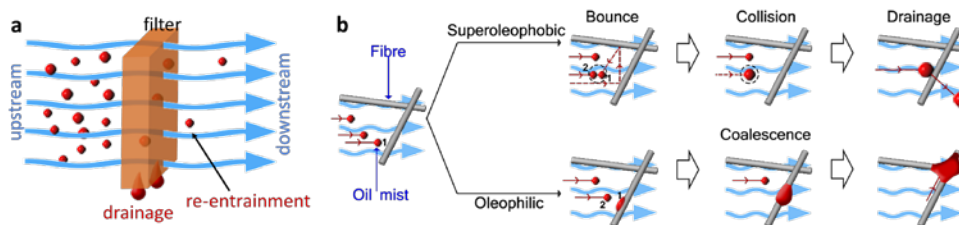


Figure 3. (a) Oil disposal routes during oil mist filtration. (b) Schematic illustration of oil mist interaction with fibres with different surface wettabilities.

CONCLUSION

We have shown that superoleophobic treatment of fibrous filters can greatly improve the filtration performance for small oil mists. A 1.12 mm thickness superoleophobic filter can reach a filtration efficiency of 99.4% for small oil mists, with only 6% higher pressure drop when compared to the untreated filter of the same thickness. For large oil mists, the quality factor was twofold higher than that of the untreated control filters. The superoleophobic filter has almost 100% filtration efficiency. A “bounce-collide-drain” mechanism was proposed to explain the improvement of the filtration performance. Such a novel concept may have great significance in development of high efficiency, low energy consumption gas-liquid coalescing filters.

REFERENCES

- [1] R. Mead-Hunter, A. J. C. King, B. J. Mullins. *Sep. Purif. Technol.*, 133, 2014: 484.
- [2] M. Wilcox, R. Kurz, K. Brun. *Int. J. Rotating Mach.*, 2012: 254.
- [3] K. R. Spurny. *Advances in Aerosol Gas Filtration*. Taylor & Francis, 1998.
- [4] T. P. Liew, J. R. Conder. *J. Aerosol Sci.*, 16, 1985: 497.
- [5] B. J. Mullins, R. Mead-Hunter, R. N. Pitta, G. Kasper, W. Heikamp. *AIChE J.*, 60, 2014: 2976.
- [6] H. Zhou, Y. Zhao, H. Wang, T. Lin. *Adv. Mater. Interfaces*, 3, 2016: 1600402.

ACKNOWLEDGMENT

Funding support from Australian Research Council through a Discovery Project (DP150100406), Alfred Deakin Postdoctoral Fellowship (to H. Z), and Institute for Frontier Materials (IFM) Research Excellence Grants scheme 2018 is acknowledged.

Anti-Tuberculosis Nanofibrous Membrane

Nakarin Subjalearndee, Chutima Vanichvattanadecha, Autchara Pangon, [Varol Intasanta](#)

Nano Functional Textile Laboratory, National Nanotechnology Center, National Science and Technology Development Agency, Klong Nueng, Klong Luang, Pathumthani, Thailand

varol@nanotec.or.th

Recurrence of TB endemic, the ubiquitous presence of MDR-TB (Multi-drug resistance tuberculosis) and the failure of recent TB vaccine clinical trials pose threats towards global public health and long-term social welfare. TB bacteria can be suspended in air or transmitted via respiratory aerosol, while conventional air filtration technologies rely heavily on micron-sized physical filtering of airborne particles, which are quite ineffective with respect to bacteria such as TB because of their relatively small sizes and thick cell walls. Even though fine filtration of HEPA filter could lead to effective blocking of small particles and bacteria, the device has no antibacterial functions. As a consequence, trapped bacteria stay alive, proliferate and eventually make the device harmful due to the densely accumulated colonies. We present a novel approach to counteract the spread of airborne tuberculosis bacteria by means of nanofiltration. Syntheses and characterizations of multifunctional nanofibers and nanofibrous membranes for antibacterial applications are presented. First, water-based multicomponent solutions containing polymer, UV resistant, antibacterial and water repellent agent are prepared and electrospun into nanofibers by nanospider machine. The unique interplay among the functional components leads to mechanically-robust, flexible and water-resistant nanofibrous membranes with flow-through capacity and size-selectivity toward TB. Three aspects of TB resistance are demonstrated: contact mode, water-based and flow-through mode as well as air-borne flow-through mode. Firstly, the contact between fluid-based TB suspension and the nanomembrane leads to clear zone on the surface of the nanomembrane as evident by a confocal laser scanning microscope and Live/Dead staining kit. Secondly, in the water-based, flow-through system, TB cells are physically blocked and killed by the miniscule pores of the potent antibacterial nanofibrous membranes. Thirdly, the membrane is assembled into a portable air filter that shows tuberculosis killing efficiency of more than 90-99% during pilot scale TB-suspended aerosol filtration in a biosafety cabinet level 3. Finally, we consider how this technological platform could further inspire other advanced developments of mechanically-robust and multifunctional nanomembranes.

KEYWORDS: Nanofibrous membrane, nanospider, antibacterial, tuberculosis, multifunction.

Multifunctional Liquid-core Fibers

Rudolf Hufenus, Sabyasachi Gaan

Empa, Swiss Federal Laboratories for Materials Science and Technology, Switzerland

rudolf.hufenus@empa.ch

In this talk we will present the continuous production of liquid-filled polymeric fibers via a stable melt-spinning process at the pilot plant scale. The ability to produce a continuous liquid-core fiber is attractive since post-filling of a hollow fiber with similar dimensions is not practical. As nonlinear and elastic flow properties of polymer melts would lead to flow instabilities in co-extrusion of a molten polymer and a liquid core, a special spin pack was designed that enables the stable melt-spinning of a bicomponent fiber with a liquid core. The polymer is supplied from extruder and gear pump, while the fluid forming the core is injected by a high-pressure liquid pump. A suitable liquid for the core has to meet several elementary requirements: It must exhibit high thermal stability, reasonable viscosity, and relatively low vapor pressure at the processing temperature of the polymer sheath to prevent exit spraying. In addition, it should not be corrosive to the extrusion equipment, and the liquid must not act as solvent for the polymer component.

With this novel technique, we could spin polymeric fibers with up to 15% of liquid core comprising of a thermally stable flame retardant. Incorporating flame retardants directly to the polymer matrix only allows for far less amounts (< 5%) to avoid impairing spinnability and mechanical properties of melt-spun fibers. Such a high loading via incorporation in the fiber core not only yields flame retardant fibers, but also provides flame-protection to surrounding material without compromising the structural integrity of a textile or fiber composite material. In addition, we could further functionalize the liquid core of the fiber with essential oils to produce fragrant melt-spun fibers. We could show that the fragrances, injected as liquid cores, survived the severe melt-spinning conditions, and that the fragrant molecules could diffuse through the polymeric sheath to reveal the fragrance. Here, the liquid core can play the role of a reservoir for the essence, providing a long-term performance.

Irradiated Hydrogel Fibers Responsive to Moisture

Jiachuan Hua, Wai Yi Cheung, Pui Fai Ng, Bin Fei

Institute of Textiles & Clothing, Hong Kong Polytechnic University, Hong Kong, China

tcfuib@polyu.edu.hk

Tough hydrogel fibers have potential applications in biomedical textiles. A few absorbent fibers have been manufactured and commercialized, such as Oasis and Lanseal-F. However, their applications are very limited due to their poor toughness in wet state. They cannot sustain fiber continuity under stress and stretch. In recent years, some novel hydrogels have been reported with high stretch over 20 times. Using a flexible “double network” model, we succeeded in creating highly stretchable hydrogels composed of polysaccharides and polyacrylamide, and further processed them into shape memory and moisture-responsive fibers. However, the thermal induction of radical polymerization process is not suitable for large scale continuous production. In order to make the manufacturing process more practical, we tried to incorporate radiation crosslinking technique into the manufacturing of hydrogel fibers.

Starting with existing polymers, polyacrylamide (PAM) and iota-carrageenan (IC), weak hydrogel fibers (WHFs) were obtained through a wet spinning process. In such WHFs, IC was physically crosslinked while PAM chains randomly entangled together as discrete chains. These WHFs were led through an electron beam to achieve chemical crosslink between PAM chains. Thus obtained hydrogel fibers presented obviously improved strength in both stretch and compression, and resistance to dissolution in water (Figure 1).

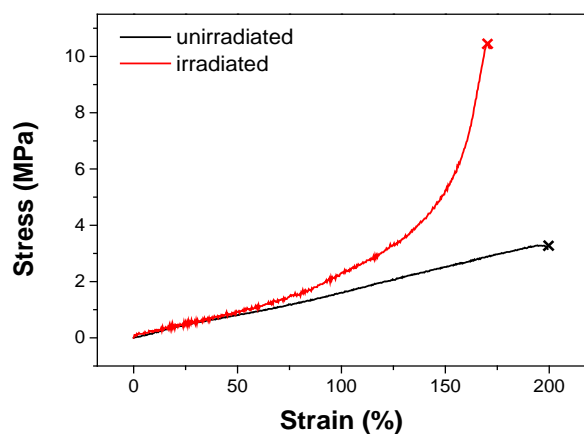


Figure 1. Tensile curves of original and EB irradiated (20 KGy) DR2 hydrogel fibers.

The irradiated hydrogel fibers were posted stretched by 100% and dried in air, then exposed to moisture or water to observe their recovery and water absorption process. In both types of media, the dry fibers were able to absorb water times of their own weight and return to their original length in limited time. In comparison, the water absorption and shape recovery in liquid media was much faster than those in humid air (by hundreds times).

KEYWORDS: Hydrogel fiber, irradiation crosslink, shape recovery.

ACKNOWLEDGMENT

We sincerely acknowledge the financial supports of NSFC fund 51373146.

Preparation and Thermo-responsive Properties of Temperature-Sensitive-Gel(TSG)/Polymer Functional Films

Jin Gong^{1,2}, Eiichi Hosaka², Hiroshi Ito²,
Yoshikazu Shibata³, Dai Nakanishi³, Shin-ichiro Ishihara³

¹Department of Mechanical Systems Engineering, Graduate School of Science and Engineering, Yamagata University, Yamagata, Japan

²Department of Polymer Science & Engineering, Graduate School of Organic Materials Science, Yamagata University, Yamagata, Japan

³KOHJIN Film & Chemicals Co., Ltd., Kumamoto, Japan

jingong@yz.yamagata-u.ac.jp; ihiroshi@yz.yamagata-u.ac.jp

Temperature sensitive gels (TSGs) exhibit physical changes in response to changes in temperature. Many kinds of TSGs were developed currently in our group, and all these TSGs show high crystallinity. TSGs also have good strength and toughness. TSGs are expected to use in many fields such as medical, robotics, MEMS and also in daily life^[1, 2]. TSGs change their modulus at transfer temperature^[3, 4]. In this paper, we report a new TSG having a lower transfer temperature at around 60°C to open up boarder-application possibilities of TSGs as functional filler for developing new functional films.

Functional films are widely used in fields such as food packaging, electronics, energy sector and daily necessities. There has been a growing demand for functional films recently. TSG sheets are synthesized from monomers with vinyl group through bulk photopolymeriazation, then ground into fine particles mechanically. The picture of obtained TSG particles is shown in Figure 1. The size of TSG particles is less than 300µm, and their mean size is nearly 100µm from the SEM image. TSG particles and calcium carbonate (CaCO₃) are added as functional fillers into polymer as Linear Low Density Polyethylene (LLDPE) using a twin-screw extruder. Then the obtained TSG/LLDPE/CaCO₃ composites were molded into films with hot press machine, and the new air and moisture permeable TSG/LLDPE/CaCO₃ membrane is prepared (Figure 2.). In this paper, we discuss the preparation of TSG/LLDPE/CaCO₃ functional films, and report the characterization of their thermal, mechanical and thermo-responsive properties.



Figure 1. TSG particles prepared by freeze-grinding.



Figure 2. Thermo-responsive TSG/LLDPE/CaCO₃ film.

REFERENCES

1. S. R. Sershen, S. L. Westcott, N. J. Halas, J. L. West. *J. Biomed. Mater. Res. Part A*, 51(3), 2000: 293-98.
2. Y. M. Kwon, S. W. Kim. "Thermosensitive Biodegradable Hydrogels for the Delivery of Therapeutic Agents." *Drugs and the Pharmaceutical Sciences*, G. S. Kwon, Ed. Boca Raton, FL: Taylor & Francis Group, 2005, 251-74.
3. J. Gong, H. Furukawa. *Expected Materials for the Future*, 13(1), 2003: 5-7.
4. S. Harada, R. Hidema, J. Gong, H. Furukawa. *Chemistry Letters*, 41, 2012: 1047-49.

Fundamentals of Fiber and Textile Science, Testing, and Characterization

Quantitative Evaluation of Odour Retention on Different Fibre Types

Jinfeng Wang, Xi Lu, Jing Wang, Xungai Wang

Deakin University, Institute for Frontier Materials, Geelong, Australia

xungai.wang@deakin.edu.au

We have successfully developed a novel odour detection system, which enables us to quantitatively evaluate the odour retention performance of different fibre samples. The new odour detection system can provide real time detection of odour adsorption in, and the subsequent odour emission from, a wide range of fibre or textile samples.

Three commonly used fibre types, polyester, cotton and wool, were selected in this study. The dynamic odour absorption by the selective fibres was monitored with our odour detection system. As shown in Figure 1, fibres gradually absorbed odour NH_3 and reached its absorption saturation after 80 min. The selected fibres showed great difference in their odour absorption capacity, with wool adsorbing the most odour NH_3 (93.7%). This is followed by cotton adsorbing 78.6% and polyester adsorbing the least, which was 57.1%.

After reaching their adsorption saturation, the odour emission or desorption from these fibres was also investigated. It was found that the emitted odour intensity from the saturated fibres followed the order of polyester>cotton>wool. We believe that wool's high odour adsorption but low emission makes it suitable for fibre based body odour management in active sportswear. The current most common method to control body odour is to apply biocides to impart antimicrobial properties on the fibres and fabrics, which may alter a person's natural microflora.

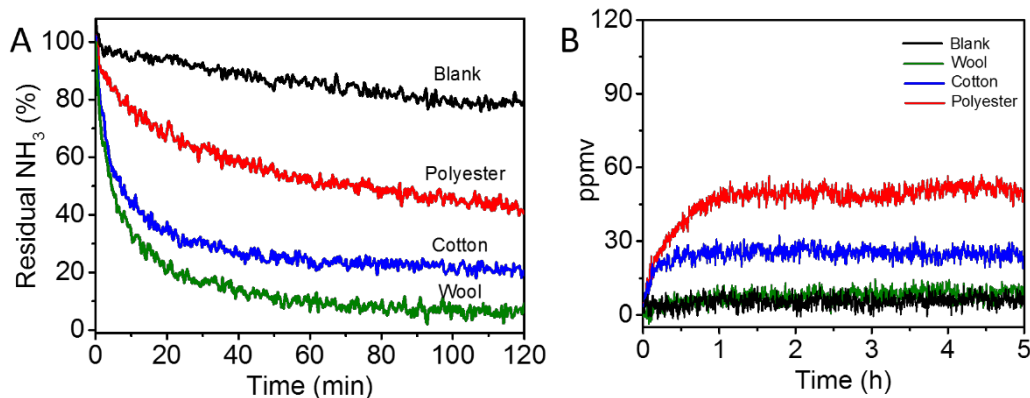


Figure 1. Time-dependent NH_3 adsorption by different fibre types (A); time-dependent gas desorption from different fibre types (B).

This study will facilitate the understanding of the relationship between textiles and body odour, especially with respect to the risk to public health from emerging antibiotic-resistant bacterial strains linked to the increased use of antibacterial and antibiotic products. It is also important to be able to control body odour through methods that do not alter a person's natural microflora.

Surface Functional Textile for Healthcare Application with Rechargeable Antibacterial Activity

Zhentan Lu, Qinwen Yuan, Dong Wang

Hubei Key Laboratory of Advanced Textile Materials & Application, College of Materials Science and Engineering, Wuhan Textile University, Wuhan, China

luzhentan@wtu.edu.cn

Nosocomial cross infection (NCI) is a great threat to human health, and caused enormous waste. However, hospitals environment were not too clean to block NCI. Textiles were necessities in hospitals, and healthcare textiles could become the reservoirs of pathogens.^[1] NCI could be aggravated by pathogens soiled healthcare textiles.^[2] It is urgent need to develop new healthcare textiles with high and rechargeable antibacterial activity.

In our work, we prepared surface modified textiles to create a clean hospital environment by surface graft polymerization or chelating adsorption.^[3] The textiles showed excellent antibacterial activity, and the property could be recharged easily. And, the textile had a high filtration rate against bacteria. Excellent antibacterial activity and high filtration rate making the textile could protect the users from direct and indirect contact with pathogenic, prevent the diseases spread with the help of textiles.

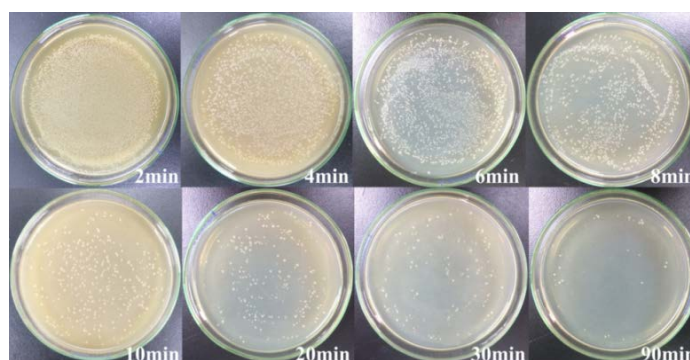


Figure 1. Antibacterial activity of the surface modified textile against *E. coli* at different times.^[3]

REFERENCES

1. K. B. JaHyun, E. S. Emily, M. B. R. Vickie, *Am. J. Infect. Control*, 40, 2012: 416.
2. A. Mitchell, M. Spencer, C. Edmiston, Jr. *J. Hosp. Infect.*, 90, 2015: 285-92.
3. Q. Yuan, Z. Lu, J. Zhang, Y. Chen, K. Liu, Y. Wang, W. Wang, Q. Liu, D. Wang. *New J. Chem.*, 2018, 0.1039/C7NJ04563H.

ACKNOWLEDGMENT

This work was supported by the National Natural Science Foundation of China (51703169, 51603154, 51503160).

Investigation of Fiber-based Influences on Bacterial Adherence

Klas-Moritz Kossel¹, Marina Handel³, Mathias Walter Hornef²,
Uwe Klinge⁴, Anja Gerhardt³, Thomas Gries¹, Andreas Blaeser¹

¹Institut für Textiltechnik of the RWTH Aachen University; ²Institute for Medical Microbiology of the University Hospital RWTH Aachen; ³Hohenstein Group, Life Science & Care; ⁴Department of Surgery of the University Hospital RWTH Aachen

klas.kossel@ita.rwth-aachen.de

Healthcare associated infections are a worldwide major socio-economic problem. In Europe, approximately 110.000 people die per year as a result of healthcare associated infections. The influence of textiles used in medicine on the infect transmission has been proven by numerous preclinical data. The bacterial adherence is one of the major fiber properties which lead to an increase of the infection rates. Therefore, the overall objective of our research projects is an interdisciplinary research on fiber-based parameters regarding the reduction of bacterial adherence. Both, in vivo applications in form of implants and ex vivo applications in form of hospital textiles will be addressed in the projects. The influence of production parameters like used polymer, draw ratio or filament number as well as different fiber cross sections (profiled vs. round) on the bacterial adherence will be investigated. Thus, a specific variation of fiber parameters will be executed which allows the determination of effects and interdependencies of the investigated parameters. In order to identify the bacterial adherence the spun fibers will be evaluated in microbiological and preclinical tests.

ACKNOWLEDGMENT

Grateful acknowledgement goes to the research association Forschungskuratorium Textil e.V., a branch of the German Federation of Industrial Research Associations (AiF), for the financial funding through AiF-IGF of the research project AiF-No. 18837 N. Additionally, we would like to thank the Bundesministerium für Bildung und Forschung (BMBF) for funding the research project (ref no. 13GW0182B).

Challenges from Wearable Technologies

Ning Pan

Biological and Agricultural Engineering, Fiber and Polymer Sciences, University of California at Davis

npan@ucdavis.edu

Wearable technologies have attracted such escalating interests from both manufacturers and consumers that some experts predict they will be “as big as the smart phone.” Given the wide coverage and extreme intimacy between the human body and clothing, the potential for wearable technologies indeed seems abundant.

For wearable technologies to gain success in today’s environment however, it is of critical importance to explore and understand the causes or reasons behind the seemingly eternity of our clothing format up to now, despite tremendous advances in both materials and fabrication, and previous failed attempts in transforming it. Textile scientists are destined for providing the guidance or answers in this regard.

This talk identifies and analyzes the major technical and non-technical issues, to explain how our current form of clothing satisfies simultaneously so many—some seemingly mutually exclusive and demanding—requirements, to have served us so well for so long; why any attempt to deviate from the basic requirements discussed here will inevitably cause severe deterioration of clothing performance and deter its consumer acceptance, and finally why searching for a new form of cloth is so difficult, if possible.

Wearable technologies should be and appear so far to penetrate first into the markets, where performance and added functionality are critical such as in the military, sports, medical fields, and under extreme conditions, e.g., firefighting and polar explorers. Applications in everyday clothing will only become possible after the technical and business issues discussed are resolved and validated.

Electrostatic Spinning—Spraying for Cell-laden Hybrid Membranes Mimicking the Native Blood Barrier

G. Fortunato¹, L. Weidenbacher^{1,2}, A. Abrishamkar^{1,3}, A. G. Guex^{1,2},
M. Brunelli¹, M. Rottmar², K. Maniura-Weber², R. Rossi¹

¹Empa, Swiss Federal Laboratories for Materials Science and Technology, Biomimetic Membranes and Textiles, St. Gallen, Switzerland; ²Empa, Swiss Federal Laboratories for Materials Science and Technology, Biointerfaces, St. Gallen, Switzerland; ³Institute for Chemical and Bioengineering, Department of Chemistry and Applied Bioscience, ETH Zürich, Switzerland

giuseppino.fortunato@empa.ch

The development of functional 3D tissues is a major goal in regenerative medicine and attracts novel applications in the field of medical equipment such as for functionalization of Ventricular Assist Devices (VAD's). For this, not only fiber surface chemistry, the morphology and the mechanical properties but also the distribution, attachment, proliferation and function of cells are of major importance. Electrospinning is a promising technology for nanofiber and respective membrane development mimicking the structure of the extracellular matrix. However, infiltration of viable cells into these scaffolds remains challenging, e.g. due to low pore size diameters or cytotoxicity of components used during the spinning procedure. To overcome these issues, we report on a combined process of fiber spinning and cell spraying both based on electrohydrodynamic procedures for the fabrication of cell-laden 3-D networks with spatially controlled distribution of the cells.

Thereby, fiber material developments are presented in terms of morphological, mechanical and surface fiber properties including measured cytotoxic effects deriving from process solvents used. To tailor the membranes for VADs, polymeric blend systems (Polyurethane PUR, Poly(vinylidene fluoride-co-hexafluoropropylene) PVDFhfp) were electrospun to obtain fibers with high elasticity, low intrinsic plastic deformation as well as anti-thrombogenic behavior. Structural examination revealed the formation of core – shell fibers incorporating PUR within the core and PVDFhfp within the shell.¹

Cell infiltration is discussed as a proof of concept both with respect to technological challenges as well as the resulting behavior of C2C12 murine myoblasts within the fibrous scaffolds. To protect the cells against toxic solvents used during the hybrid membrane production, a microfluidic encapsulation process was developed. Based on gelatine as delivery vehicle, monodispersed, micron-sized capsules with fast but adapted release kinetics of the C2C12 myoblasts were obtained. Cell e-spraying did not show any negative effects in terms of cell viability as well as phenotype after the application of high voltages.²

Globally, by exploiting a combination of fiber e-spinning and cell e-spraying, a platform for the fabrication of 3-D biografts was attained, being now further developed for VAD's. Future research is ongoing towards cyclic mechanical testing as well as stable attachment of the membranes to VAD's surface.

REFERENCES

- [1] Guex, A. G. “Hierarchical Self-Assembly of Poly(Urethane)/Poly(Vinylidene Fluoride-co-Hexafluoropropylene) Blends into Highly Hydrophobic Electrospun Fibers with Reduced Protein Adsorption Profiles.” *Macromolecular Materials and Engineering*, 302, 2017: 1700081.
- [2] Weidenbacher, L., et al. “Electrospraying of microfluidic encapsulated cells for the fabrication of cell-laden electrospun 3D tissue constructs.” *Acta Biomaterialia*, 64, 2017: 137-47.

ACKNOWLEDGMENT

This work is part of the Zurich Heart project of Hochschulmedizin Zürich (<http://www.hochschulmedizin.uzh.ch/en/projekte/zurichheart.html>).

Effect of Vapor Permeability and Aperture of Outdoor Parka and Environmental Velocity on Evaporative Heat Transfer and Ventilation Rate Using Sweating Thermal Manikin and Tracer Gas Methods

Yayoi Satsumoto¹, Takuya Aoyagi², Ayano Dempoya³, Tomoko Koshiba⁴, Teruko Tamura⁴
¹College of Education and Human Sciences, Yokohama National University; ²Former Student of Graduate School of Yokohama National University; ³Department of Architecture, Faculty of Engineering; ⁴Department of Fashion technology, Bunka Gakuen University

satumoto@ynu.ac.jp

This study aims to find out the effect of vapor permeability and aperture of outdoor parka and environmental velocity on its heat and vapor transfer and ventilation rate. Experiments using sweating thermal manikin and tracer gas method were conducted.

METHODS

To make clear the effect of the aperture and the vapor permeability of the material, outdoor parkas were made whose vapor permeable levels are 3 levels (high permeable HP, middle permeable MP, impermeable IM) and whose aperture can be changed open or closed. To make the reproducibility improve heat and vapor transfer, a sweating thermal manikin was used. The ventilation rates were estimated using tracer gas method concurrently. To make the influence of the wind velocity of the environment clear, ventilation rate was measured at wind velocity 0, 0.5 and 1.0m/s.

RESULTS

It was found that the vapor permeability of the material and the apertures were effective in improvement of evaporative heat transfer and there was a correlation in ventilation rate and evaporative heat transfer in correlation of 0.85 except for MP. When the permeability of the material for carbon dioxide were estimated, it became clear that the MP was impermeable for carbon dioxide. The indirect evaluation method of evaporative heat transfer from ventilation rate by tracer gas method can be applied except MP. Contribution of vapor permeability of the material was big and the influence of the aperture was small up to 0.5m/s, but the effect of the aperture equaled vapor permeability in 1.0m/s, and it became conspicuous. There was correlation in the wind velocity of the environment for ventilation rate.

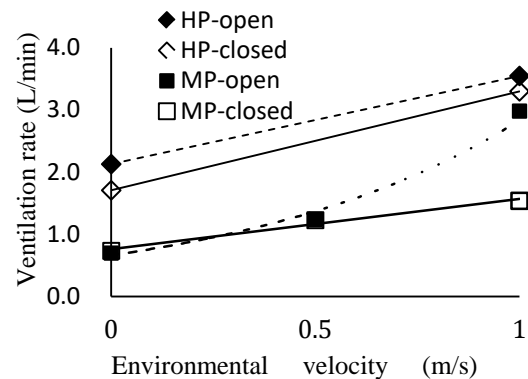


Fig.1. Relation between environmental velocity and ventilation rate.

CONCLUSION

It was found out that the vapor permeability and the apertures of outdoor parka were effective on its vapor transfer and ventilation rate by experiments using sweating thermal manikin and tracer gas methods. The validity of the indirect evaluation method of evaporative heat transfer from ventilation rate by tracer gas method was verified except MP which was impermeable for carbon dioxide but permeable for vapor. There was correlation in the wind velocity of the environment for ventilation rate. Contribution of vapor permeability of the material was big to 0.5m/s, and the influence of the aperture was small, but the effect of the aperture equaled vapor permeability in 1.0m/s.

ACKNOWLEDGMENT

This research was funded by scientific general research B (15H02888) in 2015 - 2018.

Determination of Total Comfort of Sport Caps Using Wear Trials

Rosimeiri Naomi Nagamatsu^{1,2}, Maria José Abreu², Cosmo Damião Santiago¹, Derya Tama^{2,3}

¹Federal University Technology of Paraná, Apucarana, Brasil; ²2C2T-Centre for Textile Science and Technology, Minho University, Azurém, Portugal; ³Textile Engineering Department, Ege University, Izmir, Turkey

naomi@utfpr.edu.br; josi@det.uminho.pt; cosmo@utfpr.edu.br; derya.tama@ege.edu.tr

The cap is a very popular product among young people. Previous studies regarding the production system and appearance of the product were conducted, however there is little research concerning their comfort. The total comfort is classified into 4 basic groups as thermo-physiological comfort, sensorial comfort, psychological comfort and ergonomic comfort.

This paper is part of an ongoing research aiming to establish a comprehension about function and comfort characteristics for sports caps, in this specific case using male volunteers. In this part of the study, ten models of caps of different types of raw materials, construction and structure levels were manufactured and afterwards submitted to perception tests of comfort by ten male volunteers.

The results regarding this comfort parameters shows that the volunteers felt the differences of the behavior of the caps between the different phases of the exercise and between the different caps indicating the best product concerning total comfort.

MATERIALS AND METHODS

Ten caps models were developed with different fabric characteristics for testing with volunteers (Tables I and II).

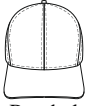
 Basebol Model	Samples	A1	A2	A4	A6	A8
	Composition	100% CO	100% CO	100% WO	65% PES 35% WO	Cork 100%PES
	Mass per unit area (g/m ²)	294	197	248	215	Cork 321 PES102
	Thickness (mm)	0,718	0,456	0,696	0,6	0,546
	Water vapour resistance (Pa/m ² /W ⁻¹)	4,2	2,88	4,48	3,22	Cork 36,5 PES -0,8
	Air Permeability (l/m ² /s)	72,4	81,8	215,6	0,6	-

Table I. Baseball caps samples.


 Snapback Model	Sample	A3	A5	A7	A9	A10
	Composition	100% CO	65% PES 35% WO	100% Cork	100%Cork 100% PES	100% PES
	Mass per unit area (g/m ²)	378	197	321	Cork 321 PES 102	430
	Thickness (mm)	0,756	0,448	0,7478	Cork 0,7478 PES 0,546	0,708
	Water vapour resistance (Pa/m ² /W ⁻¹)	5,38	2,44	36,5	Cork 36,5 PES -0,8	5,6
	Air Permeability (l/m ² /s)	45,67	178,6	-	45,67	138,2

Table II. Snapback caps samples.

The thermal sensations (comfort scale), micro-climate temperature and humidity under the cap (i-button sensor), pressure (Picopress equipment) and general comfort evaluation exerted on the user's head were measured and compared. The performance tests were performed in a climatic chamber that simulated specific climatic conditions (25°C and 75% of relative humidity, simulating the climatic conditions of Apucarana–Brazil).

The volunteers evaluated the cap in three phases: 1-Pre-exercise: sitting at rest for 5 minutes (table III); 2-Exercise on the exercise bicycle: low speed (10-15 km/h) 15 minutes, following high speed (15-20 km/h) for 5 minutes; 3-Post exercise: sitting at rest for 5 minutes.

Analysis of variance (ANOVA) was conducted to determine if there were significant differences at the $p < 0.05$ level. The data were analyzed by SPSS® software.

Thermal sensations	1 very cold	2 cold	3 cool	4 natural	5 warm	6 hot	7 very hot
Humid sensation		1 dry	2 dry somewhat	3 slightly wet	4 wet	5 very wet	
Comfort		1 comfortavel	2 slightly uncomfortable	3 uncomfortable	4 very uncomfortable	5 extremely uncomfortable	
Pressure		1 no	2 slightly	3 neutral	4 very	5 extremely	

Table III. Subjective evaluation.

RESULTS AND DISCUSSION

The ANOVA conducted on the 10 samples. The results of the evaluation with volunteers revealed that samples 3 and 9 (snapback) demonstrated a decrease in the sensation of pressure that the cap exerts on the head of the volunteer (fig.1-b). The sample 6 (baseball) presented a constant increase in pressure sensation. The other samples showed oscillations as in the comfort sensation as in the pressure sensation (fig. 1-a). Concerning the sensation of comfort, we highlight the samples 5 and 6 that remained stable during all phases and the other samples presented oscillations.

The samples follow the same trend in relation the thermal sensation (fig. 1-c). A great increase was realized in the thermal sensation after 15 minutes of cycling. After 20 minutes of testing, most of the samples follow the same trend of temperature increase, only sample 6 was different at this stage, remaining stable in relation to the previous phase and cooling faster than the other samples in the last sitting phase.

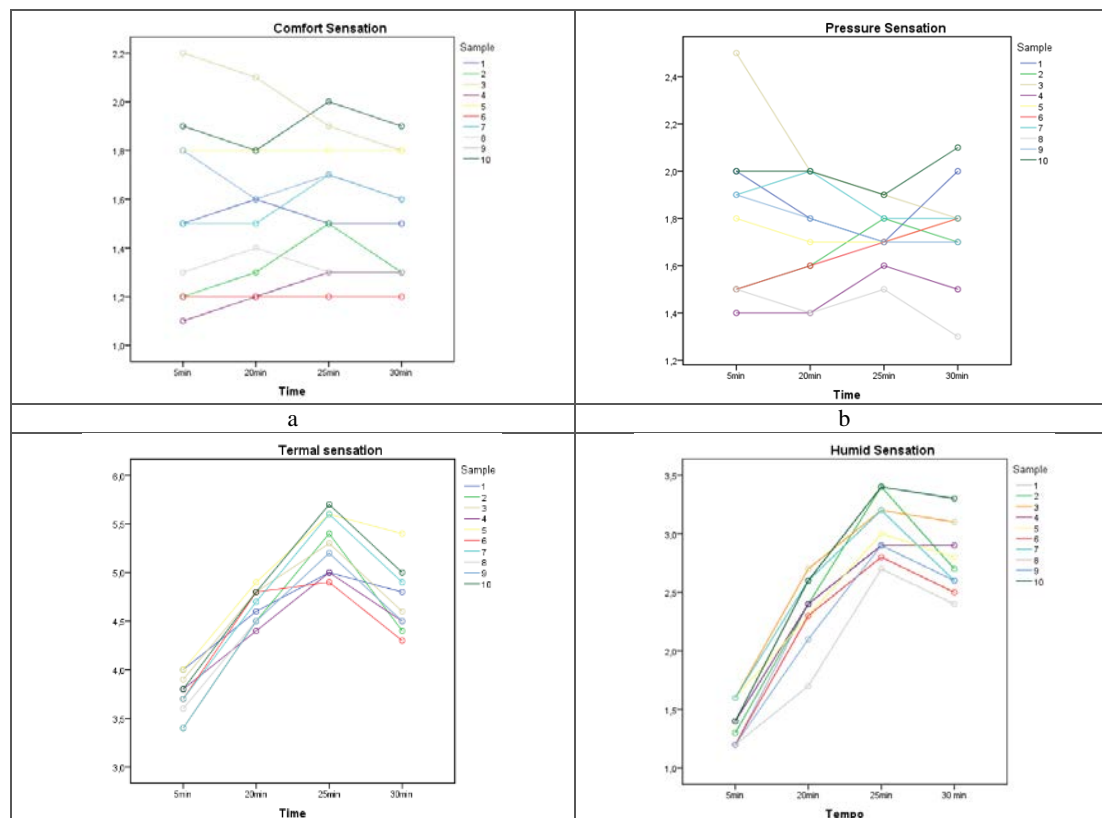


Figure 1. Objective evaluation using volunteers.

The humid sensation of all samples follows the same trend. The sample 8 that in all phases was considered by the volunteer the sample with better performance (fig. 1-d).

The results of the objective evaluation with the measuring equipment show a constant growth of both temperature and humidity. The heat dissipation in sample 6 showed the best performance. The snapback models 3, 5 and 7 had a better humid behavior.

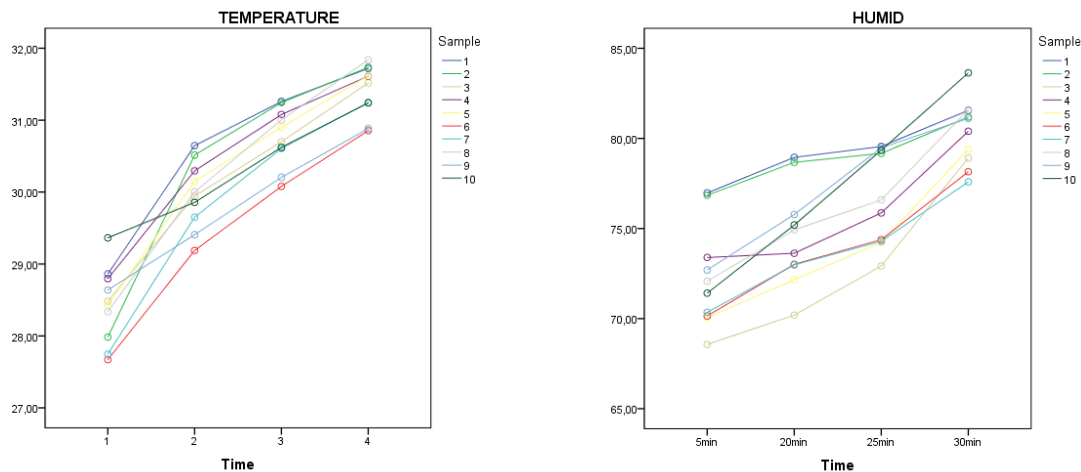


Figure 2. Objective evaluation with measuring equipment.

When comparing the two objective evaluation methods of temperature (fig.1-c, 2-a), by the end of high speed phase the graphs of the two evaluations show an increase in heat levels. In the last phase the volunteers had the sensation of decrease the temperature sensation, however using thermodata, the heat shows that the temperature continues to rise. Sample 6 had a better performance in both evaluations and the worst performing 10 sample.

When comparing the humid data of the two assessments (fig.1-d and fig. 2-c), it is realized that up to the phase of high speed cycling, there is an increase in humidity sensation in both evaluations.

The volunteer's evaluation showed that the humidity sensation was accentuated in objective evaluation (thermodata) than using the input of the inquiry of the volunteers. The last phase (sitting rested), the volunteers felt a decrease in humidity. The reason for this feeling is due to decreased physical exertion. In both evaluations sample 10 (snapback cap, 100%PES) has the poor performance and sample 8 the best (baseball cap, cork with PES) Sample 8 presented a good performance in relation to the sensation of pressure and humidity in the two of evaluation with the inquiry and evaluation using testing equipment; (front part at 100% cork and side and back straight mesh - fabric - 100% polyester, baseball model).

Sample 6 presented a good performance in relation to the comfort sensation; and heat (65% PES, 35% WO, baseball model) in both evaluations. The thermal comfort result of the evaluation using the volunteers inquiry had the worst performance of sample 5 followed by sample 10. In all evaluations the 10 sample had a poor performance (100% PES, snapback model).

CONCLUSIONS

The results regarding this comfort parameters shows that the volunteers felt the differences of the behavior of the caps between the different phases of the exercise as also between the different shapes of caps and their composition. The comparison between the results of objective evaluation with wear trial and objective evaluation with measurement equipment showed that the psychological factor influenced the volunteers' responses, mainly in the last phase of the physical test during the resting phase.

In future studies, we hope to compare these results to the results of a tactile sensory evaluation of the cap indicating the best product concerning of total sensory comfort.

ACKNOWLEDGMENT

This work is financed by FEDER funds through the Competitivity Factors Operational Programme (COMPETE) and by national funds through FCT–Foundation for Science and Technology within the scope of the project POCI-01-0145-FEDER-007136.

Evaluation Parameters for Friction Properties of Woven Fabrics by Rotational Dragging with Tactile Sensor

Toshiyasu Kinari¹, Hiroshi Tachiya¹, Lina Wakako¹, Shinnosuke Yoneda², Takumi Kyoda²

¹Institute of Science and Engineering, Kanazawa University

²Graduate School of Natural Science and Technology, Kanazawa University

kinari@se.kanazawa-u.ac.jp

INTRODUCTION

Touch feeling of fabric is one of the important evaluation factors in handling of fabric products. To cope with diversification of fabric products, the establishment of easy and detailed evaluation method is expected. The typical example of such evaluation method is Kawabata Evaluation System. This study introduces a novel method that can evaluate the hand value from the obtained frictional coefficient. We measured frictional coefficients on fabric surface, and confirmed the effectiveness of this apparatus.

TACTILE SENSOR AND ROTATIONALLY DRAGGING APPARATUS

The experimental apparatus for rotational dragging is shown in Figure 1. The contact device of the tactile sensor is made of an acrylic plate and a piano wire (5mm in the contact width to surface of fabrics). We measure the strain distribution of the contact device with strain gages, and calculate frictional force and compressive force.

We define the experiment condition as follows:

- 1) Vertical load: 0.2N
- 2) Friction speed: 1.0mm/s
- 3) Radius of rotation: 20mm
- 4) Number of dragging: 10 times

PARAMETERS OF FRICTION CHARACTERISTIC

Table 1 shows 14 woven fabric samples used in this friction test. In order to compare changes of dynamic friction coefficient μ , we focused on the following parameters; the average, the standard deviation and the variation coefficient of μ , $\bar{\mu}$ - the mean value of μ (every 5 degrees in dragging), and μ_A - amplitude on mean deviation of μ .

We conducted experiments using the apparatus for rotational dragging. The amplitude on the dynamic friction coefficient and friction characteristic values were measured.

CONCLUSION

(1) Regarding to nine types of the friction characteristic values obtained from the measurement on the fabric surface, the investigation of the correlation between each value was conducted and six characteristic values (① average value of μ , ② standard deviation value of μ , ③ variation coefficient of μ , ④ average value of μ_A , ⑤ standard deviation of μ_A , ⑥ variation coefficient of μ_A) were selected as parameters those represented friction characteristics of fabrics. (2) We obtained different friction characteristic values from the experiment by the rotating device we proposed on samples A and B those have closely similar design factors, and this result was related to subjective hand evaluation.

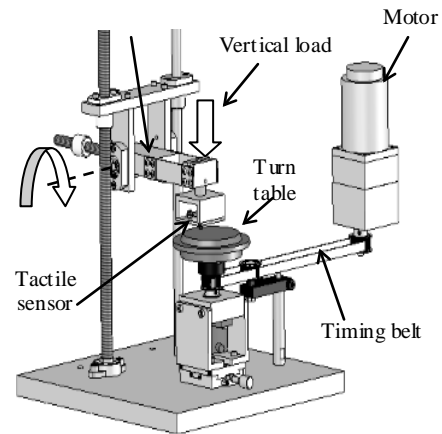


Fig.1. Experimental apparatus (rotational dragging).

Table 1. Samples of woven fabrics.

No	weave	yarn density		No	weave	yarn density	
		warp [ends/cm]	weft [picks/cm]			warp [ends/cm]	weft [picks/cm]
2	satin	99	49	A	twill	104	114
3	plain	67	35	B	twill	104	114
5	plain	92	39	E	plain	50	44
6	satin	122	57	F	satin	70	40
8	satin	103	48	G	twill	50	23
9	satin	82	43	H	twill	25.3	17.6
10	plain	46	36				
11	satin	107	57				

Effect of Different Processing Technique and Softener Treatments on the Surface Friction of Cotton Fabric

Ateeq ur Rehman, Abher Rasheed, Tanveer Hussain,
Munir Ashraf, Sheraz Ahmad, Babar Ramzan, Nau man Ali

National Textile University, Pakistan

ateequrrehman@ntu.edu.pk

Fabric sensorial properties play an important role in buying decision of textile products and they are functions of material content, yarn specifications, fabric structure, processing technique and final finish. This paper is presents the impact of processing technique and softener treatment on the surface friction of cotton fabrics. Fabric specimens were passed through four processing routes followed by treatments with soft finish at changed concentration of softener. The processed fabrics were then tested on Fabric Touch Tester (FTT) and Kawabata Evaluation System for fabrics (KES-F). The analysis of obtained results revealed that certain processing route imparted higher coefficient of friction than others. The study concluded that fabrics dyed through Pad-Thermosol dyeing process acquired more surface friction and that results obtained from KES were of much more statistical significance than those of FTT.

Optical Properties of Cashmere Fabrics

Narantogtokh Davaajav , Sachiko Sukigara

Kyoto Institute of Technology, Japan

sukigara@kit.ac.jp

Cashmere fibers are increasingly popular in the current textile market, being used for knitwear, coats, scarves, and gloves. When cashmere fibers are used as a woven fabric, the luster of cashmere is one of the components as high-grade luxury fabrics. The unique visual appearance is not the same as silk as far as consumers are concerned. Visual evaluation of the appearance of a fabric changes according to the light source, the direction from which the light strikes the fabric, and the angle at which the fabric is viewed. We have developed a method whereby a goniospectrophotometer measures the overall specular and diffuse reflection of a rotating fabric. This method proved capable of distinguishing between fuzz-surface and clear-finish wool fabrics. We applied the same method to differentiate between fine cashmere hairs on fabrics.

The light reflectance of each fabric sample was measured using a goniospectrophotometric color-measurement system (GCMC-4; Murakami Color Research Laboratory Co., Ltd., Japan). The measurements were carried out with different combinations of illumination angle θ_i , viewing angle θ_v , and rotation angle θ_ω of the fabric, as shown in Fig. 1. The rotation angle $\theta_\omega = 0$ corresponds to the fabric warp direction. The CIELAB L^* values were calculated by using a standard Illuminant D65 condition thereby obtaining spatial L^* distributions from the reflectance data.

When measurements were made for $\theta_i / \theta_v / \theta_\omega = 30^\circ / -60^\circ / 90-95^\circ$, differing surface hair morphologies were found for cashmere fabrics. It was found that L^* distributions as a function of θ_ω were influenced by weave structure. These weave structures were characterized by surface geometrical roughness (SMD). These differing surface hair morphologies were also confirmed by surface geometrical roughness SMD. The peak L^* value and its profile were strongly influenced by fabric surface irregularity, which disperses light. The larger L^* values of SMD are associated with smaller values of L^* , so more light is dispersed from the surface.

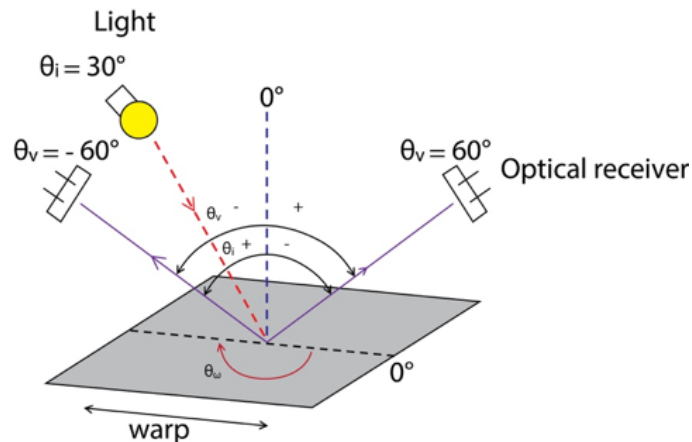


Fig. 1. Measurement geometry of illumination angle (θ_i), viewing angle (θ_v) and rotating angle (θ_ω).

Unique Multiple Melting Behavior of High-speed Melt Spun Polylactide Fibers

Midori Takasaki¹, Natsumi Fukushi², Miku Yoshizawa², Shota Onosato³, Motohiro Hanada³, Wataru Takarada⁴, Yutaka Kawahara³, Takeshi Kikutani⁴, Haruki Kobayashi¹, Katsufumi Tanaka¹

¹Kyoto Institute of Technology, Japan; ²Miyagi University of Education, Japan;

³Gunma University, Japan; ⁴Tokyo Institute of Technology, Japan

mitakas@kit.ac.jp

INTRODUCTION

Polylactide (PLA) is a biodegradable and bioabsorbable polymer produced from renewable resources such as corn starch. We previously conducted high-speed melt spinning of PLA for development of fiber materials, and investigated the melting behavior of PLA fibers by differential scanning calorimetry (DSC). Even though the DSC curves of high-speed spun PLA fibers showed a unique behavior in comparison with the high-speed spun poly(ethylene terephthalate) (PET) fiber [1,2], this reason has not been clarified.

In this study, with the aim of investigating the influence of structure of high-speed spun PLA fibers on the multiple melting behavior, wide angle X-ray diffraction (WAXD) and temperature modulated differential scanning calorimetry (TMDSC) measurements were performed.

EXPERIMENTAL

The L-lactide content of PLA was 98.7%, and the M_w was 170,000. The dried PLA polymer pellets were extruded from a spinneret with four holes of 0.5 mm diameter of each at a throughput rate of $2.0 \text{ g min}^{-1} \text{ hole}^{-1}$ at temperature of 260°C . Only one filament was taken up using a high-speed winder placed at 330 cm below the spinning head.

The WAXD patterns of the as-spun fibers were measured at room temperature. Variations of WAXD profiles during the heating process of as-spun PLA fibers were also measured at a heating rate of 2 K/min. The TMDSC analyses were performed. The temperature modulation programs were selected so as to comply with a heating only condition at an underlying heating rate of 2 K/min with different modulation periods.

RESULTS AND DISCUSSION

The TMDSC curves of as-spun PLA fibers measured at a temperature modulation period of 50 s are shown in Fig. 1. For PLA fiber taken-up at 1 km/min, an exothermic peak of cold crystallization at 88°C (Peak C), a small exothermic peak at 151°C (Peak R) and a melting endothermic peak at 169°C (Peak H) were observed in the THF. Comparing the RHF and NRHF, it can be seen as expected that the exothermic peaks of crystallization, Peaks C and R, appeared only in the NRHF, while the endothermic peak of melting, Peak L, appeared only in the RHF at the same temperature as the exothermic peak of Peak R. On the other hand, the final melting peak (Peak H) appeared both in the RHF and NRHF.

In the case of high-speed melt-spun fibers of take-up velocity at 6 km/min, the peak temperature and magnitude of the cold crystallization (Peak C) decreased in the THF and NRHF compared to the fiber spun at 1 km/min, indicating the enhancement of crystallization due to the higher molecular orientation and resultant orientation-induced crystallization in the spin-line. In addition, Peaks R and L observed in the 1 km/min fibers disappeared. Regarding the final melting, double melting peaks (Peaks M and H') were observed at around 164 and 171°C in all heat flow curves.

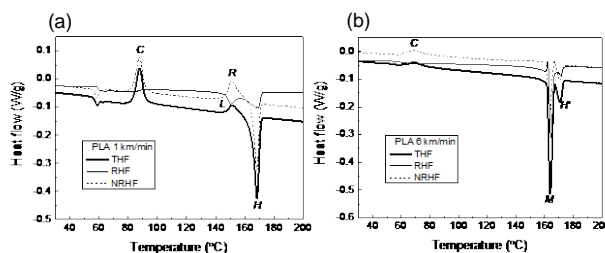


Fig.1. TMDSC curves at a modulation period of 50 s for PLA fiber taken-up at (a) 1 km/min and (b) 6 km/min.

REFERENCES

1. M. Takasaki, H. Ito, T. Kikutani. *J. Macromol.Sci. Part B Phys.*, B42, 2003: 57-73.
2. J. Shimizu, T. Kikutani, A. Takaku, N. Okui. *SEN-I GAKKAISHI*, 40, 1984: 63-71.

Fabrication of Gradient Structure in Melt Spun Polymer Blend Fibers

Long Chen, Dan Pan, Junfen Sun, Zongyi Qin

State Key Laboratory for Modification of Chemical Fibers and Polymer Materials, College of Material Science and Engineering, Donghua University, Shanghai, China

happyjack@dhu.edu.cn

This work introduces the fabrication and characterization of graded and gradient fiber. The influences of raw materials' properties and spinning parameters on the gradient structure in polypropylene/polystyrene blend fiber were studied. The morphology evolution of blend fiber during melt spinning was also studied to evaluate the droplet behaviors, such as deformation, breakup, migration and coalescence of droplets, during elongational flow. Since the morphological structure plays a vital role in the final properties of polymer blend. Once the mechanism of morphology structure evolution of blend fiber during melt spinning is clear, it is possible for us to fabric novel function fibers and improve the properties of normal fibers.

RESULTS AND DISCUSSION

Morphology Evolution of Polymer Blend Fibers

The morphological structure of blend fiber was analyzed based on the cross section and longitudinal section of blend fibers. The influences of viscosity ratio, take up speed and phase concentration were evaluated based on the morphology analysis. Results show that dispersed droplets in the center of the fiber tend to be stretched longer than those of near to the surface due to the radial temperature gradient during fiber formation. The formation mechanism of gradient structure in polymer blend during non-isothermal melt spinning process was proposed based on droplet deformation theory.

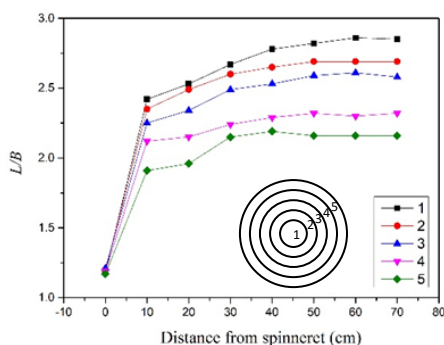


Figure 1. Aspect ratio L/B of droplets at different radial zones along spinning line.

Relation Between Droplet Deformation and Temperature

Delaby's model (equation 1) acts as a bridge between droplet deformation and viscosity ratio which is highly depended on the processing temperature. Then a relation (equation 2) between temperature, rheology, and morphology was established preliminary based on Arrhenius equation, and used to describe the radial temperature distribution in fiber from the deformation of droplets. Results show that gradient structure was attributed to the radial variation of temperature in spinning line.

CONCLUSIONS

The deformation of dispersed droplets was well described by Delaby's model. L/B in the center zone of the fiber is larger than the surface due to radial temperature gradient. The radial temperature gradients vary from 0.22 to 0.35°C/ μm at 40 cm beneath to the spinneret at the discussed take-up velocities. Based on these results, it is possible to predict and finally control the morphological structure of polymer blend fibers.

ACKNOWLEDGMENT

The authors thank the National Key Research and Development Program of China (2016YFB0302602) for financial support.

$$\lambda_d = 1 + \frac{5}{2P + 3} (\lambda_m - 1) \quad (1)$$

Where λ is the deformation ratio, P the viscosity ratio of disperse to matrix.

$$P = (A_d/A_m) \exp\left(\frac{\Delta E_{a,d} - \Delta E_{a,m}}{RT}\right) = \frac{5(\lambda_m - 1)}{2\lambda_d - 1} - \frac{3}{2} \quad (2)$$

Where ΔE_a is the activation energy, R the Boltzmann constant, A the pre-exponential factor, and the subscripts d and m are the dispersed phase and the matrix respectively.

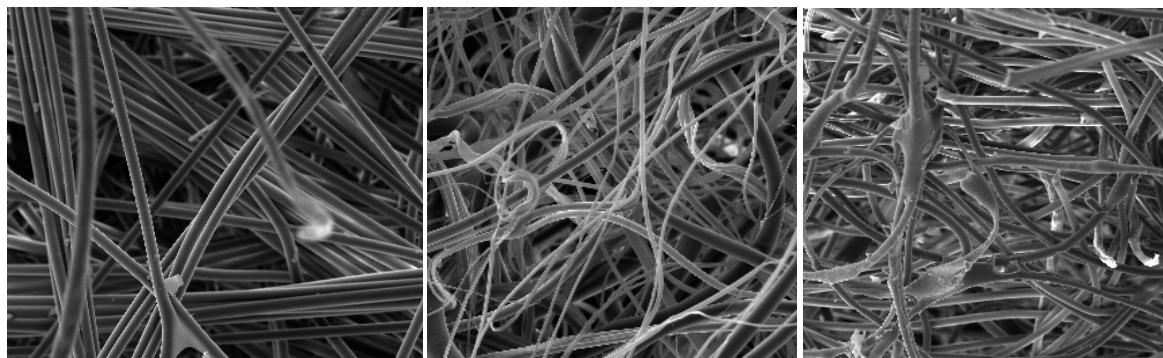
Will Polyolefin and Polytetrafluoroethylene Filaments Become the Next Generation Filter Materials?

Kyung-Ju Choi

Clean & Science, Louisville, Kentucky, USA

kchoi228@gmail.com

Filtration technology is a continuously advancing field for the last 50 years. Due to the excellent chemical resistance and higher filtration efficiency, while maintaining low resistance, polyethylene, polypropylene and polytetrafluoroethylene have become standard materials for several applications in air and liquid filtration. Furthermore, these materials are gaining momentum by replacing commodity cellulose or fiberglass-based filtration materials.

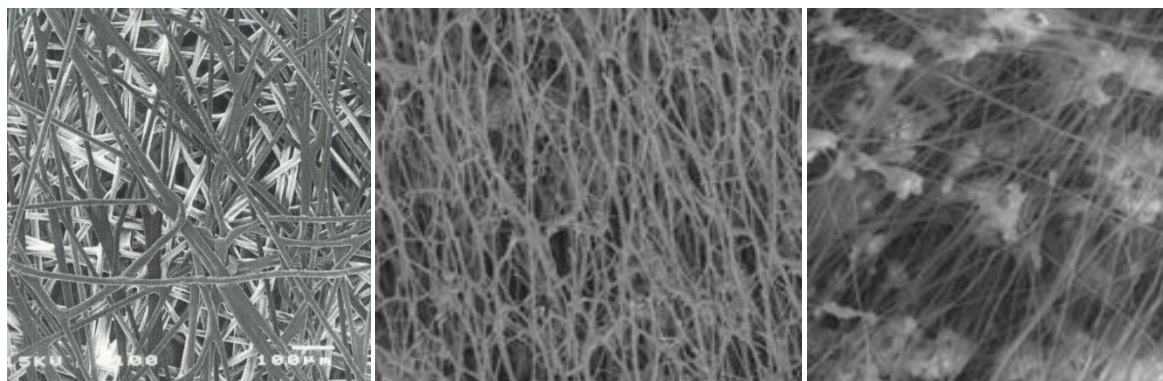


Spunbond

Meltblown

Dry Laid

Submicron meltblown polypropylene materials are being widely used, particularly in Asian markets, realized as room air purifiers, gas turbine and cabin air applications. Polyolefin spunbond materials have been dominating the HVAC and residential markets due to its high surface electric charging characteristics and low resistance for the last 20 years. Low density polyethylene (LDPE) or linear low density polyethylene (LLDPE) split thin films have been still used in air filter market. Stretched polyolefin and polytetrafluoroethylene films have been penetrating into the conventional membrane market due to its dimensional stability, chemical inertness and user-friendliness.



PP/PE Spunbond

Highly Stretched

Less Stretched

Additionally, the molecular orientation and crystal structure of polyolefins and polytetrafluoroethylene have been gradually improving embodied by positive advances in molecular structure and mechanical properties. Polyolefins and polytetrafluoroethylene are prevalent in today's filtration market and are actively being refined, which makes it plausible that these materials will persevere, if not gain more popularity, in the next generation of filter-media.

Influence of Polymer Grade, Process Parameters, and Capillary Modification on the Shape Factor of Noncircular Cross-section Fibers

Inga Noll¹, Amrei Becker¹, Gunnar Seide², Thomas Gries¹

¹Institut für Textiltechnik, RWTH Aachen University, Aachen, Germany

²Aachen-Maastricht Institute for Biobased Materials, Maastricht University, The Netherlands

inga.noll@ita.rwth-aachen.de

ABSTRACT

In the textile industry, more than 20 % of the obtained revenue goes back to product innovations. Here, an intensified use of fibers with a noncircular cross-section is observed. In particular for noncircular cross-section fibers, the development of spinning nozzles is very time consuming. This goes back to the die swell effect as for which the relaxation of the polymer at the die exit leads to a low conformity between the desired and the realized cross-sectional shape (shape factor). Therefore, multiple iteration steps are necessary to obtain the geometry of the capillaries of the spinning nozzle. Hence, the production of individual shaped fibers is inefficient and limits the degree of innovation of fiber and textile producers. Within this research study, the effects of polymer grades, process parameters and capillary modifications on an increase of the shape factor of noncircular fibers was investigated for polyethylene terephthalate. It was found that an intrinsic viscosity $> 0,8$ and an extrusion temperature of 295 °C lead to an increase of the shape factor. Modifications of rectangular capillaries of a spinning nozzle positively affect the aspect ratio of as-spun fibers.

INTRODUCTION

First developments in the extrusion of noncircular cross-section fibers began in the 1960s with trilobal fibers to mimic silk. Due to a relaxation of the viscoelastic material at the die exit - caused by the stress conditions in the spinning nozzle - and surface tension effects, there is a low correspondence between the desired and realized cross-section. The correspondence is referred to as shape factor. Throughout the past centuries, multiple approaches were made to increase the shape factor in order to reduce the number of iteration steps necessary in the spinning nozzle development and to produce novel cross-sectional geometries. Hereinafter, parameter variations, the extrusion of bicomponent fibers with soluble sheath materials and the addition of particles were investigated. Due to a change of the material properties or economic inefficiency associated therewith, none of these methods have proven to be beneficial for industrial production of shaped fibers to date.

The objective of this research study is to increase the shape factor by modifying the capillaries of a spinning nozzle. The approach is to shift the swelling behaviour into the spinning nozzle, allowing a control of the stress and strain profile at the die exit. Therefore, the effect of varying polymer grades with different intrinsic viscosities, process parameters and capillary modifications on the shape factor is investigated using cruciform and rectangular nozzles. This work highlights the most important findings of the shape factor evaluation.

HYPOTHESIS

This research study is based on the hypothesis that an increase of the shape factor requires the manufacturing of capillaries with expanded die outlets, Figure 11.

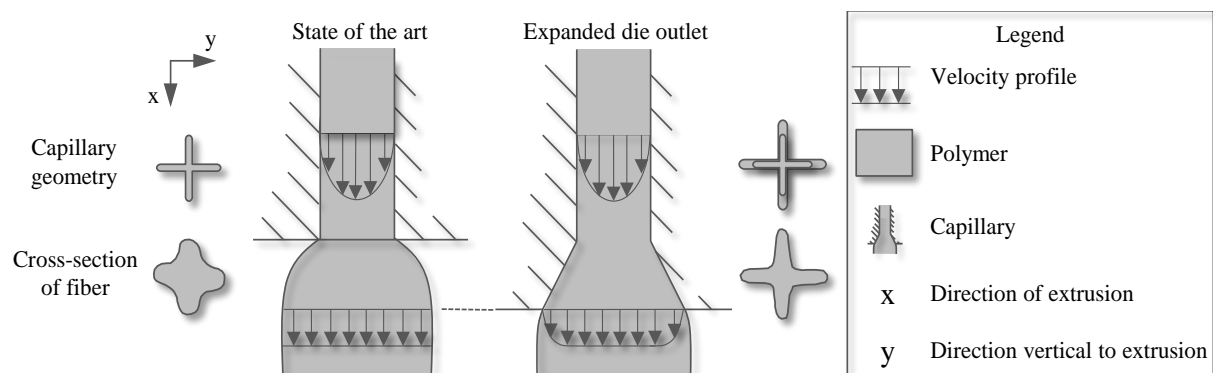


Figure 1: Hypothesis of the research project.

Therewith, the swelling of the polymer can be shifted into the capillary. The velocity component vertical to the direction of extrusion is systematically reduced. The expansion of the flow area at the die outlet results in a deceleration of the flow velocity of the polymer. The velocity profile at the die outlet is decreased. In the polymer, there is a damped stress condition. At the point where the polymer detaches from the wall, the expanded die outlet needs to end. Here, the elastic component is relieved. The polymer is hence forced to adapt the desired cross-sectional shape.

EXPERIMENTAL

The correlations between polymer grade, process parameters and capillary modification with the shape factor are investigated in the melt spinning process.

Polymer grade

The polymer grades used for the melt spinning of fibers with a cruciform cross-section are PET Polyclear® from Invista S.à.r.l., PET + TiO₂ and PET DMT (Dimethyl Terephthalate). Relevant material characteristics are listed in Table I.

Table I. Material characteristics of investigated polyester grades.

		PET Polyclear®	PET DMT	PET + TiO ₂
Intrinsic viscosity	[-]	0.83 ± 0.02	0.86 ± 0.03	0.67 ± 0.02
Melting temperature	[°C]	243	248.30	256.90
Degradation temperature	[°C]	387.89	358.23	353.89

The filaments were extruded with the least possible extrusion temperature as that the pressure in the spinning nozzle was < 140 bar. It was found that PET + TiO₂ with the lowest intrinsic viscosity shows the highest deviation from the desired shape due to stronger transverse flow component, Figure 2.

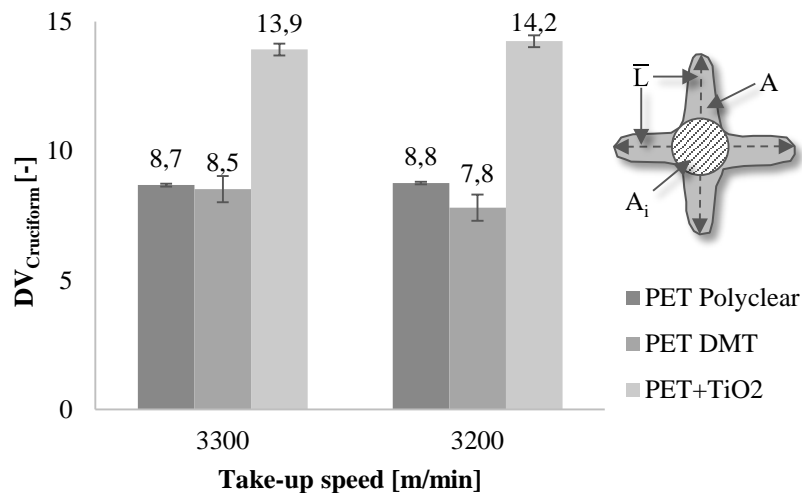


Figure 2: Deviation of the fiber cross-section from the desired cruciform shape for different polymer grades.

Process parameters

The effects of extrusion temperature ($T_{\min \text{ at } 140 \text{ bar}} + 5^\circ\text{C}$), take-up speed (3000 to 3500 m/min) and cooling air speed (0.4, 0.5 m/s) on the shape factor of cruciform of PET Polyclear® are shown in Figure 2. The extrusion temperature is found to be the major influencing factor due to the impact on the melt viscosity.

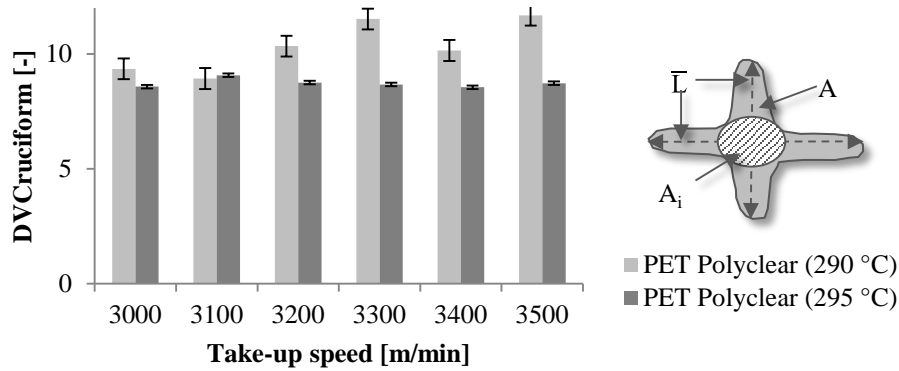


Figure 3: Deviation of the fiber cross-section from the desired cruciform shape for different take-up speeds.

Capillary modification

The effects of a capillary modification on the shape factor were evaluated with regard to the aspect ratio and the accordance with an applied rectangle to determine the rectangularity, Figure 4.

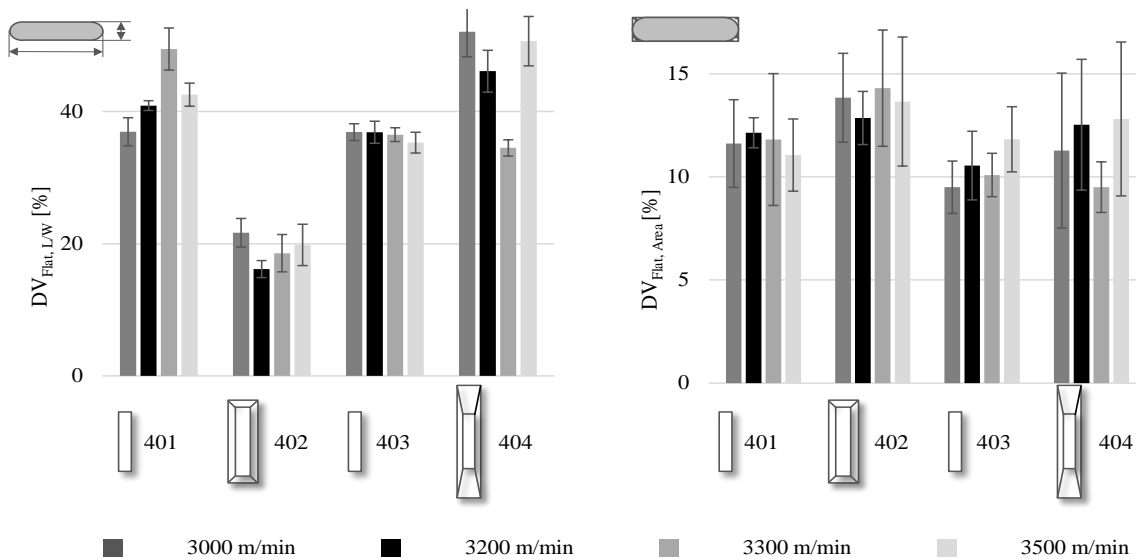


Figure 4: Deviation of the fiber cross-section from the desired rectangular shape for different capillary modifications.

It was observed that a longer effective capillary length (403 vs. 401) results in a lower deviation for both, aspect ratio and applied rectangle. A higher aspect ratio (402 vs. 404) at the die exit leads to a lower deviation from the desired aspect ratio. It is expected that the swelling behavior of the length and the width of the spinning beam is more uniform with larger aspect ratios due to less anisotropic cooling. Furthermore, a conversion of a square to a circle requires less energy than the conversion of a long rectangle to the energetically favorable state.

CONCLUSION

The intrinsic viscosity of the polyester grade is found to strongly impact the shape factor of as-spun fibers. Hereinafter, the extrusion temperature is of greater importance in achieving a high shape factor in contrast to the take-up and cooling air speed. A capillary modification increased the aspect ratio of rectangular fibers whereas a greater deviation of the filaments' cross-sectional areas from the area of applied rectangles was observed. Further research includes a design of experiments on different angles and lengths of the capillary modification and the investigation of the transferability of the effects to novel geometries and other polymers than PET.

ACKNOWLEDGMENT

This work was supported by the Federal Ministry of Education and Research (BMBF) within the framework of the funding initiative KMU-innovativ: Produktionsforschung.

Effect of Curvature on Wetting and Dewetting of Complexly Shaped Fibers

Chengqi Zhang¹, Mars Alimov², Konstantin G. Kornev¹

¹Clemson University, Clemson, South Carolina, USA

²Kazan Federal University, Kazan, Russia

kkornev@clemson.edu

The behavior of coating films and droplets on complexly shaped fibers is investigated to explain the effect of curvature of the fiber contour or the curvature of the fiber bent. By using a thin-film approximation with the air-liquid interface positioned almost parallel to the fiber surface, capillary pressure was estimated from the profile of the fiber surfaces supporting the films. The film is always unstable and the fiber shape and movements have adaptive value in collecting fluid: coiling and bending of fibers facilitate fluid collection at a particular side of the fiber surface. We discuss specifics of wetting phenomena related to finishing and spraying of elliptical and C-shaped fibers and their loops. Some practical applications of this effect are discussed with regard to fiber engineering.

Numerical Simulation of Melt Spinning Process Incorporating Crystallization Characteristic of Polypropylene in Super Cooling Conditions

Yasuhiko Otsuki¹, Yutaka Kobayashi¹, Kouya Kawai², Wataru Takarada², Takeshi Kikutani²

¹Research & Development Division, Prime Polymer Co., Ltd

²Department of Materials Science and Engineering, Tokyo Institute of Technology

yasuhiko.otsuki@primepolymer.co.jp

For the polymer processing in the industry, high processing speed is generally preferred to improve production efficiency. Accordingly, crystallization proceeds under a considerably high cooling rate condition. Particularly in the melt spinning process, the instantaneous cooling rate exceeds 1000 K/s under ordinary industrial conditions. If fundamental analysis of crystallization behavior is considered, cooling rate achievable using a conventional DSC apparatus is much lower, and it has been considered that the prediction of crystallization behavior in the industrial polymer processing based on the data obtained using a DSC is impossible. Recently, however, a novel DSC apparatus with the capability of extremely high heating and cooling rates was developed. There is an expectation that the fundamental data of crystallization behavior obtained using the high-speed DSC can be incorporated into the numerical simulation for the polymer processing of industrial conditions.

In this study, firstly, crystallization behavior of three isotactic polypropylenes (PP) with different molecular weights and molecular weight distributions were evaluated under the isothermal condition as well as under the ultra-high-cooling-rate non-isothermal conditions using the high-speed DSC. Based on these analyses, a model which expresses the crystallization behavior of PP through development of both α -form crystals and mesophase was prepared. In this model, crystallization rate is described with multiple bell-shape functions.

Secondly, melt spinning of these three polymers were carried out at the take-up velocity range of 125 to 2000 m/min. During the spinning experiment, on-line measurement of the thinning behavior of the spin-line was conducted. For the numerical simulation of the melt spinning process, non-isothermal axisymmetric two dimensional model was solved with finite element method. Multi-mode Phan-Thien Tanner constitutive equation was used to express viscoelastic characteristics of the polymer melts. Experimental results of the spin-line diameter profiles were well predicted incorporating the kinetics of orientation-induced crystallization based on the high-speed DSC results as well as crystallization-induced change of flow-ability into the simulation. The necessity of introducing the effect of tensile stress on the crystallization behavior varied among the three PPs. It was also found that the estimated crystallization behavior under high tensile stress showed good correlation with the poly morphology in the as-spun fibers.

Smart and Safe Chemical Protective Clothing

Eugenija Strazdiene¹, Inga Dabolina², Daivute Krisciuniene³

¹Vilnius University of Applied Sciences, Lithuania

²Riga Technical University, Latvia

³JSC Ansell Protective Solutions, Lithuania

e.strazdiene@mtf.viko.lt

The approach of 4th industrial revolution accelerates the efficiency growth of fashion value chains due to the integration of data analysis, robotics, sensors 3D scanning and printing, internet of things, virtual and augmented reality. Intensive digitization of the majority of design and manufacturing processes leads to mass customization, which still is not widely available option for companies producing specialized clothing, e.g. personal protective garments. Advances of digital technologies enables companies to compete by increasing the quality of the products and services, on the one hand, and by reducing the costs of labor time and material consumption on the other hand. The widespread use of CAD systems in garment industry to design patterns along with database resulting from 3D scanning technology of the human body, are prerequisites for virtual modelling of the dimensional correspondence between 2D patterns and concrete human body.

Due to the huge number of variables involved, numerous levels and types of chemical protective clothing systems has been technologically developed. It must be noted that such clothing is worn on fully dressed human body and often equipped with specialized gear, what makes comfort fitting of them more complicated. The object of the investigation was chemical protective clothing (CPC) for firefighters Trellechem®VPS of encapsulating design (type VP1). Technical characteristics of the selected type of CPC show that it is resistant to a wide range of chemicals for more than 8 hours. It is also resistant to abrasion and flame due to materials and seams multilayer structure. Trellechem®VPS CPC suit follows the requirements of standards: EN 943-2/ET; EN 943-1; EN 1073-2; EN 14126.

Thus, the aim of this research was to develop the digitized method of chemical protective clothing (CPC) prototype generation, which would comprise 3D scanning with hand-held scanner technology together with virtual fitting, 2D pattern creation and material consumption calculation software by providing maximal comfort of developed clothing. Scanned data was processed with Artec Studio 11, which is industry-acclaimed software for advanced 3D scanning and data processing. It is also important that scanning of workers with different types of equipment allows to customize clothing taking into account not only workers body shape and measurements, but the size of worn equipment. Even more that the gear, which is worn for different jobs differs in size and shape.

Additional task was to integrate smart internal and external communication systems into CPC for more efficient and safe work of firefighters' and rescue team members during different type of accidents. For this reason, a close-fitting holsters, that integrate radio transmitters, headsets, remote speaker microphones and other devices were developed. Such vests are universal. i.e. could be worn under the CPC, which covers the whole body of firefighter together with gear (breathing apparatus, breathing mask and helmet). Also, they are adjustable for lighter types of clothing, e.g. when gear is worn on the top of protective clothing. Sewing and embroidering technologies were be applied to incorporate electronic components into garment.

ACKNOWLEDGMENT

This research work was partially financed by the European Union's European Regional Development Fund, through the INTERREG BSR Programme, which awarded a grant to the SWW project (#R006). The authors gratefully acknowledge the received financial support.

Effects of Washing and Wearing Processes on Soldiers Uniforms: Friction Sound Characterization

Floriane Leclinche^{1,2}, Dominique Adolphe¹, Emilie Drean¹, Laurence Schacher¹, Véronique Zimpfer²

¹Laboratoire de Physique et Mécanique Textiles, UHA, Mulhouse, France

²Institut Franco-Allemand de Recherches de Saint Louis, France

floriane.leclinche@uha.fr

INTRODUCTION

Sound is one of the sensory comfort features required by consumer. The sounds produced by garments can be expected for instance the rustling sound of silk or can be uncomfortable for example sounds of waterproof garments. The noise generated by fabric-to-fabric friction in the frame of military applications is essential to be studied in order to improve acoustic stealth. Although a literature review revealed some works on visual stealth, not enough work has been done in terms of acoustic stealth. The sound generated by the fabric friction is not constant along the time due to the wearing process induced by washing and use of garments. These constraints can be considered as low mechanical stress and repeated frictions will gradually modify the surface of the fabric. The ageing of material can be estimated thanks to fabric friction sound analysis.

The aim of this study is to analyze the influence of wear and washing processes on fabric friction sound generated by the friction under arms or between legs when a person is moving or walking. Previous studies have shown that the sound properties of fabrics depends on many parameters like the weave patterns or the surface roughness.

APPROACH

In this study, two sets of fabrics have been used. One is composed of samples, which are worn out thanks to Martindale abrasion tester. The second set is worn out through multiple washing (50 washes). For each sample, several acoustic parameters and mechanical properties especially compression and surface properties have been measured. The mechanical properties of the fabrics are measured thanks to the Kawabata Evaluation System [1]. The fabrics were all conditioned during 24 hours in standard conditions (relative humidity $HR\% = 65 \pm 5\%$, temperature $T = 20 \pm 2^\circ\text{C}$). Acoustic measurement is achieved using an acoustic booth (Figure 1) equipped with a system reproducing the human arm motion thanks to two samples rubbing together; one sample is fixed and the other one is mobile. Both samples are placed above a silicone surface which reproduces the human skin [2]. A microphone Brüel & Kjaer 1 inch (type 4190) is used to detect the friction noise of the fabric specimen. The sound recording is performed thanks to a Brüel & Kjaer amplifier (type 2606). Duration of tests is around twenty seconds and some parameters, like the speed or the angle of scanning which were experimentally fixed, are constant.

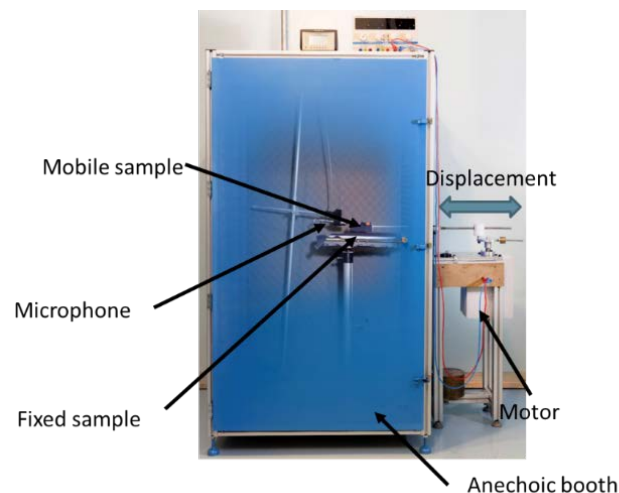


Figure 1: Experimental device.

The processing of the sound [3] is performed in three steps. Firstly, two or three seconds of the recording are selected using the Audacity® software. Secondly, the signal is processed by a high-pass filter. This filter will allow to delete the interference noises essentially in the low frequencies. Finally, the filtered sound signals are processed through FFT which allows to estimate the third octave band from 20 Hz to 20 kHz and to obtain noise level in dB.

RESULTS AND DISCUSSION

The Figure 2 represents the evolution of the total noise level according to the fabric's ageing. According to the obtained results, three domains can be observed. In the first one (from 0 to 5,000 abrasive cycles), the total noise level increases which is followed by a decrease from 5,000 to 12,000 cycles. Finally, in the last zone, the total noise level goes to a stable value. In the first two areas, two linear correlations have been found between the total noise level and the number of abrasive cycles i.e. the degree of wear of the specimens.

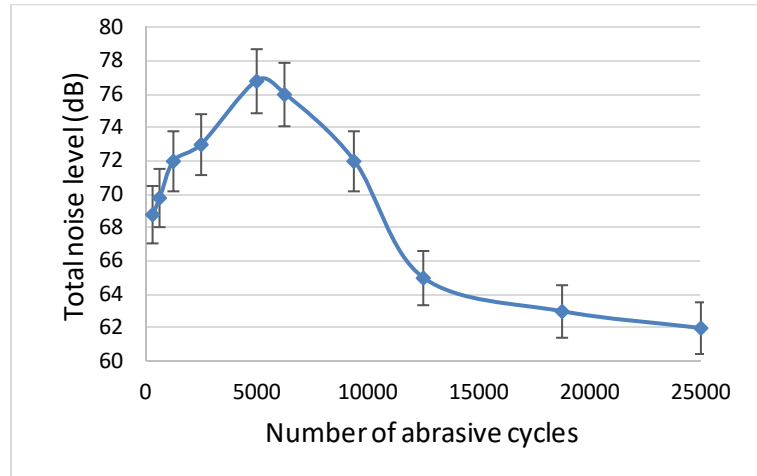


Figure 2: Evolution of the total noise level according to the degree of wear of samples.

Regarding to the influence of washing, the Figure 3 shows the evolution of the total noise level. A different behavior can be observed compared to the Figure 2. In this case, the total noise level quickly decreases to reach a stable value. After 10 washes, we can conclude that the fabric's ageing, due to washing, will have a slight influence on the noise level.

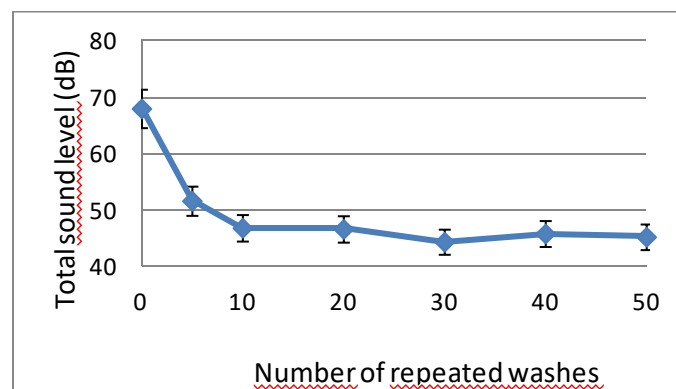


Figure 3: Evolution of the total noise level according to the number of washes.

A statistical analysis (Principal Component Analysis) has been done in order to find relationships between acoustic, compression and surface parameters for abrasion [Figure 4(a), and for the washing method, Figure 4(b)].

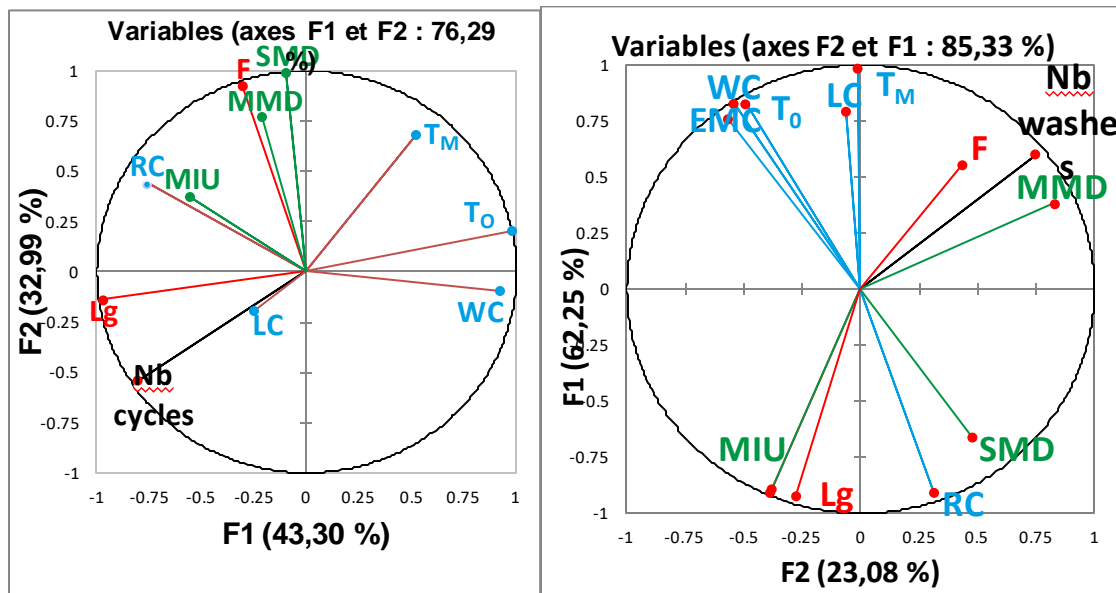


Figure 4: Principal Component Analysis: (a) set of fabrics worn out by abrasion; (b) set of fabrics washed repeatedly.

According to Figure 4(a), there are several correlations between the parameters. The total noise level (Lg) is correlated to the number of abrasive cycles (N), with the increase of it the number of free fibers on the fabric's surface will increase too. Therefore, there are more contact points between the two fabrics when they rub against each other and the total sound level is higher. The total sound level and the number of abrasive cycles are anti-correlated to compression properties (WC and T0). The fabric's thickness is going to decrease with the increase of the number of abrasive cycles because some material will be gradually removed from the fabric's surface.

Regarding to the peak frequency (F), it is correlated with surface properties (MMD and SMD). Indeed, the wear of the textile surface is going to cause a change in surface condition and thus the roughness, which is consistent with a change of acoustic signature.

If we look at the Figure 4(b), different correlations can be observed; only the surface properties are correlated with acoustics ones. The difference could be explained by the chemicals composing the detergent used for the washing which create a kind of coating around the fibers and change mainly change the surface properties.

CONCLUSION

Fabric's ageing has a significant influence on fabric friction sound but also on the compression and surface properties of the fabric. From the comparison between the two methods used to wear out the samples, we can conclude that the total sound level (Lg) is strongly correlated to compression and surface properties whereas the peak frequency (F) is more linked to the surface properties. The evolution of the total noise level is different according to the method used.

The follow-up study will be to conduct the same analysis on other kind of fabrics and to develop a sensory panel to compare instrumental and sensory approaches.

REFERENCES

- [1] Kawabata, S. *The Standardization and Analysis of Hand Evaluation*. 2nd ed. Osaka, Japan: Textile Machinery Society of Japan, 1980.
- [2] Yosouf, K., Latroch, H., Schacher, L., Adolphe, D. C., Dréan, E., Zimpfer, V. "Frictional sound analysis by simulating the human arm movement." *Autex Res. J.*, Vol. 17, 2017: 1.
- [3] Yosouf, K., Dréan, E., Schacher, L., Adolphe, D. C., Moukadem, A., Dieterlen, A., Zimpfer, V., Pellerin, V. "New Method to Characterize the Sound-Generated Fabric Friction." *The Fiber Society Spring Conference Proceedings*, 2014: 97-98.

Fundamentals for Memory Fibers and Their Potential

Jinlian Hu, Harishkumar Narayana , Shanshan Zhu

Institute of Textiles and Clothing, The Hong Kong Polytechnic University, Hong Kong

tchujl@polyu.edu.hk

Memory polymeric fibers can be made into smart materials which sense the environment, make a judgement and memorize specific properties. Two typical categories in memory polymers (MPs) are shape memory polymers (SMPs) and stress memory. SMPs have the capability to memorize a permanent shape after they are programmed for a temporary shape upon external stimuli. In general, SMPs are composed of at least two various structural components, which can be called soft segments in charge of temporary shape and hard segments in charge of permanent shape. Based on our new understanding, SMPs are composed of three structural elements, namely, netpoints, switch and rubbery chains. Recently a novel stress-memory concept was proposed by our group, in which the stress in a material can be programmed, stored, and retrieved reversibly with an external stimulus. However, this stress-memory cannot be simply guaranteed by shape-memory-effect. A significant memory stress was found in semi-crystalline MP with T_m -switch, which expresses enthalpy change, first-order transition, and was proved to take main responsibility for achieving memory-stress. For the other important SMP with T_g -switch, memory stress is generated only in small degree and by entropy change, second-order transition, which is similar to rubber. Thus, we can say that shape memory has less stringent conditions for either first order or second order thermodynamic transition, but stress-memory has much higher requirements that can only be satisfied by first order transition with enthalpy variation. Crystals which can provide enthalpy change are capable of modulating the entropic energy to possess good stress-memory ability. The three basic elements in such stress-purposeful MP: net-points to hold the whole structure, rubbery chains with entropy change and switch with enthalpy change. Based on the results of T_m type MPs, memory fibers were proved to possess higher memory stress than films, because the thermal properties, melting transition and enthalpy of memory fibers are higher than those of the films. Thus stress-memory filaments are advantageous for utilization into smart compression stockings, where the stress/internal pressure can be maintained the minimum baseline pressure and controlled externally by a thermal stimulus. Several new concepts were originated from this fundamental study. Understanding the role of switch enthalpy and extrapolates it beyond crystals such as reversible chemical bonding to non-thermal stimuli can broaden the scope of structural and behavioral design of smart fibers. We anticipate their wide-spread application in energy storage and mechanical control of this family of materials, such as electronics, artificial organs, aerospace, and biological and physical massage systems.

ACKNOWLEDGMENT

The authors would like to thank the funding support from HK Research Grants Council (RGC) with General Research Fund (GRF) for the project: Fundamental Study of Stress Memory and Its Application in Smart Compression Stockings Using Memory Polymer Filaments (#: PolyU 15204416).

Fabric Drape Model Considering Shear and Bending

Liu Yang¹, KyoungOk Kim², Masayuki Takatera²

¹Graduate School of Science and Technology, Shinshu University, Japan

²Division of Kansei and Fashion Engineering, Institute for Fiber Engineering (IFES), Interdisciplinary Cluster for Cutting Edge Research (ICCER), Shinshu University, Japan.

takatera@shinshu-u.ac.jp; 15fm227c@shinshu-u.ac.jp

A prediction model for fabric drape when shear stiffness is infinite and zero considering bending rigidity is developed. The proposed model is verified with experimental drapes. Most of the fabrics are in an area between two theoretical lines for infinite and zero shear stiffness. Drape coefficient (DC) can be predicted using a regression equation with bending rigidity, shear stiffness, weight, and dimension of fabric, drape coefficient

INTRODUCTION

Garment simulation lacks accuracy because of the conversion problem between mechanical properties of fabric and related parameters in simulators. In Fabric Research Laboratories (FRL) drape test, drape coefficient (DC) is used for evaluating fabric drapability. A similarity rule for a fabric cantilever is $K = L\sqrt[3]{w'/B}$, here L is sample length, B is bending rigidity per unit width, and w' is fabric weight per unit area. However, drape deformation is not described in any analytical formulae. In this study, a drape prediction model is proposed to clarify drape deformation in the view of bending and shearing.

DRAPE PREDICTION MODEL

In the case of FRL drape test, if the effect of shear is ignored, the drape deformation can be considered as bending deformation of circular segment beam. Hence, the deformation can be described as Equation 1.

$$-2B \frac{d^2\theta}{ds^2} = w' \frac{R}{\sqrt{1 - \left(\frac{s'+R_0}{R}\right)^2}} \left[\cos^{-1} \frac{s'+R_0}{R} - \frac{1}{2} \sin \left(2 \cos^{-1} \frac{s'+R_0}{R} \right) \right] \sin \theta \quad (1)$$

Here, w' : weight per unit area; s' : arc length from the fixed end; R : radius of the fabric sample; R_0 : vertical distance from the origin to the bending line under the critical condition; θ : slope of the fabric.

EXPERIMENTAL

To verify the theory and clarify effects of bending and other properties on fabric drape deformation, drape tests were performed on seven kinds of woven fabrics and two kinds of sheets. Bending rigidity and shear stiffness of the samples were measured by Kawabata Evaluation System. The radius r of the support disk was set from 1.5 cm to 8 cm at intervals of 0.5 cm. For each disk radius, sample radius R was set as twice of r , $R=2r$. Thus, the disk radius r is equal to the sample length L . The node number n of the drapes was manually set as 3, 4, 5, and 6.

RESULTS AND DISCUSSION

Comparison results of theoretical and experimental data indicate that fabrics, except for fabrics with lower bending rigidity and shear stiffness, are in the range of two critical conditions of zero and infinite shear stiffness. When K is small, shear deformation is resisted, while when K is large, shear deformation occurs and caused a wave-shape of drape. A multiple regression equation for prediction of DC is also given.

Effect of Drying Temperature on Shrinkage Ratio of Knitted Clothing

Yurika Hashimoto¹, KyoungOk Kim², Masayuki Takatera² Kazuhiko Hashimoto³

¹Graduate School of Science and Technology, Shinshu University, Japan; ²Institute for Fiber Engineering (IFES), Interdisciplinary Cluster for Cutting Edge Research (ICCER), Shinshu University, Japan; ³Panasonic Corporation, Kusatsu City, Japan

takatera@shinshu-u.ac.jp; 17fs209j@shinshu-u.ac.jp

The relationship between washing and drying conditions and shrinkage of knitted clothing is still unclear. We investigated the relationship between drying temperature and the shrinkage ratio of various knitted clothing by drying after wetting. It became clear that cotton knitted fabrics are not affected by the over-drying condition. Regarding socks, the shrinkage increased due to over-drying and rise in temperature during drying.

INTRODUCTION

Shrinkage of knitted clothing due to washing and drying is affected by many factors such as material, structure, laundering conditions and etc. However, the effect of drying temperature on various knitted clothing is still unclear. In this study, we investigated the relationship between drying temperature and the shrinkage ratio of various knitted clothing by drying after wetting.

EXPERIMENTAL

We investigated the effect of drying temperature conditions on shrinkage rate of knitted clothing. A cotton knitted fabric and a pair of socks (cotton 59.5%, acrylic 25.5%, polyester 13.5%, polyurethane 1.5%) were used as samples. We dehydrated the samples by pressing slightly. On the samples, marks were drawn to measure the length. The samples were pretreated in a chamber of 40 °C and 5% RH for 60 minutes. Then, we measured the sample mass and length as an initial value. After preconditioning, the samples were immersed in water of 25 ± 2 °C for 30 minutes. After immersing, the samples were dried in the chamber. The humidity in the chamber was set at 5% RH. The drying temperature was set as from 40°C to 60 °C and from 60°C to 40°C. Moreover, we over-dried the samples at 40°C and 80°C respectively for 6 hours. During drying, the mass was measured every 30 minutes. When the moisture content becomes less than 1% or when there is no change in mass, the mark distances were measured, and the shrinkage ratios ΔL were calculated by $100 \times (L_2 - L_1) / L_1$, where L_1 is initial length and L_2 is length after drying.

RESULTS AND DISCUSSION

There was no difference in the shrinkage ratio of cotton knitted fabric even when the sample was over-dried. Regarding the socks, the shrinkage ratio became larger when it is over-dried. Moreover, the shrinkage ratio of socks when raising the temperature during drying was larger than one of the socks when lowering temperature during drying. It is conceivable that high-temperature conditions before and after finishing drying affect shrinkage ratio of socks. It will be due to the shrinkage of acrylic fiber [1].

CONCLUSION

It became clear that cotton knitted fabrics are not affected by the over-drying condition. Regarding socks containing acrylic fiber, the shrinkage increased due to over-drying and rise in temperature during drying. Therefore, it was conceivable that the temperature before and after finishing drying is related to shrinkage ratio of socks.

REFERENCE

[1] Hurley, R. B. "The dimensional stability of acrylic knit fabrics." *Textile Research Journal*, 36.11, 1966: 989-93.

Evaluation of Nanoscale Structure and Mechanical Properties of Fibers Using FIB-notch Techniques

Taylor Stockdale, Yuris Dzenis

University of Nebraska-Lincoln

ydzenis@unl.edu; taylor.stockdale@huskers.unl.edu

From natural to synthetic, textile to high-performance, fibers find utility in a wide variety of applications today ranging from delicate linens and tissue scaffolding to more strenuous applications including mooring lines, ballistic fabrics, and reinforcement in structural composite materials. Correlating structure with measured mechanical properties aids in selecting fibers for specific applications. Bulk fiber mechanical properties can be measured through tensile testing, while structural properties are generally realized through spectroscopy and diffraction techniques. Useful diffraction measurements are limited to fibers that possess highly crystalline structure (e.g., high-performance polymer fibers), so other techniques are necessary to elucidate the organization of structure in fibers with lower degrees of crystallinity (e.g., textile or natural fibers). While spectroscopic techniques (Raman, FTIR, etc.) can effectively give chemical structure data with orientation, data of this type lack physical representation.

Recently, a novel technique was developed that allows rapid access to the internal surfaces of individual fibers, which can be subsequently imaged using high resolution atomic force microscopy (AFM).¹ The technique uses a focused ion beam (FIB) to introduce artificial notches in single fibers. In highly oriented crystalline fibers, a natural cleavage plane facilitates fracture between the notches, providing access to the internal surface of the fiber without disrupting the finer nanoscale morphology. Fracture surfaces are subsequently imaged using AFM. In addition to real space imaging capabilities, AFM characterization can measure nanomechanical properties of the smallest features in these fibers. In this investigation, we demonstrate the use of the FIB to notch and access the internal surfaces of several different fiber types ranging from natural (plant and silk) to textile and high-performance fibers. Fractured fibers were mounted, and internal surfaces were characterized using SEM and AFM with special emphasis on differentiating various nanoscale morphologies between fiber types. For example, highly ordered nanofibrillar structure was observed to be more pronounced in high-performance polymer fibers. The obtained results provide useful insights into characterizing nanoscale morphologies in individual fibers without having to use more aggressive techniques such as microtoming. The developed techniques can be used in ageing studies, where the degradation of internal structures in fibers can be directly observed.

REFERENCES

1. Stockdale, T.A., Strawhecker, K.E., Sandoz-Rosado, E.J., Wetzel, E.D. "A rapid FIB-notch technique for characterizing the internal morphology of high-performance fibers." *Materials Letters*, 176, 2016: 173-76.

A Novel Approach to Evaluate Thermal Protective Performance of Clothing Subjected to Stretching Forces

Yun Su^{1,2}, Rui Li², Jie Yang², Guowen Song², Chunhui Xiang², Jun Li^{1,3}

¹College of Fashion and Design, Donghua University, Shanghai, China; ²Department of Apparel, Events, and Hospitality Management, Iowa State University, Ames, Iowa, USA; ³Key Laboratory of Clothing Design and Technology, Ministry of Education, Shanghai, China

gwsong@iastate.edu

Protective clothing system used for firefighters is designed to provide effective thermal protection for firefighters in fire extinguishing or rescuing operations. However, fabric deformation occurred due to body movement and postures could dramatically change thermal protective performance. The lack of information on fabric deformation and its impact on clothing performance suggested current testing methods on clothing performance evaluation are not sufficient. Therefore, it is necessary to investigate the effect of fabric deformation on thermal protective performance.

A stretching device with a cylindrical copper calorimeter was developed. The device was designed to simulate the fabric deformation or stretch in a cylindrical configuration as the result of body movement or typical body posture in the firefighting. Stretching forces (0, 1.2, 2.1 and 3.1 psi) were applied to simulate the effect of fabric deformation and its effect on thermal protective performance of clothing under low and high intensity heat exposures was investigated with the time to generate skin burn. The correlation between skin burn time and fabric properties (thickness and density) was examined. Additionally, change of heat flux absorbed by skin over the applied stretching force was compared. The results exhibited that the fabrics were stretched around 15% under 3.1 psi stretching force and the thermal protective performance of clothing was significantly reduced. The difference of skin burn time among different stretching forces demonstrated a decrease over the increase of stretching forces. As shown in Table I, the skin burn time predicted for the configuration with an air gap was significantly larger than that of no air gaps. The difference of predicted skin burn time with different applied stretching forces demonstrated a decrease trend. Additionally, the higher intensity heat exposure (84 kW/m²) decreased the effect of stretching force on the thermal protective performance, which was relevant to fabric shrinkage and the increase of fabric thickness as the contribution of thermal degradation. Therefore, the fabric deformation due to body movement and different postures has an important impact on thermal protective performance of clothing. The findings from this study provides further understanding the thermal protective performance of clothing and it may lead to develop a new test approach to characterize and simulate the performance of clothing under real situation.

Table I. Decreasing percentage of predicted 2nd degree burn time under with/without air gap and different stretching forces.

	A1		A2		A3	
	8.5 kW/m ²	84 kW/m ²	8.5 kW/m ²	84 kW/m ²	8.5 kW/m ²	84 kW/m ²
Air gap (6.4 mm)	0	0	0	0	0	0
No air gap (0 psi)	53.68%	52.49%	55.55%	32.19%	57.08%	59.91%
No air gap (1.2 psi)	15.57%	8.14%	9.84%	4.04%	6.27%	1.18%
No air gap (2.1 psi)	3.63%	2.53%	1.59%	5.26%	0.14%	1.19%
No air gap (3.1 psi)	0.97%	-0.13%	1.00%	1.11%	1.65%	0.00%

Testing Method for the Evaluation of Flammability of Meta-aramid Blended Yarns

Jie Feng, Tao Hua, Min Zhang, Ka Hei Chan, Wong Man Ching

Institute of Textiles and Clothing, The Hong Kong Polytechnic University, Hong Kong, China

tao.hua@polyu.edu.hk

The flammability behavior of fabric depends on the fabric structure and yarn properties, particularly on the yarn flammability. However, there are no such testing methods for the evaluation of yarn flammability. Therefore, this study aims to develop a simple and effective testing method for the evaluation of flame resistance of meta-aramid/cotton blended yarns at different blended ratios, which can be used to predict and give an overview of the flammability of the resultant fabrics.

Referring to the testing standards of 16 CFR Part 1610 and ASTM D1230 for fabric flame resistance, a protocol for the testing of yarn flame resistance is setup. Figure 1 shows the designed testing samples and their testing machine for the yarn flame resistance. The blended yarns are wound on the designed testing template in the lengthwise direction and its density is 120 yarns/in. 32 Ne meta-aramid (A)/cotton (C) fiber blended yarns at five blended ratios (24A/76C, 31A/69C, 48A/52C, 65A/35C and 72A/28C) produced in a conventional ring spinning frame are used for the evaluation of their flame resistance.

As the same as the test of fabric flame resistance, three important properties, afterflame time, afterglow time and damage length, are used to evaluate yarn flame resistance. Lower afterflame and afterglow time and damage length imply a better flame resistance of yarns. Here, the length of flame and the ignition time applied on the sample are important, which obviously influences the testing results of flame resistance. In the investigation, a 16 mm length flame and flame application times of 2s and 3s were adopted for all the yarn samples.



(a) Testing yarn samples



(b) Flame resistance tester
(Model: TC-45 220V 50HZ)



(c) Testing process

Figure 1. Testing method of yarn flame resistance.

The results of yarn flame resistance evaluated by using the testing method developed showed that with the increase of the proportion of meta-aramid fiber, the afterflame and afterglow time and damage length of yarns tend to be gradually reduced at both flame application times of 2s and 3s, which indicates that the use of higher proportions of meta-aramid fibers increases the flame resistance of blended yarns. On the other side, it can be concluded that the developed testing method for the evaluation of yarn flammability is feasible and can be simply and effectively used for the evaluation of flame resistance of meta-aramid/cotton fiber blended yarns.

ACKNOWLEDGMENT

The authors wish to thank the Innovation and Technology Commission of Hong Kong SAR Government, The Hong Kong Research Institute of Textiles and Apparel, X-Fiber (Hong Kong) Limited and Hang Hui Holdings (H.K.) Limited for funding support (Grant No. ITP/054/16TP).

Beyond Fibers and Ropes: Best Practices

Rafael Chou, David S. Tseng

Samson Rope Technologies, Ferndale, Washington, USA

rhou@samsonrope.com; dtseng@samsonrope.com

At a previous Fiber Society conference, Samson discussed the various approaches to evaluating and predicting synthetic fiber rope performance from a manufacturer's standpoint — "From Fiber to Rope Performance: A Two-way Approach" — identifying the underlying challenges and describing two approaches to better predict fiber rope specifications.

In this new presentation, Samson will discuss the other two important aspects of synthetic fiber ropes: application knowledge and industry standards. In order to properly design and select a rope, one needs to match the rope properties to the key application performance requirements. While factors such as cost, rope strength, elastic elongation, size, and weight are universal rope parameters, there are other factors that are very application-specific, such as tensile fatigue, bending fatigue, abrasion resistance, spooling, surface characteristics and stiffness. Hence, specific applications require more in-depth knowledge for the best product design and selection.

In addition to selecting and designing the right product, manufacturers also need to be sure to follow best practices to maximize both the efficiency and safety of any operation. Industry standards and field experience are the two sources to develop these best practices. By looking into individual cases and viewing the collective picture as a whole, this presentation aims to demonstrate how these elements are connected to integrating into a coherent selection and compliance practice for the best results.

Specific topics for in-depth discussion of some case studies also include assignable causes for cases with poor performance, selection of ropes, accessories, hardware options, and examples of the influence and guidelines of the various industry bodies for the best practice.

Online Appearance Inspection System of DTY Packages

Fei Li¹, Pei Feng¹, Ronggen Zhang¹, Qiang Fei¹, Chongchang Yang^{1,2}

¹Donghua University; ²Engineering Research Center of Advanced Textile Machinery, Ministry of Education

ycc@dhu.edu.cn; leavel302@126.com

The quality of the finished fabric is affected by the appearance defects of the draw texturing yarn (DTY). In the production process, the draw texturing yarn will form DTY package through a wingding mechanism. It is important to inspect the appearance defects of DTY packages. The inspection process of DTY has been always manually undertaken, which causes high intensity and low accuracy work. This paper develops an online inspection system of DTY on the basis of opto-mechatronics and imaging technology.

Firstly, a close study was done on the causes, categories and effects of external appearance defects of DTY packages. According to the categories and distribution of the defects, the areas to be inspected were classified. And then, according to the categories and distribution of the defects, the areas to be inspected were classified. After that, came up with a complex image capture scenario using both liner array and area array, selected necessary equipment for image capture, determined on the image capture system which was to use multiple cameras simultaneously.

Then, defect detection standard was determined through factory inspection standards and workers inspection experience to provide a quantitative basis for detection. A large number of sample images of the appearance defects were analyzed. This paper prepared those images of DTY packages captured in the test including picture segmentation and feature detection. And then, various superficial defects of tested DTY packages against the features extracted were detected. This paper finished the overall design of online inspection software and synchronized detection results to get an overall understanding of the external appearance of those tested DTY packages.

Finally, an online comparison between manual inspection and automatic inspection was done as a test. The results show that: the efficiency of the system is less than or equal to 4.4 second per spindle; the inspection accuracy of system is not less than 94%; it is applicable to conduct automatic inspection of the external appearance of DTY packages, which would cut 95% of manual costs while basically meeting relevant standards on DTY package external appearance inspection.

Sustainable Polymer Materials/Advanced Cellulose Fibers and Textiles

Research Activities on Bio-based Fibers in Toray Industries, Inc.

Yoshitaka Aranishi, Hidekazu Kano, Yoichiro Tanaka

Fibers & Textiles Research Laboratories, Toray Industries, Inc.

yoshitaka_aranishi@nts.toray.co.jp

INTRODUCTION

Biomass utilization is a growing issue coupled with the anxiety about limited exhaustible resources. In 2016, about 90 million tons of fibers were used in the world. Synthetic fibers account for 67.3 % of the total fiber production and these are made from fossil resources. For the purpose of maintaining the sustainable society, it is a momentous issue to utilize bio-based resources as a fiber raw material.

MELT SPINNABLE NEW TYPE CELLULOSIC FIBERS

Cellulose, the hugest organic resource on the earth, is getting great interest and expectation as a raw material for many applications. Viscose rayon and cellulose acetate are typical cellulosic filaments and widely used in the world. However, conventional cellulosic filaments require harmful organic reagents as solvent during the wet spinning or dry spinning of the fibers.

The reason why cellulose doesn't have thermo-plasticity is the strong hydrogen bonds between OH groups of the cellulose molecules. Bulky aliphatic acids esterification gives thermoplasticized cellulosic composition. As long as the compositions are designed to have low melt and elongational viscosity, melt spinning of the thermoplasticized cellulosic compositions are successfully conducted. Thinning profiles of the running filaments are specific and different from common polymers because of the rigidity of the molecules. Wide variation of the fiber cross sections such as tri-lobal fibers, hollow fibers, sea-islands type conjugated fibers are one of the merit of using melt spinning for fiber making process.



Figure 1. Various cross sections of melt spun cellulosic fiber.

POLYESTER FIBERS MADE FROM BIOMASS MONOMERS

Polyester fibers are widely used around the world owing to their good mechanical properties. Production amount of the PET fibers in 2016 was 52 million tons, which is about 60% of the total fiber consumption. If we can produce bio-based polyester fibers, it would bring a favorable effect with their huge amount of the production.

PET is made from ethylene glycol and terephthalic acid. Ethylene glycol can be easily produced from bio-ethanol, however, it is quite difficult to produce bio-based terephthalic acid, which has an aromatic ring in the molecule, directly via biological procedures.



Toray succeeded in producing 100% bio-based PET fiber made from bio-EG and bio-TPA, with the aid of chemical oxidation processing with bio-based xylene. 3GT fibers which made from bio-based propylene glycol and TPA are partially bio-based fiber. Because of the polymer configuration, 3GT fibers show specific stretch properties. These bio-based polyester fibers with specific properties will be also discussed.

Figure 2. 100% bio-based PET fiber made from bio-EG and bio-TPA.

Cellulose Dissolution in Ionic Liquids: A Theoretical Study

Takuya Uto, Kazuya Yamamoto, Jun-ichi Kadokawa

Graduate School of Science and Engineering, Kagoshima University, Kagoshima, Japan

kadokawa@eng.kagoshima-u.ac.jp

INTRODUCTION

Cellulose is an important fibrous material because of its abundance in nature, while it is known to be poor in processability and solubility due to a highly crystalline feature. Therefore, solvents that can efficiently dissolve cellulose are highly in demand for practical application. Recently, ionic liquids have been attracting attention as solvents to dissolve polysaccharides since it was reported that 1-butyl-3-methylimidazolium chloride (BMIMCl) dissolved cellulose¹. Although ionic liquids are widely reported to dissolve cellulose, little has been studied on the detailed dissolution mechanism. In this study, we adopt molecular dynamics (MD) approach to study the dissolution of cellulose crystal model in imidazolium-based ionic liquids² (Fig.1).

METHODS

The crystal models were constructed from either 9, 10 or 30 cellulose chains with DP = 10 or 20 according to the structure of cellulose I β ³. The MD simulations were carried out for the models in ionic liquids under the constant temperatures (400K or 450K) and pressure (1bar).

RESULTS AND DISCUSSION

It was observed that ionic liquids penetrated between the molecular chains accompanied with cleavage of the hydrogen bonds as the dissolution process. Moreover, in the ionic liquids, which showed excellent solubility, such as 1-allyl-3-methylimidazolium chloride (AMIMCl) and 1-ethyl-3-methylimidazolium chloride (EMIMCl), after cleavage of hydrogen bonds proceeded, the molecular chains were peeled from crystal phase and dispersed (Fig. 2). On the other hand, in BMIMCl and imidazolium acetates, cellulose chains were peeled off, and the slow uptake of cations into molecular chains resulted in insufficient hydrogen bond cleavage. In addition, the MD simulation for cellulose crystal in imidazolium bromide, which did not dissolve cellulose, showed no changes in the crystal model.

The MD trajectory analysis revealed that the microcrystalline cellulose solubility⁴ vs. the number of intermolecular hydrogen bonds had relatively good correlation (Fig. 3).

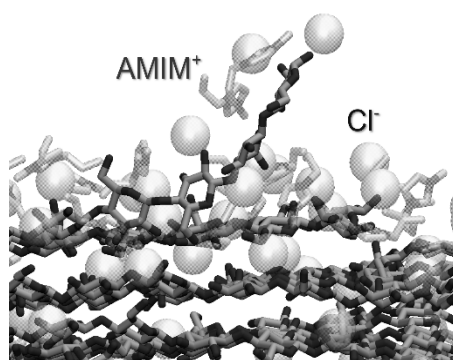


Fig. 2. Dissolution behavior of cellulose crystal in AMIMCl after 75ns at 450K.

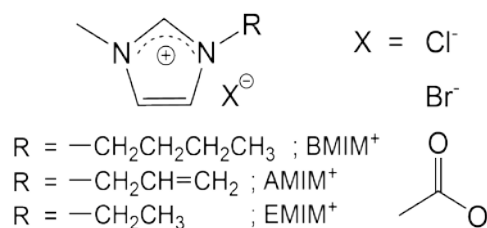


Fig. 1. Imidazolium-based ionic liquids used as solvents in this study

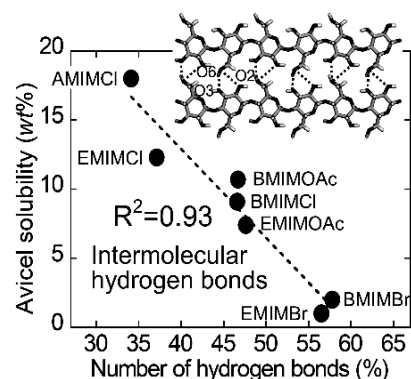


Fig. 3. Relationships between cellulose solubility and the number of hydrogen bonds in crystal model at 400K.

REFERENCES

- [1] R. Swatloski, S. Spear, J. Holbrey, R. Rogers. *J. Am. Chem. Soc.*, 124, 2001: 4974-75.
- [2] T. Uto, K. Yamamoto, J. Kadokawa. *J. Chem. Phys. B*, 122, 2018: 258-66.
- [3] Y. Nishiyama, P. Langan, H. Chanzy. *J. Am. Chem. Soc.*, 124, 2002: 9074-82.
- [4] N. L. Mai, Y. M. Koo. *ACS Sustainable Chem. Eng.*, 4, 2016: 541-47.

Highly Stiff Cellulose Fibers Spun from Liquid Crystalline Microcrystalline Cellulose Solutions Using DMSO as Co-solvent with an Ionic Liquid

Chenchen Zhu¹, Anastasia F. Koutsomitopoulou¹, Stephen J. Eichhorn¹,
Jeroen S. van Duijneveldt², Robert M. Richardson³, Kevin D. Potter¹

¹Bristol Composites Institute (ACCIS), University of Bristol, Bristol, U.K.

²School of Chemistry, University of Bristol, Bristol, U.K.

³H. H. Wills Physics Laboratory, Physics Department, University of Bristol, Bristol, U.K.

chenchen.zhu@bristol.ac.uk

There is enormous desire to develop sustainable and high-performance replacements for glass fibers, as well as alternative precursors for carbon filaments. As the most abundant natural polymer in the world, cellulose attracts public attention due to its numerous advantages (e.g. low-cost, sustainability, biocompatibility, biodegradability, good molecular order and molecular strength). Ionic liquids (ILs) are considered as a new-class solvent to replace the traditional approaches to the dissolution of cellulose, due to their chemical and thermal stabilities, reusability, and performance. An IL 1-ethyl-3-methylimidazolium diethyl phosphate (EMImDEP) has been selected in this study, due to its excellent properties such as low melting point, high hydrogen bond acceptor capability, as well as its comparatively low viscosity.

In this study, a novel and cost-effective route, with the addition of co-solvent, is presented to produce well-controlled and continuous cellulose fibers with exceptional mechanical properties (specific Young's modulus same as E-glass fibers) from liquid crystalline solutions. This route involves a one-step dissolution process followed by a dry-jet wet fiber spinning procedure. Low-cost and non-toxic dimethyl sulfoxide (DMSO) has been used as co-solvent with EMImDEP to improve the dissolution of cellulose, while reducing the dissolution time, temperature and the viscosity of cellulose solutions. Strongly optically anisotropic patterns appear for cellulose solutions, and their clearing temperatures are above 100-105°C. Highly aligned, stiff cellulose fibers (Young's modulus up to ~41 GPa) have been spun from cellulose/EMImDEP/DMSO solutions, using high concentrations of low molecular weight microcrystalline cellulose (usually used for low mechanical property applications like medical tablets and foodstuffs). The significant alignment of cellulose chains along the fiber axis has been confirmed by Scanning Electron Microscopy (SEM), Wide-Angle X-ray Diffraction (WAXD), and Powder X-ray Diffraction. This work demonstrates a route with great potential to convert low-performance cellulose waste into high-performance fibers for the applications as composite reinforcing fibers and carbon fiber precursors, while significantly reducing the processing time and cost.

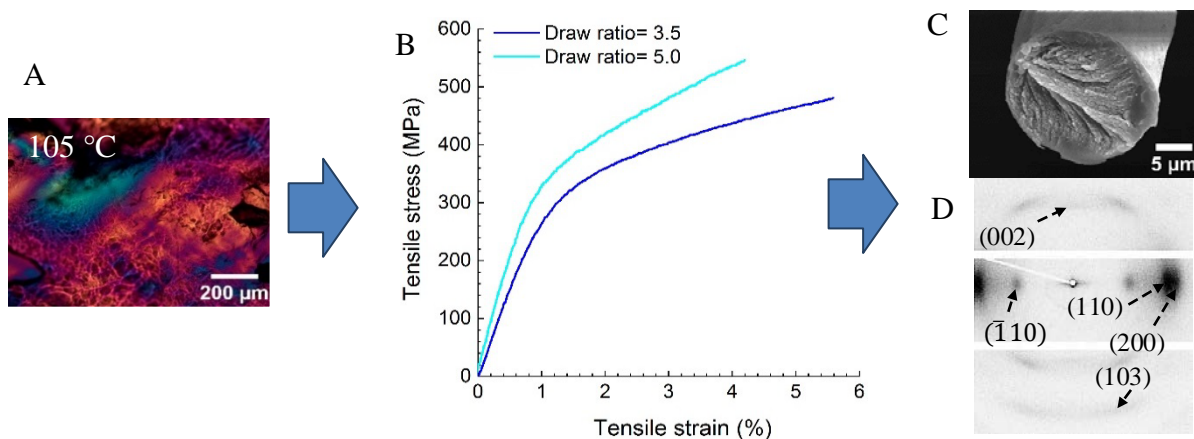


Figure 1. (A) Polarized optical micrograph of cellulose/EMImDEP/DMSO solution at 105°C; (B) tensile stress-strain curves of cellulose fibers; (C) typical fiber cross-section (SEM); (D) a typical WAXD pattern for a single cellulose fiber.

Hierarchical Core-Sheath PPy@CNT/BC Macrofibers with High Electrochemical Performance for All-Solid-State Supercapacitors

Jingjing Yao, Shiyan Chen, Huaping Wang

State Key Laboratory for Modification of Chemical Fibers and Polymer Materials,
College of Materials Science and Engineering, Donghua University, Shanghai, China

chensy@dhu.edu.cn

Fiber-based supercapacitor have gained great attention since they are convenient to integrate with wearable electronics and incorporated into fabrics easily. However, the quest for high energy and power densities of fiber-based supercapacitor remains a challenge. Herein, a highly flexible polypyrrole decorated carbon nanotube/bacterial cellulose fiber-based supercapacitor assembled by multiple nanoscale supercapacitors with hierarchical core-sheath and the porous structure is carefully designed. The bacterial cellulose in fiber-based supercapacitor not only efficiently prevent the aggregation of carbon nanotubes and significantly improve the wettability of supercapacitor, but also may act as electrolyte nano-reservoirs, which would accelerate the diffusion of electrolyte ions and improve the electrochemical performance. The inner hierarchical core-sheath structure and the mesoporous significantly increase the specific surface area of the supercapacitor and facilitate the ion transport resulting in enhanced considerably electrochemical properties. The assembled all-solid-state fiber-based supercapacitor realizes a desirable combination of outstanding electrochemical performance and excellent flexibility with excellent specific capacitance (228 F/g, 178 F/cm³ at the scan rate of 5 mV/s), high energy densities (19 mWh/cm³, 33.1 Wh/kg), and high cycling retention ability (over 6000 cycles), which would have great potential as the energy and power in various portable, miniaturized, and wearable electronic devices.

ACKNOWLEDGMENT

This work was supported by the National Natural Science Foundation of China (51573024 and 51273043), the Fundamental Research Funds for the Central Universities and DHU Distinguished Young Professor Program.

Preparation of Highly Stretchable Elastomeric Composites Reinforced with Well-defined Nanofiber Network of Bacterial Cellulose

Keita Sakakibara¹, Yoshihiko Shimizu^{1,2}, Yohei Nakanishi¹, Yoshinobu Tsujii¹

¹Institute for Chemical Research, Kyoto University, Kyoto, Japan

²Matsumoto Yushi-Seiyaku Co., Ltd., Osaka, Japan

sakaki@scl.kyoto-u.ac.jp

Cellulose nanofiber (CNF) possesses good physical properties such as elasticity and strength along the longitudinal direction. Furthermore, CNF has a high aspect ratio, having potential superiority as reinforcement fillers for polymer matrix. However, since CNF has hydrophilic nature on surface, the perfect dispersion in a polar polymer matrix is quite difficult. We are then intriguing bacterial cellulose (BC). Since native BC hydrogel is composed of highly fine and pure CNF network structure, ideal CNF/ polymer composite materials can be prepared by proper stepwise solvent exchange to any monomers following polymerization, even if CNF does not have much affinity for the corresponding polymers. In this paper, we demonstrate the preparation and highly-stretchable properties of BC/poly(ethyl acrylate) (PEA) composites materials.

The method for the preparation of BC/PEA composites is shown in Fig. 1. The key to success in the preparation is stepwise solvent exchange from water to EA by way of tetrahydrofuran (THF), in which any shrinkage, deformation, and break did not take place. Then, photo-initiated free radical polymerization of EA was conducted.

The BC/PEA composites obtained exhibited highly stretchable properties (Fig. 2a). Despite the small volume fraction of BC (approximately 0.4 vol%), the BC/PEA composite showed significant increases in Young's modulus (26 times larger than that of the neat PEA), tensile strength (3.5 times larger), and fracture energy (3.8 times larger), with its fracture strain (1520 %) almost the same as that of the neat PEA (1660 %). This composite was characterized by effective strain hardening. Confocal laser scanning microscopic (CLSM) observations revealed the structure of the nanofibers embedded in the elastomeric matrix (Fig. 2b). The enhanced mechanical properties were discussed based on the rigidity and flexibility of the BC nanofibers and their entangled network and were finally ascribed to the well-defined BC nanofiber network produced by the bacterium (Fig. 2c).

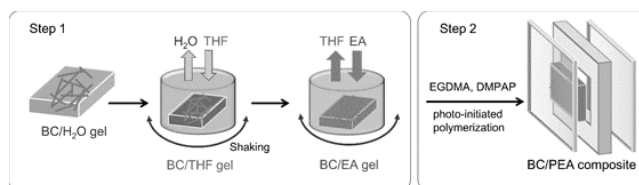


Fig. 1. Schematic illustration of the preparation of BC/PEA composites.

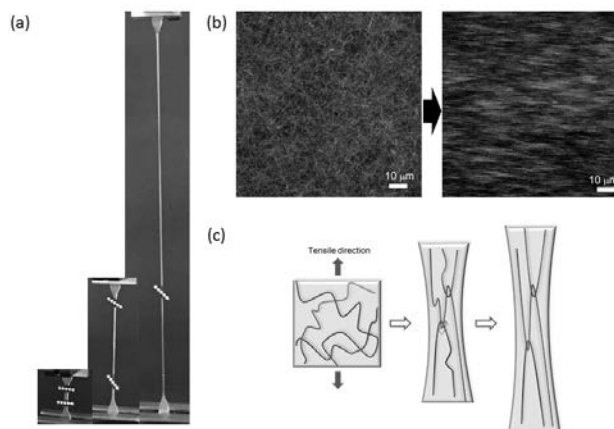


Fig. 2. (a) Images of the BC/PEA composite in tensile test; the strains were 0, 400, and 1400 % from left to right. (b) CLSM images of the composites before (left) and during (right) stretching, indicating high alignment of bacterial cellulose nanofibers. (c) Schematic illustration of the proposed BC-reinforcement mechanism of the BC/PEA elastomer.

Dynamic nanofiber network structure upon tension will be presented and critically discussed.

REFERENCE

1. Y. Shimizu, K. Sakakibara, Y. Tsujii. *J. Fiber Sci. Technol.*, 74, 2018: 17-23. (10.2115/fiberst.2018-0003)

ACKNOWLEDGMENT

This work was partly supported by JSPS KAKENHI (Grant Number 17H06238).

Effects of a Biobased Filler on the Crystallization Behaviors of Poly(L-lactic acid)

Amit Kumar Pandey¹, Rahul Patwa², Vimal Katiyar², Sono Sasaki¹, Shinichi Sakurai¹

¹Department of Biobased Materials Science, Kyoto Institute of Technology, Kyoto, Japan

²Department of Chemical Engineering, Indian Institute of Technology Guwahati, Assam, India

amitpandey886@gmail.com; shin@kit.ac.jp

INTRODUCTION

Poly (L-lactic acid) PLLA is one of the most frequently used biobased polyesters due to its biodegradability and favorable mechanical properties. However, some properties such as slow crystallization rate, low crystallinity and low thermal stability restrict its industrial applications. In order to overcome these limitations, a number of fillers from organic and inorganic origin have been investigated over the past few decades to reinforce the PLLA materials. Bio-fillers from plant and animal origins have been a subject of growing interests because of their availability and low costs. It has been found that the introduction of biobased fillers has a tendency to improve the thermal stability and slow crystallization behavior of PLA. In view of this, the current work has been focused on silk nanocrystals (SNC) and its effects on the crystallization behaviors of PLLA.

EXPERIMENTAL

PLLA, obtained from NatureWorks (grade 2003D) was used as the polymer matrix. The SNC used for this research work was prepared in the laboratory from the Muga silkworm by the acid hydrolysis treatment. PLLA/SNC composites were prepared by melt mixing of PLLA with varying loadings of the SNC in co-rotating twin screw extruder at 200°C. The thermal behavior of PLLA and PLLA/SNC composites were measured by DSC 2920 (TA Instruments). For isothermal crystallization, the samples were first melted at 200°C for 5 minutes and immediately cooled to 110°C and allowed to crystallize for 80 min.

RESULTS AND DISCUSSION

The kinetics of isothermal crystallization can be described by the well-known Avrami Equation. The degree of crystallinity (ϕ) as a function of time (t) can be expressed as:

$$\phi = 1 - \exp[-(kt)^n] \quad (1)$$

Therefore,

$$\log[-\ln(1-\phi)] = n[\log k + \log t] \quad (2)$$

where k is the crystallization rate constant and n is the Avrami exponent.

Figure 1 shows the degree of crystallinity as a function of time. It can be seen that the final degree of crystallinity increases even with the low loadings of SNC (0.5%). It is found by the isothermal crystallization experiment (DSC measurements) that the degree of crystallinity of PLLA increases but the rate of crystallization decreases with the inclusion of SNC. (Figure 2)

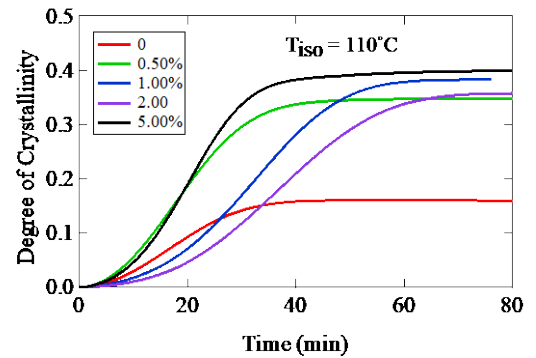


Figure 1. Degree of crystallinity as a function of time. These are the results of the isothermal crystallization experiment (DSC measurements) at 110°C upon the quickly quenching from melt at 200°C.

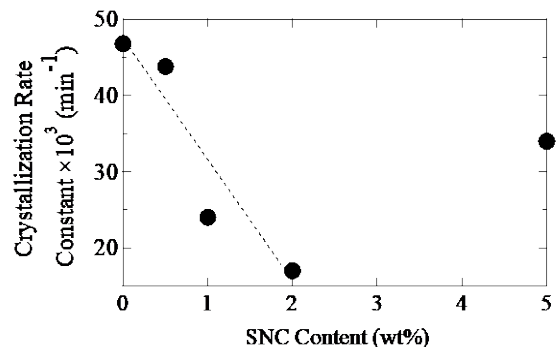


Figure 2. Crystallization rate constant as a function of the SNC loading.

Forcibly Spinning of *Bombyx mori* Silkworm Silk Ended in Complete Failure

Yutaka Kawahara

Division of Environmental Engineering Science, Gunma University, Kiryu, Japan

kawahara@gunma-u.ac.jp

Forcibly spinning method has once shown a potential to enhance tensile strength of silk fibers. Thus, the tensile data for the forcibly spun silk fibers reported so far were compared with the tensile data of commercial non-genetically hybridized F₁ silkworm fibers. The forcibly spinning method may be convenient to produce a finer filament. However, it is difficult to produce a long and strong filament comparable to the commercial silk fibers. On the contrary, the breeding technology which can reduce the number of molting from tetra to tri by feeding a specific imidazole compound was thought to be the most practical strategy to obtain a finer and stronger silk filament with a length more than 500 m.

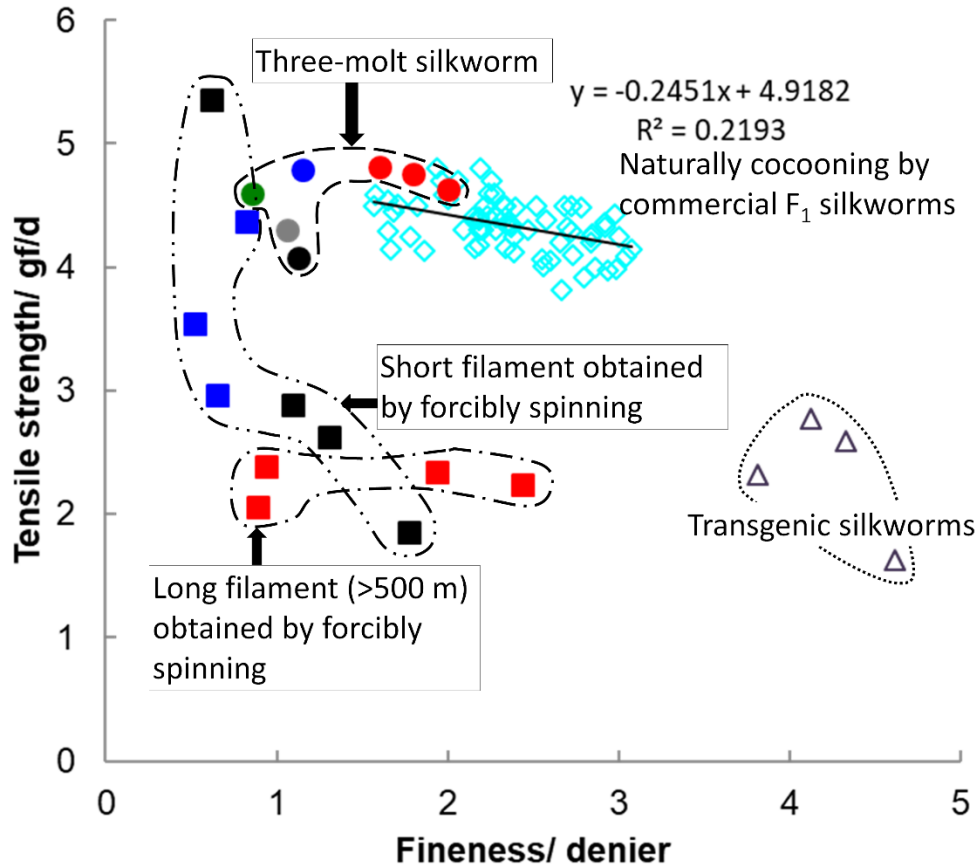


Fig. 1. Relation between tensile strength and fineness of filament. For the conversion of Pa unit into gf per denier, the density of 1.375 g/cm³ of raw silk filament containing 30 % sericin was used to convert the tensile data of as-forcibly spun fibers and the density of 1.365 g/cm³ of silk fibroin filament was used to convert the tensile data of degummed fibers.

Fabrication and Characterization of Transparent, Flexible, and Water-insoluble, Non-mulberry Silk Fibroin Films

Kelvin O. Moseti^{1,2,3}, Taiyo Yoshioka³, Tsunerori Kameda³, Yasumoto Nakazawa¹

¹Department of Biotechnology and Life Science, Graduate School of Engineering, Tokyo University of Agriculture and Technology, Tokyo, Japan

²National Sericulture Research Centre, Industrial Crops Research Institute, Kenya Agricultural and Livestock Research Organization, Thika, Kenya

³Silk Materials Research Unit, Institute of Agrobiological Sciences, National Agriculture and Food Research Organization, Japan

yasumoto@cc.tuat.ac.jp, okongok904@affrc.go.jp

We present a novel approach for the fabrication of high molecular weight, transparent, flexible and water-stable films from silk gland fibroin of the non-mulberry silkworm, *S. c. ricini*. Unlike the conventionally fabricated ones that are β -sheet rich, structural characterization of the films obtained by FTIR and ¹³C solid state NMR spectroscopy reveals that they are α -helix rich. Therefore, it is expected that they will exhibit different physical, mechanical and biomedical properties, hence the possibility of their utilization as new bio materials.

Structural Change and Its Effect on the Mechanical Property of Silk Induced by Tensile Deformation

Taiyo Yoshioka¹, Tsunenori Kameda¹, Kohji Tashiro²

¹Silk Materials Research Unit, National Agriculture and Food Research Organization (NARO)

²Department of Future Industry-oriented Basic Science and Materials, Graduate School of Toyota Technological Institute

yoshiokat@affrc.go.jp

INTRODUCTION

General silks, produced by domesticated- or wild-silkworms and spiders commonly show high toughness with excellent balance of strength and ductility in tensile deformation. However, in detailed observations, their tensile deformation behavior is not unique. While some of them, represented by the domesticated *Bombyx mori* (*B. mori*) silkworm silk, does not show any distinct yielding point in its stress-strain curve, the many of them, represented by the *Saturniidae* wildsilks and spider silks, show a clear yielding point and a subsequent plateau region before occurring the strain hardening. The aim of this study is to make clear the structural mechanism of the difference of these tensile behaviors. For this purpose, we performed a time-resolved synchrotron X-ray analysis during the stretching deformations of *B. mori* silk, showing typical former stress-strain curve, and *Antheraea assama* (*Muga*) silk, showing typical later one.

EXPERIMENTAL

The structural change of the degummed *B. mori* and *Muga* silks occurring in the stretching processes were investigated by the time-resolved simultaneous measurement of stress-strain curve and synchrotron WAXD and SAXS. The fiber bundle with a bundle thickness of about 1.5 mm of *B. mori* or *Muga* silks was set on a stretching device (micro-stretcher, Linkam Scientific Instruments Ltd., UK), which is set in a synchrotron X-ray beam line 40B2 at SPring-8 (Hyogo, Japan), and stretched with a stretching rate of 10 $\mu\text{m}/\text{sec}$. The WAXD and SAXS measurements were performed during the stretching with a time-interval of 10 seconds.

RESULTS AND DISCUSSION

As mentioned above, while *B. mori* silk showed a typical stress-strain curve without the distinct yielding point, *Muga* silk with a clear plateau region, as shown in Figures 1a and b, respectively. We simultaneously obtained a series of WAXD and SAXS patterns during the tensile deformations. For both of *B. mori* and *Muga* silks, the changes of crystal strain along the *c*-axis direction, defined as $\varepsilon_{002} = ((d_{002}(\text{initial}) - d_{002}(\varepsilon)) / d_{002}(\text{initial}) \times 100)$, were estimated and superposed with the corresponding stress-strain curve as shown in Figures 1a and b. In both cases, the changes of crystal strain ε_{002} well followed the stress-strain curve in the beginning. However, they deviated from the stress-strain curves and saturated at the macroscopic strains of about $\varepsilon = 8.5\%$ in *B. mori* silk and $\varepsilon = 5.0\%$ in *Muga* silk, respectively. The deviation point of *Muga* silk consisted with the starting point of plateau region. This indicated that the stress distribution regime was changed from homogenous to heterogeneous ones in both cases, and the plateau region of *Muga* silk appeared when the heterogeneous regime starts. This revealed that the structural origin of the appearance of plateau region is dominantly related to the structural change of amorphous part. The essential common and different parts between the *B. mori* and *Muga* silks will be discussed.

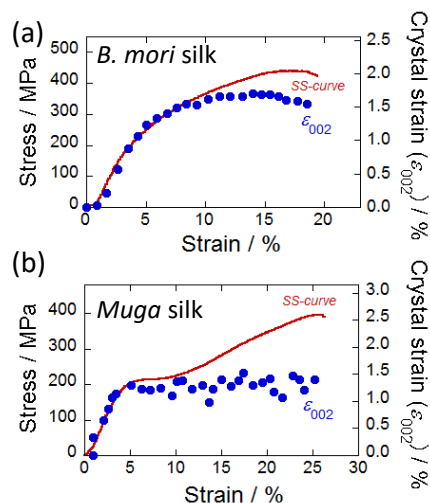


Figure 1. Stress-strain curve (red line) and the changes of crystal strain (blue plot) along the *c*-axis direction of (a) *B. mori* and (b) *Muga* silks.

High-performance, Bio-based Plastics Synthesized from Natural and Unnatural Polysaccharides

Tadahisa Iwata

Science of Polymeric Materials, Department of Biomaterial Sciences,
Graduate School of Agricultural and Life Sciences, University of Tokyo, Tokyo, Japan

atiwata@mail.ecc.u-tokyo.ac.jp

The increasing environmental and economic concerns on the utilization of petrochemicals have led researchers to rely on plant biomass as a feedstock for the synthesis of polymeric materials. Recently, our group succeeded to synthesize new thermoplastics from polysaccharides such as xylan, glucomannan, curdlan, pullulan, etc by esterification and found interesting thermal, mechanical, optical properties. Xylan is the most abundant hemicellulose with mainly β -(1 \rightarrow 4) linked xylose. Konjac glucomannan (GM) is isolated from tubers of *Amorphophallus konjac* plants and consists of β -(1 \rightarrow 4) linked D-glucose and D-mannose residues and the molecular ratio of glucose to mannose has been reported to be ca. 1.6. Curdlan is a linear polysaccharide with β -(1 \rightarrow 3) linked glucose produced by *Alcaligenes faecalis*. Pullulan is a water-soluble extracellular polysaccharide produced by strains of fungus *Aureobasidium pullulans*, consisting of a chain of maltotriose units that alternate regularly between α -(1 \rightarrow 6) linkages. In this paper, xylan, glucomannan, curdlan and pullulan ester derivatives are synthesized and thermal and mechanical properties are investigated. Furthermore, in the case of xylan ester derivatives, a possibility as bio-based nucleating agents for PLLA and PDLA is presented.

More recently, we succeeded the one-pot synthesis and development of unnatural-type bio-based polysaccharide, α -1,3-glucan. The synthesis can be achieved by in vitro enzymatic polymerization with GtfJ enzyme, one type of glucosyltransferase, cloned from *Streptococcus salivarius* ATCC 25975 utilizing sucrose, a renewable feedstock, as a glucose monomer source, via environmentally friendly one-pot water-based reaction. Furthermore, acetate and propionate esters of α -1,3-glucan were synthesized and characterized.

KEYWORDS: Bio-based polymers, polysaccharide ester derivatives, thermal property, optical property, enzymatic polymerization.

Development of Thermostable Polymers from Plant-derived Aromatic Hydroxy Acids

Daisuke Ishii^{1,2}, Tatsuya Goto¹, Kotaro Ino¹, Yukiko Enomoto¹, Tadahisa Iwata¹

¹Graduate School of Agricultural and Life Sciences, University of Tokyo

²Faculty of Life Sciences, Tokyo University of Agriculture

di206176@nodai.ac.jp

Plant biomass-derived aromatic hydroxy acids, such as ferulic (FA) and caffeic (CA) acids, are found in nature as plant metabolites and can be obtained from agricultural wastes such as rice bran and extracted coffee beans. In order to develop novel biomass plastics with improved thermal properties, molecular and thermal properties of the polyesters and poly(ester-amide)s of the aromatic hydroxy acids were investigated.

PROPERTIES OF POLYMERS SYNTHESIZED FROM PLANT-DERIVED AROMATIC HYDROXY ACIDS

(Co)polyesters of ferulic acid

While poly(ferulic acid), a homopolyester of FA, showed neither glass transition nor melting transitions, poly(ferulic acid-*co*-glycolic acid) (PFG) showed glass transition (T_g) at about 100 °C and melting transitions (T_m) at 160 and 210 °C. Furthermore, poly(ferulic acid-*alt*-glycolic acid), an alternating copolyester of FA and glycolic acid, showed melting transition at as high as 276 °C. The challenges of these copolyesters is to increase the molecular weight, that is currently up to 1.2×10^4 attained in poly(ferulic acid-*alt*-glycolic acid).

Polyester of caffeic acid

Poly(caffeic acid) (PCA) showed T_g between 100 and 110 °C. Although PCA did not show T_m , it showed shear flow behavior above the T_g and formed shear-induced mesophase. Furthermore, PCA with the molecular weight of 4.9×10^4 was successfully processed into melt-spun fiber. The PCA also showed degradation onset temperature of more than 300 °C. The broadness between the melting and degradation temperatures will contribute to the retention of material properties after thermal processing.

Copoly(ester-amide) of ferulic acid and glycine

Copolymerization of FA and glycine (Gly) was attempted by preparing three types of precursors: *N*-feruloyl glycine methyl ester (FAMG), *N*-feruloyl glycine (FAG), and *N*-(4-*O*-acetylferuloyl) glycine (AcFAG). These precursors were synthesized by amide coupling reactions between FA and the methyl ester of Gly, followed by protection/deprotection of the end groups. Polymerization of the these precursors was attempted in bulk or solution state to obtain poly[(ferulic acid)-*alt*-(glycine)] (P(FA-*alt*-Gly)), namely the alternating copoly(ester-amide) of FA and Gly. As the result, only AcFAG yielded P(FA-*alt*-Gly) containing a high-molecular weight fraction of more than 10^4 g/mol. Poly(AcFAG) (P(AcFAG)) is an amorphous polymer with the T_g of 189 °C, the 5-% weight-loss temperature ($T_{d5\%}$) of 297 °C, and the 50-% weight-loss temperature ($T_{d50\%}$) at 495 °C. The thermal property values are comparable to polyarylate, an existing petroleum-based aromatic polyester.

KEYWORDS: Aromatic polymers, ferulic acid, caffeic acid.

Utilization of Plant Biomass as Valuable Materials via Sustainable Process

Kazuhiro Shikinaka¹, Yuichiro Otsuka², Haruka Sotome³, Yoichi Tominaga³

¹National Institute of Advanced Industrial Science and Technology; ²Forestry and Forest Products Research Institute; ³Tokyo University of Agriculture and Technology

kaz.shikinaka@aist.go.jp

We report a simple yet effective method for processing lignocellulosic biomass by simultaneous wet-type ultrafine bead milling and enzymatic saccharification at pH 4.0 ~ 6.0 and 50 °C. This generates nanoscale particles that allow close to 70% saccharification of cellulose and recovery of a glassy, flame retardant, and transparent non-deteriorated lignin film. Furthermore, small amount of non-deteriorated lignin greatly enhances the heat-tolerance properties of a synthetic polymer without the need for inorganic, halogen, or phosphorus compounds.

The utilization of non-edible plant biomass, such as polysaccharides and lignin, is essential to the transition from using petroleum-based material resources to sustainable and renewable ones. Polysaccharides (cellulose and hemicellulose) have been used as pulp and nanofibrous materials. By contrast, lignin, which is an aromatic network polymer consisting of propenyl phenol units, has potential as a renewable alternative to synthetic aromatic polymers. However, the extraction of non-edible plant biomass requires treatment with toxic reagents at heating, which prevents utilization of the biomass on an industrial scale due to the environmental load.

In our study, a simple yet effective method for extraction of lignocellulosic biomass by simultaneous enzymatic saccharification and comminution (SESC) was established¹. Our basic procedure for SESC operation involves the following simple steps: a mixture of plant powder and commercial enzyme (min. 30 FPU / g-g lucan) in phosphate buffer (pH = 4.0 ~ 6.0) was milled for a maximum of 4 h by wet ultrafine bead milling apparatus at 50 °C and 1 psi that employs zirconia beads (0.5 mm ϕ) (Figure 1). As needed, further saccharification at 50 °C for 48 h was allowed to proceed, after which, the final slurry was centrifuged. The supernatants, which contain sugar products, were pooled while the precipitate, which is mainly composed of lignin, was washed with pure water. The dispersed particles in the final slurry had an average diameter of 38 nm for softwoods. We have also applied the SESC to hardwoods and herbaceous biomass. The saccharification ratio from SESC was max. 83% for cedar (*i.e.*, softwoods). The saccharification ratio is higher than other chemical treatments for cedar. The *in situ* fermentation of the supernatant of SESC (Figure 1) using a 'sake' yeast inoculum generates ethanol at a conversion ratio with maximum theoretical value. The dried SESC precipitate (later denoted SESC lignin) is transparent film with pale brown color (Figure 1) that is significantly different from the black-colored lignin extracted via typical chemical processing. The SESC lignin can be mixed with an ordinary polymer simply by heating. Kneading and hot-pressing of the lignin-polymer mixture gave self-standing composite films. The SESC lignin has the superior ability relative to that of conventional petroleum-based materials to serve as an excellent heatproof filler for poly(ethylene carbonate) (PEC), *i.e.*, the 5% decomposition temperature (T_{d5}) of PEC increased about 70 °C with the addition of only 5 w/w% of SESC lignin².

In summary, the SESC offers a promising approach for lignocellulosic plant biomass treatment to produce sugar, ethanol, and high-performance polymer materials. The almost full recovery of plant biomass components, which has a positive impact on the generation of high value secondary products, could considerably contribute to its economic viability as well.

REFERENCES

- ¹K. Shikinaka, et al. *Green Chem.*, 18, 2016: 5962.
²K. Shikinaka, et al. *J. Mater. Chem. A*, 6, 2018: 837.

ACKNOWLEDGMENT: This work was supported by a grant from the Advanced Low Carbon Technology Research and Development Program of the Japan Science and Technology Agency (No. 16200591400).

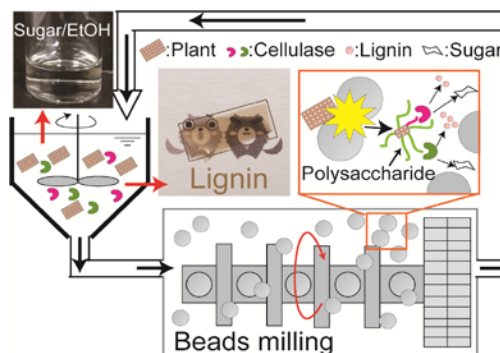


Figure 1. Schematic image of SESC

Dyeing and Finishing/Design and Merchandising

Developing a Natural Dyeing Method for Obtaining Turkey Red Color

Recep Karadag

Marmara University Faculty of Fine Arts, Laboratory for Natural Dyes, Acibadem, Kadikoy Istanbul, Turkey
Turkish Cultural Foundation Cultural Heritage Preservation and Natural Dyes Laboratory, Istanbul, Turkey

rkaradag@marmara.edu.tr; rkaradag@turkishculture.org

A dyeing recipe invented by dyers in 15th century Ottoman Empire, Turkey Red, sometimes referred to as Edirne (Adrianople) Red, was a highly guarded trade secret handed from master dyer to apprentice. The technique was introduced to Europe in 1746 when two master dyers from Izmir were taken to France where they continued their craft. The technique then spread to England where in the 19th Century, Glasgow boasted six dyeing factories that dyed in Turkey Red. With the spread of synthetic dyes and the diminishing application of natural dyes in the textile industry, the recipe for Turkey Red was lost.

The present invention relates to a natural dyeing method which enables to dye 100% cotton fiber and fabric products by using roots of madder (*Rubia tinctorum* L.) plant in particularly textile sector and to obtain Turkey red color. Although Turkey Red is a color which is known theoretically since 15th century, obtaining cotton textile products with Turkey Red color still requires difficult and long steps. When all steps are not applied as it should be or in cases where it is not waited for necessary periods, the desired color tone cannot be obtained completely.

In this study; coloring compounds, mordant materials and color value were analyzed in the different historical Turkey red textiles in the Topkapi Place Museum and Military Museum in Istanbul. All the analysis results were used for obtaining Turkey Red color by developed dyeing machine and developed dyeing process. The developed process was result in take out a patent.

According to the analysis results of historical Turkey Red textiles and developed Turkey Red color have same characterizations. In addition to fastness and antimicrobial tests were done on the developed Turkey Red color.

We regard the rediscovery and scientific documentation of Turkey Red as an important contribution to the preservation of our cultural heritage, as well as to science. The work on Turkey Red is one more important milestone in our long-standing efforts for the preservation and contemporary application of natural dyes. By perfecting natural dyes and making them fully usable in contemporary textile manufacturing and other consumer products, we aim to contribute to responsible productions that save our environment and protect human health.

ACKNOWLEDGMENT

This work was supported by the Turkish Cultural Foundation and Armaggan Company.

Structural Change and Guest Release from Cyclodextrin Inclusion Complex Treated at Ultra-high Pressure

Kenji Hisada, Sayaka Kasakawa, Kyosuke Takeshita, Chie Kato, Mikiaki Kakasawa, Toyoaki Hirata

Department of Frontier Fiber Technology and Science, University of Fukui, Japan

k-hisada@u-fukui.ac.jp

INTRODUCTION

The inclusion phenomenon of cyclodextrin (CD) is used for sustained release, stabilization, solubilization of guest molecules. When pressure is applied to inclusion compounds, the equilibrium of the system is shifted so that the total volume decreases in accordance with Le Chatelier's principle. On the other hand, when applying ultra-high pressure to solid inclusion complexes, the hysteresis was observed in the release of guest molecules. In this study, we examined the influence of matching of guest size and host molecular void size on the hysteresis.

EXPERIMENTAL

Menthol, limonene, camphor, 2-methylthiazoline (2MT), 4-ethyl-2-methylthiazoline (4E2MT) and hinokitiol (HT) with different molecular sizes were used as volatile guest molecules. d_1 and d_2 are defined as two axes orthogonal to the long axis direction of the guests. Inclusion complexes of these guests with β -CD or γ -CD were prepared and hydrostatic pressure or dynamic pressure was applied on them. Guest release with time were measured from weight loss of inclusion compound weight with a quartz crystal microbalance (QCM) to obtain the guest release rate. The composition of the inclusion compound before and after application of pressure was measured by $^1\text{H-NMR}$ spectroscopy, and the influence of pressure application on inclusion structure was evaluated by FT-IR measurement.

RESULTS AND DISCUSSION

The $^1\text{H-NMR}$ spectra of the inclusion complexes did not change before and after application of pressure, and no decomposition was recognized during the treatments. Comparing the guest release rates before ultra-high pressure treatment (k_0) with the release rates after treatment (k_p), the release rates of menthol, camphor and limonene are decreased, and conversely, release of HT was accelerated. The pore size of β -CD is 0.70 nm. The molecular size of menthol was almost the same as the intramolecular void size of β -CD in d_1 direction. In this system, the decrease in release rate due to pressure application was remarkable. Stretching vibration for methyl CH bonds of the guest molecules was suppressed by pressure application. For camphor/ β -CD inclusion compounds whose molecular size matches the pore size of cyclodextrin, the release of guest molecules was slow down from that for as prepared complex. Inclusion compounds of 2MT and 4E2MT in which d_1 and d_2 were both 0.60 nm or less had a high release rate and no deceleration effect by pressure application. In these inclusion compounds, the affinity was so low that guest molecules would leak out as a liquid phase due to the application of ultrahigh pressure.

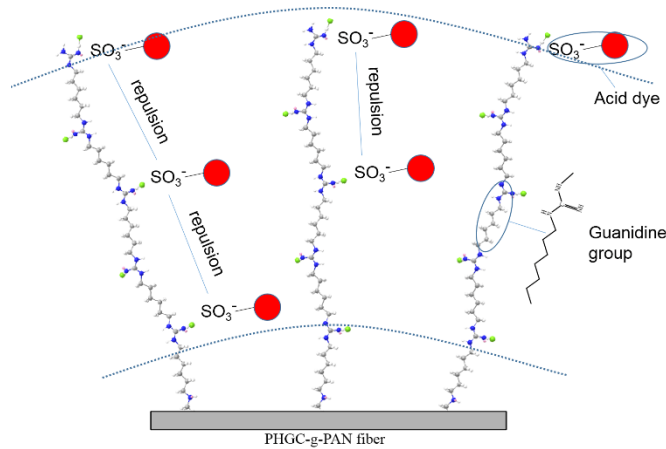
Adsorption of Acid Dye on Guanidine Groups Grafted Polyacrylonitrile Fibers

Biao Wang, Fengmei Li, Chengran Yang

State Key Laboratory for Modification of Chemical Fibers and Polymer Materials,
College of Material Science and Engineering, Donghua University, Shanghai, P.R. China

wbiao2000@dhu.edu.cn

Guanidine groups grafted polyacrylonitrile (PHGC-g-PAN) fibers were prepared by hydrolyzing polyacrylonitrile (PAN) fibers with sodium hydroxide followed by reacting with polyhexamethylene guanidine hydrochloride (PHGC). The content of guanidine groups in the obtained PHGC-g-PAN fibers was 0.44mmol/g. The structure of PHGC-g-PAN fibers was characterized by FTIR and SEM. The PHGC-g-PAN fibers were effective for the adsorption of acid dye from aqueous solutions with a high sorption capacity of 275.4 mg/g and the adsorption behaviors including isotherms and kinetics were investigated. Langmuir and Freundlich isotherm models were used to describe the adsorption process. The results indicated that Freundlich model was better in describing the adsorption isotherm, suggesting a heterogeneous adsorption behavior. The adsorption kinetic was found to follow pseudo-second-order model. Results from adsorption regeneration tests demonstrated that the PHGC-g-PAN fibers could be regenerated by NaOH solutions and the regenerated fibers could still provide at least 70% of the initial adsorption capacity even after 10 adsorption–desorption cycles.



Development of Multifunctional Surfaces for Advanced Textile Applications

Mehmet Daşdemir, Hatice İbili

Textile Engineering Department, Gaziantep University, Gaziantep, Turkey

dasdemir@gantep.edu.tr; haticeihatice@gmail.com

The focus of the study is the development of multifunctional nonwoven fabric with superhydrophobic and antibacterial characteristics via electrohydrodynamic atomization (electrospraying). Superhydrophobic and antibacterial finishing agents were mixed as emulsion with different ratios and applied to nonwoven fabric to compare the effectiveness on water repellency characteristics. Commercial chitosan and fluorochemical finishing agents were used to prepare finishing agent solutions at 2 w/v% and 3 wt% concentrations respectively. Electrospayed finishing solutions were prepared as 100% fluorocarbon, 25/75 v/v% fluorocarbon/chitosan, 50/50 v/v% fluorocarbon/chitosan, 75/25 v/v% fluorocarbon/chitosan and 100% chitosan. Electrospaying application was carried out for 10 minutes for each run. Processing parameters for electrospaying were 20 kV applied voltage, 10 cm tip to collector distance, and 22 gauge needle size. Applied flow rates was $10 \mu\text{l}\cdot\text{min}^{-1}$. After the application, water repellencies of the coated fabrics were characterized with water contact angle measurements. According to our findings, the contact angle of electrospayed fabric were increased with the increasing fluorocarbon rate on emulsion. Increasing fluorocarbon rate enhanced water contact angle values, which reached a maximum level (up to 161°) while average water contact angle was $150^\circ \pm 3.2$ (Figure 1). Also size distribution of these nanoparticles was examined with particle size analyzer by means of intensity (Figure 2). As a result of this study, nanoparticles were formed with narrow size distribution. The results showed that the distribution of electrospayed nanoparticles were improved with addition of chitosan to electrospayed solution compared to electrospaying of 100% fluorocarbon solution. In conclusion, electrospayed nonwoven fabrics achieved both superhydrophobic and antibacterial characteristics as satisfactory level. One of the other important outcomes of this study is that there was no significant change on the comfort properties of nonwoven fabrics after the electrospaying application.

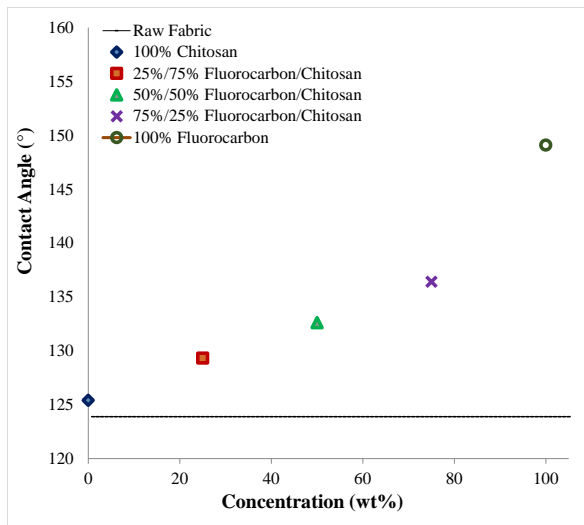


Figure 1

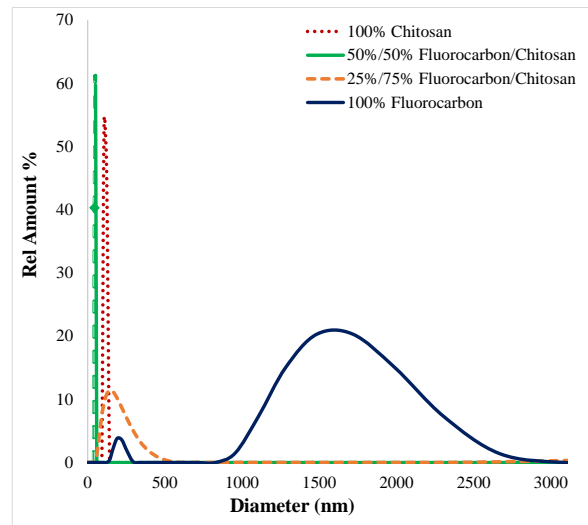


Figure 2

Figure 1. Water repellencies of raw and electrospayed fabrics. Figure 2. Size distribution of electrospayed nanoparticles.

Parameters Affecting the Electrospraying Process with Flame Retardant Agent

Bilgen Kapar, Cem Güneşoğlu

Gaziantep University, Engineering Faculty, Textile Engineering, Gaziantep, Turkey

bilgen.celikturk@gantep.edu.tr

The purpose of the study is to see the parameters effect on deposition time during electrospraying process of flame retardant agent solutions. The solutions were prepared with 50/50 v/v ethanol/water and then the parameters were adjusted with three different electric field (1.5 kV/cm, 2 kV/cm and 2.5 kV/cm), with two different concentrations (1:5 v/v, 1:10 v/v). Determined amount of flame retardant solution (4mL) were electrosprayed on aluminum foil and deposition time was measured to finish the determined solution. Flow rate was determined as 20 μ L/min, needle diameter was selected as 0,7 mm (22G). During experiments, the ambient temperature was measured as 20-23 ° C and the humidity value was measured as 27-32%. In normal conditions, 4 ml solution should finish in 20 minutes, because the set up is horizontally arranged and there isn't any forces acting on liquid droplet like gravity force. Güneşoğlu found an equation related with electrospray process parameters. According to this equation deposition time is affected most viscosity. When the viscosity is higher, the deposition time is lower. In conclusion, increasing flow rate, electric voltage, solution viscosity and decreasing working distance caused lower deposition time. In this study, when electric field increases, deposition time decreases for each concentration value. The effect of constituents and verification of process are identified with statistical analysis and the formulation of deposition time is formed with regression analysis. According to regression analyses, conductivity and surface tension values of flame retardant solution were highly correlated so when the formula was formed, just electric field and viscosity values were added to formula by Minitab. Adjusted R² was found 85,5% which explains that approximately 86% variation in data can be explained by the model. The model affecting parameters model can be showed in following equation:

$$\text{Deposition time (minute)} = 32,3 - 2,46 \text{ Viscosity (cP)} - 0,525 \text{ Electric Field (kV/cm)}$$

According to formulation, the most effective parameter on deposition time is viscosity. The effect of viscosity and electric field were in negative way, when they increase deposition time decreases. Viscosity and electric field should be chosen high levels as much as it can be.

Structural Coloration of Textile Controlling Structure of Colloidal Crystal Array on Fiber and Textile

Kazumasa Hirogaki¹, Kazushi Sekiguchi¹, Daichi Nakamura², Isao Tabata², Teruo Hori³

¹Graduate School of Engineering, University of Fukui; ²Faculty of Engineering, University of Fukui;

³Headquarters for Innovative Society-Academia Cooperation, University of Fukui

hirogaki@u-fukui.ac.jp

Structural coloration of a textile has been expected as a novel coloration method in order not to use a dye with suspicion of toxicity and large amount of waste water. We focused attention on a colloidal crystal structure in opal which nano-sized particles are arranged cyclically. A fiber and a textile will be colored structurally by forming the colloidal crystal on its surface. A polyester fiber was dip-coated with water suspension of uniform sized silica particles (diameter 310nm) and then it was dried. The particles were ordered along the fiber surface by self-assembling through lateral capillary force while drying. The particles ordered on the surface become the first layer of the crystalline lattice, and the crystal grows from it. It is considered that the crystalline structure can be controlled by influencing mobility of particles through the interaction between the particles and the surface. We investigated the effect of hydrophilicity and charge of the fiber surface to formation of colloidal crystal on the fiber. Surface modified polyester fiber was prepared with O₂ plasma treatment or a sol-gel method using 3-Aminopropyltriethoxysilane (APS). Hexagonal arrangement and Square arrangement were observed for the particles deposited on the fiber surface. It is considered that the former was derived from hcp or fcc and latter was derived from bcc. On the plasma treated fiber, the ratio of hexagonal arrangement to square arrangement was 3:1. On the APS treated fiber, the ratio was 1:8. Inducing amino groups on the fiber surface resulted in increasing bcc structure due to lowering the mobility of particles on the fiber surface while self-assembling through the electrostatic interaction between the negative charged silica particles and the positive charged fiber surface in water. The fiber fabricated colloidal crystal on its surface exhibited red color and it has a peak with wavelength of 637 nm in the reflection spectrum. In the presentation, we will also mention about controlling color exhibition such as angle dependence of the textile structural colored with a colloidal crystal (fig. 1) through preparing a higher-order structure of a colloidal crystal imitated with a peacock feather structure.

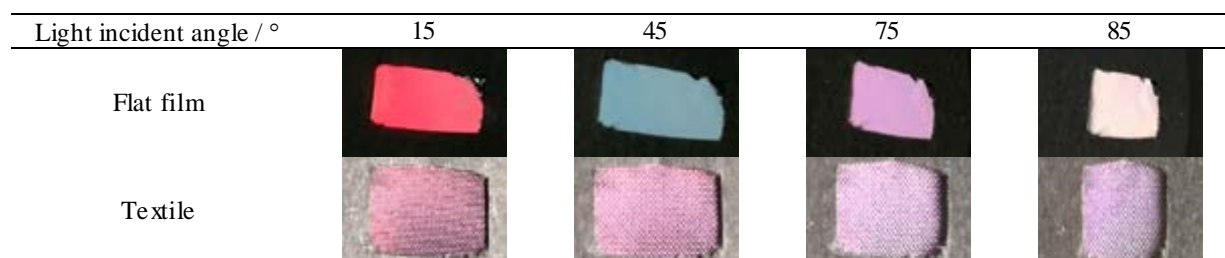


Figure 1. Photos (exposure angle at 15 °) of colloidal crystal flat film (angle-dependent coloration) and colloidal crystal deposited textile (angle-independent coloration).

Development of a New Outdoor Sport Shirt Using a Thermal Manikin Under Different Climatic Conditions

Maria José Abreu¹, Andé Catarino¹, Derya Tama^{1,2}

¹University of Minho, Center for Textile Science and Technology, Guimaraes, Portugal

²EgeUniversity, Department of Textile Engineering, Izmir, Turkey

josi@det.uminho.pt; white.man@det.uminho.pt; derya.tama@ege.edu.tr

INTRODUCTION

Humans are endothermic organisms and have much higher basal energy consumption, which is mainly necessary to keep their body temperature constant within a wide range of different environmental temperatures. The human body temperature is around 37 °C in the body core such as cranial, thoracic, abdominal cavities and in the extremities, the temperature is lower (28-36°C) [1]. Especially in active sports, the muscles produce heat from metabolic activity and this causes greatest thermal stress during exercise. In order to provide heat balance, the heat is lost from the body through four independent processes; evaporation, convection, conduction and radiation [2].

The clothing is one of the parameters that affects heat balance of the athlete during exercise. Combining clothing functions with wear comfort is a growing market trend, and for all active sports, it is one of the vital factors for achieving high level of performance. Functional requirement of high active sportswear depends on the nature of sport, climatic conditions and amount of physical activity. As Bhatia and Malhotra (2016) concluded in their overview research about thermo-physiological wear comfort of clothing, heat and moisture transmission mechanism through clothing, need to be analysed together with material properties and other influencing parameters [3].

In the present research, the mostly used fabrics in outdoor sports were determined and evaluated by using thermal manikin. Outdoor rowing was chosen as outdoor sport and since it is a water sport, a water repellent finishing was applied to all fabrics. In order to achieve the optimum shirt design, which enhances the comfort and performance of the user, the environmental conditions were analysed first. Moreover, the thermal responses of human body was investigated as well by literature research. With respect to thermal manikin test results and literature review, suggestions were done for outdoor rowing clothing.

MATERIALS AND METHODS

The mostly used fabrics for outdoor rowing were determined and tested. The fibres and the knitting structures were presented in Table I. The fabrics were evaluated by using thermal manikin (PT-Teknik/Denmark). In order to perform thermal manikin tests, three long sleeve basic shirts were produced from each fabric and were treated with a water-repellent finishing (5% of a fluorocarbon-based product).

Code	Composition	Knitting Structures
F1	60% Polyamide	False Rib 1
F2	35% Polyester 5% Elastane	Single Jersey jacquard 1
F3	60% Polyamide 35% Polypropylene 5% Elastane	Single Jersey jacquard 2

Table I. The composition, knitting structures and the codes of shirts.

Two test series were conducted in order to evaluate the effect of air temperature and humidity change on thermal insulation properties of the shirts. The test series were set with respect to “ISO 9920:2007: Ergonomics of the thermal environment—Estimation of thermal insulation and water vapour resistance of a clothing ensemble.” The specimens were dressed up to the thermal manikin and the manikin was kept in a stationary standing position. The skin temperature was set and during the test periods maintained at 33 ±0,2°C. The values of skin temperature and heat loss were recorded every minute during the test time (60 minutes). The tests were

conducted in different climatic conditions in a climatic chamber at constant ambient temperature and relative humidity. “Test Series 1” were performed at constant of $24,5\pm 1^{\circ}\text{C}$ temperature and $60\pm 5\%$ relative humidity, “Test series 2” were conducted at of $19\pm 1^{\circ}\text{C}$ temperature and of $77\pm 2\%$ relative humidity, in which colder climatic condition was simulated.

RESULTS AND DISCUSSION

The heat loss values of Test Series 1 and Test Series 2 for eight body parts were graphically evaluated and compared (Figure 1). According to obtained data, F3 had the greatest heat flow in all body parts than other structures in Test Series 1. In Test Series 2, all fabrics showed similar heat flow values. In addition, it can be seen in the graph that, at the chest, all fabrics had the least heat flux values.

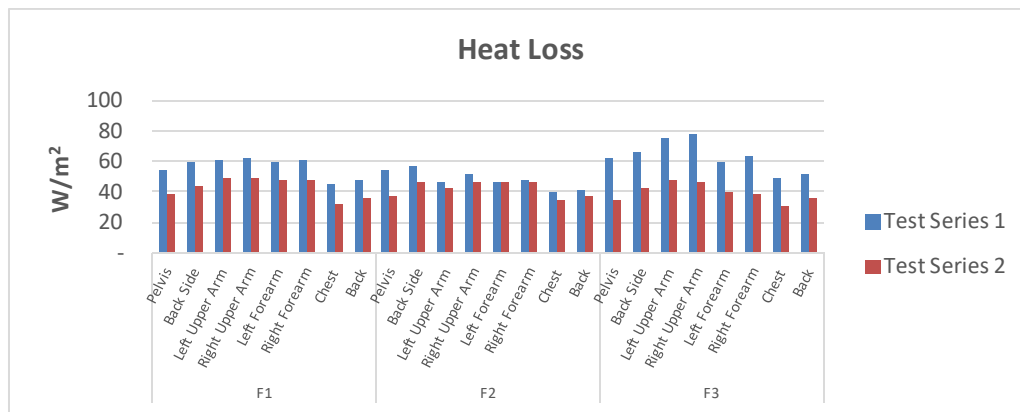


Figure 1. The heat loss values of structures for body parts according to test series.

Moreover, the comparisons were performed for each test series by calculating the effective thermal clothing insulation I_{cle} . The temperature difference of fabrics in two different conditions were evaluated regarding to the body parts (Figure 2). With respect to obtained data, it can be clearly seen that, in Test Series 2, F3 had the greatest effective clothing insulation. In addition, the fabrics showed similar effective clothing insulation properties in Test Series 1. Test Series 2 simulates colder environment and therefore it can be concluded that F3 was able to adapt effective clothing insulation properties in different conditions.

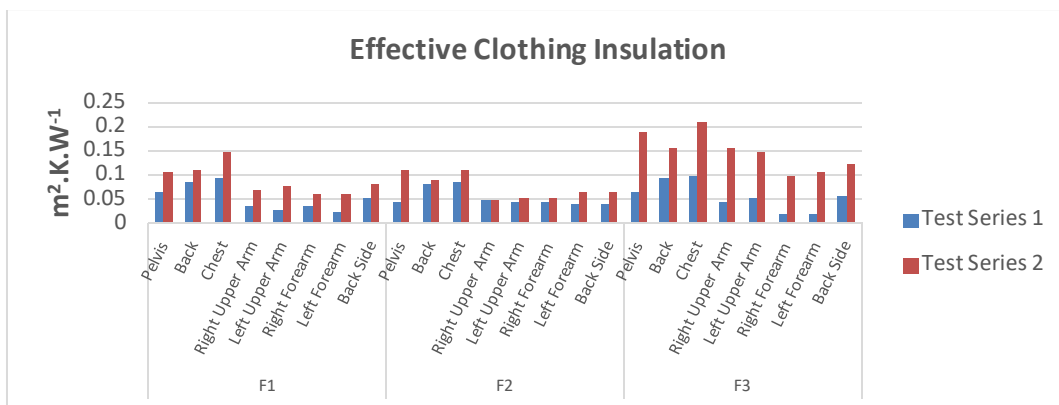


Figure 2. The effective clothing insulation values of structures for body parts according to test series.

CONCLUSIONS

The air temperature, water temperature and wind are the factors that affect the performance of the rowing as well as the safety rowing. Some clubs have the rules, which are, if the sum of the water temperature and air temperature is below 18°C [4] or the air temperature is below 5°C [5], the conditions are not considered “safe” for rowing. Moreover, in some clubs the wind conditions are defined critical above 5.1 m/s [4] whereas others allow going out only very experienced crews in the wind above 14 m/s [6]. In this wide range of climatic

conditions, the garment needs to assist the active body, support the performance of the wearer and provide thermoregulation. In order to achieve the garment, which matches these needs, the thermal and sweating responses of human body need to be considered together with environmental conditions and thermal and physical properties of fabrics.

The thermal response of a thermal manikin in different temperatures dressed with 100% Cotton long sleeved shirt was studied as a previous study [7] and the infrared images taken in this study were presented here as examples (Figure 3).

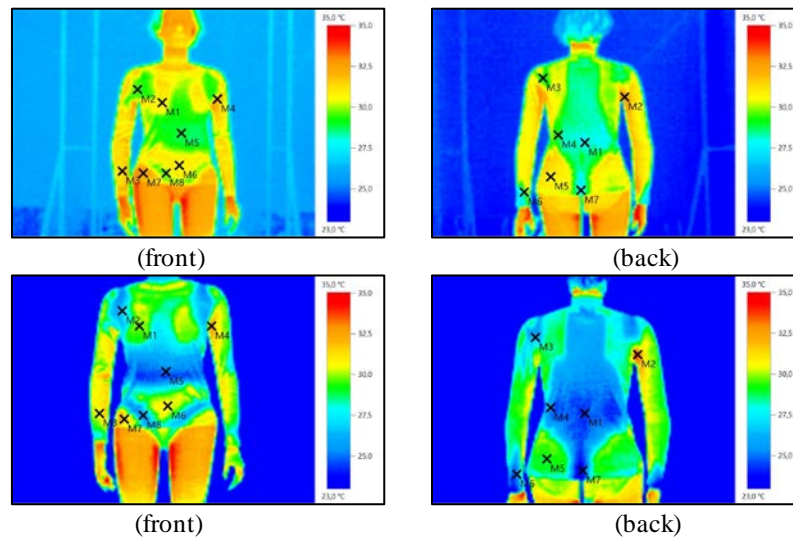


Figure 3. IR images at 24,5°C (top) and at 19°C (bottom).

With respect to all obtained data, it can be said that, a shirt for outdoor rowing can be produced with only F3. However, combining the evaluated fabrics may provide better thermoregulation for human body. Therefore, in the chest and back, which have lower skin temperatures, F3 was suggested to be put on for both in cooler and warmer air conditions. Moreover, F2 was suggested to be put on the sides of the garment and F1 on arm pits due to higher heat loss and lower thermal effective thermal insulation values.

REFERENCES

- [1] Hanns-Christian Gunga. *Human Physiology in Extreme Environments*. Boston, MA: Academic Press, 2015, p. 163, ISBN 9780123869470.
- [2] Ayres, B., White, J., Hedger, W., Scurr, J. "Female upper body and breast skin temperature and thermal comfort following exercise." *Ergonomics*, 56:7, 2013: 1194-202, DOI: 10.1080/00140139.2013.789554.
- [3] Bhatia, D., Malhotra, U. "Thermo-physiological wear comfort of clothing: an overview." *J. Textile. Sci. Eng.*, 6:2, 2016, <http://dx.doi.org/10.4172/2165-8064.1000250>.
- [4] https://www.nk.com.au/cmsimages/File/Kestrel_Wind_and_Weather_Instruments_for_Rowing_web.pdf.
- [5] <http://www.swancreekrowing.com/safety-weather/>.
- [6] http://www.bournemouthoutriggercanooclub.com/uploads/4/2/4/6/42465823/oc6_safety_and_operating_procedures.pdf.
- [7] Abreu, M. J., Catarino, A. P., Haeussermann, N. "Comfort Effects of Weft-knitted Structures on Rowing Shirts Using IR Thermography." *The Fiber Society 2016 Spring Conference Proceedings*.

ACKNOWLEDGMENT

This work was supported by FEDER funds through the Competitvity Factors Operational Program (COMPETE) and by national funds through FCT–Foundation for Science and Technology within the scope of the project POCI-01-0145-FEDER-007136. We would like to thank Nadine Häußermann and Silke Küblbeck for their kind support.

Colorful Fluorine-free Superhydrophobic Polyester Fabric Developed via Disperse Dyeing Process

Ji-Hyun Oh, Chung Hee Park

Department of Textiles, Merchandising and Fashion Design, Seoul National University, Korea

junghee@snu.ac.kr; popuka88@snu.ac.kr

Superhydrophobicity treatments have been developed focusing on industrial materials and with little consideration of clothing materials, which results in various problems such as surface color change, decrease of breathability, handle and safety of substances. Moreover, most superhydrophobic technologies have been applying to white fabrics and they have limitation to be used as fashion textiles. Thus, technologies that consider not only superhydrophobicity, but also aesthetic aspects and human-friendly are needed. Thus, in this study, we used disperse dyeing process to fabricate colorful fluorine-free superhydrophobic polyester fabric without having additional energy-consuming process.

The conventional polyester dyeing process was modified to create a streamlined process for the colorful fluorine-free superhydrophobic polyester fabric. Dyestuffs having different chemical structures were used. Wettability was evaluated with static contact angle and shedding angle and color change was characterized with a spectrophotometer. Color fastness against light, abrasion and washing was also analyzed. Water vapor transmission rate and air permeability were measured.

After the modified dyeing processing, the surface of polyester kept its nanocraters made by alkaline hydrolysis. Furthermore, due to thermal hydrophobic aging process during drying, the developed polyester fabric showed superhydrophobicity exhibiting the static contact angle of $163.7 \pm 2.6^\circ$ and shedding angle of $9.3 \pm 1.1^\circ$. Regardless of types of dyestuff, color strength was reinforced when polyester was alkaline hydrolyzed, but the polyester fabric dyed with anthraquinone dyestuff had decreased color strength after drying, with the decrease of ΔE value by 2.7. On the other hand, the polyester fabric dyed with coumarin dye showed stronger color after drying, increasing ΔE value by 4.06. Not only color fastness but also water vapor transmission rate and air permeability of the superhydrophobic polyester fabric were improved.

ACKNOWLEDGMENT

This work was supported by BK21 Plus project (22B20130000043) of the National Research Foundation of Korea (NRF) grant funded by the Korean Government and by the National Research Foundation of Korea (NRF) grant funded by the Korea government (MSIP) (No. NRF-2016M3A7B4910940 and No. 015R1A2A2A03002760).

Safer Hair Dyeing by Using Biobased Materials: Techniques, Dyeability, and Protection Effect

Hidekazu Yasunaga¹, Akiko Takahashi¹, Kazue Ito¹, Masahisa Ueda¹, Saina Taniguchi¹, Asami Yano¹, Shota Morimoto¹, Takanori Hagino¹, Chinami Seki¹, Aya Shomura¹, Takanori Matsubara²

¹Kyoto Institute of Technology; ²College of Industrial Technology

yasunaga@kit.ac.jp

INTRODUCTION

The oxidation dyes are most frequently employed for dyeing human hair throughout the world at present and the number of the people dyeing their hair is increasing. Particular components of oxidation hair dye products and the side products formed during the dyeing work occasionally as strong allergens. Sensitisation symptoms and severe dermatitis are caused for some people following their use. Under such the situation, it is very important and desired to create a novel hair dyeing technique, which is milder and safer for a human body. The author has studied such the safer hair dyeing by using biobased materials in order to decrease the risks accompanying hair dyeing. The preparation techniques, dyeability, safety and colour fastness to washing and light for the dyed hair of the dyestuffs obtained from biobased materials are reported.

RESULTS AND DISCUSSION

It was found that human hair can be dyed by a colourant, “catechinone” (4-(3,4-dihydro-3 α ,5,7-trihydroxy-2*H*-1-benzopyran-2 α -yl)-1,2-benzoquinone) prepared from (+)-catechin in aqueous buffer solution by the oxidation using tyrosinase. The obtained orange or reddish orange colourant shows enough dyeability for decolourised white hair. It was found through acute skin irritation tests according to the OECD Guidelines that catechinone does not cause erythema or oedema on skin. The resulting colour of hair is controlled by the combination of 1)[catechinone, (+)-catechin or rosmarinic acid] and 2)[each of the biobased material or Fe²⁺]. A variety of coloured hairs are acquired as shown in Fig. 1. The fastness to washing or light for hair dyed by the technique is high enough for practical use. The catechinone is also obtained by the reaction of (+)-catechin with O₂ under basic condition without enzymes.

Moreover, it was clarified that hair is dyed by the oxidation technique using biobased materials including (-)-epicatechin, caffeic acid, haematoxylin, rosmarinic acid, chlorogenic acid, L-3,4-dihydroxyphenylalanine (DOPA) and brazilin or the heating technique using D-xylose and amino acids.

Furthermore, a protection effect for hair against lights (UV and visible one) was found for the dyed or treated hair with biobased materials such as (+)-catechin, curcumin and rosmarinic acid.



Fig. 1. Photographs of hair samples: initial undyed hair (a); dyed by catechinone (cat.) (b); cat. with L-cysteine (c); cat. with L-tyrosine (d); cat. with DOPA (e); cat. with naringenin (f); cat. with lac (g); cat. with tamarind (h); cat. with hematoxylin (i); cat. with Kaoliang (j); cat. with gardenia blue (k); cat. with red cabbage (l); (+)-catechin with iron(II) lactate (m); rosmarinic acid with iron(II) lactate (n).

Fiber Manufacturing and Characterization

Comparison of Solution Spinning Setups for PLA Monofilaments

Georg-Philipp Paar¹, Elisabeth Wistuba¹, Klas-Moritz Kossel¹, Catalina Molano-López²,
Andreas Blaeser¹, Andrij Pich², Thomas Gries¹, Stefan Jockenhoevel³

¹Institut für Textiltechnik of the RWTH Aachen University; ²DWI-Leibniz Institute for Interactive Materials;

³NRW-Schwerpunktprofessur Biohybrid & Medical Textiles (BioTex) at AME-Helmholtz Institute for Biobased Materials

georg.paar@ita.rwth-aachen.de

INTRODUCTION

Biodegradable materials, such as polylactic acids (PLA), have been successfully used in suture and osteosynthesis systems. By using PLA as implant material a second operation for implant removal and long-term foreign body reactions are prevented. In vivo PLA is degraded by hydrolysis and degradation products are released, which can cause local acidosis. A successful approach for buffering of the acidic degradation products is incorporation of amine based microgels. These additives are heat sensitive therefore solution spinning was selected as method for production of PLA monofilaments. Dry spun PLA monofilaments are inferior because tensile strength is low and variation of tensile strength is high. This may result from the kidney shaped cross-section of the filaments. Thus a solution spinning process is desired, which allows production of PLA filaments with round cross-section and higher tenacity.

MATERIALS AND METHODS

PLA monofilaments were dry spun from a solution of PLA in a chloroform/toluene mixture as solvent. Wet spun monofilaments were extruded from PLA/chloroform solution into various coagulation baths (methanol, ethanol, isopropanol). Evaluation of filament cross-section was carried out by light microscopy. Those processes resulting in filaments with round cross-section were further investigated by tensile testing.

RESULTS

Kidney shaped cross-section was observed for dry spun monofilaments and those monofilaments produced by wet spinning into methanol. Wet spinning into ethanol and isopropanol resulted in fibers with a round cross-section. Therefore those processes were selected for further investigation of the influence of spinning parameters (e.g. polymer concentration in spinning solution, residence time in coagulation bath, jet stretch) on filament morphology and tensile strength. For filaments spun into ethanol cross-section changed with increasing polymer concentration from kidney shaped to round. This was not observed using isopropanol as coagulation medium. Instead filaments showed round cross-section for all polymer concentrations. The tensile strength of PLA filaments produced by wet spinning was high compared to those of dry spun PLA filaments.

CONCLUSION

The study shows that wet spinning is more suitable to produce PLA monofilaments with round cross-section and high tensile strength.

ACKNOWLEDGMENT

The project "pHMed" (EFRE-0800639) is supported by the European Regional Development Fund North Rhine-Westphalia (EFRE.NRW).

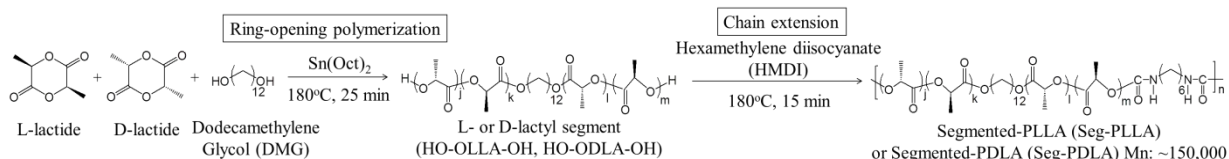
Stereocomplexation of the Melt-spun Fibers of Blends of Segmented PLLA/PDLA with a Low Optical Purity

Masaki Yamamoto¹, Miho Sakai², Kazunari Masutani¹, Yoshiharu Kimura¹, Hideki Yamane²

¹The Center for Fiber and Textile Science, Kyoto Institute of Technology, Kyoto, Japan

²Department of Biobased Materials Science, Kyoto Institute of Technology, Kyoto, Japan

hyamane@kit.ac.jp; myamamoto@kit.ac.jp



Scheme: Synthetic route of Seg-PLLA and -PDLA with a low optical purity by ROP and the subsequent chain-extension.

INTRODUCTION

Segmented PLLA (Seg-PLLA) is obtained by the chain extension of bis-hydroxyl-terminated oligo(L-lactic acid) (lactyl segment) synthesized by the direct polycondensation of L-lactic acid. Seg-PLLA with a short segment hardly crystallizes unless it is annealed and its T_m and the crystallinity decrease with decreasing segment length. The stereocomplex crystal (SC) forms in an equal blend of PLLA and PDLA and its T_m is about 50°C higher than that of the homochiral crystal (HC). So the stereocomplexation is one of the solutions to improve poor thermal resistance of Seg-PLLA. However, both SC and HC tend to coexist in the simple mixture of PLLA and PDLA. It is a purpose of this study to investigate the stereocomplex formation behavior of the melt-spun fibers of the blends (Seg-(L/D)) of Seg-PLLA and Seg-PDLA with a low optical purity. Seg-(L/D) melt-spun fibers were drawn and annealed at various conditions and the structure and the thermal property were determined.

EXPERIMENTAL

A synthetic route of Seg-PLLA and Seg-PDLA with a low optical purity is shown in the scheme. L- (or D-) lactyl segment with 5 mol% of D- (or L-) lactic acid unit was synthesized by the ring-opening polymerization of L- and D-lactide by using dodecamethylene glycol (DMG) as an initiator. Then these lactyl segments were extended into Seg-PLLA and -PDLA by adding hexamethylene diisocyanate (HMDI). L- and D-lactyl segments with 10,000 and Seg-PLLA and PDLA with 150,000 in molecular weight were obtained. Equal amounts of Seg-PLLA and PDLA were melt blended at 170°C (Seg-(L/D)) and melt-spun into an amorphous fiber. The fiber was drawn and annealed at various temperatures under the tension. Thermal property, the higher-order structure, and the mechanical property were determined by using DSC, WAXD and the tensile test

RESULTS AND DISCUSSION

DSC curves of the Seg-(L/D) and that of the fiber are shown in Fig. 1. DSC curve of the PLLA/PDLA blend is also shown for comparison. It should be noted that Seg-(L/D) and its melt-spun fiber only show a melting of SC around 195°C. This suggests that the SC is a unique crystalline structure in the Seg-(L/D) and its fiber. On the other hand, both HC and SC were observed for the PLLA/PDLA blend. The lower T_m of Seg-(L/D) than that of the SC of the PLLA/PDLA blend made the melt spinning possible without causing a serious thermal degradation. WAXD patterns and the equatorial spectra of the fiber drawn to $\times 8.2$ at 70°C and that subsequently annealed at 120°C are shown in Figs. 2 and 3. Drawn fiber only shows a broad halo indicating the amorphous nature of the fiber. On the other hand, the annealed fiber shows the arc reflections of SC at $2\theta = 12, 20.5$ and 24° without showing any trace of the reflection of HC although annealing temperature is lower than T_m of HC. These results indicate that the crystallization of HC is suppressed in the blend of Seg-PLLA and -PDLA with a lower optical purity blend. This may be due to the longer L- and D-sequences required for the HC crystallization than that for SC.

ACKNOWLEDGMENT: This work was partially supported by Council for Science, Technology and Innovation (CSTI), Cross-ministerial Strategic Innovation Promotion Program (SIP), “Technologies for creating next-generation agriculture, forestry and fisheries” (funding agency: Bio-oriented Technology Research Advancement Institution, NARO).

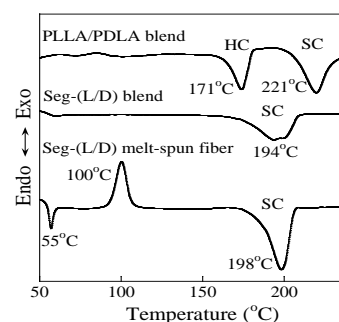


Fig. 1. DSC curves of PLLA/PDLA blend, Seg-(L/D) blend and its fiber.

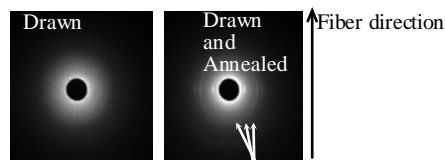


Fig. 2. WAXD patterns of the drawn fiber and the fiber annealed.

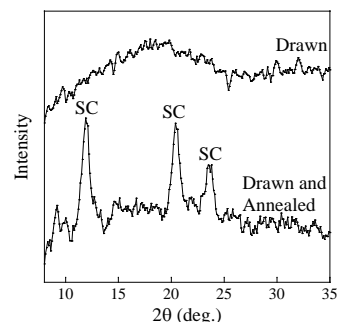


Fig. 3. WAXD equatorial spectra of the drawn fiber and the fiber annealed.

Study on High-resolution, On-line Diameter Measurement of PET Fiber in High-speed, Melt-spinning Process

Young Chan Choi¹, Hyun Ju Oh¹, Do-Kun Kim¹, Takeshi Kikutani², Wan-Gyu Hahm¹

¹Technical Textile & Materials R&D Group, Korea Institute of Industrial Technology (KITECH), Ansan, Korea

²Department of Materials Science and Engineering, Tokyo Institute of Technology, Tokyo, Japan

wghahm@kitech.re.kr; ycchoi@kitech.re.kr

Although PET fibers have been commonly used in many industrial applications, the PET fibers still have a lot of potential to improve their performance via control and optimization of molecular structure of the fibers. Many researchers have studied the deformation of PET fiber by using on-line measuring techniques to evaluate the mechanism of structure development in high-speed melt-spinning process. However, the reported on-line measurement systems still have a limitation to utilize high-speed spinning process, due to their low resolution.

Herein, the on-line diameter measurement systems, which can scan diameter of running PET fibers with high scanning rate (16 kHz) and adjust location and height of sensor stage by automatic tracking systems, were used for precise scanning fiber diameter profile. The PET of IV 1.17 was used for melt-spinning. And spinning temperature in the vicinity of spinneret was controlled with 290 and 334 °C, respectively. Hole diameter of spinneret was 0.5 mm and throughput rate was 3 g/min·hole. The PET fibers were taken at 1.0 ~ 5.0 km/min. The on-line diameter measurement systems successfully obtained the fiber diameter profiles in spin-line at 16 kHz. From the diameter profiles, the velocity and density of running fiber could be estimated, and also the structural development of PET fibers accompanying strain-induced crystallization was evaluated. In conclusion, we could observe structural development of running and molten PET fiber via different spinning conditions in high-speed melt-spinning process by using high-resolution on-line diameter measurement systems in detail.

KEYWORDS: High-resolution, on-line fiber diameter measurement, high-speed melt-spinning.

High Modulus Nylon 66 Yarn for Tire Cord Fabric Development

N. Uğur Kaya, Tuğba Elele, Emine Güven

Kordsa Teknik Tekstil A.Ş.

ugur.kaya@kordsa.com

Nylon 66 (NY 66) is a widely used polymer as tire reinforcement with its excellent tensile, and thermal properties together with its exceptional fatigue resistance. As cap ply, it restrains the belt package and prevents the undesirable tire growth under centrifugal forces at high speeds, thus maintains a stable carcass shape. The cap ply material is expected to have a high modulus to restrain growth and prevent belt edge separation. NY 66 congregates low cost, proper adhesion to the rubber, high modulus, dimensional stability and manufacturability.

In this study, development and commercialization of novel high modulus NY66 cord fabrics for cap ply application in high- and ultra-high performance (HP & UHP) tire segment was targeted. Thinner high performance nylon tire cord fabric brought lighter tire manufacturing and lower rolling resistance, thus ensuring fuel saving and contributing in CO₂ emission reduction (Figure 1).

High modulus Nylon 66 yarn was achieved by executing new design conditions in polymerization and spinning process. Physical properties of standard and developed yarns were investigated regarding breaking strength (BS), initial modulus, load at specific elongation (LASE %4) and shrinkage (%), whereas microstructural properties included crystalline perfection index (CPI), crystalline orientation (F_c), amorphous orientation (F_a) and birefringence. Significant increase in the orientation of high modulus yarn was revealed via microstructural analysis under all different heat treatment conditions.

Substantial improvement in the LASE (4%) was reported in final tire cord fabric (TCF) and single end cord (SEC). The enhanced restraining effects on belt package and rolling resistance improvements were confirmed by the customer's tire performance tests.

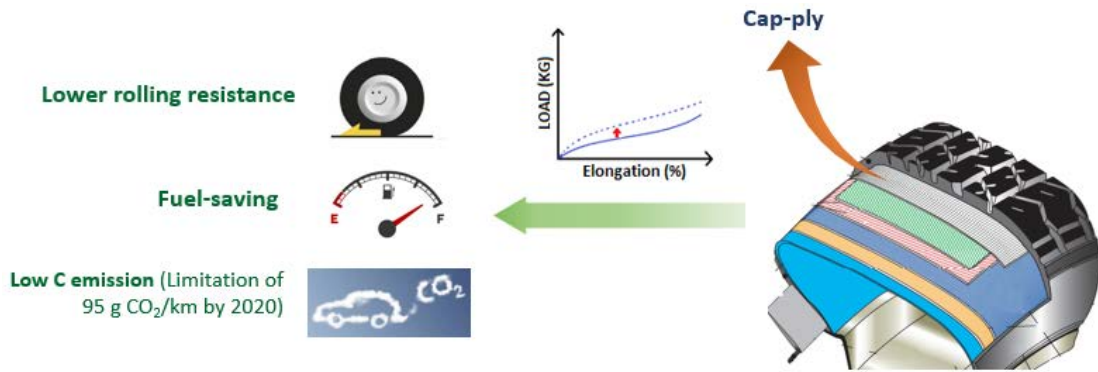


Figure 1. Added value of improved high modulus NY 66 cap ply fabric.

Auxetic Structures from 3D Printed Hybrid Textiles

David Schmelzeisen¹, Daniel Buecher¹, Subin Shajoo³, Julian Haller¹, Christopher Pastore², Thomas Gries¹

¹Institut für Textiltechnik (ITA) of RWTH Aachen University; ²Thomas Jefferson University, Kanbar College of Design, Engineering and Commerce; ³Karunya University, Karunya Nagar, India

daniel.buecher@ita.rwth-aachen.de; thomas.gries@ita.rwth-aachen.de

Auxetic materials are materials that have a negative Poisson's ratio. When a material is subject to normal tensile deformation in a single direction, the material will demonstrate normal compressive deformation in the other directions. The ratio of the strains applied and observed this way is called the Poisson's ratio, and for the vast majority of materials this value is positive. There are a few materials that are fundamentally auxetic from their molecular structure, and these tend to be highly porous foam-like structures. In fact, the auxetic behavior comes from the microstructural geometry of the foam.

Expanding the auxetic microstructure to a larger scale, there is a well-established field of research to evaluate structural systems that demonstrate auxetic behavior through the use of structural elements at a much larger scale than molecules or pores, by combining triangles, squares, or auxetic hexagons.

There are a range of applications for auxetic materials, including biomedical, sports, textiles. One of the interesting properties is the ability of auxetic materials and structures to form synclastic shapes (including domes and spheres), as opposed to traditional materials which form as anticlastic surfaces (positive Poisson's ratio) or even monoclastic (high shear modulus). A synclastic curve are formed from an increase in dimensions in both direction and shearing of the surface, monoclastic requires no stretch and no shear, and anticlastic has shearing as well as an increased length in one direction and decreased length in the other.

Design and modeling of novel auxetic materials and structures is a developing field. In this paper, we are examining a methodology for creating auxetic membrane structures using 3D printing upon textile materials. The result is a quick method of producing parametric auxetic structures that are durable and suitable for a range of applications.

Figure 1 shows a 7x7 print, again slit between the squares, demonstrating significant auxetic behavior and also the ability to form into synclastic surfaces.

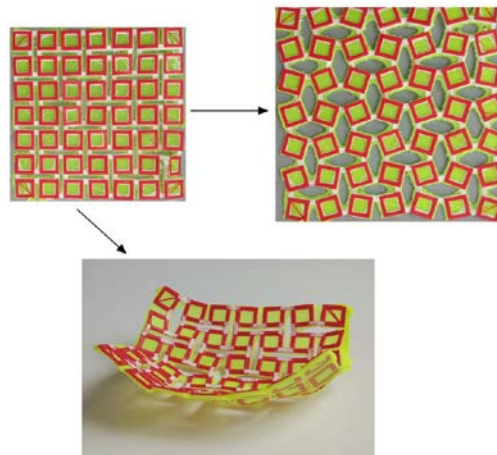


Figure 1. 7x7 printed auxetic square structure on elastic jersey knit showing auxetic behavior with a Poisson's ratio of -0.9 (right) and also ability to form synclastic surfaces (bottom).

Properties and Applications of New, Heat-resistant Polyamide Fiber

Satoshi Koizumi, Ryokei End, Jirou Tanaka

Fiber Textiles Company, Kuraray Co., Ltd.

satoshi.koizumi@kuraray.com

PROPERTIES OF POLYAMIDE RESINS AND FIBERS

Genestar™ is a new semi-aromatic polyamide which is provided from C9-diamine and terephthalic acid by Kuraray (Figure1) [1]. Genestar™ has high chemical resistance, low water absorption, high heat resistance, and good stability of dimension because of its high Tg (= 120 °C). Thanks to these excellent performances, Genestar™ widens the range of applications and increases the usage for automotive parts and electronic components. Genestar™ resin is suitable for injection and extrusion molding, and it also can be converted to the film and fiber applications. We, Kuraray, have already succeeded to get the Genestar™ fiber by means of our original spinning technologies. Genestar™ fiber has a lot of excellent performances as well as resin. (Table 1).

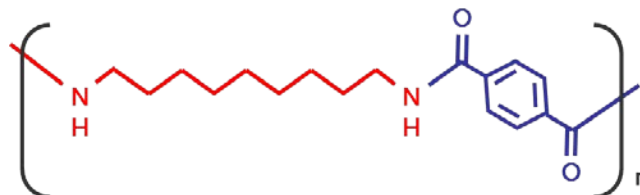


Figure 1. Molecular structure of Genestar™.

APPLICATIONS OF GENESTAR™ FIBER

Genestar™ fiber is actually used as a raw material of paper application in battery separators and filter media with utilizing its excellent performance. Genestar™ fiber can be processed to the thermoplastic composite materials which have light weight, high strength, and stiffness in addition to the original properties of resin. [2] Recently we developed Genestar™ fiber with high heat aging resistance whose tensile strength is stable under the long term of heating condition (150 °C, 500 hours). This fiber is suitable for automotive parts that both chemical resistance and heat aging resistant are required. We take advantage of the excellent performance of Genestar™ fiber and expand its applications in wide range of fields. In this presentation, we will show details of new applications of Genestar™ fiber including its properties and examples of use.

Table 1. Typical properties compared to other fibers.

		Genestar™	Ny6	Ny66
Melting Point (Tm)	°C	265	220	260
Glass transition Temp. (Tg)	°C	120	50	50
Density	g/cm ³	1.14	1.14	1.14
Water absorption (20 °C x 65 RH)	%	1.8	4.5	4.5
Tensile Strength	cN/dtex	4.2	5.6	5.7
Tensile Modulus	cN/dtex	49	35	40
Dry Shrinkage (180 °C)	%	3	24	11

REFERENCES

[1] Kuraray Co., Ltd. *A Catalogue for Genestar™ Resin*.

[2] Y. Washitake, R. Endo. "Preparation and characterization of new semi-aromatic polyamide fiber." Aachen-Dresden International Textile Conference 2013.

Three-component Composite, Anti-counterfeiting Fiber Based on Cross-section Pattern

Ronggen Zhang¹, Pei Feng¹, Fei Li¹, Qiang Fei¹, Chongchang Yang^{1,2}

¹Donghua University; ²Engineering Research Center of Advanced Textile Machinery, Ministry of Education

ycc@dhu.edu.cn; bensonreed@163.com

As a high-tech, high-added value product, anti-counterfeiting fiber has a unique place in the field of anti-counterfeiting field. This paper focuses on three component composite anti-counterfeiting fiber based on cross-section pattern and researches on the producing techniques of fiber via theoretical and experimental research. Development of a new product is also discussed.

Firstly, based on the basic principles of polymer rheology and rheological properties of the melt spinning, the flow mechanism of the melt in the composite spinning assembly was investigated. Design spinning components for three-component composite fiber with cross-section pattern for "fish bones" and "letter H" POLYFLOW was used to simulate the melt flow of different spinning solutions. The component structure was optimized by analyzing the flow rate profile and the shear rate profile of the different components within the module.

Then, through the rheological control equation, the numerical simulation of melt in cylindrical guide hole and conical guide hole were carried out by using POLYFLOW, the velocity distribution, the pressure distribution and the shear rate distribution were analyzed, the rationality and feasibility of the conical guide hole were verified. the theoretical design of the spinneret micro-hole was calculated and the size was determined. In addition, the extrusion forming of three components of composite anti-counterfeit fiber with the "fish bone" was simulated and analyzed.

Finally, the three component composite anti-counterfeiting fiber base on cross-section pattern was studied and prepared. Research and analysis of the cross-sectional boundary layer shape, when the three components were PP(red), PA6, PP(black). The influence of different spinning processes on the fiber cross-section forming was investigated through experiments, especially the traffic ratio. Experimental shows cross-section pattern — "fish bones" and "letter H" — are clear, with a high degree of anti-counterfeiting efforts.

Can Fibers Lead the 4th Industrial Revolution?

Moon Won Suh

State University of New York, Korea
North Carolina State University, USA

msuh@ncsu.edu

Textile industry led the First Industrial Revolution with shuttle looms and multi-spindle spinning frames in England in the middle of the 18th century. Textile and clothing industry also led the Second Industrial Revolution with steam-powered electricity to witness a global explosion of productivity in the late 19th century manufacturing. The Third Industrial Revolution during 1960-1980 brought a quantum jump in textile productivity via automated control, computer integrated systems (CIM), electronic sensors, and robotics along with fabulous machine development in Japan and Europe.

The Forth Industrial Revolution has just begun, and the question is: “Can fibers, fibrous products and the allied industries lead this revolution?” This talk will examine the possibility based on recent developments in innovative fibers, explosive growths in fiber-based products, massive digitization revolutions, AI-driven decisions for smart manufacturing at the presence of the ongoing cultural revolution in fashion and prevailing consumer behaviors around the world. Linking factories, machines and machine components with fibers, yarns and the end products the fastest and the most economical way became a mandate for satisfying instantaneously the most demanding customers globally. The author will critically examine the weakest links stemming from lack of fundamental research in fiber sciences and the void in creating an innovative system for converting fibers into multitudes of usable products scattered in equally large number of industries under the ongoing “grasshopper manufacturing” practices around. The author will also present a model for “Mini-Lot Manufacturing” and “Chaos-Based Textile Design” for the culturally revolutionized 21st century consumers as examples of the needed innovations.

Yarn and Fabric Performances in a Modified Ring Spinning System

Rong Yin, Xiao-ming Tao, Bin-gang Xu

Institute of Textiles and Clothing, The Hong Kong Polytechnic University, Hong Kong, China

xiao-ming.tao@polyu.edu.hk; vincentyr@hotmail.com

Recently, a novel spinning technology, named Nu-Torque™, has been proposed by introducing a false-twisting unit into the conventional ring frame for producing low twist and soft handle single yarns.^{1,2} Based on a new version of the false-twisting unit, performances of Ne 40 yarn and fabric has been evaluated.^{3,4}

Firstly, potential influencing factors on yarn properties were identified, and the fractional factorial methodology was employed to find out the statistically significant factors on yarn tenacity, evenness and hairiness. According to the experimental results, twist factor, speed ratio and wrap angle were confirmed as the significant parameters on yarn properties, therefore, these three parameters were then selected for further study using response surface methodology to find the optimal value for yarn production. The second-order equations were obtained to examine and estimate the relationships between the factors and responses, and the overlaid contour plot was employed to find the optimal results. The optimized yarn with 11.1% twist reduction apparently outweighed the conventional yarn in hairiness, slight improvements in yarn evenness as well as comparable tenacity.

Secondly, this study explores the surface characteristics and properties of knitted fabrics produced by the modified yarns and compares with the fabrics made from the conventional ring yarns. For preparing fabric samples, quantities of the Ne 40 modified yarns as well as conventional yarns were spun, respectively. Then, the prepared cop yarns were wound on the cone before knitting. After that, three single yarns were fed into the gauge of flat knitting machine and the interlock structure was adopted to avoid the fabric spirality. Properties and performances of the knitted fabrics were evaluated and compared, including fabric weight, thickness, loop length, bursting strength, air permeability, thermal property, pilling resistance, etc. The knitted fabrics made from the modified yarns show a 6.28% higher in bulkiness than that of the conventional yarns, resulting to a better capacity of thermal insulation and warmer feeling. Moreover, these two fabrics show similar bursting strength and same pilling grade.

REFERENCES

- [1] P. C. Chi, L. C. Ki, X. M. Tao. U. S. Patent 7,841,161 B2 (2010).
- [2] R. Yin, X. M. Tao, B. G. Xu. *Scientific Reports*, Vol. 6, 2016: 24432.
- [3] R. Yin, X. M. Tao, B. G. Xu. Submitted to *Textile Research Journal*.
- [4] R. Yin, X. M. Tao. Patent Submission (PolyU Ref: PAT-1083-CN-NP).

ACKNOWLEDGMENT

This research was funded in part through research grants from the Hong Kong Research Institute of Textiles and Apparel, Innovation and Technology Commission of the Hong Kong Special Administrative Region, China, High Fashion Group Management Limited (Project No. ITP/021/17TI), and a postgraduate scholarship by The Hong Kong Polytechnic University.

Fabric Defect Detection and Classification by Applying Convolutional Neural Networks

Maximilian Kemper¹, Sven Windau¹, Thomas Gries¹

¹Institut für Textiltechnik der RWTH Aachen University (ITA) Aachen, Aachen, Germany

maximilian.kemper@ita.rwth-aachen.de

INTRODUCTION AND MOTIVATION

The quality of industrially produced fabric highly depends on the number of defects within the material. Fabric defects appear in various forms, such as broken ends, reed marks, tight ends, mispicks, or loops (see Figure 1).

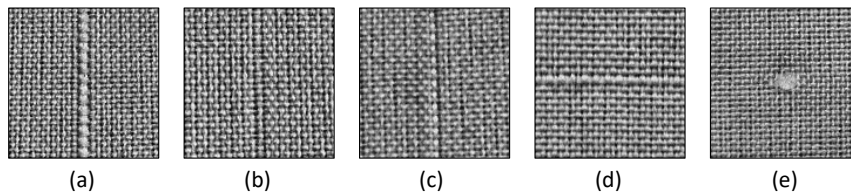


Figure 1. Examples of fabric defects: (a) broken end, (b) reed mark, (c) tight end, (d) mispick, (e) loop.

In order to provide fabric material with fewer and fewer defects, the challenge to automate fabric quality control is an important research topic. One major challenge of most automated machine vision inspection systems and their machine learning based algorithms is the requirement of a manually selected set of suitable features for the visual inspection task. In case of fabric inspection, various features have to be identified and chosen that adequately describe the different defects. This so called feature engineering demands a proficient knowledge of the problem. In order to avoid the non-trivial feature engineering, we propose to use a learning algorithm to learn relevant features for fabric defect detection and classification by itself. Hence we present the application of a Convolutional Neural Network (CNN) for automatic visual inspection of fabric defects.

METHODOLOGY

The methodology for creating the CNN is adapted from the process for applying supervised machine learning to a real-world problem. At first, the initial problem has to be defined. Then, the data for the learning or training process has to be acquired and to be pre-processed. Typical preprocessing operations comprise data normalization or contrast enhancement. After the definition of training and test sets, the initial CNN architecture and several hyperparameters have to be defined. The CNN is then trained with the training data and tested with the test data. During the training process, the CNN learns to detect and classify fabric defects by adjusting its parameters according to a training rule. To improve the accuracy of the classifier, architecture and hyperparameter tuning are performed.

EXPERIMENT RESULTS

With the proposed network architecture and hyperparameters, a classification performance of 99.51 % on white plain and twill weave fabric could be achieved. Overall, the classification performance is promising and demonstrates the capability of CNN for fabric defect detection and classification. Out of 1,216 test images, the classifier correctly classified 1,210 test images.

ACKNOWLEDGMENT

The authors would like to thank the German Research Foundation DFG for the kind support within the Cluster of Excellence “Integrative Production Technology for High-Wage Countries.”

Electrospinning vs. Centrifugally Spinning— Processing and Applications

Mahmut, Dirican, Pei Zhu, Chaoyi Yan, Xiangwu Zhang

College of Textiles, North Carolina State University, Raleigh, NC, USA

xzhang13@ncsu.edu

Nanofibers are an important class of material that is useful in a variety of applications, including filtration, tissue engineering, protective clothing, composites, battery separators, energy storage, etc. Electrospinning and centrifugal spinning are two useful methods for producing nanofibers with various structures and properties. The electrospinning method mainly uses electric force to draw charged threads of polymer solutions or melts to form fibers with diameters in the order of several hundred nanometers (Figure 1A). So far, electrospinning is the most studied method for producing nanofibers. A literature search using the Web of Science™ database shows that Year 2017 alone had publication of over 3000 articles in the electrospinning of nanofibers. Among these publications, over 50% focused on the investigation of the electrospinning process and the characterization of the resultant nanofibers, and the others mainly address the innovative use of electrospun nanofibers for various applications. Although, significant R&D efforts have been taken to scale up the electrospinning process, the wide-spread commercial use of electrospinning is still limited due to its low production rate, poor safety, and high cost. Centrifugal spinning is gaining attention as an alternative nanofiber preparation approach. Centrifugal spinning produces nanofibers by using centrifugal force to eject and stretch polymer solution or melt jets from a high-speed rotary and perforated spinneret (Figure 1B). Since the centrifugal spinning process does not use high-voltage electric field, it alleviates the related safety concern. In addition, the high rotational speed allows fast and scalable fiber fabrication, which can dramatically improve the production rate by two to three orders of magnitude and reduce the production cost when compared with the electrospinning process. Moreover, the centrifugal spinning process enables the fabrication of nanofibers from polymer solutions with much higher concentrations than the electrospinning process, which also reduces the production cost by using less solvent. However, centrifugally-spun nanofibers normally have larger diameters than electrospun nanofibers. This presentation compares the electrospinning and centrifugal spinning methods, and discusses the applications of prepared nanofibers in energy storage, chemical and biological protection, biomedical materials, and laser ultrasound.

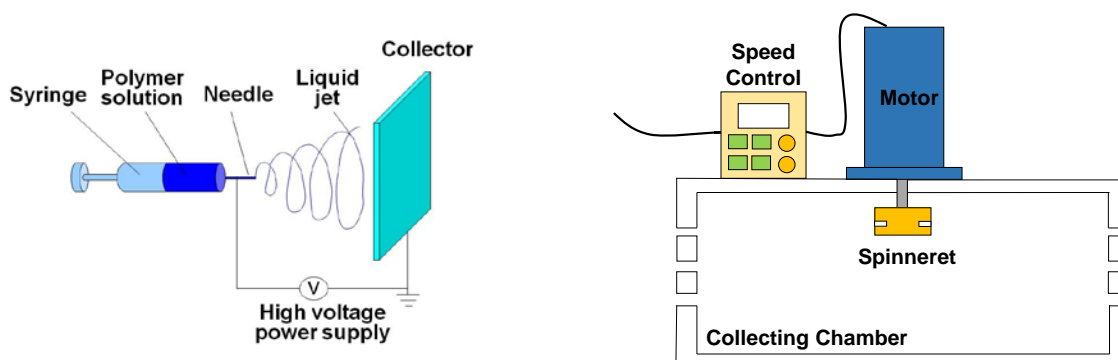


Figure 1. Electrospinning and centrifugal spinning methods for producing nanofibers.

Control of Structure and Mechanical Behavior of Continuous Nanofibers Through Addition of Small Amounts of Nano-inclusions

Dimitry Papkov, Mohammad Nahid Andalib, Yuris Dzenis

University of Nebraska-Lincoln

dpapkov@huskers.unl.edu; ydzenis@unl.edu

Recent analysis of electrospun polyacrylonitrile (PAN) nanofibers (NFs) in the ultrafine (100-250 nm) diameter range showed extraordinary simultaneous size effects in strength, modulus, and toughness. Finest nanofilaments exhibited strength approaching that of advanced structural fibers, while exceeding their toughness by more than an order of magnitude. Structural investigations showed that this unique and highly desirable mechanical behavior may be due to high degree of macromolecular alignment in conjunction with low crystallinity. Small additions of nano-inclusions such as carbon nanotubes and graphene oxide resulted in significant changes in nanofiber structure after carbonization. Here, we compare the impact of different nano-inclusions, such as carbon nanotubes, graphene oxide, cellulose nanocrystals, and para aramid nanocrystals, on the morphology, structure, and mechanical properties of nanofibers. Interaction between the precursor polymer matrix and the nano-inclusions with different geometry, size, and surface chemistry are examined. Effects of these interactions, nano-inclusion alignment and dispersion on nanofiber crystallinity and crystal alignment are examined. Mechanical properties of the different composite nanofibers are compared. Results show significant differences in the impact of the different nano-inclusions on nanofiber modulus and strain to failure. Addition of Double Wall Carbon Nanotubes improved nanofiber modulus well in excess of what was expected from the rule of mixtures. At the same time, strain to failure of the nanofibers was reduced. On the other hand, cellulose nanocrystals had little effect on nanofiber modulus, but increased the strain at failure almost two-fold. Structural explanations are offered for the differences in the observed properties. Effects of different nano-inclusions on nanofiber shrinkage, polymer chain relaxation, and crystal orientation after heat treatment are also examined. These effects can play an important role in the final structure and properties of the nanofibers after carbonization. Results obtained in this work can form the basis for future development of a new generation of advanced nanofibers for structural applications.

Polymer Nanofiber-based Filter Media with Tailored Three-dimensional Structure for High-efficient Air Filtration Through Suspension Drying Techniques

Ke Liu^{1,2}, Pan Cheng^{1,2}, Zhibing Yi^{1,2}, Xu Wang^{1,2}, Ying Liu^{1,2}, Dong Wang^{1,2}

¹Hubei Key Laboratory of Advanced Textile Materials & Application, Wuhan, China

²College of Materials Science and Engineering, Wuhan Textile University, Wuhan, China

luicole@foxmail.com

A mixed solution of tert-butyl alcohol (TBA) and water was employed to stably disperse PVA-co-PE nanofibers. Nanofibrous filter media based on PP nonwoven fabric substrate with various porosity were then prepared via three drying techniques of nanofiber-suspension: spray-air drying, spray-freeze drying and container loading-freeze drying. The prepared nanofiber composite filter media present controllable three-dimensional structure. Nanofiber layer porosity increased from 76.6% to 97.3% with a increased nanofiber layer thickness from about 10 to 55.3 μm for filter media with the given nanofiber coverage density (2.667 g/m^2). Based on the structure, filter media possess a best comprehensive filtration performance with the quality factor=1.110 mmH₂O-1 (99.955% and 6.73 mmH₂O) and a best efficient performance with efficiency=99.999% (0.645 mmH₂O-1 and 17.86 mmH₂O) at NFCD=2.677 g/m^2 and 6.583 g/m^2 , respectively. The promising properties are mainly derived from the stable three dimensional structure of nanofiber network offering the superior torturous channels for capturing airborne nanoparticles and facilitating the penetration of air flow, which presents a typical deep bed filtration. The result of electret treatment test shows that the filter media exhibits remarkably stable filtration properties and basic insusceptible to the electrostatic charges rather than the commercial PP nonwoven fabric substrate. This suggests the superiority of present nanofiber composite filter media in the application as a high cost-effective air filter.

KEYWORDS: Nanofiber, air filtration, 3D structure.

ACKNOWLEDGMENT

The authors were thankful to the financial support of Nature Science Foundation of Hubei Province (No. 2016CFA076), National Science-technology Support Program of China (No. 2015BAE01B01).

Electrospinning PAN of Increasing Isotacticity

Reva M. Street¹, Masatomo Minagawa², Andrew Vengrenyuk¹, Caroline L. Schauer¹

¹Department of Materials Science and Engineering, Drexel University, Philadelphia, PA, USA

²NPO, Dream-Create-Laboratories, Yamagata, Japan

cls52@drexel.edu

Polyacrylonitrile (PAN) is a semicrystalline hydrophobic polymer commonly electrospun for filtration applications and as a precursor for carbon nanofibers. Using the urea-clathrate synthesis, PAN of various isotacticities can be created. Electrospinning of urea-clathrate polymerized PAN with isotacticity 25% and 52% was achieved in N, N-dimethylformamide (DMF) at room temperature. The non-woven meshes had a cylindrical morphology and ranged in diameters from 200-600 nm. X-ray diffraction (XRD) analysis demonstrated that the polymer retained semi-crystalline structure, and that crystallinity was correlated with increasing isotacticity. The electrospun isotactic PAN nanofiber mats also exhibited ~30% of the piezoelectric response of electrospun (65:35) poly(vinylidene fluoride-trifluoroethylene) (PVDF-TrFE), a current gold-standard for piezoelectric polymers. Conversely, commercially purchased free-radical polymerized PAN exhibited no observable piezoelectric response. This is significant, as previous studies of PAN piezoelectricity required stretching and poling or blending with copolymers to measure a significant piezoelectric effect. Future work is ongoing studying the effect of carbon nanofiber production due to increasing isotacticity.

Carbon Fibers and Advanced Composite Materials

Consideration of the Impregnation Process of Polymer Melt to Carbon Fiber Bundle by Steady-state Viscoelastic Flow Simulation

Shuichi Tanoue, Hayato Otake, Hideyuki Uematsu

Frontier Fiber Technology and Science, Faculty of Engineering, University of Fukui, Japan

tanoue@matse.u-fukui.ac.jp

INTRODUCTION

The impregnation process of the polymer melt to the carbon fiber bundle can be modeled by the polymer melt flow through the cylinder group region. In this study, we tried to discuss the impregnation process of the polymer melt to the carbon fiber bundle by viscoelastic flow simulation of the polymer melt through the cylinder group region.

CALCULATION METHOD

Figure 1 shows the calculation model. In the cylinder group region, the cylinders locate in the equal interval and zigzag alignment. The length of the cylinder group region is changed by the number of cylinders in this region. The steady-state flow of the viscoelastic fluid is assumed. The Phan-Thien Tanner (PTT) model was employed as the constitutive equation. Figure 2 shows the steady-state flow characteristics of the test fluids. Three kinds of the test fluids with the same shear viscosity curves and the different elongational viscosity curves were considered.

RESULTS AND DISCUSSIONS

The ratio V_f between the total cross-section area of cylinders in the cylinder group region and this region area corresponds to the volume ratio for carbon fiber reinforced plastic. In this abstract, we discuss the calculation results at $V_f = 40\%$ and the cylinder diameter R_f of $3.5 \mu\text{m}$. The pressure difference between the pressure at the entrance of the cylinder group region and that at the exit of this region, named as the pressure drop, corresponds to the necessary pressure when the fluid flows in this region at a mean velocity. Figure 3 shows the pressure drop as a function of the length of the cylinder group region at the mean velocity of $70 \mu\text{m/s}$. The average of the pressure at the plane perpendicular to the flow direction were employed for calculating the pressure drop. The pressure drop increased linearly with the length of the cylinder group region, and the pressure drop gradient increased with the elongational viscosity of the fluid. There are acceleration and deceleration flows in this region. Therefore, a large pressure is needed for flowing the fluid having large elongational viscosity in this region.

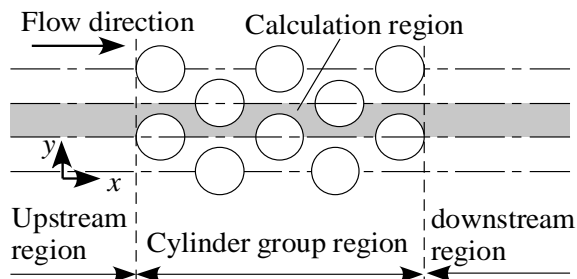


Fig. 1 Calculation region.

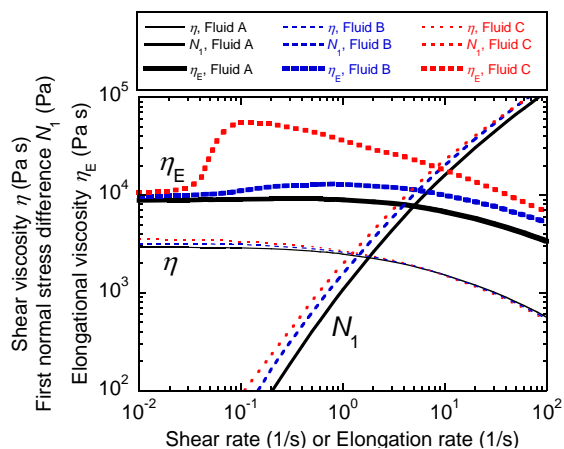


Fig. 2 Steady-state flow characteristics used in this study.

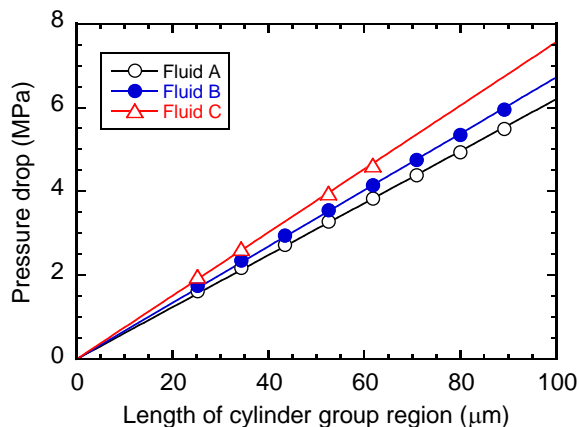


Fig. 3 Pressure drop as a function of the length of the cylinder group region at mean velocity of $70 \mu\text{m/s}$ at $V_f = 40\%$ and $R_f = 3.5 \mu\text{m}$.

Improvements in Determination of Carbon Fibre Strength Distribution Using Automation and Statistical Data Analysis

Faisal Islam¹, Steve Bucknell², Yann Leray², Anthony Bunsell¹, Lucien Laiarinandrasana¹, Sébastien Joannès¹

¹MINES ParisTech, PSL–Research University, France

²Dia-Stron Ltd., Andover, United Kingdom

sebastien.joannes@mines-paristech.fr; steve.bucknell@diastron.com; faisal.islam@mines-paristech.fr

INTRODUCTION

Carbon fibres are widely used in composite materials to make light-weight and high-strength products. For failure modelling and to simulate the effective properties of the products, detailed information about tensile strength distribution and its parameters are required. Many studies have acknowledged difficulties in obtaining fibre strength data which can accurately represent the entire fibre population in a given application. These mainly include premature specimen failure during handling, improper alignment between the fibre and the loading direction, time and labour requirement, etc. An automated single fibre testing process (referred to as the LDS/LEX) has been developed at Dia-Stron Ltd. and described here, which could assist in overcoming most problems. It increases the efficiency of the process and enhances quality of the data generated. The errors occurring due to manual handling of fibres are eliminated and human effort is reduced notably.

CHARACTERIZING CARBON FIBRES

It is known that strength of fibre composites is primarily dependent on fibre properties. So, fibre strength is a very critical input parameter for computer modelling of composite materials for different applications such as composite Pressure vessels and automotive components. Failure in fibre composites usually originate inside fibres and using tow data may not be very useful. Also, for recycled carbon fibres, SFT is the best method for quantitative analysis and quality control.

Issues in testing carbon fibres

Carbon fibres are usually tested manually which is associated with many issues. If unaddressed, it can be the reason behind huge variations in reported results. Some of these issues include:

1. Fibre cross-section may vary between individual fibres and also along the length, hence accurate measurement of fibre diameter is critical for accurate determination of fibre strength.
2. The gauge length used for testing would affect the measured strengths, but there has been no general agreement on an optimum gauge length in the results that have been reported.
3. The confidence on the reported results would depend on the number of fibres that are tested. Since manual single fibre testing is a very time-consuming process, most authors have reported results only for a small number of fibres.
4. It is difficult to avoid fibre misalignment in manual single fibre testing, which may lead to inaccurate results.

Manual method for single fibre testing

Manual SFT required separate instruments for measuring fibre diameter and applying tensile load. Card frames are used for mounting the fibres as shown in Figure 1(a). Sample preparation starts by extracting a single fibre from a bundle in placing it on the paper tab. The ends of the fibre are then fixed using epoxy or wax. This is followed by diameter measurement after which the specimen is transferred to the universal testing machine. The sides of the paper tab are then cut and the tensile load is applied. Cutting the paper often leads to fibre failure before the test commences.

One of the major problems with this process is avoiding fibre misalignment and ensuring an accurate gauge length as shown in Figure 1(b). It depends very strongly on the position of the epoxy which is very difficult to control manually, especially when the gauge length becomes very small. In addition to being very time consuming, a significant number of specimens break during the preparation process.

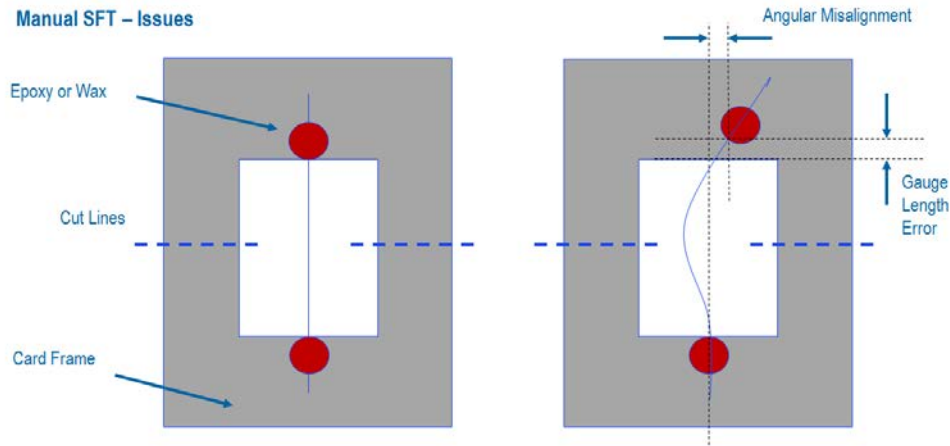


Figure 1. (a) Scheme of a single fibre mounted on card frames, (b) major issues with sample preparation.

Automated single fibre testing

To overcome the problems faced by the conventional method, Dia-Stron has developed an automated testing method which includes a dedicated sample preparation technique. Card frames are replaced by plastic tabs (Fig 2a). Each end of a fibre is held by a plastic tab. The tabs are arranged on a cassette in sets of 20 (Fig 2b). Each tab has v-shaped slots which help in proper alignment of fibres. UV Curing adhesives are dropped inside the wells at the end of the tab which locks the fibre in place, and defines the fibre bonding point very accurately (Fig 2c). UV curing of adhesive is done by flood illumination which takes between 3-10 secs (Fig 2d).

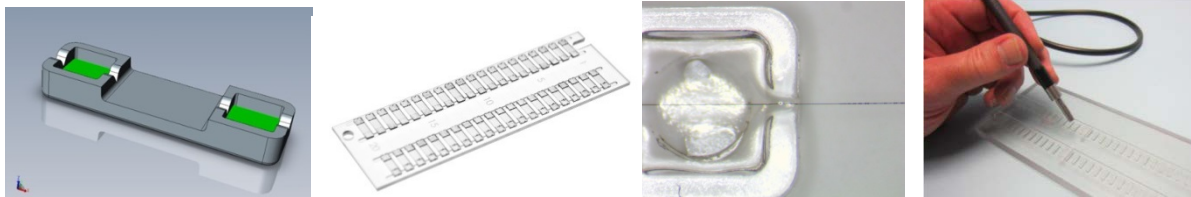


Figure 2. (a) Plastic tab for holding a fibre, (b) 20 sample cassette, (c) wells in tabs for accurate gauge lengths (d) UV curing of adhesives.

Dia-Stron automated testing setup is a combination of a tensile tester and a laser diffraction system for measurement, together known as the LEX/LDS system (Figure 3a). The automated pick-up system transfers the specimens from the cassette to the test location, where the fibre is straightened, diameter is measured and the tensile load is applied. After test completion, the system automatically transfers the plastic tabs back to the cassette and proceeds to the next test. The advantages of this system include reduction in testing time due to automation, improved alignment due to the presence of grooves in tabs, gauge length correction due to straightening of fibres before testing, reduced specimen failure due to elimination of operator handling, among others. The system allows the testing of fibres at several different gauge lengths.

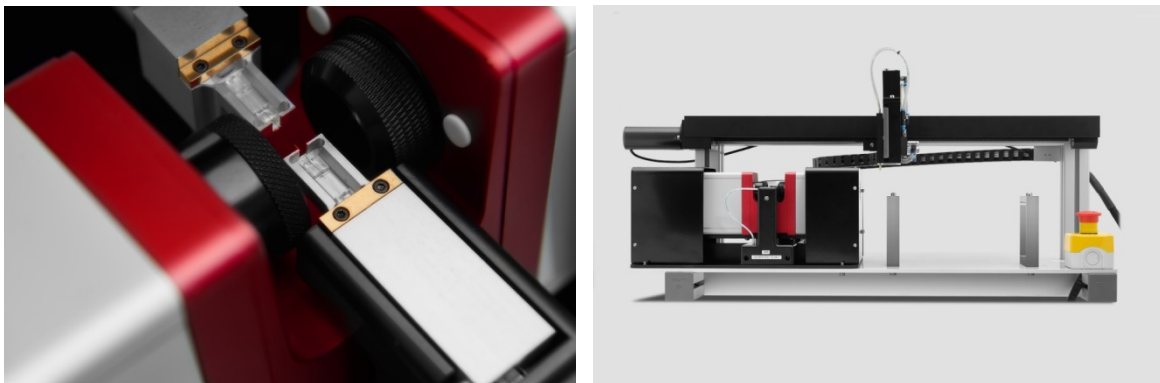


Figure 3. (a) Combined Linear Extensometer and Laser Diffraction system, (b) complete automated testing setup.

STATISTICAL ANALYSIS

According to the weakest link theory each fibre is a chain composed of multiple small links connected to each other. Strength of the weakest link determines the strength of the fibre. The statistical function that best describes the weakest link theory is the Weibull distribution (Eq. 1). It is characterized by the scale (σ_0) and shape (m) parameters. One of the advantages of using the Weibull distribution is that it gives us a very useful 2D representation of the observation. The experimental data generated for carbon fibre strength was used to fit to a Weibull distribution (Fig 4a). The dots represent the experimental data and the straight line represents the best fit Weibull model. The vertical axis represents unreliability (or failure probability), which is the percentage of population that is expected to fail and the horizontal axis represents the corresponding strength. B50 life, or the median failure strength can be read directly from the graph and is 4.01 GPa. This means that 50% of the fibre population is expected to have strength of less than 4.01 GPa.

$$P(\sigma_f) = 1 - \exp\left\{-\left(\frac{L}{L_0}\right)\left(\frac{\sigma_f}{\sigma_0}\right)^m\right\} \quad (1)$$

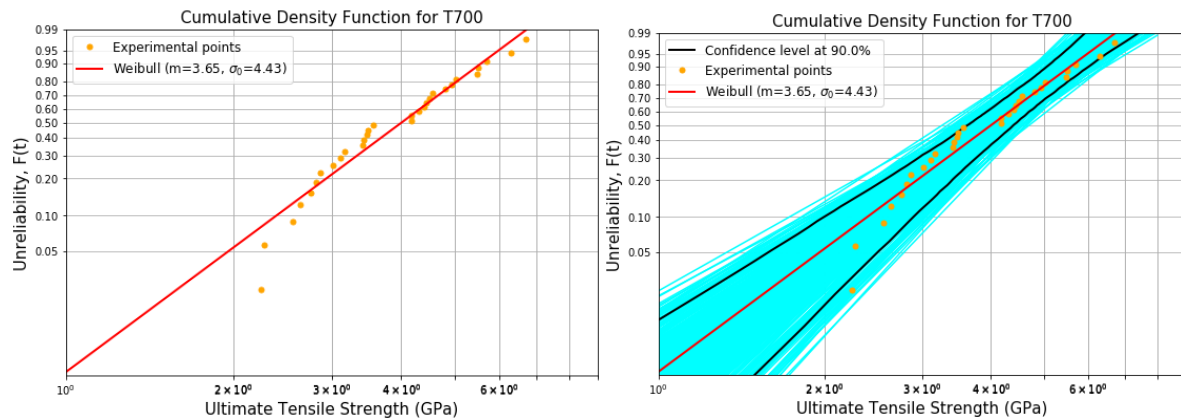


Figure 4. (a) Best fit Weibull plot for experimentally generated carbon fibre strength, (b) simulated Weibull distributions and confidence region.

To get an indication of the confidence that can be associated with the results, a confidence interval has been calculated. Monte Carlo simulations of the Weibull distributions were generated, as shown in blue in Fig. 4(b). Using these distributions, the confidence region was obtained which is the area between the 2 black curves. Using this, the Confidence interval can be calculated. The B50 life (or the median strength) can be seen to fall between 3.65-4.37GPa. It would be more appropriate and useful to report this Confidence Interval along with every point prediction.

However, this Confidence Interval is very large and needs to be narrowed down for more accuracy in reported results. More experimental data points are required for that purpose. Thanks to the automated test setup, it was possible to generate a large number of fibre strength data and for different gauge lengths, as shown in Table I. The experimental data set was fitted with the two-parameter Weibull distribution using the method of truncation. This was required because the experimental data set does not contain the strength of weak fibres, as they were too weak to survive the testing process. So, to represent this data set, we used the method of truncation to predict the actual Weibull distribution. Monte Carlo simulations were made and the Confidence Interval was calculated. The width of the 90% Confidence Intervals reduce to less than half the original size. For example, the new Confidence Interval for the B50 life (or the median strength) is calculated to lie between [4.01-4.31] GPa. This increased accuracy has been possible because of the very large number of data points that were generated using the automated testing system.

Gauge Length (mm)	No. of fibres tested
04	140
20	140
30	200

Table I. No. of fibres tested for different gauge lengths.

ACKNOWLEDGMENT: The research leading to these results has been done within the framework of the FiBreMoD project and has received funding from the European Unions Horizon 2020 research and innovation programme under the Marie Skłodowska-Curie grant agreement No. 722626.

Strength Reduction in Liquids and Its Application in Defect Analysis for Carbon Fibers

Masatoshi Shioya¹, Masayoshi Ido¹, Yoshiki Sugimoto²

¹Tokyo Institute of Technology; ²The National Institute of Advanced Industrial Science and Technology

shioya.maa@m.titech.ac.jp

Tensile break of carbon fibers (CFs) is initiated by the crack propagation from the initial crack developed during fiber production process. The Griffith strength relation shows that the crack in a brittle material starts to propagate when the tensile stress reaches to a value of

$$\sigma = \frac{1}{Y} \left(\frac{2E\gamma}{\pi c} \right)^{1/2} \quad (1)$$

where E is the tensile modulus, γ the free energy at the crack surface, c the length of a crack with a sharp tip at one end and Y the geometric constant. This equation predicts that the tensile strength decreases in a liquid as compared with that in air if the newly created crack surface is covered by the liquid or its vapor immediately after the crack starts to propagate and, as a result, the value of γ decreases. Actually, this tensile strength reduction can be observed for a polyacrylonitrile(PAN)-based CF as shown in Figure 1 (M. Shioya *et al*, *Carbon*, Vol.65, p.63 (2013)).

Since this strength reduction takes place only when the critical defect (i. e. the initial crack that causes fiber fracture) locates on the fiber surface, it is possible to know whether it locates on the fiber surface or inside the fiber by the tensile tests in air and a liquid. However, once a given single fiber specimen is broken in air, it is impossible to make it back to the unbroken state and test it again in a liquid. It is assumed, therefore, that the order, i , of the strength value of a given specimen among the strength values of N specimens, when arranged from the lowest to the highest values, does not change in different media. Then, the strength value of a given specimen in different media can be known by conducting the tensile tests on groups of specimens in different media and following the strength values at a given value of the fracture probability, F , defined as

$$F(\sigma) = \frac{i - 0.5}{N} \quad (2)$$

where the value of 0.5 has been introduced for taking into account of the finite number of the specimens in a group. Figure 2 indicates that the larger critical defects tend to locate at the fiber surface.

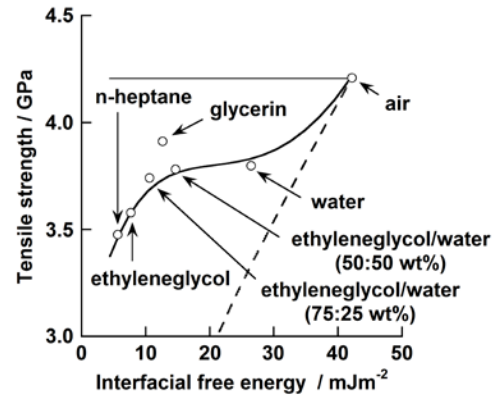


Fig. 1. Tensile strength of a CF in various media versus the interfacial free energy between CF and test media. In figures 1 and 2, the horizontal solid line shows the strength level in air and the dashed line represents the strength value calculated with the Griffith strength relation using the interfacial free energy for γ .

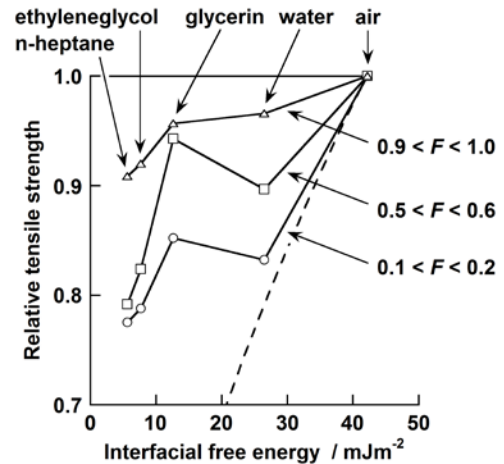


Fig. 2. Relative tensile strength of CF specimens in various test media normalized to the strength in air versus the interfacial free energy between CF and test media. The plots with the larger value of F corresponds to the CF specimens containing the larger critical defects. The plots shift downwards from the horizontal solid line to the dashed line as the fraction of the surface cracks increases.

Influence of Chemical Pretreatments on Processing, Structure, and Properties of Rayon-based Carbon Fibers

Gajanan Bhat¹, Kokouvi Akato², Wesley Hoffman³, Farhad Mohammadi⁴

¹The University of Georgia, Athens, GA, USA

²Oak Ridge National Laboratory, Oak Ridge, TN, USA

³AFRL, Edwards Air Force Base, CA, USA

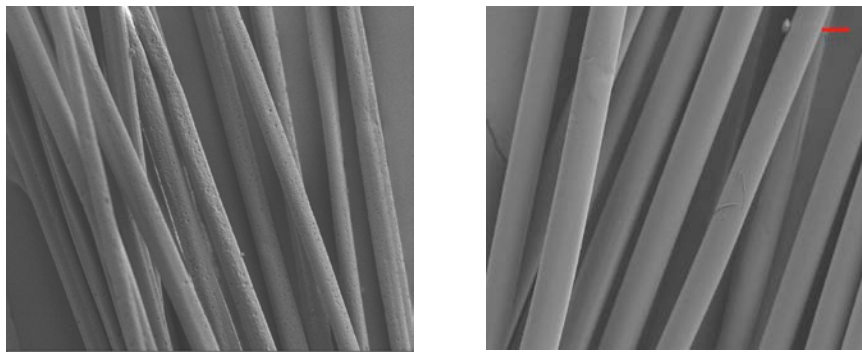
⁴Advanced Cerametrics, Lambertville, NJ, USA

gbhat@uga.edu

Although carbon fibers are predominantly produced from polyacrylonitrile (PAN) and pitch precursors, rayon also is of interest as a precursor fiber since rayon-based carbon fibers have some unique properties. Rayon was the first precursor investigated for high modulus carbon fibers. Rayon-based carbon fibers are produced by a limited number of companies in the world, and no rayon is commercially produced in the United States. Experimental studies are being conducted to optimize the processing conditions for conversion of a domestically produced rayon precursor into carbon fibers. For comparison, a commercially available rayon fiber was also investigated.

The transition of rayon fibers to carbon fibers consist of oxidation in air at lower temperatures, and carbonization and graphitization in an inert environment at a higher temperature. The oxidative stabilization is a complicated process involving multiphase reactions in a complex chemical pathway. For rayon, the decomposition starts with desorption of chemically bonded water followed by dehydration of cellulosic structure (150–240°C). It is known that phosphorous based chemicals help control the oxidation reactions in a way resulting in higher carbon yield and possibly in reduction of the carbon fiber cost. The precursor fibers used were pretreated in 1N phosphoric acid before stabilization. The stabilized fibers were carbonized to various temperatures, and the effects of high temperature treatment and tension during carbonization were investigated by elemental analysis, x-ray diffraction studies and tensile testing.

It was observed that chemical pretreatment was critical in successfully converting rayon into carbon fibers and increasing the carbon yield. The SEM photographs show that high quality carbon fibers can be produced from proper pretreatment, controlled pyrolysis and high temperature carbonization. The carbon content of the fibers was relatively lower even after heat treatment till 1200°C. The tensile strength and modulus were much higher with the use of tension during the heat treatment process. To achieve high carbon content and tensile properties, high temperature treatment above 2000°C is required. Results from this ongoing research will be presented.



SEM photographs of carbon fibers from untreated and pretreated precursor fibers.

The Effects of Interfacial Adhesion for Mechanical Properties of CFRTPs Made with Polyamide 6

Toshihira Irisawa, Kento Ujihara, Sarasa Kobayashi, Yasuhiro Tanabe

Graduate School of Engineering, Nagoya University

irisawa.toshihira@material.nagoya-u.ac.jp

Carbon fiber reinforced thermoplastics (CFRTPs) have been focused on their low cost and high production rate, so many investigations about CFRTPs have been performed from various directions. Especially, commodity thermoplastics such as polypropylene (PP), polyamide (PA) or polycarbonate are selectively used as a matrix resin for CFRTPs in automotive applications. Therefore, CFRTPs made with commodity plastics have been developed worldwide. In this study, PA6 were chosen as matrix polymer for CFRTPs, because PA6 have been expected as matrix polymer for automotive application in terms of the balance of properties and cost.

It is known that the surface of CFs has the oxygen-containing functional groups by surface treatment such as electrolytic oxidation process, and that these functional groups form covalent bonds to epoxy resin at the time of traditional CFRP molding, which causes high interfacial shear strength (IFSS). On the other hand, it has not been clear that the functional groups efficiently work for the IFSS between CFs and PA6. Furthermore, it is also known that the impregnation of thermoplastics into CFs fabrics is difficult because the melt viscosity of thermoplastics is very high. To solve this problem, CFRTPs made with in-situ PA6 by a vacuum assisted resin transfer molding (Va-RTM) (Fig. 1) have been proposed. This study focuses on the interfacial adhesion between CFs and in-situ polymerizable PA6, and the influence of the functional groups on carbon fibers for mechanical properties of the CFRTPs have been discussed.

In the case of using the CFs which have the functional groups on the surface, interfacial adhesion between CFs and PA6 became high because of interaction of each other (Fig. 2). Furthermore, it was revealed that these effects apparently improved the mechanical properties of these CFRTPs (Fig. 3).

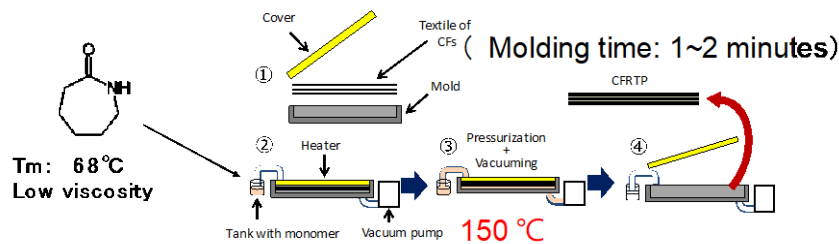


Fig. 1. Schematic illustration of Va-RTM methods.

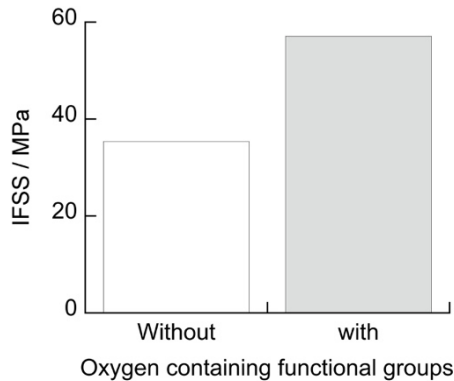


Fig. 2. IFSS between PA6 and CFs with/without the functional groups.

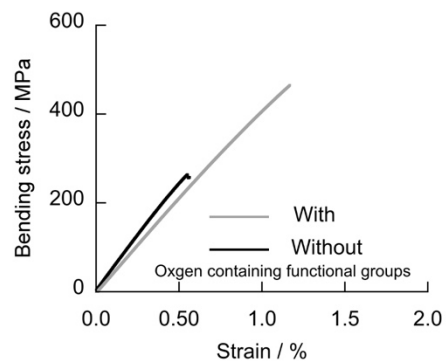


Fig. 3. S-S curves of CFRTP made with PA6 and CFs with/without the functional groups.

Highly Transparent PVA-co-PE Nanofiber/Epoxy Film

Dong Wang¹, Mufang Li¹, Weibing Zhong²

¹Wuhan Textile University, Wuhan, China; ²College of Chemistry, Chemical Engineering and Biotechnology, Donghua University, Shanghai, China

wangdon08@126.com

The development of electronics towards a more functions-integrated, flexible and stretchable direction requires mechanically flexible substrates with high thermal and dimensional stability and optical transparency. Herein, rolls of an optically transparent PVA-co-PE nanofibrous membrane/epoxy composite with synergistically enhanced thermal stability, very low CTE, and outstanding mechanical properties are reported. The nanoscale size, the unique inter-stack structure, and the strong interfacial interactions between the PVA-co-PE nanofibers and the epoxy contribute to the synergistic effects. Because of the match between the refractive index (RI) of the PVA-co-PE nanofibers and the epoxy matrix, the visible light transmittance of nanocomposite film could be as high as 85% and the composite film was still optically transparent with a nanofiber loading content of up to 61.7 wt%. The break strength and compliance matrix of the composite film with a high fiber loading of 61.7 wt% increased by 2.3 times of that of the neat epoxy film and exceeded $3000 \text{ m}^2 \text{ N}^{-1}$, respectively. PVA-co-PE nanofibers have a very low CTE value ($3.634 \times 10^{-6} \text{ K}^{-1}$) and could be applicable as a reinforcement to reduce the thermal expansion of epoxy. Furthermore, we developed a flexible alternating current electroluminescent (ACEL) device based on the transparent composite film and the experimental results showed that the transparent composite film could serve as substrate for flexible electronic devices. In addition, their electrical and optical properties were evaluated.

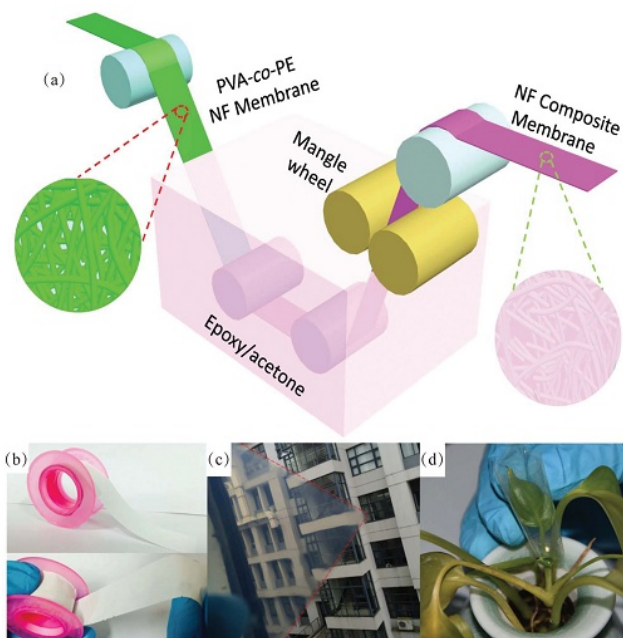


Figure 1. An illustration of the preparation process of transparent PVA-co-PE/epoxy composite films, (b) A digital image of a reel of PVA-co-PE nanofibrous membrane, (c) An image of transparent composite film ($6 \times 6 \text{ cm}$) from which we can see the distant building, (d) A digital photographic image showing the high transparency and flexibility of the composite film.

Ionic Liquid-based Electrolytes Containing Inorganic Nanofibers for Quasisolid Energy Devices

Hidetoshi Matsumoto¹, Takahiro Yuuki¹, Yuki Takano¹, Minoru Ashizawa¹, Hajime Matsumoto²

¹Tokyo Institute of Technology; ²National Institute of Advanced Industrial Science and Technology

matsumoto.h.ac@m.titech.ac.jp

In the present study, surface amino-functionalized silica nanofibers (NFs) were prepared by electrospinning and used as one-dimensional (1-D) fillers of ionic liquid (IL)-based quasisolid electrolytes. On adding NFs to an IL (1-ethyl-3-methylimidazolium bis(trifluoromethanesulfonyl)amide, EMITFSA) containing lithium salt (lithium bis(trifluoromethanesulfonyl)-amide, LiTFSA), the well-dispersed 1-D nanofillers easily form a three-dimensional network structure in the IL, function as physical cross-linkers, and increase the viscosity of the composites, consequently providing a quasisolid state at a small fraction of the NFs (above 2 wt %). Rheological measurements demonstrated that the prepared composites exhibit “gel-like” characteristics up to 200°C. All prepared IL-NF composites show high ionic conductivities, on the order of 10^{-3} S cm⁻¹, around room temperature. It is also found that thinner NFs enhance the lithium transference numbers of the composites. Fourier transform infrared measurements revealed that surface amino groups of the NFs interact with the SO₂ group of TFSA anion. This supports that the surface amino groups of the NFs plays a crucial role in not only quasisolidification at a low fraction of the NFs but also ionic transport behavior through the IL-NF composites. In addition, quasisolid lithium-ion cells containing the prepared composites demonstrate relatively high rate characteristics and good cycling performance at high temperature (125°C). These results clearly indicate that IL-NF composites can be promising electrolytes for use in quasisolid energy devices, including secondary batteries, supercapacitors, fuel cells, and dye-sensitized solar cells.

ACKNOWLEDGMENT

This work was supported by the Advanced Low Carbon Technology Research and Development Program, Specially Promoted Research for Innovative Next Generation Batteries (ALCA-SPRING) from Japan Science and Technology Agency (JST).

Preparation of Few-layer Graphene Using Ionic Liquid as Green Media and Its Application in Polymer Composite and Fibers

Ye Chen¹, Chenyu Wang¹, Fuyou Ke¹, Peng Ji¹, Huaping Wang^{1,2}

¹State Key Laboratory for Modification of Chemical Fibers and Polymer Materials, College of Materials Science and Engineering, Donghua University; ² Research Institute of Donghua University

chenye@dhu.edu.cn

The application of graphene in materials and fibers has been widely attracted attention, due to its distinguished properties. However, preparation of large-scale and high-quality graphene is the premise. In addition, how to avoid the re-aggregation of graphene in materials processing is the key for obtaining high-performance composites and fibers with graphene. In this research, a simple method to obtain fewer-layer graphene was reported, by grinding and sonicating the mixture of ionic liquids (ILs) and multilayer graphite. The strong π - π and cation- π interactions between ILs and graphene layers provided driving force for exfoliating graphite to few-layer graphene. Then the obtained fewer-layer graphene was composited with polymers and the improvement on the mechanical and electrical properties of polymer matrix was investigated. The result indicated that the tensile strength of the composites was improved by adding few-layer graphene in polymers. SEM showed a good dispersion of ionic liquid modified graphene in polymer matrix.

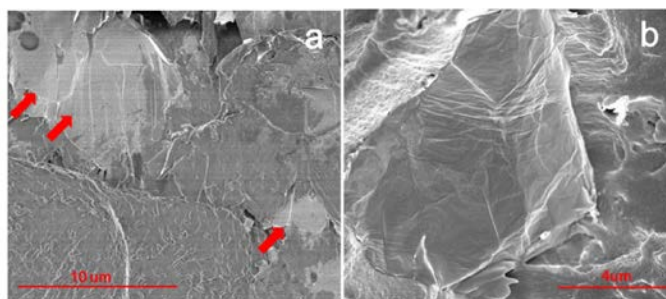


Figure 1. SEM images of PEI/GNPIL composite film with 0.5 wt% GNPIL (a) GNPIL intercalated in PEI matrix; (b) full structure of graphene in PEI matrix.

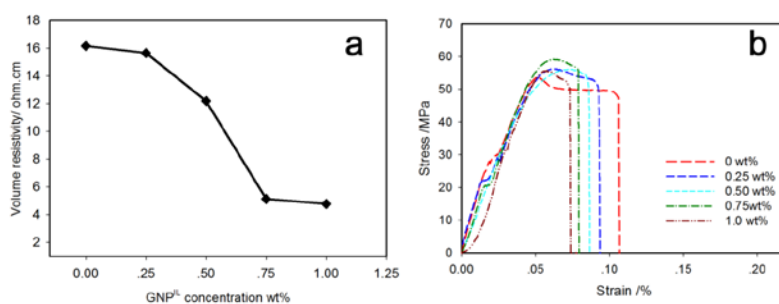


Figure 2. Volume resistivity (a) and stress-strain curves (b) of PEI composites with different GNPIL contents at room temperature.

REFERENCES

1. Y. Chen, C. Wang, W. Fan, F. Ke, S. Chen, F. Guan, H. Wang. *Compos. Sci. Technol.* ASAP.
2. Y. Chen, J. Tao, L. Deng, L. Li, J. Li, Y. Yang, N.M. Khashab. *ACS Appl. Mater. Interfaces*, 5(15), 2013: 7478-84.

ACKNOWLEDGMENT

The authors gratefully acknowledge the supports from the National Natural Science Foundation of China (51703021), Shanghai Pujiang Program (16PJ1400500).

On the Development of Sustainable Composites Reinforced with High-performance Regenerated Cellulose Fibers

Anastasia F. Koutsomitopoulou, Chenchen Zhu, Marco Longana, Stephen J. Eichhorn, Kevin D. Potter

Bristol Composites Institute (ACCIS), Department of Aerospace Engineering, University of Bristol, Bristol, United Kingdom

an.koutsomitopoulou@bristol.ac.uk

The future demands for a significant reduction of the CO₂ emissions have forced the composite sector (e.g automotive and wind energy) to explore more sustainable manufacturing processes for lightweight composite materials. To reduce the petroleum-based, non-renewable polymers dependency, large scale utilization of natural polymers such as cellulose needs to be developed. However, one of the major challenges in large scale utilization of cellulose from biomass is dissolution and processing of cellulose to prepare industrial products such as high-performance textile fibers.

For that purpose, a continuous and high-speed manufacturing process for regenerated cellulose fibers using Ionic Liquids (ILs) as benign solvent is developed to produce strong fibers with high stiffness by achieving high-fiber stretching during the spinning process. The novel regenerated cellulose fibers demonstrate mechanical properties similar with those of the commercially available glass fibers. The physical structure as well as the mechanical properties of these fibers using the manufacturing methods developed for the purposes of this study, indicate the feasibility of use these fibers in sustainable composites for automotive and sports equipment applications.

The development of sustainable composites with competitive mechanical properties suitable for applications in automotive, sports equipment and other sectors is still ongoing. This study gives an initial insight into the incorporation of high-performance regenerated cellulose fibers into thermosets and thermoplastic materials for the production of composites. This study aims to demonstrate the capability to manufacture hybrid carbon-regenerated cellulose long-fiber reinforced composites with high fiber volume fractions as well as highly aligned short fibers composite materials using the HiPerDiF method.

Inducing the Crystallization in Cotton Cellulose Ion Gel Films for Enhanced Mechanical Properties

Muhammad Abdul Haq^{1,2}, Yasuhiro Habu¹, Kazuya Yamamoto¹, Akihiko Takada³, Jun-ichi Kadokawa¹

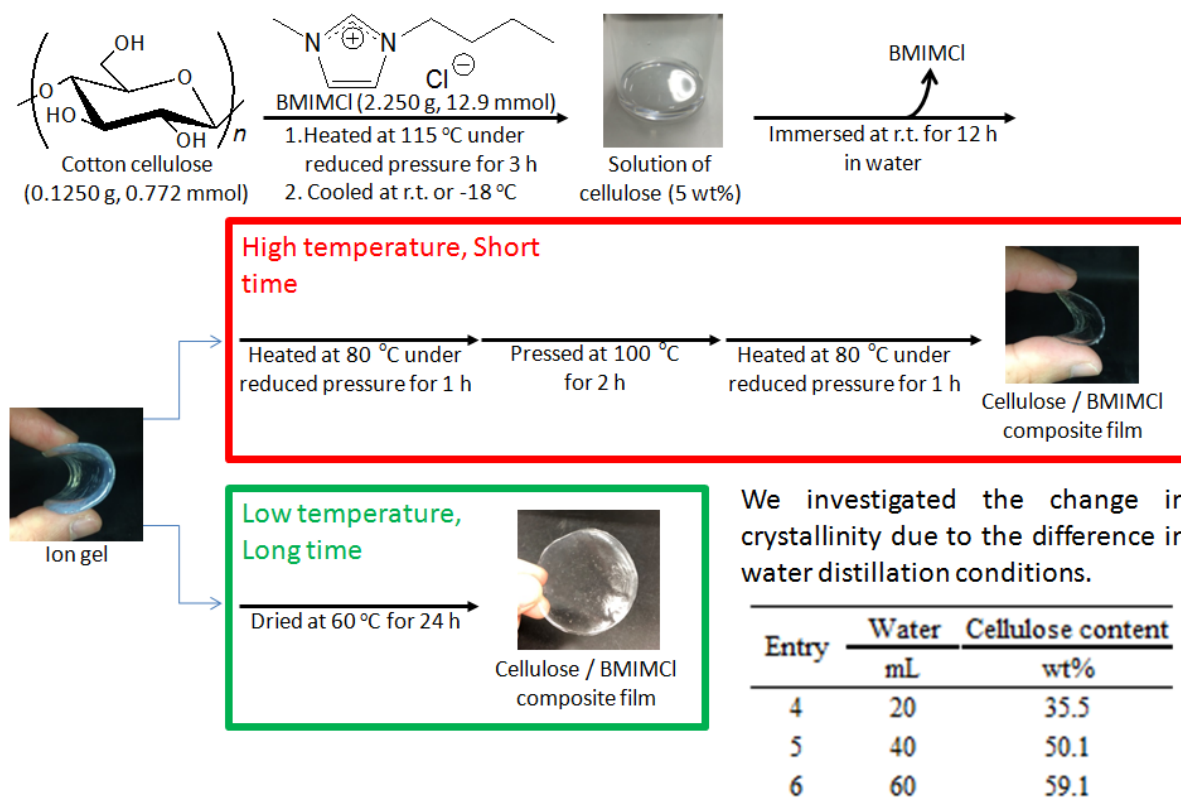
¹Department of Chemistry, Biotechnology and Chemical Engineering, Kagoshima University, Japan

²Laboratory of Food Engineering, Department of Food Science & Technology, University of Karachi, Pakistan

³Institute for Materials Chemistry and Engineering, Kyushu University, Japan

abdul.haq@eng.kagoshima-u.ac.jp; kadokawa@eng.kagoshima-u.ac.jp

Cellulose films can be prepared by the gelation from their solutions in ionic liquid. However the regenerated cellulose films exhibit very low elasticity. In this report, the effects of pre-gelation and post gelation conditions on mechanical properties and crystallinity of the regenerated cellulose film are presented. The films were prepared by dissolving cotton (5 wt%) into 1-butyl-3-methylimidazolium chloride (BMIMCl) for three hours at 115°C under vacuum. Subsequently, the cellulose/ionic liquid solutions were either kept at -18°C for 24 h or cool to room temperature followed by coagulation in different amount of water. After coagulation, water was either quickly distilled off at 80°C under reduced pressure (1 h) or slowly at 60°C for 24 h. The resulting films were characterized by tensile test, differential scanning calorimetry (DSC) and X-ray diffraction (XRD) measurements. The amount of water during coagulation and distillation condition significantly affected the elongation and strength of the film. These films also exhibited the thermoprocessability above the phase transition temperature, i.e., 155°C. It is suspected that processing conditions altered the degree of crystallization in regenerated film as evidence by XRD analysis and a mixed amorphous/crystalline phase is good for both high elongation at break and high tensile strength.



ACKNOWLEDGMENT

This work was partially supported by Japanese Society for Promotion of Sciences (Grant No. FY2017 P17347).

Antibacterial Nano-crystalline Cellulose Modified with N-halamine/Quaternary Ammonium Salts

Xuehong Ren¹, Ying Liu¹, Yan Zhang¹, Tung-Shi Huang²

¹College of Textiles and Clothing, Jiangnan University, Wuxi, Jiangsu, China

²Department of Poultry Science, Auburn University, Auburn, Alabama, USA

xuehongr@hotmail.com

Nano-crystalline cellulose (NCC) has generated much attention recently and has great potential in many applications due to its availability, high specific surface area, biodegradability, biocompatibility and reproducibility. While, many studies have shown that NCC is able to serve as film reinforcement and has been incorporated into cellulose acetate, polyurethane, polyvinyl alcohol, and poly (lactic acid) matrices to prepare composite membranes, few research has been performed on the functional modifications of NCC prior to forming composites. In this study, noncyclic N-halamine precursor, cyclic N-halamine precursor, and quaternary ammonium salts with different alkyl chain lengths were used to chemically modify NCC particles, and the modified NCC particles were incorporated into CA film, CS/PVA composite film, and chitosan film, respectively. In the antibacterial efficacy test, the results showed that all these three types of films demonstrated good biocidal property. The mechanical strength, thermal stability, and in vitro cytocompatibility of the composite films were also evaluated. The bio-based nanocomposite films with good antibacterial properties could have potential applications in packaging materials.

Hydrogel Surface Functionalization of Cotton to Improve Wound Dressing Applicability

Eva Pinho, [Graça Soares](#)

Center for Textile Science and Technology, Campus de Azurém, Universidade do Minho, Portugal

gmbs@det.uminho.pt

INTRODUCTION

Cotton still are the most used substract for wound management. However, textiles can cause wound dehydration and became mechanically anchored to the wound' surface, turning their change in a painful process. To overcome these drawbacks, modification of cellulosic textiles has been extensively study to improve their application as wound dressing. Thus, our group developed a composite material of cotton functionalized with hydroxypropylmethylcellulose /cyclodextrin hydrogel to be used as antimicrobial wound dressing (Figure 1).

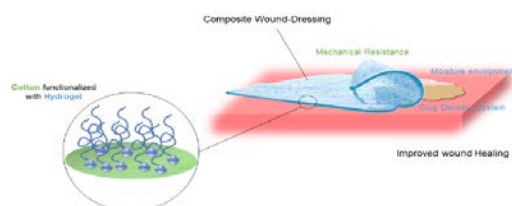


Figure 1. Schematic representation of a cotton substract functionalized with hydrogels for improved wound healing.

METHODS

The composite synthesis was performed by one-step chemical crosslinking. The reaction parameters, such as crosslinker concentration and polymeric solution concentration, were optimized. The obtained composites were characterized base on their physicochemical and mechanical properties. Moreover, to confirm the drug delivery ability of the system, antimicrobial molecules were loaded, and their antimicrobial activity assessed.

RESULTS AND DISCUSSION

The composites, obtained from the crosslinking between cyclodextrins, hydroxypropyl methylcellulose and cotton substract, were developed to be applied as wound dressings capable of preventing wound infections. The hydrogel will improve the wearability and drug delivery capacity of cotton textiles. And the cotton will improve the hydrogel' mechanical properties, facilitating the handle process. The composites were easy to handle and soft, thus suitable for the contact with injured skin.

The hydrogels' swelling profile was transferred to the composite. To the best of our knowledge, loading of gallic acid (as antibacterial agent) into composites wound dressings, and its release for control wound infections, have not been evaluated until now. The swelling and gallic acid loading profiles were similar. The results obtained (DSC, FTIR and release) suggested that gallic acid may be inside the cyclodextrins cavity and, also, trapped in the polymeric network. Regarding the biological properties of the composites, the gallic acid antibacterial activity was preserved after its incorporation within the wound dressings.

CONCLUSIONS

In conclusion, the developed composites showed the combined properties of cotton and hydrogel. Moreover, the loaded composites were able to destroy bacterial cells, preserving the gallic acid antibacterial activity. Based on the results from the present work, the developed composites showed suitable properties for application as antibacterial wound dressing.

ACKNOWLEDGMENTS

Authors wishing to acknowledge the project TSSiPRO—NORTE-01-0145-FEDER-000015—supported by the regional operational program NORTE 2020, under the PORTUGAL 2020 Partnership Agreement, through the European Regional Development Fund. The authors, also, acknowledge the Portuguese Foundation for Science and Technology (FCT) funding from the project UID/CTM/00264/2013 and FEDER funds through the COMPETE 2020—*Programa Operacional Competitividade e Internacionalização* (POCI) with the reference project POCI-01-0145-FEDER-007136.

**Fundamentals of
Polymer Material:
Synthesis,
Polymerization,
Characterization,
and Its Physics**

Syntheses and Wettability of Poly(fluoroalkyl (meth)acrylate)s with Carbamate Linker

Yi Liu^{1,2}, Yuji Higaki², Atsushi Takahara²

¹Department of Chemistry and Life Science, Guizhou Normal College, Guiyang, China

²Institute for Materials Chemistry and Engineering, Kyushu University, Fukuoka, Japan

takahara@cstf.kyushu-u.ac.jp

INTRODUCTION

Wetting properties of comb-shaped polymers with perfluoroalkyl (R_f) side-chains have been widely investigated so far in terms of surface orientation of fluoroalkyl segments¹. However, the factors determining the wetting properties of fluoroalkyl polymers have not been revealed clearly. In the present work, we discuss the effect of the carbamate linker between backbone and R_f side-chains on the wettability and surface structure of poly[fluoroalkyl (meth)acrylate]s on the basis of DSC, wide angle X-ray diffraction (WAXD), XPS and contact angle measurements.

EXPERIMENTAL SECTION

The poly[fluoroalkyl (meth)acrylate]s with carbamate linker, PMAUrC₈^F and PAUrC₈^F (Fig 1), were prepared by free radical polymerization in THF under reflux with 2,2'-azobisisobutyronitrile (AIBN) as a radical initiator.

RESULTS AND DISCUSSION

As observed in Fig. 2, the DSC curves of PMAUrC₈^F and PAUrC₈^F exhibit two endotherms with quite different magnitudes of enthalpy variations: higher for T_1 , and lower for T_2 . The phase in the temperature range between T_1 and T_2 shows birefringent textures on the heating and cooling process, which enable us to verify the two transitions: the first peak, T_1 , was attributed to a crystal/liquid crystal phase transition, whereas the second, T_2 , was assigned to the liquid crystal/isotropic phase transition. The structure transition was also confirmed by temperature controlled WAXD measurement. The surface chemical compositions of PMAUrC₈^F and PAUrC₈^F films were revealed by XPS measurement (Fig. 3). The C1s peaks were composed of five chemically different types of carbons. The higher surface concentration of fluorine atoms compared with the bulk values indicated the orientation of R_f side-chains.

CONCLUSIONS

The poly[fluoroalkyl (meth)acrylate]s with carbamate linkage show liquid crystalline ordered structure after melting of the crystalline ordered structure of R_f groups. The fluoroalkyl groups were highly oriented to the film surface.

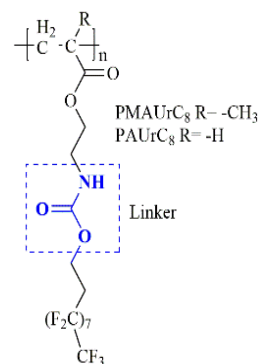


Fig. 1. Chemical structures of PMAUrC₈^F and PAUrC₈^F.

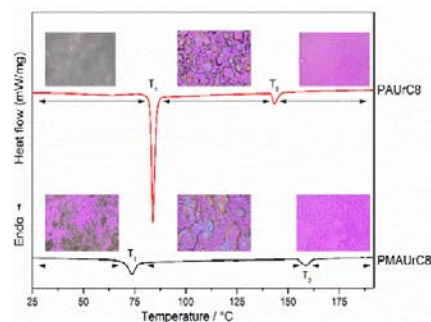


Fig. 2. DSC thermograms and POM images of PAUrC₈^F and PMAUrC₈^F.

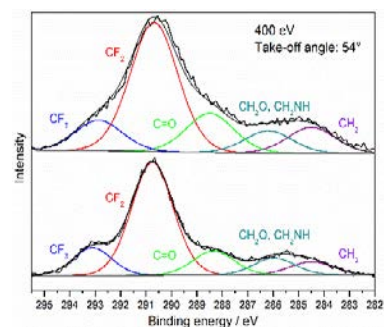


Fig. 3. C_{1s} XPS spectra of PMAUrC₈^F and PAUrC₈^F.

Polymer Hybrid Membranes for CO₂ Capture

Shinji Kanehashi^{1,2}, Kenji Ogino³, Sandra Kentish²

¹Graduate School of Engineering, Tokyo University of Agriculture and Technology, Japan; ²Department of Chemical Engineering, University of Melbourne, Australia; ³Graduate School of Bio-Applications and Systems Engineering, Tokyo University of Agriculture and Technology, Japan

kanehasi@cc.tuat.ac.jp

INTRODUCTION

Carbon dioxide (CO₂) capture remains a priority in many countries as the world seeks to address climate change. In particular the most recent report from the Intergovernmental Panel on Climate Change shows that geological storage is required for all scenarios that can meet 430–550 ppm CO₂ atmospheric concentrations (Working Group III, IPCC 5th Assessment Report, 2014). Polymeric membrane-based separation for CO₂ capture is known as an advantageous cost-effective technology. However, to be successful, the membrane materials require high gas permeability and selectivity under the trade-off relationship.

Mixed Matrix Membranes (MMMs) combine the benefits of both polymer substrates and fillers and have become attractive materials for gas separation in recent years. The nanofiller can improve not only gas separation performance, aging behavior but also physical properties such as mechanical strength and abrasion resistance. In the present work, MMMs consisting of a commercial aromatic polyimide and various nanoparticles were prepared.

RESULTS AND DISCUSSION

The dry gas permeability of all MMMs increased with increasing particle loading without a significant reduction in the CO₂/CH₄ selectivity. Furthermore, upon increasing the porosity of the particles, the permeability was enhanced, relative to that of pure Matrimid. We show that the gas separation performance of a range of nanoparticles suspended within a polyimide matrix can be readily described by a single free volume relationship, if the gas is dry. This free volume in the mixed matrix system is simply determined from the pore volume of the filler and the calculated fractional free volume of the polymer, multiplied by their respective volume fractions.

The gas permeability of MMMs in the presence of water vapour was strongly affected by the nanoparticle hydrophobicity, with membranes composed of hydrophobic fillers out-performing hydrophilic fillers of comparable porosity. These results suggest that MMMs prepared using highly porous, hydrophobic nanoparticles can be effective in gas separation applications such as natural gas sweetening, biogas purification and post-combustion carbon capture, when water vapour is present as an impurity.

Facile Fabrication of Poly(glycidyl methacrylate)-*b*-polystyrene Functional Nanofibers Under Shearing Field

Deli Xu, Wenwen Wang, Zhifeng Zhang, Dong Wang

School of Materials Science and Engineering, Wuhan Textile University, Wuhan, China

wtuwang@126.com

Glycidyl methacrylate (GMA) containing epoxide groups, offers a dual functionality and gives the user freedom and flexibility in polymer design. The epoxide groups could react irreversibly with nucleophilic groups, such as $-NH_2$, $-SH$, and $-COOH$. Thus, the block copolymer nanofibers with a high density of epoxide groups is well-suited for the immobilization of proteins, enzymes and other biomolecules under a gentle condition for biosensors. Moreover, the large specific surface area is benefit for adsorption of proteins besides the immobilization reaction. In this work, poly(glycidyl methacrylate)-*b*-polystyrene (PGMA-*b*-PS) block copolymers with epoxide groups were synthesized by two steps with 1,1-diphenylethylene as chain transfer reagent. The molecular weight and chemical structures of block copolymers were characterized. Then PGMA-*b*-PS nanofibers were fabricated under shearing field by using methanol as antisolvent and glycerin as the shear medium. The shear speed, concentration of block copolymer solution and ratios of methanol to glycerin were controlled and regulated. The morphologies of block copolymer nanofibers were investigated by SEM.

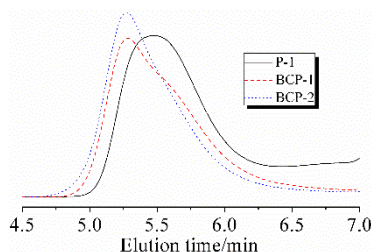


Figure 1. GPC curves of the precursor and PGMA-*b*-PS block copolymers.

Table I. Molecular characteristics of the precursor and block copolymers.

Poly mers	M_n (g/mol)	M_w (g/mol)	M_w/M_n	Tg ₁ (°C)	Tg ₂ (°C)
P-1	27631	44384	1.6	66	-
BCP-1	29749	60137	2.0	67	103
BCP-2	35507	73405	2.1	61	106

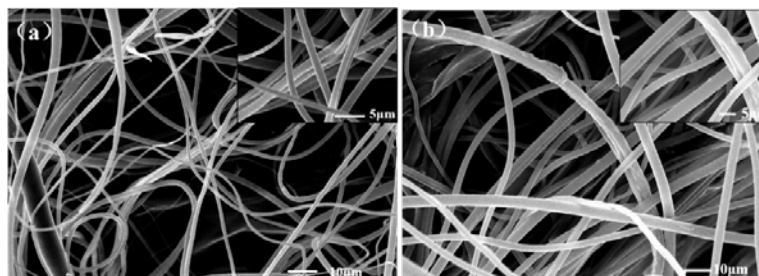


Figure 2. SEM image of PGMA-*b*-PS (BCP-1) fibers, (a) the solution concentration and rotation speed were 0.3 g/ml and 1500 r/min, respectively; (b) the solution concentration and rotation speed were 0.4 g/ml and 1500 r/min, respectively.

Fibers with the diameter from 500 nm to 1500 nm were obtained when the concentration of block copolymer solution was 0.3 g/ml and the contents of glycerin and methanol were 40 ml and 410 ml under the rotation speed of 1500 r/min.

ACKNOWLEDGMENT: We thank the National Natural Science Foundation of China (Grant No. 51603154), Nature Science Foundation of Hubei Province (Grant No. 2016CFB259) and Science and Technology Research Project of Educational Commission of Hubei Province (Grant No. Q20161603) for the financial support.

Photonic Films of Block Copolymers Comprising a Main-chain Liquid Crystalline Central Segment Connected to Amorphous Segments at Both Ends

Junpei Kuribayashi, Maito Koga, Masatoshi Tokita

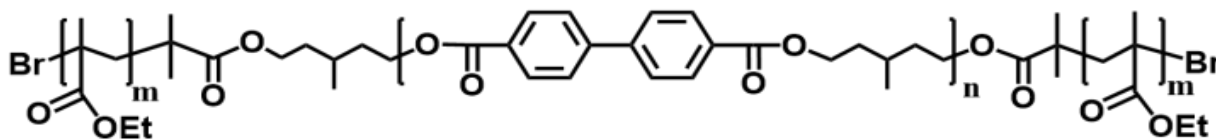
Department of Chemical Science and Engineering, Tokyo Institute of Technology

mtokita@polymer.titech.ac.jp

The incorporation of a liquid crystalline (LC) segment into a block copolymer produces an LC block copolymer, and the LC polymer represents a powerful tool for manipulating the orientation of the self-assembled structures. LC polymers have a unique orientation ability to respond to external fields such as magnetic, electric, and shear flow fields. Thus, LC block copolymers enable the introduction of this responsive ability. Also, LC polymers can affect the self-assembly behavior of block copolymers through several factors, including the conformational and structural asymmetry of the LC polymer and the anchoring of the LC to the microdomain interface.

We have investigated the microphase-separated structures of a series of T_x - y - x copolymers consisting of a main-chain LC B5 polyester connected to amorphous poly(ethyl methacrylate) (PEMA) segments at both ends at PEMA volume fraction of ϕ (Scheme 1). The B5 polyester consists of 4,4'-biphenyl dicarboxylic acid and 3-methyl-1,5-pentanediol. The numbers of x and y correspond to the number average molecular weights (M_n) of each PEMA segment at both ends of the B5 segment and the B5 segment, respectively, in units of kg/mol. T_x -10- x copolymers with x and ϕ in the range of 1.2–5 and 0.19 to 0.50, respectively, form lamellar microdomains. The LC director lays along the lamellar normal, indicating that LC segments having the contour length longer than the lamellar thickness are most extended perpendicular to the lamellar interface but folded and accommodated in lamellae.

T25-90-25 form lamellar microdomains stacked at a spacing of 130 nm and the cast films are colored blue. This blue color is ascribed to 390 nm wavelength light reflected by a lamellar structure having the spacing and the average refractive index of 130 nm and 1.5, respectively. With doping a B5 homopolymer to T45-90-45 copolymer, the lamellar spacing is increased from 160 to 210 nm, and the film color changes from blue to green. Thus T_x - y - x copolymers with the total M_n of 140 kg/mol can offer photonic films although amorphous block copolymers typically required the M_n more than 500 kg/mol to form photonic crystals.



Scheme 1. Chemical Structure of T_x - y - x copolymer.

Regularity of Spherical Microdomain Ordering in a Triblock Copolymer Ultrathin Film

Rasha Ahmed Hanafy Bayomi, Sono Sasaki, Shinichi Sakurai

Department of Biobased Materials Science, Graduate School of Science and Technology,
Kyoto Institute of Technology, Kyoto, Japan

shin@kit.ac.jp; rashaaa.moussa.88@gmail.com

We investigated the ordering regularity in confined spaces (in dewetted islands). We used a poly(methylmethacrylate)-*block*-poly(*n*-butylacrylate)-*block*-(polymethylmethacrylate) (PMMA-PnBA-PMMA; MAM) triblock copolymer, in which PMMA spherical microdomains are formed in a PnBA matrix. The volume fraction of PMMA was 0.20. An ultrathin film was prepared by spin coating. Before annealing, the film exhibits a homogeneous state with a full coverage on the silicon wafer (Film thickness ~ 15 nm). In order to measure the film thickness before annealing, we engraved a line in the film using a stationery cutter, then we measured the film thickness by the atomic force microscopy (AFM) using the contact mode. After five hours thermal annealing at 180°C , the dewetting took place, forming islands, with a height ~ 22 nm. Fig. 1a shows the islands due to dewetting by the thermal annealing, and many spherical microdomains regularly ordered can be detected in Fig. 1b. The Fourier transform (FT) pattern clearly displays the six spots. This significantly indicates a single grain state inside of the island. In order to discuss the ordering manner of the spherical microdomains in the dewetted islands, the FT patterns of many islands were examined in details. The packing manner of the spheres is examined in terms of the island shape (degree of circularity of the island). The islands having a high circularity (mostly complete round shape) exhibit a well-ordered arrangement of the spherical microdomains mainly ordering on a symmetry hexagonal lattice and forming a single grain. According to Black et al., over time the defects in the islands diffuse towards the island's perimeter and vanish, resulting in a well-ordered structure [Soft Matter 2017, 13, 3275-3283], which attests to the validity of our results. On the contrary, the islands having less circularity exhibiting a deformed hexagonal ordering, forming more than one grain (polygrain state) inside of one island (not showing the result in this abstract). The polygrain state could be a result of the islands coalescence over time.

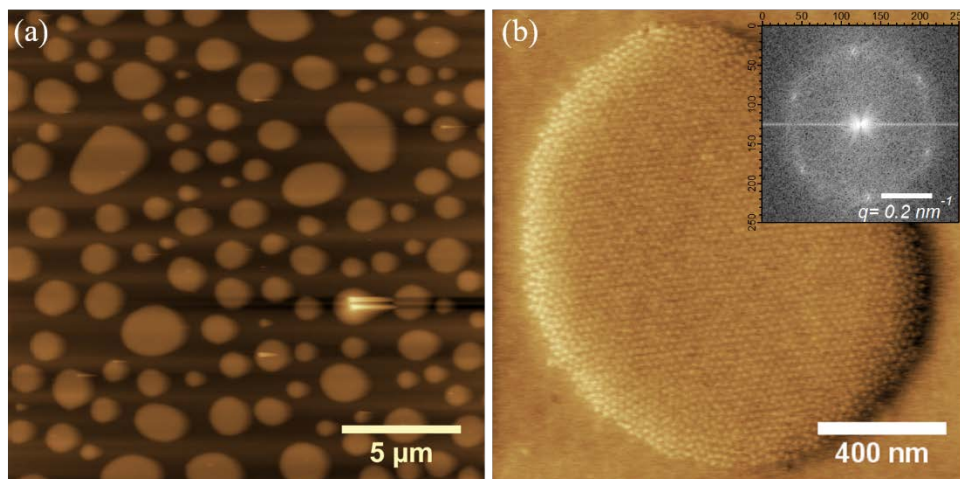


Fig. 1. AFM images of the monolayer film after annealing. (a) Height image showing the island-like dewetted portion on the silicon wafer. (b) Phase image focusing on one island, which contains many spherical microdomains regularly ordered. The inset shows the Fourier transform pattern.

Effect of Alkyl Chain Length of Fatty Acids on Adsorbed Layer Formation of the Acids and Local Viscosity at Metal/Fluid Interface

Toyoaki Hirata, Hina Takamura, Shinya Ozawa, Kenji Hisada

Department of Frontier Fiber Technology and Science, University of Fukui, Fukui, Japan

k-hisada@u-fukui.ac.jp

INTRODUCTION

The physical and chemical information about the actual solid–fluid interface would be quite useful for clarifying the friction reduction mechanism because the formation of a boundary layer greatly affects the coefficient of friction under boundary lubricated and hydrodynamic lubricated conditions. In this study, we investigated the local viscosity around metal/fluid interface with a quartz crystal resonator and the alkyl chain length of the additive was focused as a key factor to propagate a boundary layer.

EXPERIMENTS

Tetradecanoic (C14A), hexadecanoic (C16A) and octadecanoic (C18A) acids were used as additives in base oil, hexadecane (C16). Cu electrodes on quartz resonators were used as metal substrate. The quartz resonator and solutions were incubated in thermostat chamber at 296 K before resonator measurement. The resonators were dipped into C16 and fatty acid/C16 solution sequentially. After the resonators were placed into fatty acid/C16 solution, impedance amplitude and phase angle around resonance frequency were monitored at elapsed times. Resonance resistances (R_r) were defined as diameters of the admittance circles and local viscosity (η_l) around metal–fluid interface were estimated from R_r .

RESULTS AND DISCUSSION

Figure 1 shows specific relative resonance resistance ($R_r/R_{r,0}$) in each acid solution with different concentration. In the case of C16A solutions, $R_r/R_{r,0}$ increased in two stages over time. In the previous studies, the adsorption layer was revealed to be constructed with C16A monolayer and C16A/C16 mixed layer^{1,2} and the molecular layers grew up more than 20 nm thick after 1 h immersion.³ Our measurement shows that the adsorbed layer cause the viscosity increase, the enhancement phenomenon is depend on the alkyl chain length of fatty acid, and the phenomenon is remarkable for chain matching condition. Local viscosity is proportional to the square of the resonance resistance ($\eta_l \propto R_r^2$).⁴ For 0.2wt% C16A solution, the equilibrium viscosity at interface was 29.4 times higher than that for initial stage. The dense and viscous molecular layer could be sustainable and durable on tribological surfaces

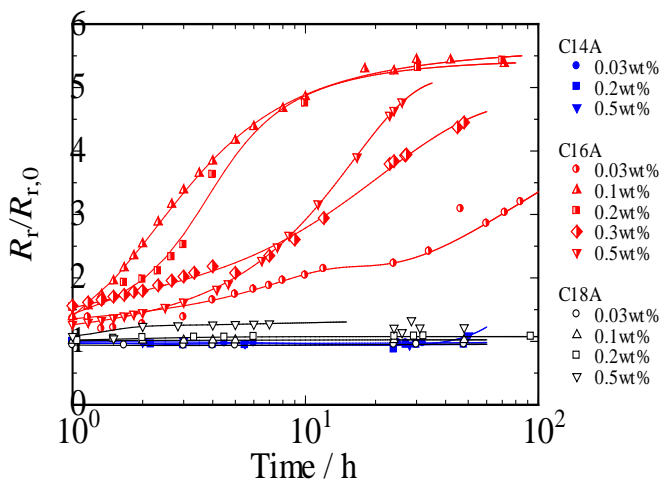


Figure 1. Time courses of the specific relative resonance resistance ($R_r/R_{r,0}$) in C14A, C16A and C18A/C16 solutions with different acid concentrations, respectively.

REFERENCES

1. Campana, et al. *Langmuir*, 27, 2011: 6085-90.
2. Clark, et al. *Langmuir*, 32, 2016: 534-40.
3. Hirayama, et al. *Langmuir*, 33, 2017: 10492-500.
4. Muramatsu, et al. *Anal. Chem.*, 60, 1988: 2142-46.

Fully Return-to-Nature Polymer Research for Sustainability of Resources

Seong Hun Kim

Department of Organic and Nano Engineering, Hanyang University, Korea

kimsh@hanyang.ac.kr

Upcycling of resources becomes an important social issue because of the extensive utilization of non-biodegradable polymers. Land fill is undesirable due to space limitation and ground pollution. Incineration is not also preferred because of emission of toxic gases which is generated from decomposition of polymer chains and residual additives.

To resolve these waste management problems, the recycling method and fully return to nature biocomposites were investigated in this research. The poly (ethylene terephthalate) (PET) bottle wastes were chemically recycled. The recycled PET was melt blended with virgin PET to improve the thermal and mechanical properties of recycled PET.

Biomass derived polylactide is fully return to nature polymer and expected to replace petroleum-based commodity polymers because of its excellent physical properties. Polylactide biocomposites reinforced by nanofillers such as nanocellulose and nanosilica, were prepared for high performance biocomposites. The various modifications of nanocellulose such as acid hydrolysis, acetylation, and alkylation were performed for dispersion enhancement, resulting in efficient reinforcement effect of modified nanocellulose in the polylactide matrix. The mechanical properties, crystallinity, and thermal stability of polylactide biocomposites were investigated. Furthermore, the theoretical prediction in the mechanical properties and crystallization behaviors of polylactide biocomposites were additionally analyzed to clarify the reinforcing potential of modified nanocellulose and nanosilica. Biobased polyurethane (BPU) was also successfully synthesized from castor oil to replace petroleum-based polyurethane and the properties of BPU composite and nanoweb were investigated.



Figure 1. Resource recirculation loop.

Continuous Supernanofibers for the Next Generation Tough Structural Composites

Yuris Dzenis

University of Nebraska-Lincoln

ydzenis@unl.edu

Advanced fibers produced a revolution in structural and functional materials in the 20th Century and are now used in a myriad of applications from aerospace to automotive and sporting goods. However, there was no major breakthrough in advanced fiber development since the last carbon fiber introduction more than three decades ago. Classical processing techniques for ultrahigh-performance polymer fibers rely on combination of high polymer crystallinity and macromolecular alignment to achieve superior mechanical properties. As a consequence, advanced fibers such as Kevlar and Spectra possess extraordinary strength but low strain to failure (<3%) and, therefore, low toughness. Our recent analysis of electrospun polyacrylonitrile (PAN) nanofibers (NFs) in the ultrafine (100-250 nm) diameter range (~100 times thinner than conventional advanced fibers) showed extraordinary simultaneously high strength, modulus, AND toughness. Finest nanofilaments exhibited strength on the par with the best advanced fibers while exceeding their toughness by more than an order of magnitude. Structural investigations showed that this unique and highly desirable mechanical behavior may be due to high degree of macromolecular alignment in conjunction with low crystallinity. Here, we demonstrate that it is possible to further improve NF mechanical properties by changing nanomanufacturing parameters and macromolecular chemistry. Specifically, polymer chain rigidity is shown to have an important effect on structure and mechanical behavior of individual nanofibers. 3D nanofiber assemblies and yarns as well as nanofiber reinforced composites are explored and characterized experimentally. Explicit mechanical models of NF assemblies and composites are developed and validated. Reported dramatic (2-3 orders of magnitude) simultaneous improvements in mechanical properties of NFs can lead to inexpensive, simultaneously strong and tough composites and structures for safety critical applications. The proposed structural explanation of our discovered NF mechanical behavior challenges the prevailing paradigm in advanced fiber development calling for high polymer crystallinity and can lead to the entirely new class of advanced fibers with ultrahigh toughness, in addition to strength. Such fibers can ultimately result in ultralight structures with the strength higher than carbon-epoxy composites (the current state-of-the-art) but significantly higher toughness, rivaling that of metals.

Derivation of Statistical Principle: Explaining the Heating Rate Dependence of Degradation Temperature of Ziegler-Natta Poly(styrene)

Masatomo Minagawa¹, Toshiki Taira², Yoshiaki Fujikura³

¹NPO, Dream-Create-Laboratories, Yamagata, Japan

²Graduate School of Science & Engineering, Yamagata University, Yonezawa, Japan

³Faculty of Engineering, Yamagata University, Yonezawa, Japan

gakusai-minagawa@memoad.jp

ABSTRACT: A simple statistical principle of chemical degradation system was derived by using isotactic poly(styrene). From a single TG-DTA curve, T_m (melting) and T_d (degradation temperature) were obtained. These values were traced under different heating rates (20-0.6 °C/min). The results were summarized as a function of heating time in a semi-logarithmic scale (Figure 3). It is indicated that a shaded area of the figures was almost constant irrespective of the heating rate employed (Figure 4), which was directly connected with the thermal energy (dQ^*) to cause the macroscopic thermal degradation.

INTRODUCTION: In the thermo-analytical field, the degradation behavior of many compounds has been investigated. We know that the value of T_d is strongly dependent on the heating rate employed (20-0.6 °C/min). This heating rate dependence of T_d is quite natural and is observed not only for organic polymers but also for inorganic ones. There is no theory which explains the reason why T_d varies or when degradation occurs under the given linear heating rates. We present a simple statistical theory ($dQ=const.$) explaining these two problems based on a chemical fluctuation.

EXPERIMENTAL: The sample was isotactic poly(styrene) (PSt.) (crystalline powder) prepared by Ziegler-Natta catalyst. The instrument was Rigaku TG-DTA (micro-type) and the heating conditions were as follows: sample weight, 10mg, heating rate, 20-0.6 °C/min, atmosphere, in N_2 stream (flow rate, 20ml/min). For comparison, an inorganic material (CaC_2O_4/H_2O) was used partly.

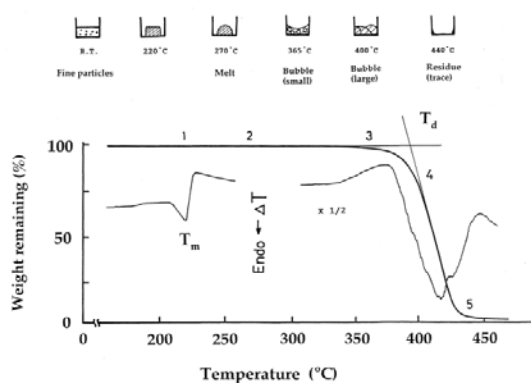


Fig. 1. Typical TG-DTA curve of isotactic PSt

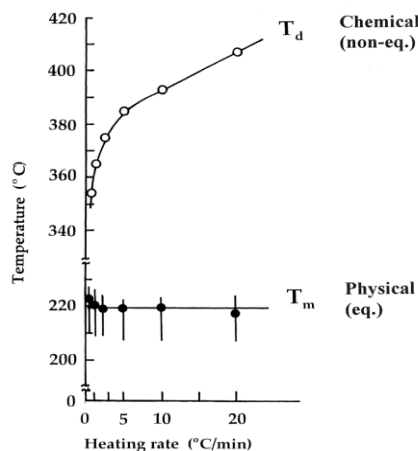


Fig. 2. Variation of both T_m and T_d

RESULTS AND DISCUSSION: Typical TG-DTA curves are shown in Figure 1. A clear melting point (T_m ; endothermic) was observed at 220 °C. Above 350 °C, gradual weight loss started. The degradation temperature (T_d) was defined as a cross-over point between two lines. It is possible to trace the process by a sample morphological change. This TG-DTA curve was traced under different heating rates. These T_m and T_d values

are summarized in Figure 2. The value of T_m was almost constant, whereas that of T_d was not. The slower the heating rate, the lower the T_d . This is quite natural that the former is physical eq. phenomenon, whereas the latter does chemical one (non-eq. one).

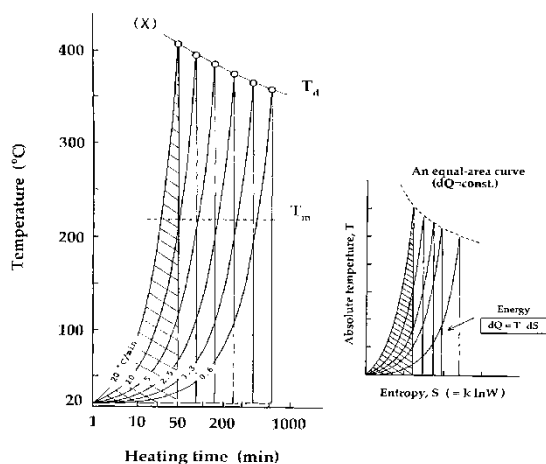


Fig. 3. Heating rate dependence of T_d and T_m

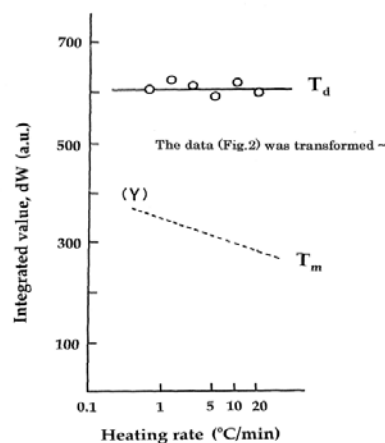


Fig. 4. Constancy of integral value

When the T_d was plotted against the heating time in a semi-logarithmic scale, Figure 3 was obtained. Pay attention to the figures enclosed by the shaded area by T_d curve. Geometrical shape was analogous, and the shaded area may be constant. In fact, this was true as shown by Figure 4. The area was almost constant irrespective of the heating rate employed. That is, the apparent heating rate dependence of T_d is caused not by accident but by a valid simple statistical principle that has been overlooked. We consider that the area is equal to the thermal energy (dQ^*) stored in the bulk sample, which causes the macroscopic thermal degradation of the system in question.

Theoretical Consideration

This is directly verified by the following way. Thermodynamics defines the energy (dQ) in terms of entropy (dS) in the following form, eq. (1). Statistical mechanics defines it (dS) in terms of the probability ($dS=k \ln W$) as follows, eq. (2).

$$dS = dQ/T \dots\dots(1)$$

$$dS = k \cdot \ln W \dots\dots(2)$$

These relations, which are defined in the equilibrium state, appear to be valid here. That is, as shown in Figure 3 right, when the ordinate is absolute temperature (K), and the abscissa is a logarithmic function of heating time (\ln/t), therefore the area must be equal to the energy ($dQ=\text{const.}$), since entropy is generally given in the logarithmic form ($S=k \ln W$),

Constancy of T_d and Its Universality

To tell the truth, the thermal degradation is a kind of fluctuation phenomenon (direct verification is given in the forthcoming paper), and therefore the above relationship ($dQ^*=T \cdot dS$) has a wide universality. For example, an inorganic material, calcium oxalate monohydrate ($\text{CaC}_2\text{O}_4/\text{H}_2\text{O}$), is a well-known standard substance in thermal analysis field. It decomposes in three steps, liberating H_2O , CO and CO_2 , respectively. We can analyze the results as in Ziegler-Natta PSt. Figure 5 shows the results.

It is apparent that the decomposition liberating each component occurs when an inherent critical thermal energy (dQ^*) is stored in the bulk sample. In other words, the value of critical thermal energy (dQ^*) to cause the degradation is constant, although degradation temperature itself varies depending on the linear heating path employed. Thus, the constant-area principle was confirmed not only for organic polymer but also for inorganic compound (Figure 6).

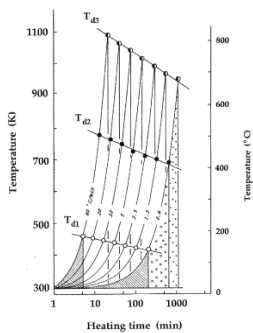


Fig. 5. Constancy of T_d of $\text{CaC}_2\text{O}_4/\text{H}_2\text{O}$

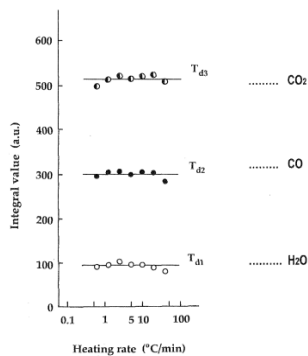
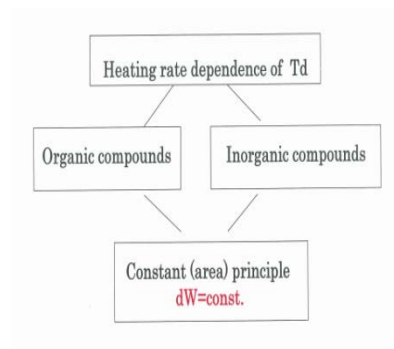


Fig. 6. Universality of equal area principle



Important point is that the results (Figure 2) contain the factor relating to the time (t), whereas the theory (Figure 3) doesn't contain the factor of time (t). How to compromise these two controversies is quite a difficult problem in this discussion. The answer is given by Figure 7.

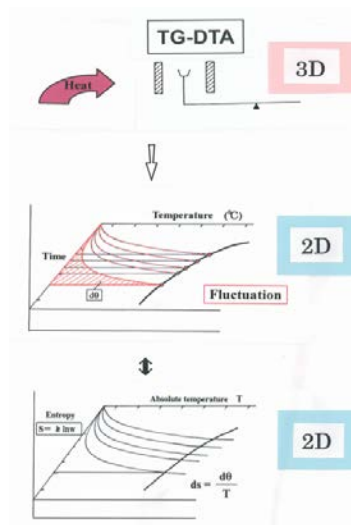


Fig. 7. Projection-mapping of analytical data

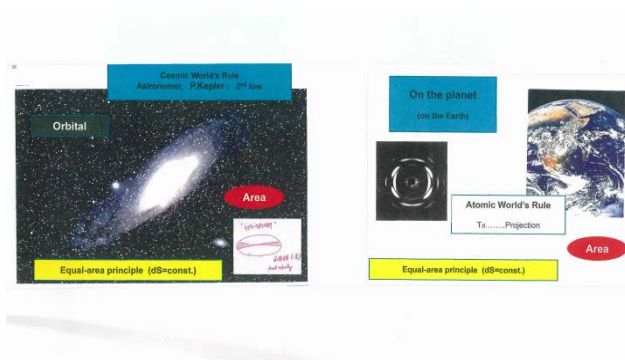


Fig. 8. Existence of Equal Area Principle in Cosmic World and Atomic One

Projection-mapping-method in thermo-analytical data is presented. Namely, experiments were carried out in 3D space (top), and the results were transformed by a logarithmic function in 2D space (middle). In 2D space, further, we can discuss the results freely based on a valid theory (statistical mechanics and thermodynamics), since time factor is excluded there (bottom).

Thus, the mechanism and universality of constant area principle in thermo-analytical field were clarified. At the same time, it is worthwhile noting that the constant area principle has already been found in Astronomy (the 2nd law of Kepler's principle). The area enclosed by an area velocity within a finite time is exactly constant. It is interesting to note that the similar type of law (statistical principle) exists in both Cosmic World and Atomic World as disclosed here (Figure 8).

ACKNOWLEDGMENT: We wish to express sincere thanks to the late Prof. H. Morawetz, Prof. E. Pearce, the late Prof. E. Turi, and Dr. C. Chiew in Polytechnic University for many suggestions and technical support.

Preparation and Characterization of Modified Polyesters with Flame Retardancy and Anti-droplet Properties by Copolymerization

Peng Ji¹, Zhenling Jiang², Chaosheng Wang^{1,2}, Fuyou Ke², Ye Chen², Huaping Wang^{1,2}

¹Co-Innovation Center for Textile Industry, Donghua University, Shanghai, China

²College of Materials Science and Engineering, Donghua University, Shanghai, China

jipeng@dhu.edu.cn

In this paper modified PET polyesters have been prepared by copolymerization with phosphorus flame retardant [(6-Oxido-6H-dibenz[*c, e*] [1, 2] oxaphosphorin-6-yl) methyl] butanedioic acid (DDP) and nano-SiO₂ silica sol. The structure and properties of flame retardant DDP were measured by nuclear magnetic resonance (NMR), thermal gravity analysis (TGA). The results indicate that DDP flame retardant is more suitable for polymerization. TGA, limiting oxygen index (LOI), vertical flame test, and scanning electron microscope (SEM) methods were devoted to discuss the flame retardancy and anti-droplet properties of modified polyesters. The results show that the silica sol increases its char residue. The silica sol is conducive to the formation of dense stable carbon layer, inhibiting the expansion of the carbon layer forming holes, and then improving the droplet of modified polyester. The highest LOI of modified polyester is 34.8±0.1%, the UL94 is V-0 grade. The modified polyesters have good flame retardancy and anti-droplet properties. It can be used for preparation of fiber in the textile decoration.

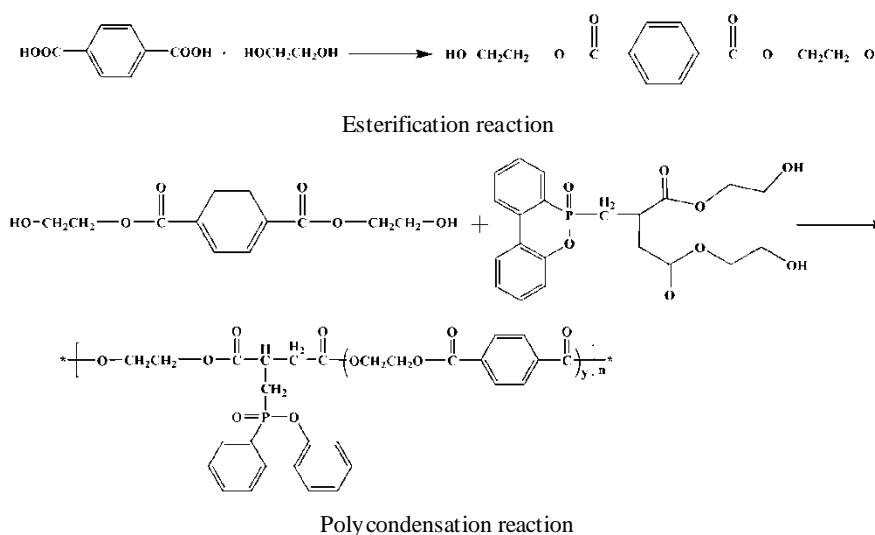


Figure 1. Preparation of modified polyesters with flame retardant by copolymerization.

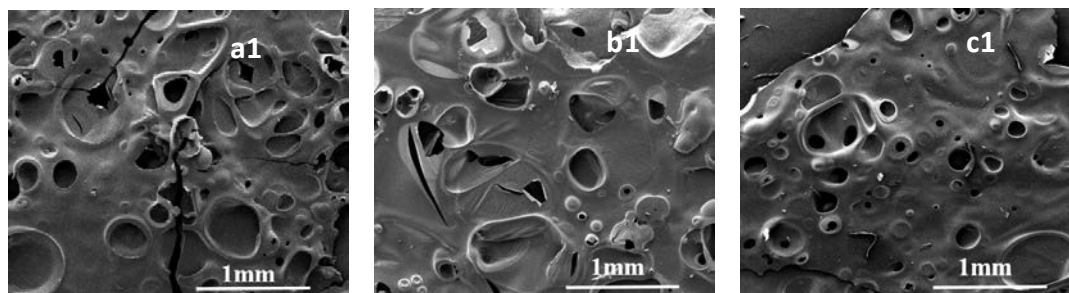


Figure 2. The SEM of residual char after 700 °C flame experiments (a1 was PET, b1 was PETP, c1 was PETP-3Si).

ACKNOWLEDGMENT: The authors gratefully acknowledge the supports from the National Natural Science Foundation of China (51703023), supported by China Postdoctoral Science Foundation (2017M621321).

Dye Decomposition and Cr(VI) Reduction Under Visible Light by a Cellulose Acetate Fiber Cross-linked with Amorphous TiO₂

Hanako Asai, Shinya Kato, Koji Nakane

University of Fukui, Japan

h_asai@u-fukui.ac.jp

INTRODUCTION

In the past few decades, crystalline TiO₂, such as rutile and anatase, has been studied as a photocatalyst under UV light irradiation. However, Wang et al. used not crystalline but amorphous TiO₂ for the reduction of Cr(VI) and decomposition of dye molecules under visible-light irradiation. According to their study, the cleaning mechanism is different from that in the case of crystalline TiO₂, where the amorphous TiO₂ acts as an electron mediator for electron transfer from the excited dye to Cr(VI) and the reaction does not involve excitation of the photocatalyst. Here, Cr(VI) is very harmful to human health and it is contained in the wastewater from electroplating and textile industries. Therefore, treating Cr(VI) effluent at the same time as the dye wastewater is suitable, especially in the textile industries.

In recent studies, we have investigated cellulose acetate (CA)-metal dioxide hybrid fibers, where metal dioxide was contained in amorphous state. Therefore, we propose the application of CA-TiO₂ fibers to wastewater treatment. Our material is in fibrous form, so it is more suitable for use as a filter, rather than the membrane or powder form. In this study, we investigated the relationship between the fiber preparation conditions and the Cr(VI) reduction properties as well as dye decomposition ability.

EXPERIMENT

The sample preparation method is schematically represented in Fig. 1. The 15 wt% CA solution was set in a syringe, and ejected by syringe pump into the stirred Ti(OR)₄ solution bath with various concentrations, instantaneously forming a fibrous material, CA-TiO₂ fiber.

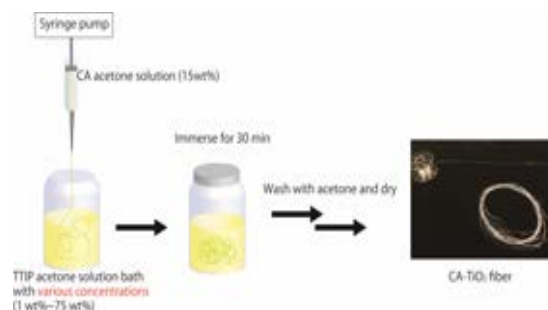


Fig. 1. CA-TiO₂ fiber preparation methods.

RESULTS

We immersed the CA-TiO₂ fibers in a solution containing methylene blue (MB) and Cr(VI). After the adsorption of MB and Cr(VI) to the fiber, we irradiated visible light to the system. Fig. 2 shows the variation in absorbance, A/A_1 of (a) MB and (b) Cr(VI) at the predetermined wavelength. As you can see, MB was decomposed and Cr(VI) was reduced by the existence of CA-TiO₂ fiber. We will discuss the detail mechanism at the presentation.

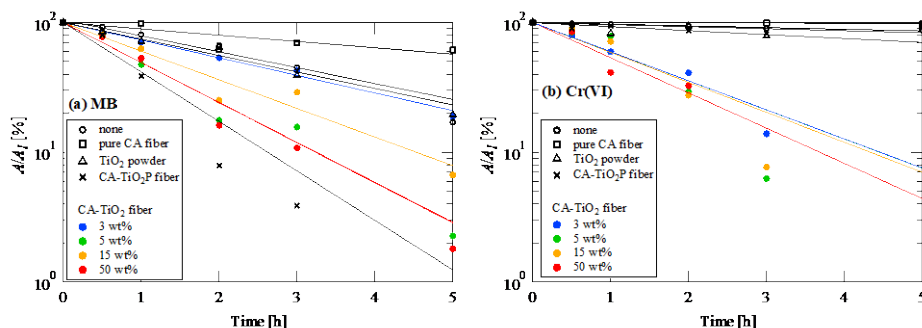


Fig. 2. Variation in normalized (a) MB and (b) Cr(VI) concentration under irradiation by visible light, as a function of immersion time.

Isothermal Crystallization Experiments for Poly(L-lactic acid) Containing A Liquid-type Nucleation Agent by Small- and Wide-angle X-ray Scattering

Thi Ngoc Diep Pham¹, Masatsugu Mochizuki², Mikio Doi², Hideaki Takagi³,
Nobutaka Shimizu³, Noriyuki Igarashi³, Sono Sasaki¹, Shinichi Sakurai¹

¹Department of Biobased Materials Science, Kyoto Institute of Technology, Kyoto, Japan;
²Taiyo Kagaku Co., Ltd, Mie, Japan; ³High Energy Accelerator Research Organization, Tsukuba, Japan

shin@kit.ac.jp; ptndiep90@gmail.com

INTRODUCTION

Poly(L-lactic acid) (PLLA) is a biodegradable and biocompatible polymer. Moreover, PLLA can be synthesized from renewable sources such as sugar, carbohydrate, etc. In recent several decades, scientists are interested in PLLA because of environment-friendly characteristics. However, there existing some big problems of PLLA, which are low crystallization rate and low crystallinity. In order to overcome such drawbacks, nucleation agents have been incorporated into PLLA. In this study, we added a special liquid-type nucleation agent (organic acid monoglyceride; OMG) into PLLA in order to increase the crystallization rate and to reduce the induction period. In this study, we conducted time-resolved small and wide-angle X-ray scattering (SWAXS) to follow crystallization of PLLA/OMG.

EXPERIMENTAL

There are two types of neat PLLA samples (such as PLLA4032D and PLLA2500HP from Nature Works with different D% content and MFR (Melt Flow Rate) value); and PLLA with OMG (1% addition) samples, as designated by PLLA4032D/OMG and PLLA2500HP/OMG. The code names of samples are shown in Table I. The time-resolved WAXS measurements in

Table I. Sample characteristics.

Code name	Samples	D% content	MFR	Nucleation agents
D1.4	PLLA4032D	1.4%	7.0	--
D1.4/OMG	PLLA4032D/OMG	1.4%	7.0	1%
D0.5	PLLA2500HP	0.5%	8.0	--
D0.5/OMG	PLLA2500HP/OMG	0.5%	8.0	1%

each 5 s step were conducted at BL-6A beamline in KEK, Tsukuba, Japan upon temperature jump from 200 °C to 110.2 °C (cooling rate was approximately 385 °C/min, T-jump was completed within 14 s). The wavelength of the X-ray (λ) was 0.150 nm. In order to determine the onset time of crystallization, we examined temporal evolution of the most intense reflection peak which is overlapping (200) and (110) reflections. Computational peak decomposition was conducted to separate the peak from the amorphous halo peak.

RESULTS AND DISCUSSION

WAXS results

The crystallinity is plotted as a function of time in Fig. 1. The plots of crystallinity show a tendency such that PLLA/OMG has higher crystallization rate in an early stage. The crystallinity increases up to 42 % finally, excepting for D0.5/OMG. Although this specimen showed the most rapid crystallization, the ultimate crystallinity was lowest (at $t = 2500$ s). The reason is not clear at present. It is speculated that the morphology of the higher-order structure for D0.5/OMG is different from those for the other specimens, as a result of the very rapid crystallization which may induce self-termination of the crystallization around $t = 300$ s. Namely, very quick crystallization may induce higher order structure which automatically terminate the further crystallization.

SAXS results

The lamellae thickness (L) and long period (D) are evaluated from the 1d-SAXS profiles by using correlation function $\gamma(r)$:

$$\gamma(r) = \frac{\int_0^\infty I(q) q^2 \cos(qr) dq}{\int_0^\infty I(q) q^2 dq}$$

As clearly seen in Fig. 2, the lamellar thickness increases as a function of time. The lamellar thickness increases in early stage (<500 s) and turns to stabilization. The linear fitting of the increasing tendency in the early stage was made to evaluate the rate of growing of the lamellar thickness. The rate was found in the following order: D1.4 < D1.4/OMG < D0.5 < D0.5/OMG. Thus, the thickening rate of lamellae is found to be affected by the nucleation agent OMG and the amount of D-content. Furthermore, by focusing on the ultimate value of the lamellar thickness, the specimens with OMG have thinner lamellar thickness. This result shows a good agreement with the DSC result that the specimens with OMG have lower melting temperature than neat PLLA.

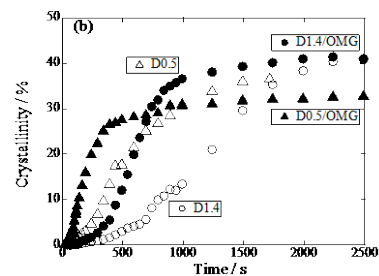


Fig. 1 Crystallinity as a function of time.

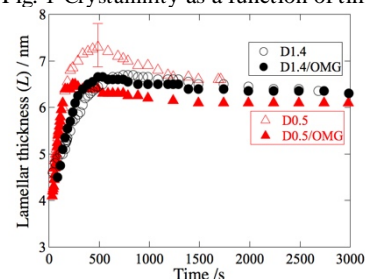


Fig. 2 Lamellae thickness (L) as a function of time.

Microspheres with Dimple Morphology of Poly(*p*-oxyferuloyl) Prepared by Reaction-induced Phase Separation

Hironori Atarashi, Masahaya Sugimoto, Shinichi Yamazaki, Kunio Kimura
Graduate School of Environmental and Life Science, Okayama University

h-atarashi@okayama-u.ac.jp, polykim@okayama-u.ac.jp

Aromatic polymers are used in various industrial fields as high-performance materials due to their excellent properties, such as thermal stability, mechanical properties, or chemical stability. However, processing of these polymers, especially in micrometer or nanometer scale, is extremely difficult because of their intractability. We have been studied morphology control of rigid polymers during polymerization and succeeded in preparing many morphologies consisted of aromatic polymers, for instance whisker, microsphere, ribbon and so on. In this study, we newly obtained the aromatic polyester microsphere with dimple morphology, shown in Figure 1 (c), synthesized from ferulic acid as a starting material.

The polymer, poly(*p*-oxyferuloyl) (POF), was synthesized by the reaction-induced phase separation during polymerization using *p*-acetoxyferulic acid (AFA) as a monomer (Scheme 1). The polymerizations were carried out at a concentration of 1.5 wt% at 300-340°C for 20 min – 6 hours in liquid paraffin. After polymerization, the precipitated POFs were filtered with a glass filter, washed with acetone and *n*-hexane, and dried under vacuum. Morphologies and chemical structures of the precipitated POFs were evaluated by SEM, FT-IR, and WAXS. Figure 1 shows morphologies for POF prepared at (a) 300, (b) 310, (c) 320, and (d) 330°C, respectively. Only in the panel (c) microspheres with dimple morphology were observed, of which the average diameter was 6.1 μm. They didn't possess crystallinity, even though the POFs shown in Figure 1 (a), (b), and (d) had crystallinity. The microspheres frozen in liquid nitrogen were crushed and the inside structure was observed. It was clear that the insides of them were homogeneous. This indicates that the dimple morphology was formed only at the surfaces of the microspheres. In order to reveal the formation mechanism of the POF microspheres with dimple morphology, time dependence of the morphologies and the chemical structures were evaluated. The results suggest that the formation of dimple on the surface of the POF microspheres might be caused by the reaction of the double bond in the main chain during the polymerization.

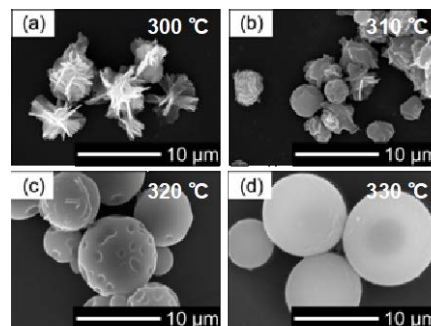
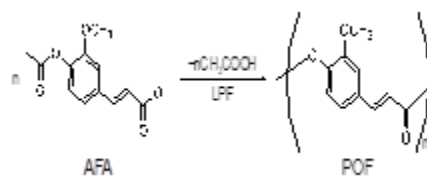


Figure 1. Morphologies of POF prepared at (a) 300, (b) 310, (c) 320, and (d) 340°C.



Scheme 1. Synthesis of POF.

Measuring the Interfacial Tension of Polymer Melts: A Modified Fiber Retraction Method

Yurong Yan^{1,3}, Zuyun Xie¹, Youim Chang², Rudolf Hufenus³

¹School of Materials Science and Engineering, South China University of Technology, Guangzhou, China

²Department of Chemical Engineering, Tunghai University, Taichung, Taiwan

³Empa, Swiss Federal Laboratories for Material Science and Technology, St. Gallen, Switzerland

yryan@scut.edu.cn; rudolf.hufenus@empa.ch

Polymer blends considerably expand the field of application of polymer materials, but the final properties of the alloy critically depend on the morphology of the immiscible and/or miscible domains that develop in blending and processing. A variety of parameters can influence the final morphology of a polymer blend, such as viscosity ratio, composition, processing method, and types of melt flow; but the most important factors are interfacial properties.

The so-called breaking thread method was adopted to measure the interfacial tension of polymer melts. Here, surface contamination and good contact between thread and applied film are two difficult to control key points that may influence the test result. With the help of core-sheath bicomponent spinning technology, a novel interfacial tension test sample preparation and measuring method were designed, which can avoid said problems. In this study, interfacial tensions of PA6/LDPE with and without compatibilizer were studied. Results showed that the modified system is more accurate due to the uncontaminated surface and a short procedure, especially in bi-component fiber processing, which has almost no blending process. LLDPE/PA6 bi-component fibers were used to measure the relative interfacial tension change of molten LLDPE and PA6 polymers with different MAPE concentrations in LLDPE, and the tendency is consistent with the pull-out test results. The reliability of this new method to measure relative interfacial tensions of polymer melts is strongly dependent on the of core/sheath ratio of the bicomponent fibers.

Preparation of Poly(1,4-phenylene terephthalamide) from Poly(ethylene terephthalate) by Means of Reaction-induced Crystallization

Tatsuya Kohara¹, Hironori Atarashi¹, Shinichi Yamazaki¹,
Tetsuya Uchida², Kunio Kimura¹

¹Graduate School of Environmental and Life Science, Okayama University, Japan

²Graduate School of Natural Science and Technology, Okayama University, Japan

polykim@cc.okayama-u.ac.jp

Poly(ethylene terephthalate) (PET) has been widely used in our daily life. Synthesis of value-added materials from wasted PET is of importance as an effective upgrade recycling technology. Poly(1,4-phenylene terephthalamide) (PPTA) is a representative of high-performance fiber materials and well known as Kevlar. The conversion of PPTA from PET had been previously examined by ester-amide exchange reaction in the melt phase or solution phase. [1,2] In these studies, the content of 1,4-phenylene terephthalamide (PTA) moiety in synthesized polymers was limited to at most 60 % owing to the intractability of PPTA. In this study, the conversion of PET to PPTA was examined by using reaction-induced crystallization to overcome the above limitation.

PET ($M_w = 2.8 \times 10^4$) and dibenzyltoluene mixture were placed in a vessel, and the mixture was heated up to 320°C to dissolve PET. Concentration of PET was 5 wt%. When the PET was entirely dissolved, the equal amount of *p*-phenylene diamine (PPDA) to terephthaloyl moiety of PET was added to the solution under stirring. Then the reaction was heated at 320°C for 12 h without stirring. Precipitates were obtained with the yield of 62%, but the content of PTA moiety in the precipitated polymers was 92 mol%, indicating that the precipitated polymers contained a small amount of ethylene terephthalate moiety. The reaction was next carried out at 350°C for 12 h in the slight excess of PPDA to accelerate the exchange reaction. PPTA which did not contain ethylene terephthalate moiety was formed as plate-like crystals with the yield of 75-92%. The obtained PPTA crystals possessed high crystallinity, and electron diffraction indicated that the PPTA molecules aligned perpendicular to the plane of the plate-like crystals. The small amount of PET moiety left in the oligomers was excluded by the ester-amide exchange reaction during crystal growth. M_w of PPTA crystals was 1.02×10^4 . The M_w of PPTA increased to 1.18×10^4 by the stepwise addition of PET and PPDA during the reaction. High molecular weight PPTA could be prepared under non-stoichiometric condition by using crystallization. Poly(1,4-phenylene benzimidazole) which was a typical high-performance fiber was synthesized by the similar procedure.

REFERENCES

- [1] Y. Kim, H. D. Roh, H. C. Le. *J. Appl. Polym. Sci.*, 91, 2004: 2502.
- [2] S. Nakano, U.S. Patent No. 5837803 (1998).

Poster Session

Ultra Small-angle X-ray Scattering Analysis of Block Copolymer-grafted Silica Nanoparticle Hybrid Films Under Mechanical Deformation

Chao-Hung Cheng¹, Shuhei Nozaki¹, Chigusa Nagano¹, Shiori Masuda¹, Tomoyasu Hirai^{1,2,3}, Yuji Higaki^{1,2,3}, Ken Kojio^{1,2,3}, Atsushi Takahara^{1,2,3}

¹Graduate School of Engineering; ²Institute for Materials Chemistry and Engineering; ³International Institute for Carbon-Neutral Energy Research, Kyushu University, Japan

takahara@cstf.kyushu-u.ac.jp; c.cheng@ms.ifoc.kyushu-u.ac.jp

INTRODUCTION

Nanohybrids prepared by self-assembly of polymer-grafted particles have been reported. These hairy particles can strongly improve the particles dispersion. The mechanical properties can be tuned by the ratio of hard and soft components. However, the structure changes during mechanical deformation in the hybrid films are not clarified. In this study, colloidal crystal structure changes under mechanical deformation were investigated by *in-situ* ultra small-angle X-ray scattering (USAXS).

EXPERIMENTS

The block copolymer brushes on silica nanoparticles were prepared by two-step surface-initiated atom-transfer radical-polymerization (SI-ATRP). Poly(butyl acrylate) (PBA) and poly (methyl methacrylate) (PMMA) were chosen as the inner and outer layers, respectively. The film was prepared by heat-pressing under 170°C and 10 MPa. Glass transition temperatures (T_g s) were measured by differential scanning calorimetry (DSC) and dynamic viscoelastic measurement. Tensile test was performed to obtain stress-strain curves. The colloidal crystal structure of nanohybrid films was analyzed during elongation by *in-situ* USAXS.

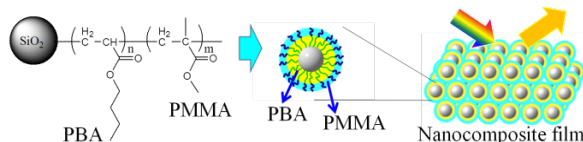


Fig. 1. Nanohybrid films with structural colors composed of block copolymer-grafted particles

RESULTS AND DISCUSSION

DSC and dynamic viscoelastic measurement revealed that two different T_g s, indicating that the formation of phase separated structure of copolymer in the nanohybrid film. The film became stretchable with incorporation of the rubbery PBA interphase. The Young's modulus and strain at break of block copolymer-grafted samples could be tuned by changing the weight ratio of soft and hard blocks. The nanohybrid films exhibited the structural colors due to the presence of ordered structure. An ordered arrangement of particles was observed in local regions by atomic force microscope (AFM). Fourier transform of AFM images revealed that the colloidal particles form a paracrystalline ordering. Also, the structure factors and form factors of silica particles were clearly observed in USAXS profiles as shown in Figure 2. The experimental data fit to the theoretical function of face-centered cubic (FCC) structure. While elongation, the peaks of [111] plane shifted, and the decrease of [111] plane distance in the direction perpendicular to elongation were varied among samples with different weight ratios of hard/soft blocks. The film behaved more rubber-like with increasing the PBA weight ratio. The detail will be discussed in the poster.

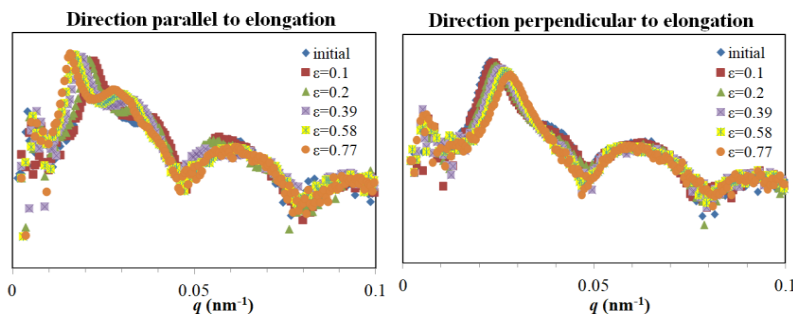


Fig. 2. USAXS profile during elongation of PBA-*b*-PMMA-grafted silica nanoparticle hybrid films.

Effect of Spacer Geometry on Reverse Electro dialysis (RED) Resistance

Soroush Mehdizadeh, Takakazu Abo, Masahiro Yasukawa, Yuriko Kakihana, Mitsuru Higa
Graduate School of Sciences and Technology for Innovation, Yamaguchi University, Japan

mhiga@yamaguchi-u.ac.jp; g002we@yamaguchi-u.ac.jp

Renewable energy has attracted considerable attention to be the new source for world energy production in last decade. Reverse electro dialysis (RED) is an efficient membrane-based technology which can convert SGP into electricity energy. In RED process, concentrate and dilute solution flow alternatively through ion exchange membranes (IEMs) which selectively allow the passage of cations and anions from the concentrate to dilute stream as shown in Fig. 1. The ionic passage is converted into electric current with redox reaction by means of suitable electrodes at both end of the RED stack.

In RED, spacers which are made by non-conductive material are used to keep distance between membranes, and to improve ion distribution in both compartments. Although the effect of spacers on RED resistance have been always measured by using alternative and direct current through RED stack, there are few systematic analyses about the spacer geometric properties on the RED resistance more quantitatively. In this work, the effect of spacer geometrics on their resistance have been precisely evaluated by measuring different spacer's resistance in the same solution. In addition, RED experiments with 5 types of different spacer dimensions have been also performed to compare the ohmic resistance of RED stack estimated from spacer geometry with the obtained RED actual resistance and literatures.

The results showed that the resistance and shadow effect of the spacers have reasonable relationship with their thickness, porosity, area fraction, and volume fraction. In addition, the spacer shadow effect on membranes due to covering the membrane area, measured by subtracting different spacers resistance beside membrane from just spacers resistance in solution without membrane, were also related to the spacers geometric properties. As a result, the ohmic resistance estimated from spacer geometry has a good agreement with ohmic region of RED stack resistance which were measured by means of AC and DC. Therefore, this knowledge is promising to be useful for designing RED stack especially about the spacers.

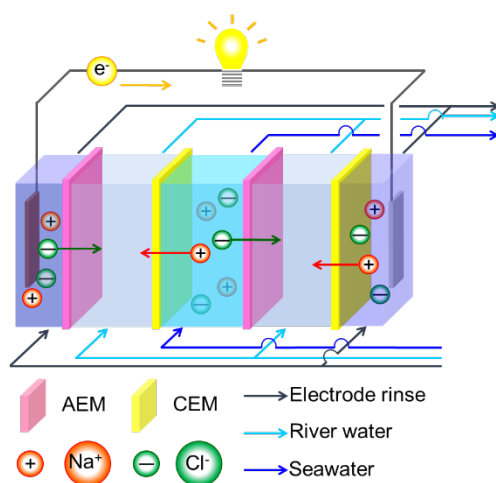


Fig. 1. Simple schematic of RED stack which sea water and rivers water have flow alternatively between anion exchange membrane (AEM) and cation exchange membrane (CEM)

ACKNOWLEDGMENT

This research is supported by JSPS KAKENHI Grant Number JP16H01796 [Grant-in-Aid for Scientific Research(A)].

Electric Heating Performance and Superhydrophobicity of Cotton Fabric In-situ Polymerized with Pyrrole Using Binary Oxidants

Suhyun Lee, Chung Hee Park

Department of Textiles, Merchandising and Fashion Design, Seoul National University, Seoul, Korea

sjj1413@gmail.com; junghee@snu.ac.kr

This study aims to develop a conductive fabric with superhydrophobicity through an in-situ polymerization of pyrrole onto fabric using binary oxidants, ammonium persulfate (APS) and ferric chloride (FeCl_3). For this purpose, pyrrole was directly polymerized onto the cotton fabric surface, varying the mixing ratios of the oxidants to control electric conductivity and to adjust the surface roughness as well. And then n-dodecyltrimethoxysilane (DTMS) sol-gel solution was coated to lower the surface energy. Conductivity, electric heating property, superhydrophobicity, and mechanical properties were compared according to the polymerization conditions of pyrrole.

The in-situ polymerization of pyrrole using the binary oxidants succeeded in depositing polypyrrole particles of approximately 80 nm in diameter on the surfaces of the cotton fabrics. On the contrary, the diameters of the polypyrrole particles were 254 nm for APS 100% oxidant and 167nm for the FeCl_3 100% oxidant. The surface resistivity decreased and heating performance was improved as the FeCl_3 ratio in the oxidants increased, resulting in an up to 20°C increase in the surface temperature of the specimen. Meanwhile, in terms of surface wettability, the contact angles of the developed fabrics increased from 0° to 165° and their shedding angle decreased from 90° to 5°. It is interesting to note that the specimens polypyrrol treated with binary oxidants exhibited a somewhat higher shedding angles than single oxidants possibly because of their small nano-scale roughness. Investigation of the physical properties of the developed specimens revealed that the tensile strength and flexibility decreased by the polypyrrole deposition. Samples treated with the binary oxidant maintained about 80% of their tensile strength and flexibility compared to the untreated sample. The superhydrophobic surface of polypyrrole fiber composites effectively protected the conductive layer from oxygen and moisture, thus retarding oxidation aging and enhanced rubbing fastness and washing durability.

ACKNOWLEDGMENT

This work was supported by a grant (no.2015R1A2A2A03002760 and no.NRF-2016M3A7B4910940) of the National Research Foundation of Korea funded by the Korean government (MSIP).

Performance and Efficiency Comparison Between Pressure-retarded Osmosis and Reverse Electrodialysis

M. Yasukawa¹, T. Sakurada², R. Horie², M. Kuno¹, Y. Kakihana¹, M. Higa¹

¹Graduate School of Sciences and Technology for Innovation, Yamaguchi University

²Graduate School of Science and Engineering, Yamaguchi University

mhiga@yamaguchi-u.ac.jp; myasu@yamaguchi-u.ac.jp

Owing to rapid growth of environmental concerns especially about CO₂ emission and subsequent impact on the world climate, renewable energy without CO₂ and its-related technologies have gained a definite promise to improve our life. Among the renewable energy resources, salinity gradient energy (SGE) which generates by mixing two solutions with different salinities such as seawater and river water has attracted and recognized as a relatively new energy resources because of their potential as well as the other energy resources such as solar, geothermal, biomass and so on. Up to now, pressure-retarded osmosis (PRO) and reverse electrodialysis (RED) have been recognized as major techniques to convert SGE into electricity using membranes, and were demonstrated for the practical use by using a combination of real solutions such as of seawater brine from seawater desalination plants and municipal wastewater, and seawater and river water. However, although the current developments of the componential issues in both PRO and RED allow us the practical demonstration, to our best knowledge, a systematic investigation of the both PRO and RED performance especially with their performance comparison in a pilot-scale is still not available because their pilot-scale studies are still few. In this study, we have performed pilot-scale PRO and RED experiments with the effective membrane areas of 65 m² and 40 m², respectively. The PRO and RED performances were evaluated under a wide range operating conditions by changing the operating parameters such as concentrations, flow rates, applied hydraulic pressure difference and loading current. The evaluated performances were then compared each other in the view point of the energy utilization rate, energy conversion efficiency and total systematic positive power output (Fig. 1). In the case of PRO, these efficiencies and final power output depended on not only the membrane (module) characteristics, operating conditions, but also mechanical efficiency such as turbine, pressure exchanger and high pressure pump. Whereas, in the RED case, they mainly depended on the stack resistance originated from the ion-exchange membranes and spacers, and loading current. These comparisons provide a useful knowledge for the optimum choice of PRO and RED systems depending on the operation conditions.

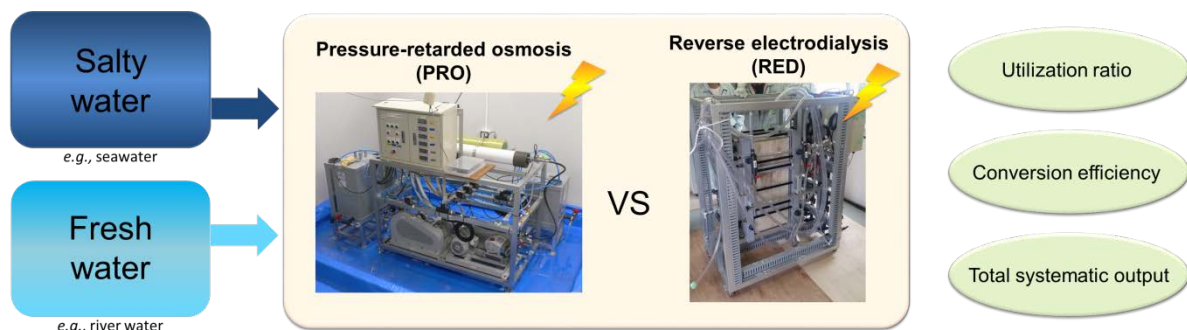


Fig. 1. A pilot-scale performance comparison between PRO and RED.

ACKNOWLEDGMENT

This research is granted by (1) the Japan Society for the Promotion of Science (JSPS) through the “Funding Program for World-Leading Innovative R&D on Science and Technology (FIRST Program),” initiated by the Council for Science and Technology Policy (CSTP), (2) JSPS KAKENHI Grant Number JP16H01796 (Grant-in-Aid for Scientific Research(A)) and (3) feasibility study of the Breakthrough by Dynamic Approach in Sewage High Technology (B-DASH) Project conducted by the Ministry of Land, Infrastructure, Transport and Tourism.

Characterization of Charge Mosaic Membranes Prepared by Ion-track Graft Polymerization

M. Omori¹, T. Yamaki², H. Koshikawa², S. Sawada³, Y. Kakihana¹, M. Yasukawa¹, M. Higa¹

¹Graduate School of Sciences and Technology for Innovation, Yamaguchi University, Japan

²Takasaki Advanced Radiation Research Institute, National Institutes for Quantum and Radiological Sciences and Technology, Japan

³Research Group for Radiation Materials Engineering, Fuels and Materials Engineering Division, Nuclear Science and Engineering Research Center, Japan Atomic Energy Agency, Japan

mhiga@yamaguchi-u.ac.jp

Charge mosaic (CM) membranes has parallel arrays of cation- and anion-exchange domains passing through the membranes. Hence, the membranes have high permselectivity for salt, and have potential to desalination and concentration of salt solution in food and water treatment applications. In this study, we prepared CM membranes by using ion-track graft polymerization. CM membranes prepared by this method will be expected to have high ion permeability because it has nano-order size ionic channels with high charge density. An anion-exchange membrane, FAS-30 (fumasep[®]: FUMATECH) used as a base film was irradiated with a 560 MeV ¹²⁹Xe ions from a cyclotron. The ion-beam fluence was 3.0×10^8 or 1.0×10^9 ions/cm². After the irradiation, the membrane was immersed in a solution of *p*-styrenesulfonate (SSS) for graft polymerization of negatively-charged chains, which has opposite charges to the base film, to form charge mosaic structure inside the anion-exchange membrane. The ion-exchange capacity of the cation- and anion-domains of the cation-exchange membranes, IEC_{cation} and IEC_{anion} , respectively, were measured, and permeation experiment in a dialysis system consisting of a CM membrane and solutions of KCl or sucrose were performed to examine the permselectivity of the CM membrane using the same methods described elsewhere¹⁾. Table 1 shows the experimental conditions and results of the prepared CM membranes. IEC_{cation} of the membranes increased with increasing ion beam fluence and grafting time. The increase in IEC_{cation} will be due to the fact that more radicals were produced by higher-fluence ion beams, and the longer grafting time the membrane has, the longer grafting chains of the negatively-charged groups it has. The flux of KCl and permselectivity between KCl and sucrose increased with increasing IEC_{cation} . CM4 with 3.8×10^8 of ion beam fluence and 9 hours of grafting time showed both the highest KCl flux and highest permselectivity in all the CM membranes. Hence, a CM membrane prepared by ion-track graft polymerization will be expected to have higher performances by optimizing the ion irradiation conditions and polymerization conditions. Therefore, the CM membranes will have potential applications to desalination at low salt solutions.

Table 1 Experimental conditions and experimental results of the prepared CM membranes

Sample	Fluence [ions/cm ²]	t_G [h]	IEC_{cation} [meq/g]	IEC_{anion} [meq/g]	λ [-]	J_{KCl} [10^{-10} mol/cm ² s]	α [-]
CM1	1.0×10^8	6	0.02	0.46	0.03	1.23	25
CM2		9	0.14	0.37	0.38	369	100
CM3	3.0×10^8	6	0.11	0.38	0.29	281	67
CM4		9	0.16	0.30	0.52	553	291

REFERENCE

1) M. Higa, M. Kobayashi, Y. Kakihana, A. Jikihara, N. Fujiwara. *J. Membr., Sci.*, 428, 2013: 267-74.

Characterization of Cation-exchange Membranes Prepared by Ion-track Graft Polymerization

S. Harada¹, M. Goto², T. Yamaki³, S. Sawada⁴, H. Koshikawa³, A. Kitamura⁴, M. Yasukawa¹, M. Higa^{1,2}

¹Graduate School of Sciences and Technology for Innovation, Yamaguchi University, Japan

²Graduate School of Science and Engineering, Yamaguchi University, Japan

³Takasaki Advanced Radiation Research Institute, National Institutes for Quantum and Radiological Sciences and Technology, Japan

⁴Research Group for Radiation Materials Engineering, Fuels and Materials Engineering Division, Nuclear Science and Engineering Research Center, Japan Atomic Energy Agency, Japan

mhiga@yamaguchi-u.ac.jp; u038fj@yamaguchi-u.ac.jp

Ion-exchange membranes (IEMs) have been widely applied in many fields such as the concentration or desalination of electrolyte solutions using electrodialysis (ED) systems etc. Almost all IEMs have styrene-*co*-divinylbenzene polymer matrix. Recently, many novel IEMs have been developed to get higher ionic transport properties (high transport number and low membrane resistance) than commercial IEMs. A heavy ion with huge kinetic energies can pass through a polymer material and induce a continuous trail of excitation and ionizations, leaving a latent track. The latent track contains high-density and localized macromolecular radicals, which can act as an initiator of graft polymerization of negatively-charged monomers to prepare a cation-exchange membranes (CEMs). The prepared CEMs had straight and high aspect ratio of cylindrical cation-exchange domains perpendicular to the membrane surfaces and the domains had high concentrations of the cation-exchange groups. Therefore, the CEMs will have high performance for ED applications. In this study, we prepared novel CEMs by ion-track grafting polymerization method and measured the characteristics of obtained CEMs. Poly(ethylene-*co*-tetrafluoroethylene) (ETFE) films as a base film were bombarded with a 560 MeV ¹²⁹Xe ions from a cyclotron with 3.0×10^8 or 1.0×10^9 ions/cm² of the ion-beam fluence. The irradiated films were immersed in 1 M of ethyl *p*-styrenesulfonate (EtSS) solutions for graft polymerization. The EtSS-grafted membranes were hydrolyzed in ultrapure water at 80 °C for 24 h to remove the ethyl groups. The water content, *H*, membrane resistance, membrane charge density and ion-exchange capacity (*IEC*) of the CEMs was measured using the same methods described elsewhere¹⁾. In the case that the ion-beam fluence was 3.0×10^8 ions/cm², the degree of EtSS grafting (*D_G*) was less than 2.5% at 12 h of reaction time. In the case of 1.0×10^9 ions/cm², *D_G* was 13.4 and 75.1 % at 3h and 12 h, respectively. The increase in *D_G* will be due to the fact that more radicals were produced by higher-fluence ion beams. The prepared IEMs with 13.4 and 75.1 % of *D_G* showed 0.38 and 1.70 mmol/g of *IEC*, respectively. The charge density of the prepared CEMs obtained from the membranes potential measurement were 2.19 and 0.43 mol/dm³, respectively. The water content of the CEMs increased with increasing in *IEC*. The membrane resistance of the CEM with the *IEC* of 1.70 mmol/g was 0.18 Ω cm², which was only around one tenth of that of a commercial CEM, Neosepta® CMX. The IEMs prepared in this study have higher ionic selectivity than commercial IEMs; hence, the IEMs have potential application to an ED desalination process for high salt concentrations.

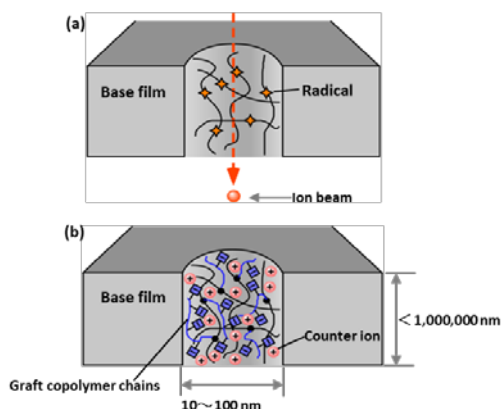


Fig. 1. Schematic diagram of the preparation process of a CEM using the ion-track grafting technique. (a) a base film after ion-beam irradiation, (b) a CEM after the grafting of cationic monomers that was initiated from the radicals in the base film

REFERENCE

- 1) M. Higa, M. Nishimura, K. Kinoshita, A. Jikihara. *Int. J. Hydrogen Energy*, 37, 2012: 6161-68.

Preparation and Characterization of PVA-based Charge Mosaic Membranes Prepared by Polymer Coating Method

Tsuyoshi Saito, Yuriko Kakihana, Masashiro Yasukawa, Mitsuru Higa
Graduate School of Sciences and Technology for Innovation, Yamaguchi University, Japan

mhiga@yamaguchi-u.ac.jp; kakihana@yamaguchi-u.ac.jp

A charge mosaic (CM) membrane consists of cation- and anion-exchange regions passing through the membrane. Due to this specific structure, it can selectively permeate electrolytes against non-electrolytes. Therefore, a CM membrane has a potential usage for desalination and concentration of salty solution in food and water treatment applications. Although there are various reports on preparation methods of CM membranes, there have been no commercial CM membranes because of their low mechanical strength and low salt flux. In this study, we prepared poly(vinyl alcohol) (PVA)-based CM membranes by using polymer coating method, and performed permeation experiments using salt and sucrose to examine its permselectivity for salts. Two types of PVA copolymers, PVA-*b*-polystyrene sulfonate (PVA-*b*-PSSS) and PVA-*b*-poly(vinylbenzyl trimethylammonium chloride) (PVA-*b*-PVBTAC) were synthesized *via* thiol-ene click reaction between thiol-terminated PVA (SH-PVA) and the respective monomers (SSS and VBTAC). Two aqueous solutions of the each synthesized PVA-based copolymers were alternately coated on a nonwoven fabric or glass plate with designed regular pattern by using a dual dispensing machine to form a base film. After then, the base films were prepared by physical and chemical cross-linking treatments to obtain CM membranes. To confirm the formation of the cation and anion-exchange domains, a prepared membrane was immersed into both in methyl orange solution and in methyl violet solutions for 1 hour. Diffusion dialysis experiment using KCl and sucrose were performed to check the CM membrane performance. The flux and permeability coefficient of J_{KCl} and P_{KCl} , and those of sucrose, J_{SUC} and P_{SUC} , were obtained from the slope of the time-concentration curves. Permselectivity between KCl and sucrose, $\alpha \equiv P_{KCl}/P_{SUC}$, was obtained from the ratio of the coefficients. Figure 1 shows the surface of the CM membrane (DCM). The size of the anion- and cation-exchange domains are 1110 and 633 μm , respectively. The diffusion dialysis experiments showed that the slope of the time-concentration curve of KCl was much higher than that of sucrose, indicating that the CM membrane has high permselectivity for salts. The characteristics of the CM membranes prepared in this study as well as those in literature were listed in Table 1 to compare their characteristics where DCM and DNCM are the prepared CM membranes with and without nonwoven fabric as the reinforce material. Although the permselectivity of our membrane is less than that of PBCM, the salt flux of our membrane is more than about 2 times higher than that of PBCM because of the lower flux of sucrose through the membrane.

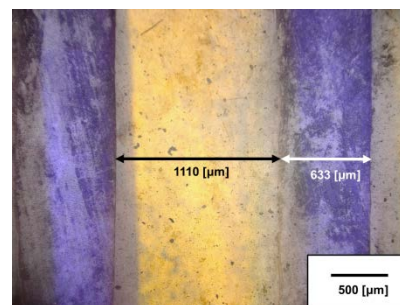


Fig. 1. Photograph of the surface of the CM membrane prepared in this study. The orange parts, anion-exchange domains dyed with methyl orange; the purple ones negatively charge-domains dyed with methyl violet.

Table 1. Characteristics of charge mosaic membranes obtained in this study: thickness, d , flux of KCl, and sucrose, J_{KCl} and J_{suc} , respectively, and permselectivity between KCl and sucrose, α .

Sample	d [μm]	J_{KCl} [10^{-10} mol/cm ² s]	J_{SUC} [10^{-10} mol/cm ² s]	P_{KCl} [10^{-9} mol/cm ² s]	P_{SUC} [10^{-9} mol/cm ² s]	α [-]
DCM	282	113	11.3	31.9	2.79	11
DNCM	82	142	14	11.6	1.15	10
PBCM ¹⁾	200	72	2.3	1.4	42	32

REFERENCE

- 1) M. Higa, M. Kobayashi, Y. Kakihana, A. Jikihara, N. Fujiwara. *J. Membr. Sci.*, 428, 2013: 267-74.

Polymer Alloy of Polybutylene Terephthalate and Polyrotaxane and Its Physical Properties

Fumiya Sakakibara, Akira Ishigami, Takashi Kurose, Hiroshi Ito
Graduate School of Organic Materials Science, Yamagata University, Japan

ihiroshi@yz.yamagata-u.ac.jp; tyk97200@st.yamagata-u.ac.jp

Physical properties of polymer alloy between Polybutylene Terephthalate (PBT) and Polyrotaxane (PR) were investigated. Two types of PBTs were used. PBT① (1401X06, Toray Co., Ltd., MFR=17.4 g/10min) and PBT② (1401X31, Toray Co., Ltd., MFR: 54.0 g/10min). A supramolecular PR which was composed of three parts (Fig. 1): the linear chain (polyethylene glycol (PEG)), cyclic molecule (cyclodextrin (CD)), and stopper molecule (adamantanamine). Three different PRs were used (PR①: SH1300P, Mw=180,000 g/mol, PR②: SH2400P, Mw=400,000 g/mol, PR③: SH3400P, Mw=700,000 g/mol). They are kindly provided by Advanced Softmaterials Inc.. The blending ratio of PBT/PR was 95/5 wt% in this study. An 8-axis melt kneading extruder (WDR 15OT-45MG-NH, Technovel Co., Ltd.) was used for the polymer blending. The kneading process at the temperature of 230 °C and the screw rotation speed of 100 rpm was applied. The blended samples were molded using micro-injection molding machine (AU3E-s, Nissei Plastic Industrial Co., Ltd.) and that was followed by fabricating small dumbbell specimen (JIS7162 1BB).

Tensile test results of blending materials were shown in Fig.2 (a) and (b) with the test speed of 10 and 500 mm/min, respectively. When the 5 wt% of PR was added, the strain at break reduced or did not change compared with the neat PBT and Mw of PRs did not affect mechanical properties at the strain rate 10mm/min. On the other hand, higher Mw of PR reduced the strain at break at the strain rate 500mm/min. It is assumed that the PR should become the starting point of the fracture caused by heterogeneous dispersion of PR in PBT or the lack of interfacial adhesion between PBT and PR due to low interfacial interaction between them. Blending condition and materials will be modified to improve dispersion of PR in PBT and the mechanical properties.

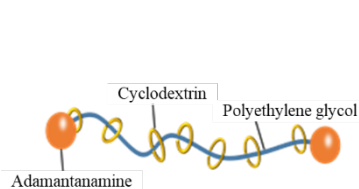


Fig. 1. The structure of polyrotaxane.

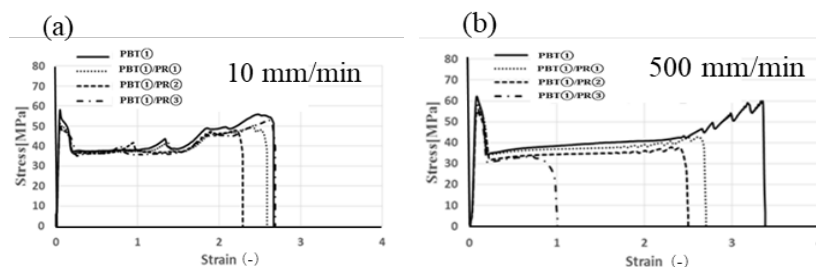


Fig. 2. Stress strain curves of PBT and PBT/PR alloys at strain rate 10 mm/min (a) and 500 mm/min (b).

Sensory Evaluation of Female Jeans Using the CALM Scale to Assess Total Comfort

Iara Braga¹, Maria José Abreu², Madalena Oliveira²

¹Federal University of Piauí/University of Minho; ²University of Minho

iarabraga@yahoo.com.br; josi@det.uminho.pt; madalena.oliveira@ics.uminho

The present paper consists on the experimental stage of a PhD research, on the study of the popular female jeans comfort, referring to the process of subjective evaluation of comfort to wear. The popular jeans in study, refers to the jeans created, produced and consumed by the poor classes of Fortaleza, in the state of Ceará, Brazil (Braga and Abreu, 2017). The purpose is to investigate the female jeans, with the objective of collecting information about the comfort / discomfort perceptions of the consumers of the Fortaleza popular markets.

MATERIALS AND METHODS

The sensorial evaluation to use of the jeans was made according to the following phases:

1) The inquiry was the instrument used for data collection (Braga, Abreu and Oliveira, 2017). The inquiry was constructed from the combination of three different steps: with the combination of scales (Figure 1) (numerical, attributes and faces).

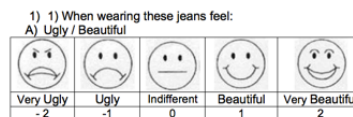


Figure 1 – Combination of scales

With two leaves consisting of a front and back body map, with each side (front and back) (Figure 2) being divided in 15 parts, referring to the body zone dressed in jeans, adaptation of the Discomfort Opinion Scales developed by Corlett; Bishop (1976).

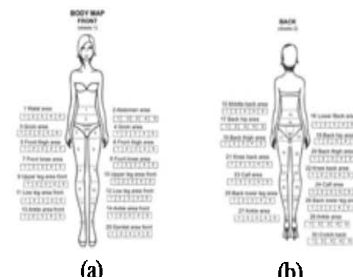


Figure 2 – Body map (a) front, (b) back

The final question, concerning the assessment of the total comfort of the jeans through the CALM scale (Comfort Affective Labeled Magnitude) (Figure 3).



Figure 3 – CALM scale (Comfort Affective Labeled Magnitude) (Kamalha et al., 2013)

2) The five jeans models were bought at popular malls and fairs in the city center.



Models	Jeans 1	Jeans 2	Jeans 3	Jeans 4	Jeans 5
Composition	98% cotton 2% spandex	77% cotton 21% polyester 2% spandex	98% cotton 2% spandex	96,5% cotton 3,5% spandex	77% cotton 21% polyester 2% spandex
Structure	Twill (2/1 1)	Twill (2/1 1)	Twill (3/1 1)	Twill (3/1 1)	Twill (3/1 1)
Mass (g/m ²)	281	332	322	289	323
Thickness (mm)	0,70	0,83	0,75	0,72	0,75
Count threads (yarns/cm)	29 x 21	37 x 23	39 x 22	40 x 26	38 x 23
Air Permeability (l/m ² /s)	38	48	50	47	39
Water vapour resistance (Pa·m ² /W)	60	56	64	69	62

Figure 4 – Characterization of the five popular jeans models

3) The group of evaluators consists of 101 female volunteers, aged between 18 and 40 years, consumers of the Fortaleza popular markets.

4) The locations for the tests applications were in real environments. The means of temperature and humidity were between 28°C with variation of ± 2°C and 65%, with variation of ± 2%.

5) The time of the experiment: 30 minutes for each jeans model.

RESULTS

Through the analysis of the data collected, the evaluators pointed out: the jeans 1 and jeans 2 showed very close data in all parameters analyzed, and the jeans 1 and jeans 4 showed the same data, as the most uncomfortable jeans.

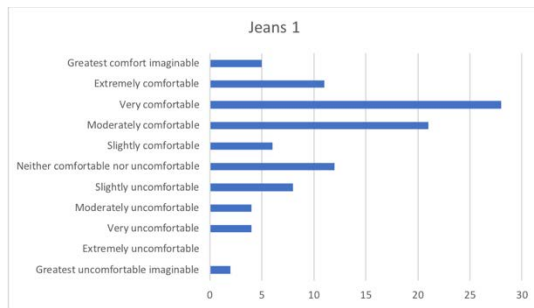


Figure 5 – Evaluation of jeans 1 data

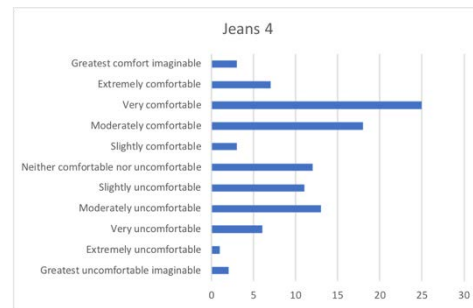


Figure 6 – Evaluation of jeans 4 data

The jeans 3 and jeans 5 showed the very close data, as the most comfortable imaginable jeans.

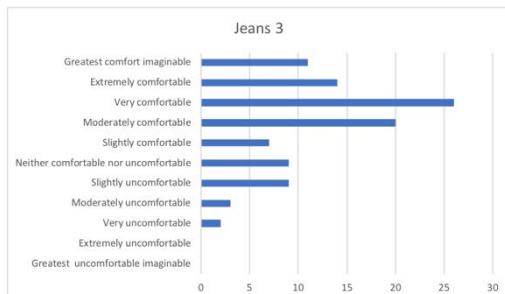


Figure 7 – Evaluation of jeans 3 data

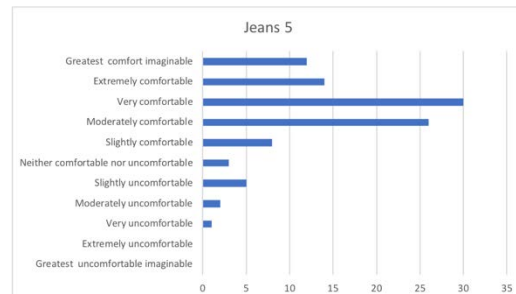


Figure 8 – Evaluation of jeans 5 data

When comparing the data of all models of the jeans tested it was observed that, in general, the models were evaluated as comfortable as showed in the Figure 9. Being that the jeans 5 stood out by having the greater number of positive evaluations of comfort and therefore it was considered most comfortable jeans. While the data of jeans 4 demonstrated to be regarded as most uncomfortable.

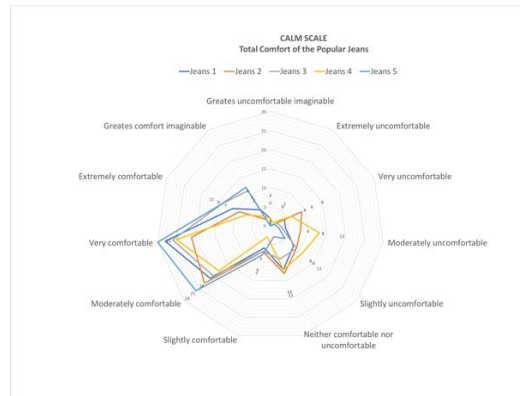


Figure 9 – Comparison of jeans evaluation data

CONCLUSIONS

During the application of the tests, it was possible to observe the level of satisfaction/dissatisfaction to wear, relating not only to the jeans aesthetics attributes, but also to the sensorial aspects brought when the skin is in contact with the jeans. When the collected responses were correlated, it was found that the perception of comfort/discomfort of the jeans is directly related to the touch sensation.

REFERENCES

Braga, I., Abreu, M. J. "Social Aspects in Denim Production, Sustainability in Denim." doi: 10.1016/B978-0-08-102043-2.00011-3. (2017)

Braga, I., Abreu, M. J., Oliveira, M. "Subjective Evaluation of the Comfort of Popular Denim: Elaboration and Validation of the Data." in *IOP Conference Series: Materials Science and Engineering*. doi: 10.1088/1757-899X/254/18/182001. (2017)

Kamalha, E., et al. "The Comfort Dimension; a Review of Perception in Clothing." *Journal of Sensory Studies*, 28(6), 2013: 423-44. doi: 10.1111/joss.12070.

ACKNOWLEDGMENT

This work is financed by FEDER funds through the Competitiveness Factors Operational Program (COMPETE) and by national funds through FCT–Foundation for Science and Technology within the scope of the project POCI-01-0145-FEDER-007136.

Industry 4.0 and the Future of Textile Production in High-wage Countries

Maximilian Kemper, Thomas Gries
Institut für Textiltechnik der RWTH Aachen University (ITA), Aachen, Germany

maximilian.kemper@ita.rwth-aachen.de

INTRODUCTION

This research initially reflects the particular challenges of textile production in high-wage countries. Later, the vision of the future of smart textile production will be outlined. In addition, pilot solutions and current research approaches which pave the way for Textile Production 4.0 are described.

CHALLENGES OF TEXTILE PRODUCTION IN HIGH-WAGE COUNTRIES

The use of Industry 4.0 in textile machinery and textile production has been examined at the Institute of Textile Technology at RWTH-Aachen University. The challenges regarding Industry 4.0 include standardization, process and work organization, protection of know-how, availability of technology and shortage of skilled workers. Important preconditions for the successful implementation of Industry 4.0 require information gathering, testing technologies, convincing decision-makers in the company and, ultimately, the ability to raise capital. Another challenge for textile production in high wage countries is the average return on sales of around 2.5%. The low profit margins make it difficult for textile producers to accumulate reserves and thus indirectly force major investments.

The particular features of textile production in high wage countries can be defined by the following:

- fragmented production chain
- switching between continuous-production and piece-production
- different orders of magnitude
- lack of standardization of communication interfaces
- low return on sales and resulting investment affinity

These peculiarities complicate the introduction of cross-process technological innovations such as Industry 4.0. Solving these problems will be the chance for the high wage countries to keep their technical leadership.

CONCEPT OF TEXTILE PRODUCTION 4.0

To be able to continue production of textiles in a highly competitive environment, several factors have to be considered. Cost reductions and efficiency improvements ensure economical production. However, the individual production processes are already highly automated. Hence it is expensive to archive cost reductions and higher efficiencies via technological enhancements.

To reduce costs and stay competitive Industry 4.0 comes into play. Linking the whole textile process chain makes information available everywhere in the process. With use of enhanced machine-cognition, those machines become capable to react on changing process- and boundary conditions. Successful pilot projects like the smart-bobbin using RFID information carrier or the self-optimizing weaving machine lead to measurable reductions of processing costs.

ACKNOWLEDGMENT

The authors would like to thank the German Research Foundation DFG for the kind support within the Cluster of Excellence “Integrative Production Technology for High-Wage Countries.”

Fabric Movement and Washing Performance in the New Front-loading Washer with Built-in Pulsator

Hyewon Kim¹, Changsang Yun², Sungmin Kim¹, Chunghee Park¹

¹Department of Textiles, Merchandising and Fashion Design, Seoul National University, Korea

²Department of Fashion Industry, Ewha Womans University, Korea

junghee@snu.ac.kr; hyewonk@snu.ac.kr

Washing efficiency for small loading in the drum washer can be improved with the complex fabric movement including falling behavior by changing the position. On the other hand, when the laundry loads are heavier, the interactions between fabrics have a major impact on the washing performance. But this mild movement of conventional drum washer has limitation and thus it is difficult to impart strong mechanical force to actual laundry load. Therefore, the purpose of this study is to analyze the relationship between the fabric movement and washing efficiency in the drum washer with built-in pulsator newly developed to increase the complex movement and interaction between the fabrics. For this, the fabric movements were observed from front and side, and visualized in 3-D coordinate.

Cotton pillowcases and soiled fabrics (EMPA 108, sebum/pigment, carbon black/mineral oil, blood, cocoa, red wine) were used for specimens. Fabric movements of XY plane (front-view), YZ plane (side-view) were observed using the two high speed cameras. Washing efficiency was evaluated for the introduction of pulsator washer and conventional. Then correlation between the fabric movement and detergency was analyzed.

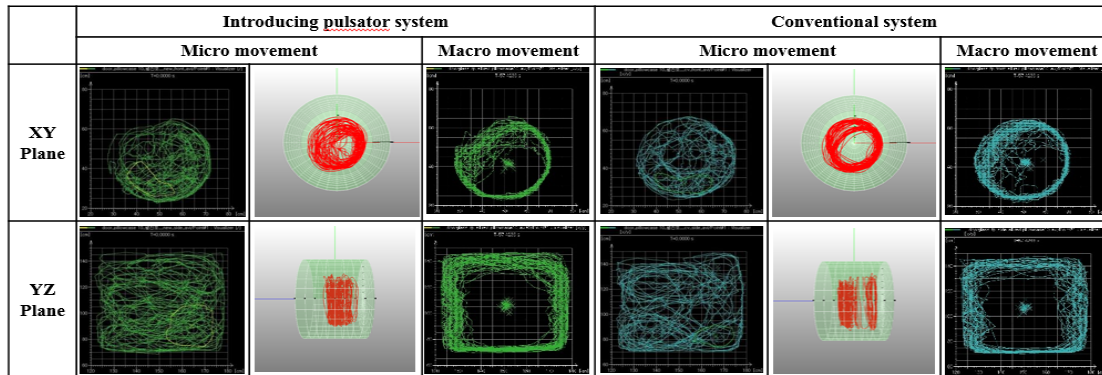


Figure 1. Comparison of the washing systems.

Fabric movements were observed from front and side, and analyzed by 3-D diagram and cylindrical coordinate system. By the introduction of pulsator in the drum washer, the fabric showed more complex movements at XY plane. Especially fabric movement of to-and-pro motion in YZ plane was remarkable throughout the washing time. On the other hand, in the conventional washer, the fabric showed mainly rotation behavior and retained same position for some time, and showing less to-and-pro motion in YZ plane.

It was shown that washing performance was improved 5.1% p (7.6%) by introduction of pulsator in the drum washer, within this experimental condition. Especially this improvement was remarkable in case of sebum/pigment, carbon black/mineral oil soiled fabrics, whose detergency seems to be more influenced by the mechanical action.

ACKNOWLEDGMENT

This work was supported by the Samsung Electronics Co., Ltd. (Grant number 350-20170041).

Textile Production Theory for Digital Applications in Fiber Production and Processing

Daniel Buecher, Bernhard Schmen, Thomas Gries
Institute for Textile Technology (ITA) of RWTH Aachen University, Aachen, Germany

daniel.buecher@ita.rwth-aachen.de

The theory of textile production is a sub-section of the general business management theory and considers the connection between input (mean use) and output (material goods or services). Interactions and the general dynamics of the process are difficult to grasp. Production systems are also not predictable or definable.

A theory is needed, to make a prediction as accurate and realistic as possible. A previous economic analysis was usually carried out with a strong focus on cost theory because the primary purpose of the company is to maximize profit. The technical side, on the other hand, considers production processes, logistics and machinery used. These approaches lead to a consideration and optimization of the production steps and less of the holistic system. With the introduction of a production theory, it is possible to represent the fraction of the detectable relationships in quantifiable action formulas. The Aachener textile production theory is intended to combine economic and business research into economics with engineering research into technical aspects and to create a holistic model.

Aachen's textile production theory regards the five main stages of the textile value chain in one approach: raw material, fiber processing, yarn production, fabric production and finishing.

In addition, eight focus points were selected and derived for the production theory. These focuses are based on the four fundamental principles: Expertise of research, fields of action industry 4.0, expert analyzes and literature. Subsequently, the eight focus points were projected onto the five main processing stages of the textile value stream. The focus is on an empirical survey in the form of expert interviews. The experts were involved in subprocesses from all main processing stages in the textile value-added chain. Subsequently, the focus of Aachen's production theory for the textile industry was integrated and future fields of action were derived.

Analysis of Tactile Sensation of Synthetic Leather Using Logistic Regression Analysis

Tsuyoshi Chiba¹, Shota Kuroda², Masaki Yamaguchi^{1,2}

¹Interdisciplinary Graduate School of Science and Technology, Shinshu University, Japan

²Graduate School of Science and Technology, Shinshu University, Japan

masakiy@shinshu-u.ac.jp; chiba-t16@mail.dnp.co.jp

INTRODUCTION

A texture on synthetic leather has an important role in controlling the appearance and the tactile sensation of a product. The purpose of this study is to propose a model for the tactile sensation expressed by several physical quantities. Firstly, five kinds of tactile sensations were quantitatively evaluated by a sensory evaluation method using 13 kinds of synthetic leather samples. Logistic regression analysis was used on the results to create a model for each tactile sensation. The diagnostic capabilities of models were evaluated by Receiver Operating Characteristics (ROC) analysis.

MATERIALS AND METHODS

Thirteen kinds of synthetic leather samples were fabricated by coating urethane on twilled fabrics (Figure 1). The sensory evaluation was performed using 30 female adult subjects (mean \pm SD, 22.3 \pm 1.1 yr). Five adjectives such as “coarse”, “uneven”, “sticky”, “soft”, and “moist” were used to evaluate the tactile sensation. Six kinds of physical quantities such as surface roughness (Sa), surface waves (Wa), elasticity (E'), viscosity (E''), contact angle hysteresis (CAH), and apparent contact angle (θ') were measured for each synthetic leather sample. The sensory evaluations and the physical properties were analyzed by logistic regression analysis to build each model of tactile sensation.

RESULTS AND DISCUSSION

Five kinds of tactile sensation model (Z) were created by logistic regression analysis. A model of coarse was derived as follows:

$$Z = 0.365 Sa - 0.081 E'' + 0.025 CAH \quad (1)$$

To confirm the above findings, ROC analysis was performed. Figure 2 shows the ROC for the presence of tactile sensation of coarse when 3 kinds of physical properties were used. The AUC was 0.90 which demonstrates the excellent capability for describing the tactile sensation.

CONCLUSION

A ROC analysis indicated a possibility that a model using physical quantities can express the tactile sensation of synthetic leather quantitatively.

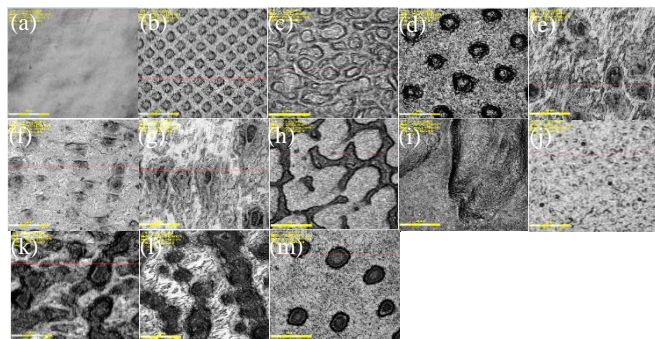


Figure 1. Images of synthetic leather surfaces using a laser scanning microscope. (a) Enamel (b) Smooth (c) Nubuck (d) Fine grain (e) Textie (f) Sheep A (g) Sheep B (h) Lamb A (i) Lamb B (j) Cow (k) Calf (l) Cordova (m) Elk.

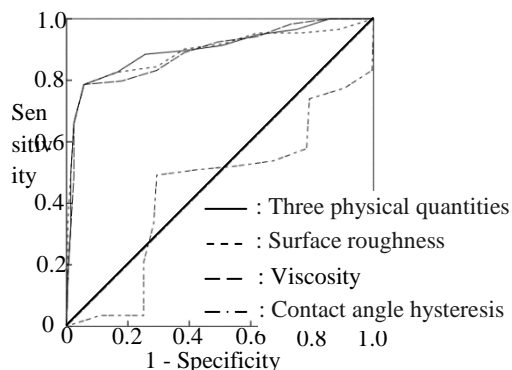


Figure 2. ROC analysis of tactile sensation “coarse” using surface roughness, loss modulus and contact angle hysteresis.

Structure Analysis of a Colorful Woven Fabric Based on Colored Weft Yarn Mixing

Tao Hua, Lau Yiu Tang, Xiao Tian, Nga Sze Sea Yeung, Hai Bo Hu

Institute of Textiles and Clothing, The Hong Kong Polytechnic University, Hong Kong, China

tcthua@polyu.edu.hk

Colorful and figured woven fabrics produced by mixing colored warp and/or colored weft yarns are widely used for fashion, home furnishings and decorations. There are two main approaches used to produce the colored-yarn mixed woven fabrics. The first approach is to employ both colored warp and weft yarns for producing colorful woven fabrics. The main advantage of this approach is its created good color mixing effect but the preparation of warp yarn is complicated and time-consuming. Another method that provides fabrics with a color mixing effect is by only using colored weft yarns, together with the raw white warps. In comparison to the colored warp and weft mixing method, this approach has several advantages such as easy and flexible production. The key issue of this approach lies in the fabric structure that determines the assignment of the desired colored weft yarns to the fabric surface.

A colored-yarn mixed woven fabric has been developed based on the multicolored wefts and raw-white warps and specially designed weft-backed structures in our previous studies. The results on the resultant color-mixed fabrics demonstrate that such kind of fabric structure enables the fabrics with varied color proportions and lowered lightness and thus reduce the negative effect from the raw-white warps used. Therefore, it is necessary to conduct extensive structure analysis on the colored-weft-yarn mixed woven fabrics.

The main goal of this study is to characterize the fabric surface and cross-section structures as well as comprehend the effects of weave and weft density on the characteristics of fabric structure and the resultant fabric color attributes. A unit of fabric surface structure is identified and then characterized in terms of the size of each mixing yarn float and yarn spacing. Based on this, the real proportion of each yarn component can be calculated. In terms of fabric cross-section, the warp yarn path is established and the height, width and length of warp and weft yarns are used to describe the fabric structure. The influence of weave and density on the geometry of fabric structure and thus the color attributes of fabric can be fully understood.

ACKNOWLEDGMENT

The authors wish to thank the Innovation and Technology Commission of Hong Kong SAR Government for funding support (Grant No. ITS/057/16).

Cleaning Liquid of Dilute Emulsion System Containing Fatty Alcohol for Removing Non-polar Oil from Fabrics

Masaki Tanaka¹, Masaru Oya²

¹Graduate School of Environment and Information Sciences, Yokohama National University

²Faculty of Environment and Information Sciences, Yokohama National University

moya@ynu.ac.jp; tanaka-masaki-xv@ynu.jp

INTRODUCTION

Many difficulties have emerged in degreasing process of textile producing industry because of green policy related to organic solvents and surfactants. Especially, it is required to develop the alternative method for replacing APE (alkyl phenol ethoxylates) system the removal efficiency of which is the greatest in general surfactant system. We have been trying to develop a new aqueous cleaning system using dilute emulsion in which fatty alcohol is used as a oily phase. This paper will show the cleaning mechanism of the system.

EXPERIMENTAL

Emulsion liquid was prepared using three kinds of linear fatty alcohols (C7 to C9) and sodium dodecyl sulfate (SDS). Artificial soiled fabric was prepared by soiling cotton cloths with n-octadecane which contains Sudan III as a tracer. Cleaning test was conducted using Terg-0-Tometer and the detergency was calculated from K/S value (Kubeika-Munk equation) derived from reflectance measured using a digital color difference meter.

RESULTS AND DISCUSSION

The removal efficiency with the emulsion system was much greater than that of surfactant solution system, especially the emulsion system of C8-C9 alcohol gave superior removal efficiency (Fig. 1). The washing mechanism was presumed not to be solubilization but to be emulsification because the results of simple emulsification test using filtration with a proper membrane filter showed the similar tendency to the cleaning test. Suitable emulsion size was decided to be 71-730 nm by particle size distribution measurement. The analysis of 4-repetitive cleaning test results using probability density functional method also supported the mechanism of emulsification (Table 1). This emulsion system can be regarded as one of the most promising methods in the future aqueous cleaning process for removing non-polar oily soils.

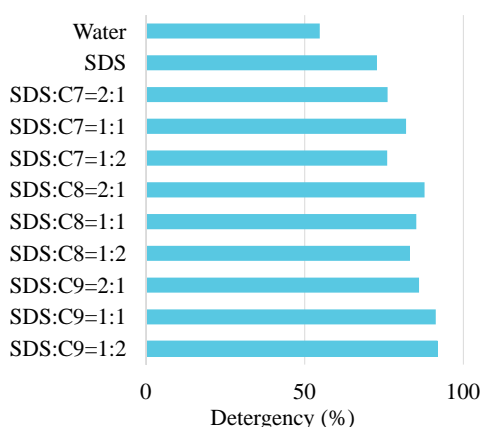
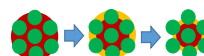


Fig. 1. Detergency of octadecane soil from cotton fabric with emulsion liquid of SDS/fatty alcohol system.

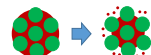
Table 1. σ_{rl} calculated for octadecane removal process using emulsion liquid of SDS and C7-C9 fatty alcohol.

	SDS: C7	SDS: C8	SDS: C9	SDS
2:1	1.58	3.75	3.45	0.92
1:1	1.97	2.90	3.51	
1:2	2.53	1.94	4.23	

$\sigma_{rl} < 2$: largely solubilization



$\sigma_{rl} > 2$: largely emulsification



New Method for Estimating Synergic Effect or Offsetting Effect in Removal Process of Soils and Dyes from Fabrics

Yosuke Taniguchi¹, Masaru Oya²

¹Graduate School of Environment and Information Sciences, Yokohama National University

²Faculty of Environment and Information Sciences, Yokohama National University

moya@ynu.ac.jp; taniguchi-yosuke-mg@ynu.jp

INTRODUCTION

Probability density functional method has been developed to express the cleaning ability of a certain cleaning system. Two parameters, σ_{r1} and μ_{r1} can be used to express the mechanism of soil removal and the level of cleaning efficiency, respectively. In this paper, additional law of μ_{r1} will be discussed to develop a new method for estimating synergic effect or offsetting effect in removal process of soils and dyes from fabrics.

EXPERIMENTAL

The assumption of this method is that both adhesion force of adhered materials and removal force follow a normal distribution. The mean value (μ) and the standard deviation (σ) of the adhesion force are assumed to be 0 and 1.0, respectively. The mean value and standard deviation of removal force μ_{r1} and σ_{r1} were calculated from 4-repetitive cleaning test. Test fabrics were prepared by soiling cotton fabrics (5cm x 5cm) with some water soluble dyes, oily dyes, iron(III) oxide, carbon black, hemoglobin and fatty acids. 5 pieces of the identical fabrics were washed with Terg-O-Tometer (1L surfactant solution) for 5 min x 4 repetition without ballast cloth. Removal percentage was calculated from K/S values in order to derive μ_{r1} and σ_{r1} using PC simulation application.

RESULTS AND DISCUSSION

The values of σ_{r1} increased if the soil varied in the order of particulate soil, water soluble soil, oily soil (by solubilization), oily soil (by emulsification). As for μ_{r1} , additive law was observed in many cases, for example $\Delta\mu_r$ (mechanics + alkaline) came to be the same value of $\Delta\mu_r$ (mechanics) + $\Delta\mu_r$ (alkaline) for the cleaning of iron(III) oxide particulate soil. Similar tendency was observed for hemoglobin cleaning varying pH and temperature (Fig. 2). As for fatty acid soil, $\Delta\mu_{r1}$ (temperature + alkaline) became much greater than $\Delta\mu_{r1}$ (temperature) + $\Delta\mu_{r1}$ (alkaline), which indicates the existence of synergic effect between temperature and alkaline strength. Offsetting effect was sometimes observed when the surfactant concentration and mechanical power were used as variables.

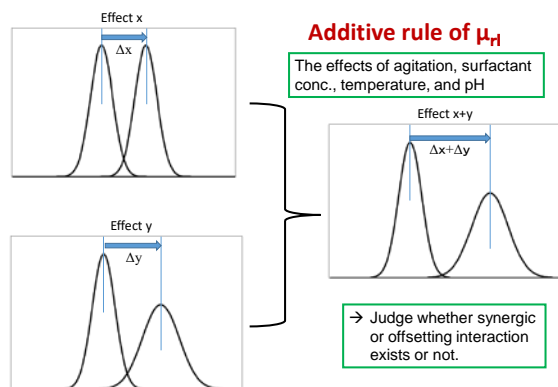


Fig. 1. Additive rule of μ_{r1} in provability density functional method between different conditions such as agitation and temperature.

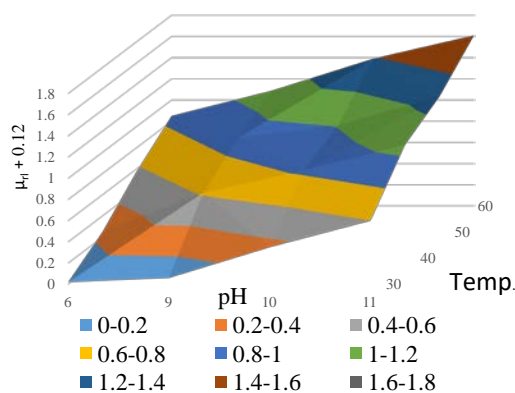


Fig. 2. μ_{r1} (+0.12) obtained from hemoglobin cleaning varying pH and temperature.

Preparation and Characterization of Kapok Nonwoven for Oil-separation Filter

Seung Woo Han, Jung Yeon Kim, Yeong Og Choi

Technical Textile R&D Group, Korea Institute of Industrial Technology, Ansan, Korea

yochoi@kitech.re.kr; seungwoo@kitech.re.kr

Kapok fiber has not only a hollow structure representing a large lumen but also a high degree of oil absorbing properties which are compared to the performance of the synthetic fibers applied to various industrial fields. The oil-water separation filter is connected to the fuel pump and mounted on a transport engine to remove moisture from the fuel to increase the engine's durability life.

In this study, the basic nonwovens to be applied as an oil-water separation filter were prepared using Kapok fiber which is a natural hollow fiber and LM-PET bicomponent is used as a binder fiber. Kapok/LM-PET basic nonwovens were manufactured through carding, cross-lapping, thermal-bonding and calendaring processes. Also, composite nano-fiber layers were formed by electrospinning using nylon and PVDF polymer on the surface of Kapok/PET basic nonwovens for improve the oil-water separation efficiency and durability. The manufactured Kapok nonwovens were evaluated in terms of various physical properties including tensile properties, pore diameter, air permeability, contact angle, and oil separation efficiency.

Study of Comfort of Japanese Traditional Uniforms: Shinto Priest Costumes

Mariko Sato, Yuko Matsui, Shinko Kumagai
Bunka Gakuen University, Tokyo, Japan

mari-sato@bunka.ac.jp

INTRODUCTION

The priesthood is those who serve God in the shrines and perform ceremonies and clerical work at the shrines. The uniforms worn by priests, i.e. costumes, have inherited the tradition of the Heian era while preserving its tradition while slightly changing the shape. It is obvious that the costumes of the priests have cultural value, but it is unknown whether they fit the present day's climate in Japan or life of priest. The purpose of this research was to cast a spotlight on "kariginu" and "sashiko" which are regarded as everyday attire among Shinto priest costumes, and to focus on their thermal characteristics, thereby to clarify the present condition of comfortable or discomfort.

METHODS

Questionnaire Survey on Clothing Life and Costumes of Priests

We asked for cooperation with the priests of Kanda Myojin and Atago Shrine.

Physical Property Test

Samples: Two types of "kariginu" cloth [with woven cloth pattern (A), motif cloth (B)]; four types of "hakama" fabric [polyester / "Shiose" (C), "Shya" (D), "Habutae" (E), Tetoron rayon blend (F)].

Measurement items: Yarn density, thickness, air content rate, surface observation by microscope, airflow resistance, contact cold sensation, skin model.

Measurement of CLO Value by Thermal Manikin

Environmental conditions: Climate chamber at 20°C · 50% RH

Measuring equipment: Thermal manikin

RESULTS AND DISCUSSION

As a result of the questionnaire survey, many respondents said that costumes gave hot feeling in summer, and cold feeling in winter, and the belt was easy to get sweaty. Meanwhile, excellent points were also raised, including the feelings tightened towards Shinto rituals, being able to wear regardless of body shape changes, things can be put into the cuffs and necks. The physical property test indicated that A and C for winter were thicker, had larger thread density, and larger tendency of airflow resistance than the summer B and D. In the skin model, both R_d and R_e were higher in the order of $C > B \geq A > D$. In the clo value measurement, summer costumes exhibited 1.6 clo and winter costume 1.8 clo. Assuming that the priests spend in an environment similar to the outdoor, based on the openness of the building unique to the shrines, the possibility that wearing of costumes is not thermally comfortable in summer and winter has been indicated from the average temperature and humidity in Tokyo.

Relationship Between Fabric Surface Texture and Friction Using Tri-axial Force Plate

Davaajav Narantogtokh, Sachiko Sukigara
Kyoto Institute of Technology, Kyoto, Japan

sukigara@kit.ac.jp; narnaa67@yahoo.com

Tactile properties of fabrics are imperative evaluation indicators in the field of textile production and also consumer preference. KES system use a force sensor to check the surface roughness and friction of fabric in a constant speed and force. During the subjective assessments, the fabric touch and its finger force might be varying for each participant. We consider the individual finger force might be related to detect the different fabric surface such as hairiness and slippery. A tri-axial force plate can record changes in force and speed when human touch the fabric. The objective is to find how the finger forces are affected by the different surface texture during the touch.

Seven black woven cashmere and wool fabrics were used. Mean coefficient of friction (MIU) and its average deviation (MMD), surface roughness (SMD) were measured using KES-surface tester. 30 participants (15 female and male students) were asked to slide their 3 fingers (index, middle and ring) on the sample fabrics. The X, Y axis corresponds to the weft, warp fabric direction, the Z axis shows finger force. Finger forces from each participant were obtained and the average peak force (F_{max}) by force plate was calculated. Peak forces produced by males were consistently larger than those produced by female participants. The coefficient of friction (CoF) was calculated.

The values of mean coefficient of friction (MIU) for cashmere fabrics with hairy texture in the warp-backward direction were larger than those in the warp-forward direction (MIU=0.132~0.272). There was not much difference between the MIU values in different directions for the fabrics with disordered surface hairiness. CoF and F_{max} obtained by force plate were related to the MIU, MMD and SMD. Also, it shows more slippery and less hairy texture fabric caused lower CoF and F_{max} .

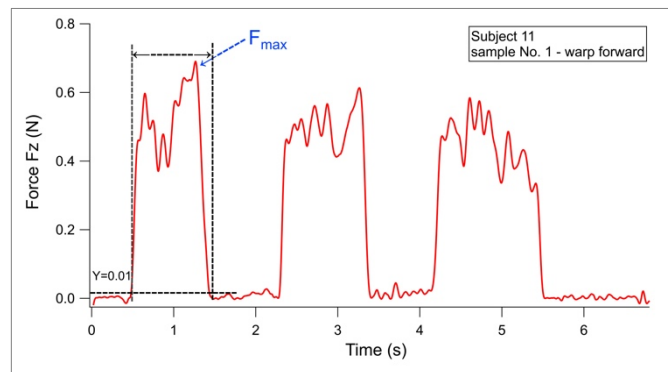


Figure 1. A data from Tri-axial force plate. Sample No. 1 – Subject 11.

Evaluation of Performance Such as Hygroscopic Exothermic Property and Heat of Vaporization of Clothing Materials

Maika Tamari¹, Atsumi Takezawa¹, Chihiro Suzuki¹, Kaname Katsuraya¹, Masami Asano²

¹Wayo Women's University; ²Asano Nenshi Co., Ltd.

katsuraya@wayo.ac.jp; tamari@wayo.ac.jp

INTRODUCTION

Recently, in Japan, winter underwear that claims hygroscopic exothermicity has become popular. Also, for the 2020 Tokyo Olympic Games to be held in the midsummer, fabrics that cool people down are being sought.

In this study, we first compared the contact thermal sensation and moisture absorption heat performance of winter underwear on the market with conventional cotton.

Next, we measured the exothermic property of moisture absorption and endothermic property of moisture release on commercially available sport shirts expressing the heat of vaporization. We also evaluated SUPER ZERO[®], which is a quick drying cotton yarn having fine and uniform voids in the yarn structure newly developed by Asano Nenshi Co., Ltd.

In addition, the decrease in temperature due to the vaporization heat of these shirts was evaluated.

METHOD

The temperature characteristics were evaluated using an infrared thermo camera in an environmental chamber. The temperature was maintained at 20°C and the relative humidity was varied between 40% and 90%.

RESULTS AND DISCUSSION

Winter Warming Underwear

Hygroscopic exothermicity was observed in all winter underwear that claimed hygroscopic exothermicity. However, these calorific values were inferior to those of ordinary cotton.

At the same time, an endotherm at moisture release corresponding to moisture absorption heat was observed for all materials. This result suggests that the thermal balance obtained from each material is zero.

Furthermore, it was found that relatively high humidity is necessary to generate heat, but such high humidity was not observed between the underwear and skin in winter.

Summer Cooling Shirts

First, the thermal characteristics of commercial shirts advertised as cool were evaluated using the heat of vaporization. Next the thermal properties of a SUPER ZERO[®] shirt were also investigated.

Both exothermic and endothermic properties were overwhelmingly greater in cotton than synthetic fibers. It was considered that because of the high polarity of cellulose of cotton, the energy during adsorption and desorption of water molecules was large.

These shirts were soaked in water and while they were dried in front of a blowing fan a decrease in the surface temperature was measured. Almost the same degree of temperature decrease was observed in all samples. SUPER ZERO[®] shirts dried in half the time of normal cotton.

Effect of Wearing Cloche Hat on Comfort Sensation of Young Women Mountain Walking in Summer in Shiga Highlands

Noriko Fukuda

Shinshu University, Japan

norikof@shinshu-u.ac.jp

OBJECT

We wear various types of hats when mountain-walking in order to protect ourselves against cold, wind, rain, insects, and sunlight. Research has shown that as the percentage of head coverage increases, heat radiation decreases. However in summer or during hard exercise, our body also relies on perspiration to maintain a constant brain temperature. With these points in mind, this study aimed to clarify the effect of cloche hats on the comfort sensation of young women mountain-walking in summer at Shiga Highlands.

METHOD

This experiment was conducted over a period of four years. Two young women participated each year. In total, eight healthy subjects (age, 20 ± 1 years; weight, 50.0 ± 4.6 kg; height, 160 ± 5.1) took part. Four subjects wore cloche hats while the other four did not. After two hours of walking, the amounts of perspiration on the back of the neck, on the chest, and on the abdomen were measured. During the rest time, the skin temperature on their left side was recorded and two sensory tests (wet sensation and comfort sensation) were conducted.

RESULTS

The average amount of perspiration depended on the region of the body. The greatest amount was from the chest area, and the least was from the back of the neck. The average amount of perspiration on the subjects wearing hats was larger than that of non-wearing subjects ($p < 0.05$), while the average skin temperature was lower (*NS*). The average score for wet sensation for subjects wearing hats was higher than that of non-wearing subjects (*NS*), and the average score for comfort sensation for subjects wearing hats was lower (*NS*). Based on the data, I concluded that wearing a cloche hat does not necessarily lead to greater comfort when mountain-walking in summer at Shiga Highlands.

Effect of Homologous Modeling of Three-dimensional Human Body Shape Data on Body Types Analysis

Ayumi Takemoto, Michiko Ohtsuka
Japan Women's University

takemotoa@fc.jwu.ac.jp

INTRODUCTION

Homologous modeling of three dimensional human body shape involves set procedures as well as aspects arbitrarily specified by the modeler. When homologous models are created based on those settings, the shapes of the models will change. But no studies have examined those settings in detail. An aim of this study was to identify how to create homologous models best suited to a given objective.

METHODS

The data used in this study were from 45 women in their 30–40s. Three dimensional body measurements were obtained using the Bodyline Scanner from Hamamatsu Photonics. Body shapes were captured using BLM Dhaiba 13545, and 64 landmarks were defined for homologous modeling.

A female model in Dhaiba Model ver.1.5 was used as a template for homologous modeling. Homologous modeling and statistical processing of those models were done using HBM-Rugle homologous modeling software from Medic Engineering Co.

RESULTS

In order to examine the effect of extension of the arms, spreading of the legs and the shape of the head on the results of principal component analysis, a set of homologous body models and a set of homologous torso models were created. Ascertaining body shape characteristics with the homologous body models was difficult since elements other than body shape were evident in the characteristics of principal components. However, body shape characteristics were better ascertained with the homologous torso models.

In order to examine the effect of differences in the surface shape of the template on homologous modeling, homologous models were created using a torso template with increased constituent data points and a smoothed surface shape. Discrepancies between the surfaces of the 2 types of homologous models and three dimensional body shapes were determined using HBM-Rugle. Significant (0.01) differences were noted, so homologous models with numerous data points allowed more accurate homologous modeling.

The average shape of both sets of models was matched results indicated large projections and depressions at sites such as the clavicles, chest, and abdomen and substantial differences between the 2 sets of models at the thighs (Fig. 1).



Fig. 1. Matching of the average shape of 2 sets of models.

ACKNOWLEDGMENT

This work was supported by a grant-in-aid for scientific research (Basic research A, grant no. 25242010).

Preparation and Characterization of Gelatin/Arabic Gum Microcapsules Containing Methyl Salicylate Deposited onto a Cotton Fabric

Samira da Silva Mendes¹, Andrea Zille², Fabricio Maestá Bezerra¹,
Nádia Regina Machado Fernandes Camargo³, André Paulo Almeida Whiteman Catarino²

¹Federal Technological University of Paraná, Paraná, Brazil

²2C2T – Center for Textile Science and Technology, University of Minho, Guimarães, Portugal

³Department of Chemical Engineering, State University of Maringá, Paraná, Brazil

samiramendes@utfpr.edu.br; whiteman@2c2t.uminho.pt

INTRODUCTION

In the last years the micro encapsulation technique has been of particular interest for researchers, due to be an efficient technique for physical capturing of active substances that are sensitive to external agents and thus allowing a sustained release of these substances. In this context, the mixture of polymers have been shown very effective and promising due to the high microencapsulation rates that are obtained, being this technique known as complex coacervation. The microencapsulation technique has been applied in different industries, namely on textile industry, resulting in new finishing and differential properties. The present study evaluated the effects of Methyl Salicylate complexation, using Gelatin and Arabic Gum as wall membrane components of the microcapsule and impregnating a jersey 100% cotton fabric.

MATERIALS AND METHODS

The materials used for the preparation of the microcapsules were Gelatin (Sigma Aldrich, Germany) and Arabic Gum (Sigma Aldrich, Germany), both as components for the wall, and Methyl Salicylate as the core material. The method used was the complex coacervation, for which three different solutions were prepared separately in order to be further mixed by means of mechanical agitation, using a temperature controlled system. The adjustment of the pH was necessary to allow the electrostatic interaction between the gelatin's amino groups and the Arabic Gum's carboxylic groups. The microcapsule's wall formation was induced by a controlled cooling of the solution, below the gelification temperature. With the purpose of obtaining a more rigid wall membrane, glutaraldehyde at 25% was added, due to be a powerful reticulation agent. In order to evaluate the formation of the microcapsules the following characterization techniques were used: FTIR, SEM, TGA/DTG and UV-VIS efficiency.

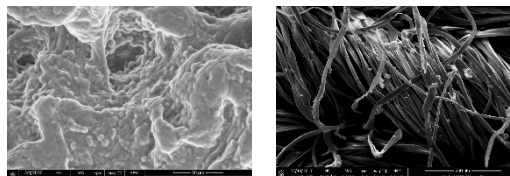


Figure 1. Electronic microscopic scan images of the microcapsules and the impregnation on a 100% cotton jersey fabric.

By means of the characterization techniques it was observed that the mixture of the two biopolymers successfully formed the Methyl Salicylate microcapsules, showing that the complex coacervation technique is driven by the electric charge difference between the materials present in the solution at the coacervation phase and the hydrophobic material. As it can be observed with Figure 1, SEM images show the microcapsules with a spherical shape and the former impregnated in a 100% cotton jersey fabric, thus showing the possibility of using them as a functional finishing in a conventional textile fabric.

ACKNOWLEDGMENT

This work was supported by FEDER funds through the Competitivity Factors Operational Program – COMPETE and by national funds through FCT – Foundation for Science and Technology within the scope of the project POCI-01-0145-FEDER-007136.

Crystalline Structure in High-speed Melt Spun Fibers of Blend of Poly(L-lactic acid) and Poly(D-lactic acid)

Nanjaporn Roungpaisan, Wataru Takarada, Takeshi Kikutani

Department of Materials Science and Engineering, Tokyo Institute of Technology, Japan

kikutani.t.aa@m.titech.ac.jp

INTRODUCTION

Enantiomeric poly(lactic acid) was prepared by the melt-blending poly(L-lactic acid) (PLLA) and poly(D-lactic acid) (PDLA) of high optical purity using a twin-crew extruder with a blend ratio of 50/50. The polymer was expected to exhibit crystalline structures of stereo-complex crystals of PLLA and PDLA and homo-crystals of individual polymers depending on the processing conditions. It is well-known that the stereo-complex crystals have the melting temperature about 60 degrees higher than the homo-crystals. With the aim of attaining good thermal and mechanical properties, high-speed melt spinning of the PLLA+PDLA blend was carried out, and the formation of the two types of crystalline structure in the obtained fibers was investigated.

RESULTS AND DISCUSSION

In this research PLLA and PDLA with the melt flow indices of 6 and 25 g/10 min, respectively, were used. High-speed melt spinning of the blend was performed setting the extrusion temperature higher than the melting temperature of the stereo-complex crystals. Melt spinning of the blend was possible up to the take-up velocity of 5 km/min, whereas the attainable maximum take-up velocities for the PLLA and PDLA were 8 and 10 km/min, respectively. WAXD patterns of the as-spun fibers shown in Fig.1 indicated that the orientation-induced crystallization started to occur at 5 km/min, where only homo-crystals were formed. DSC thermograms of the prepared fibers measured at the heating rate of 5 K/min exhibited the exothermic peak of cold crystallization and the exothermic peaks of the melting of homo- and stereo-complex crystals as shown in Fig.2 (a). DSC measurement was also performed in the cooling process of -5 K/min as shown in Fig. 2 (b). It is interesting to note that the thermograms for the high-speed spun fibers exhibited higher tendency for the formation of stereo-complex crystals, indicating a certain memory effect of structure formation in the spinning process.

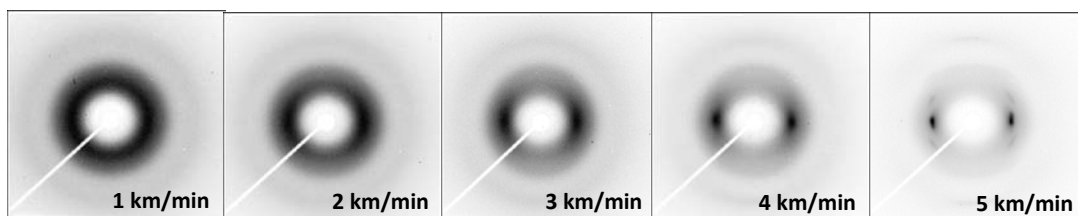


Figure 1. WAXD patterns of the PLLA+PDLA blend fibers prepared at various take-up velocities.

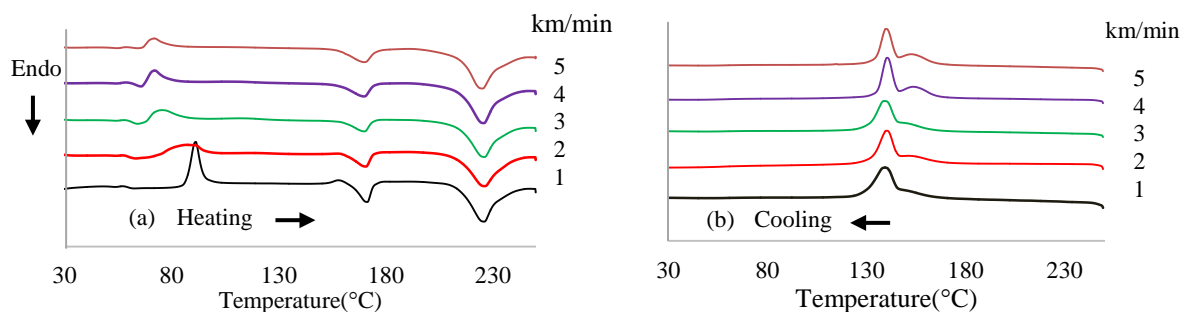


Figure 2. DSC thermograms of the PLLA+PDLA blend fibers prepared at various take-up velocities.

ACKNOWLEDGMENT

The poly(lactic acid) pellets used in this experiment were supplied by Corbion. Our gratitude to Corbion for supporting our research.

Separation of Oil-in-Water Emulsions Stabilized by Different Types of Surfactants Using Electrospun Fiber Membranes

Yi-Min Lin¹, Gregory C. Rutledge²

¹Department of Materials Science and Engineering, Massachusetts Institute of Technology, Cambridge, MA, USA; ²Department of Chemical Engineering, Massachusetts Institute of Technology, Cambridge, MA, USA

ymlin12@mit.edu

The compositions and properties of oil-in-water emulsions encountered in industry or the environment vary widely in the nature of surfactants that stabilize them. This variety poses challenges for applications of membrane separation. Electrospun fiber membranes have shown high permeability and improved robustness against fouling in emulsion separation, but the interaction between the emulsion and the membrane, and the fouling mechanism that results, remains unclear. In this work, electrospun polyamide membranes were challenged by model emulsions of dodecane stabilized by anionic, cationic, non-ionic and zwitterionic surfactants in both dead-end and cross-flow filtration configurations under constant pressure of 2 psi. The membrane was shown to have high oil rejection ($92.7 \pm 1.5\%$), sufficient to meet EPA's regulatory limit, when separating emulsions stabilized by anionic surfactant in cross-flow filtration, while maintaining a steady flux of 44.3 ± 2.6 LMH. Analysis of permeate flux and oil rejection revealed that the types of surfactants influenced the membrane fouling in both dead-end and cross-flow systems but in different ways. Fouling in dead-end filtration was found to be a function of the electrostatic interactions between the oil droplets and the membrane, while fouling in cross-flow filtration was mainly determined by the hydrophilic/hydrophobic interactions due to the adsorption of surfactants at the interfaces. Blocking filtration models are used to corroborate these findings and illustrate the transition between modes of fouling in dead-end filtration. A de-fouling process was found in dead-end configuration when separating emulsions stabilized by cationic surfactant, which was attributed to coalescence of oil droplets at the membrane surface, based on the kinetic model and direct observation. These results indicate that not only membrane-foulant but foulant-foulant interactions can influence the membrane fouling.

Preparation and Characterization of High-tenacity PTFE Filament Using Melt Spinning Process

Seung Jin Lee, Do Kun Kim, Ju Seok Hong, Byeong Jin Yeang

Technical Textile R&D Group, Korea Institute of Industrial Technology, Ansan, Korea

sjlee@kitech.re.kr

Polytetrafluoroethylene(PTFE) fibers are excellent material for heat resistance, resistance to corrosion and weatherproof. Based on these unique characteristics, it is widely used in industries such as environment, architecture, protection, and medical applications. But because of PTFE has a high molecular weight($10^7 \sim 10^8$ g/mol) and crystallization rate(90~95%) is extremely difficult to apply the manufacturing process based on the melt-spinning. Currently, PTFE fibers are manufactured through a extrusion or compression sintered process using a high pressure molding machine. These fibers have poor mechanical properties and are difficult to expanding their application. The purpose of this study was to develop methods for melt spinning PTFE filament fiber and characterize its properties. For this purpose, we investigated its properties through scanning electron microscopy(SEM), differential thermal analysis(DSC), and performed a comparative analysis of the mechanical properties of PTFE filament fiber. These results indicate that the properties of PTFE fibers using melt-spinning process can be adjusted by controlling spinning speed and thermal treatments.

Structure and Properties of Poly(ethylene terephthalate) Fiber Webs Prepared Through Laser-heated Electrospinning and Biaxial Stretching Processes

Tomoki Tokuda¹, Takuya Hara¹, Atsuya Odake¹, Wataru Kita¹, Midori Takasaki¹, Haruki Kobayashi¹, Katsufumi Tanaka¹, Wataru Takarada², Takeshi Kikutani²

¹Kyoto Institute of Technology, Japan; ²Tokyo Institute of Technology, Japan

mitakas@kit.ac.jp

INTRODUCTION

Poly(ethylene terephthalate) (PET) has been widely used for fibers, films, bottles etc. In recent years, many studies on nanofiber webs have been carried out with the intension of applying the webs for filters and batteries. In this study, to enhance the thinning of PET fibers in the web, PET fiber webs were prepared through the laser-heated electrospinning (LES) and subsequent biaxial stretching processes. In addition, the structure and mechanical properties of the obtained webs were evaluated.

EXPERIMENTAL

PET fibers (fiber diameter, $151 \pm 8 \mu\text{m}$) prepared by the melt spinning process were used for the LES process. Simultaneous equi-biaxial and planar stretching of the PET fiber webs obtained by the LES was performed up to the stretch ratios of 1×1 to 4×4 and 1×1 to 1×4 , respectively. Initial size of the web was $30 \times 30 \text{ mm}$, stretching speed of 10 mm/min , and stretching temperature of $90 \text{ }^\circ\text{C}$ were adopted. After the stretching, subsequent heat treatment was carried out at $116 \text{ }^\circ\text{C}$ for 5 minutes. Characterization of web samples was performed by scanning electron microscopy (SEM), wide angle X-ray diffraction (WAXD) measurement, tensile test and atomic force microscope (AFM) measurement.

RESULTS AND DISCUSSION

PET nanofiber webs with average fiber diameter of $0.85 \mu\text{m}$ and a coefficient of variation of fiber diameter of 18% were successfully prepared through the LES and subsequent simultaneous equi-biaxial stretching (stretch ratio: 4×4) processes. The WAXD patterns (through view) of PET films and webs are compared in Fig.1.

The machine direction (MD), i.e. stretch direction in the planar stretching and the transverse direction (TD) are displayed in the figure. Appearance of only an amorphous halo was confirmed for the un-stretched film and web samples. For the samples of planer stretching (stretch ratio: 1×4), concentration of reflection intensities along the TD direction, which corresponds to the crystalline orientation along the MD, was confirmed both for the film and web samples. The azimuthal intensity concentration was clearer for the film sample. In the case of simultaneous equi-biaxial stretching (stretch ratio: 4×4), crystalline reflections of isotropic ring appeared for both samples. Comparing the reflection intensities of different crystal planes, it was confirmed that the film samples exhibited preferential orientation of (100) plane, which includes benzene ring in the main chain of PET, along the film surface, while for the web samples, preferential orientation of only molecular chain along the web surface was confirmed.

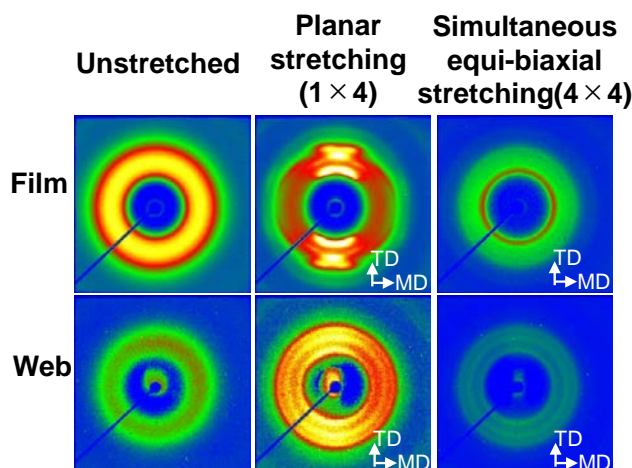


Fig. 1. WAXD patterns of PET film and web samples.

Preparation of Amorphous Super-engineering Plastic Fibers by Melt-spinning

Moo Sung Kim, Hyunjung Choi, Damiro Ahn, Sang Young Yeo

Technical Textile R&D Group, Korea Institute of Industrial Technology (KITECH)

miracle@kitech.re.kr; prairie11@kitech.re.kr

Super Engineering Plastics (SEPs) are at the highest end of the spectrum, generally with very high strength and thermal resistance. They are used in high temperature, high stress, in harsh environments, and low to medium volume production. We investigated three types of SEPs as the base materials: polysulfone (PSU), polyethersulfone (PES), and polyetherimide (PEI). PEI, PES and PSU, the amorphous high-temperature plastics generally offer very similar characteristic profiles; they differ predominantly in terms of the thermal values service temperature and glass transition temperature.

In this study, SEPs fibers were prepared by melt-spinning with high-speed winding process. Optimum spinning temperatures of PSU, PES, and PEI were 360 to 380°C. Winding speed was controlled by rotation winding machine from 1,000 to 2,000 mpm. We investigated with properties of the spun SEPs fiber through SEM, XRD, and UTM. Fig.2 shows the SEM image, of PSU, PES, and PEI fibers. The PSU fibers provides average 3.3 denier, but the PES and PEI fibers indicates the 4.6 and 5.7 denier. Fig.3 indicates the tensile properties of PSU, PES, and PEI fibers. In this experiment, there are one of the tendency to decrease tensile properties with winding speed. As the result of tensile properties test, PSU was 2.53 g/den, PES was 2.69 g/den and PEI was 3.78 g/den.



Fig. 1. Amorphous super engineering plastics fibers

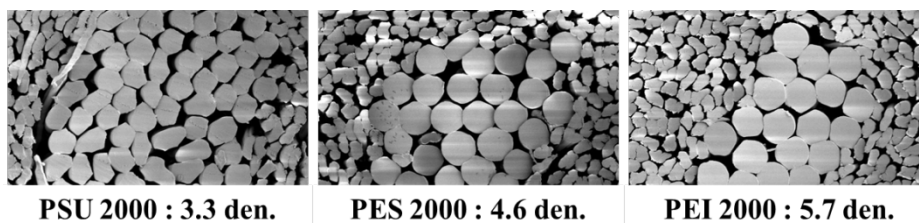


Fig. 2. The SEM images of SEPs fibers

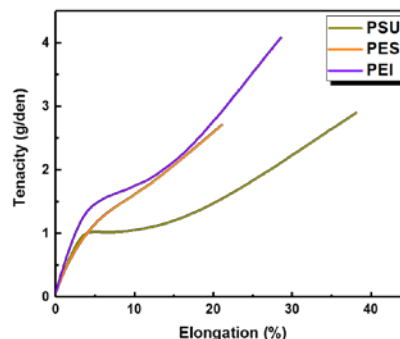


Fig. 3. Tensile properties

PET Fiber Formation Through Continuous Cold Drawing Process with Infusion of Organic Solvent

Dongwoo Go¹, Wataru Takarada¹, Arun Aneja², Takeshi Kikutani¹

¹Department of Materials Science and Engineering, School of Materials and Chemical Technology, Tokyo Institute of Technology, Tokyo, Japan

²Department of Engineering, East Carolina University, Greenville, NC, USA

kikutani.t.aa@m.titech.ac.jp; go.d.aa@m.titech.ac.jp

INTRODUCTION

Our earlier research focused on the studies for drawing of amorphous poly(ethylene terephthalate) (PET) fibers immersed in ethanol at room temperature. The formation of multiple-necking, infusion of ethanol into filament along with dye, and the occurrence of solvent-induced crystallization were observed. It should be noted that neither diffusion of ethanol into PET fiber nor solvent induced crystallization occurs if PET fibers are simply immersed in ethanol. Based on these previous results obtained through batch-type drawing, and with the aim of exploring the possibility of applying this unique behavior to industrial process, continuous drawing of PET fibers in ethanol was performed. The fiber formation behavior in ethanol as well as the structure and properties of drawn fibers were investigated in detail.

EXPERIMENTAL

As spun PET filaments were prepared at the take-up velocity of 400 m/min. Continuous drawing process was carried out in ethanol using a set of rollers operating at different rotation speeds. In some experiments, a drawing pin was placed in ethanol channel to improve process stability as shown schematically in figure 1. A tension meter and a high-speed camera were applied for continuous monitoring of the tension and multiple-necking behavior. Tensile tests, and WAXD and DSC measurements were performed to estimate the molecular structure, mechanical properties and content of ethanol in the drawn PET fibers.

RESULTS AND DISCUSSION

The occurrence of multiple-necking was observed in the continuous drawing process. Higher the drawing speed, higher number of necks were initiated on the filament as shown in figure 2. The number of necks decreased as the filament moved downstream with the vanishing of undrawn part through the merging of a pair of necks at its both ends. Distributional homogeneity of the initiation of the necks and the tension stability were improved by the installation of a drawing pin. From the endothermic peak in the DSC curve caused by the vaporization of ethanol, the presence of ethanol in the filaments was confirmed, and the ethanol-induced crystallization was also confirmed from the crystalline reflections in the WAXD images. At the same draw ratio, the elongation at break of PET fibers drawn with ethanol was found to be higher than that of drawn fibers without using ethanol, indicating the possibility of achieving higher tensile strength through additional drawing.

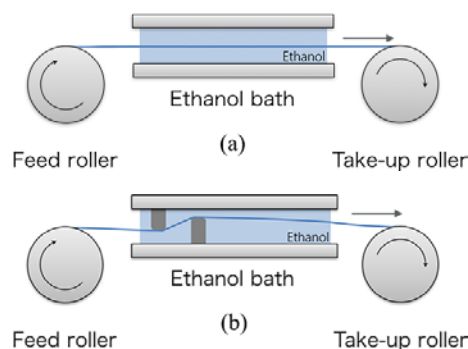


Figure 1. Schematics of (a) continuous cold drawing system in ethanol channel and (b) drawing system equipped with pin.

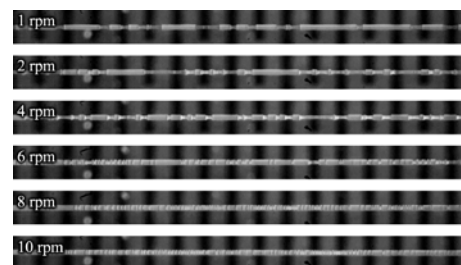


Figure 2. Photographs of PET fiber drawing line in ethanol of various feed roller rotation speeds. Draw ratio was maintained at 4x.

Computational Fluid Dynamics Analysis on Capillary Flow Through Cross-section Profiled Fibers

Eunjin Park¹, Giwon La², Jongkwang Lee², Eunae Kim¹

¹Functional textile system research lab, Department of clothing & textiles, Yonsei University, Korea

²Micro systems lab, Department of mechanical engineering, Hanbat National University, Korea

blessedjina@yonsei.ac.kr; eakim@yonsei.ac.kr; rldnjsaos101@gmail.com; jongkwang@hanbat.ac.kr

INTRODUCTION

The fabrics that make up the clothes should allow perspiration to pass through them to avoid discomfort. The perspiration/liquid water transports by means of the capillary action which is determined by pore structure and distributions in the yarns and fabrics. To maximize the liquid water transport, various kinds of profiled fibers have been used. Attempts to relate the fiber cross section and the geometrical structure of the fabrics with liquid water transport have been made experimentally or theoretically by modeling the structure. To offset the limitations of the objective experiments or theoretical modeling, a computational fluid dynamics (CFD) was used to predict the wicking height, capillary flow rate and the optimum sizes of pores between fibers.

EXPERIMENTAL

The capillary pressure according to the capillary radius and the fiber arrangement were examined by using computational fluid dynamics analysis. ANSYS 15 (ANSYS, computational fluid dynamics program, Frontis, Version 4.5) was used to start the graphic process of the capillary flow and calculate the flow in the pores which were formed by the capillary radius of profiled fibers.

A structured array of four profiled fibers in 3-D geometries was employed with capillary radius of 10, 20, 40, 60 and 80 μm . In the program, after the lines for each cylinder which has a different capillary radius was drawn, air and water were formed by filling the space between pores and fibers with the mesh. The mesh has been generated with GAMBIT program. Almost 12,000 cells were used in the numerical computation to calculate the capillary flow in the pore generated by profiled fibers. The flow of fluid in the domain of this study is assumed to be column in steady and isothermal state. The surface tension coefficient was assumed to 0.07275 N/m and the contact angle between liquid and wall of pore column was assumed 75°. The pressure outlet condition for the boundary condition was applied on the top of yarn. The time step size and the number of time step were selected as 0.05 μs and 2000 iterations, respectively.

RESULTS AND DISCUSSION

From the results of the numerical solution of CFD, the capillary flow pattern and the resistance in the pores in accordance with their size and arrangements were obtained. As the capillary radius decreases from 80 to 10 μm , the height increased up to 20 μm . At 10 μm the height was rather decreased which is probably due to the influence of cohesion between water molecules and adhesion between liquid water. Depending on the complexity of the pore structures, different capillary actions were observed. When fibers are packed in the yarn, the distribution and size of the pores between fibers changes, which leads to change of the moving paths of liquids. When the fibers are arranged to form large perimeter pores, capillary height showed value at the same porosity. Also, depending on the arrangements of the fibers, the flow rate was changed and increased up to 3 times after 100 micro seconds at the same porosity as the shape of the capillary formed by the fibers were different. The importance of perimeter is well known, but it was interesting to find the effect of pore size and path of the capillary simultaneously.

CONCLUSION

The capillary action is primarily dependent on the capillary radius but the arrangements of the fibers are also very important as the flow rate is determined by this. This suggests the importance of the yarn twists. The pores formed by fibers must be above a certain size. Further study will give information for the engineering of profiled fibers and yarns with predetermined liquid water transfer properties.

ACKNOWLEDGMENT

This work was supported by the Brain Korea 21 Plus Project of Dept. of Clothing and Textiles (No. 31Z20151113283), Yonsei University, in 2017.

Preparation and Characterization of PSA/Cellulose Alloy Fibers with N-methylmorpholine-N-oxide Monohydrate as Solvent

Tong Cheng, Kaijian Wu, Yumei Zhang, Huaping Wang

State Key Laboratory for Modification of Chemical Fibers and Polymer Materials,
College of Materials Science and Engineering, Donghua University, Shanghai, P. R. China

chentong94@163.com

Aromatic polysulfonamide (PSA) fiber is a kind of inherent flame-retardant fibers with excellent thermal stability and high limit oxygen index (LOI>31%). However, the poor hygroscopicity of PSA fiber limit its application in the protective textile field. Cellulose fiber, as its unique advantages including renewability and hygroscopicity, can be used to improve the wearing comfort of PSA fibers. In this work, N-methylmorpholine-N-oxide monohydrate (NMMO·H₂O) as a green solvent was used to dissolve PSA and cellulose, and the PSA/cellulose alloy fibers were prepared by dry-jet wet spinning.

The blended solution properties were firstly measured, the microscope images showed that PSA and cellulose dissolved completely in NMMO·H₂O. The rheology of the solutions indicated a strong interaction between PSA and cellulose. The phase morphology and properties of PSA/cellulose alloy fibers were discussed as below. From the laser scanning confocal microscope (LSCM) images, a “sheath-core” morphology was easily observed in the alloy fibers as PSA distributed more in the sheath domain of the alloy fibers due to the viscosity of PSA in blend solution is much lower than cellulose. This result contributed more to the flame retardant properties of the fibers. When the PSA content was 70 wt%, the LOI was up to 26.6% and the self-extinguishing time was less than 5 s. The SEM images showed a rough morphology, and only cellulose II crystalline structure could be observed from XRD patterns, the crystallinity was promoted with increasing of cellulose. Therefore, the mechanical properties of the alloy fibers were improved as the tenacity of 2.17 cN/dtex and the E-modulus of 74.5 cN/dtex. The moisture regain was up to 8.0 % when the cellulose content reached 30 wt%, which showed better hygroscopicity. The dyeability of the alloy fibers was also strengthened as the cellulose can be easily dyed using reactive dye, which was of great significance in the dyeing of PSA fibers. Interestingly, the alloy fibers appeared many well-distributed fibrils with diameter of 100~150nm under ultrasonic treatment, which can be a feasible way to prepare superfine fibers.

This work provided a green method to prepare PSA/cellulose alloy fibers with good flame retardant properties and better wettability.

ACKNOWLEDGMENT

This work was financially supported by the National Natural Science Foundation of China (51773032).

Polyurethane Nanofibrous Membranes Prepared via Suspension Electrospinning

Youjung Song, Seungsin Lee

Department of Clothing and Textiles, Yonsei University, Seoul, Korea

SL158@yonsei.ac.kr; yjssong@yonsei.ac.kr

INTRODUCTION

Waterborne polyurethane (WBPU) is a binary colloid system, in which (PU) particles are dispersed in an aqueous medium. WBPU is nonflammable and environmentally friendly compared with solventborne PU. Suspension electrospinning is a simple method of producing water-insoluble polymer fibers directly from aqueous dispersions. Using this method, pure PU fibers can be prepared from WBPU using a small amount of water-soluble polymer acting as a template polymer and its subsequent extraction by water. In this study, we fabricated PU nanofibrous membranes using WBPU through suspension electrospinning and assessed the effect of membrane thickness on air/moisture vapor transport and mechanical properties of PU nanofibrous membranes.

EXPERIMENTAL

WBPU (solid content = 35%) was obtained from Bokwang Chemical Co., Korea. Poly(ethylene oxide) (PEO) ($M_v \approx 600,000$, Sigma Aldrich Co., USA) was used as the template polymer to facilitate the formation of WBPU fibers. Distilled water was used as the solvent.

A 4-wt% PEO precursor solution was prepared and then a PU/PEO dispersion (35:1 w/w) was prepared by mixing the PU dispersion and the PEO aqueous solution. Polymer dispersions were electrospun for different processing durations (1, 3, 6, 9, and 12 h) to fabricate membrane samples having varied thickness. PU/PEO fibrous membranes were then put into distilled water for 24 h at room temperature to remove the template polymer (PEO).

Morphology of the electrospun PU/PEO fibers was characterized before and after water treatment using a field emission scanning electron microscope (FE-SEM). Mechanical properties of pure PU membranes after removing the template polymer were measured according to ASTM D5035-11 using a universal testing machine (Instron 5543, Instron Co., USA). Air permeability was determined according to ASTM D737-04 using an air permeability tester (FX3300, TEXTTEST, Switzerland). Water vapor transmission rate was measured according to ASTM E96-00.

RESULTS AND DISCUSSION

SEM images demonstrated that the PU/PEO fibers were successfully electrospun. The addition of a template polymer to WBPU dispersions enabled the electrospinning of continuous fibers with an average diameter of 814 nm. After the template polymer was extracted using water treatment, the fibers preserved their shape and pure PU fibrous membranes were obtained. The average diameter of PU fibers was found to be 603 ± 97 nm. By increasing the membrane thickness, the tensile strength increased. In addition, the tensile strength and strain of PU nanofibrous membranes fabricated by suspension electrospinning were comparable to those of the membranes prepared from solventborne PU. Besides, air permeability and water vapor transmission rate of the PU nanofibrous membranes decreased as the membrane thickness increased.

CONCLUSIONS

PU nanofibrous membranes were successfully fabricated by electrospinning WBPU dispersions using PEO as a template polymer followed by its water extraction. PU nanofibrous membranes exhibited mechanical properties comparable to those of membranes electrospun from conventional solventborne PU systems. Air/moisture vapor transport decreased with increasing membrane thickness. PU membranes fabricated by clean and safe electrospinning without the use of organic solvents may have high potential for various biomedical applications, where the toxicity of organic solvents is of great concern.

Preparation of Islands (High Molecular Weight PET) in the Sea (PP)-type Bicomponent Fibers by Using High-speed Melt Spinning

Hyung Joo An^{1,2}, Young Chan Choi¹, In-Woo Nam¹, Ho-dong Kim², Wan-Gyu Hahm¹

¹Technical Textile & Materials R&D Group, Korea Institute of Industrial Technology (KITECH), Ansan, Korea

²Department of Fiber System Engineering, Dankook University, Yongin, Korea

wghahm@kitech.re.kr; hodong@dankook.ac.kr

Islands in the Sea type (SI) bicomponent melt spinning is one of the most widely used processes to produce high functional and special fibers. It has been reported that the structure development in the individual components of bicomponent fiber in high-speed melt spinning show different behavior with those of single component fiber.

In this study, high-speed melt spinning for PP/high molecular weight PET (HMW-PET) SI fiber was conducted. HMW-PET(IV 1.18) and PP(MFR 25) were used for islands and sea components, respectively. The weight ratio of PP/PET components were 0.5:0.5, and the number of islands in single fiber was 74. The PP and PET components were melted at 230 °C and 290 °C and extruded at the spinning temperature of 290 °C. The hole diameter of nozzle are 0.5 mm and throughput rate was 2g/min per hole. To evaluate the structural development of PP/PET SI fibers, prepared as-spun fibers were characterized by DSC, SEM, tensile test, and Boil-off shrinkage, compared with PET and PP single-component fibers. PP/PET SI fibers could be obtained up to the spinning speed of 4km/min, and SEM images for cross section of the obtained SI fiber confirmed that islands component of HMW-PET were formed evenly in the sea component, and diameter of HMW-PET around 2 μ m at 4km/min. The PP/PET SI fiber could be obtained at higher spinning velocity than single-component fibers. These results indicate that melt structure of PET can be controlled by bicomponent spinning process.

The Impact of Pre-orientation on the Crystallization of Poly(ethylene terephthalate) Fiber During Uniaxial Tension

Jiaxiong Zou, Kang Chen, Hong ji, Yumei Zhang, Huaping Wang

State Key Laboratory for Modification of Chemical Fibers and Polymer Materials,
College of Materials Science and Engineering, Donghua University, Shanghai, China

1749568085@qq.com

The mechanical properties of polyethylene terephthalate (PET) fibers are primarily a function of crystalline texture, crystallinity and its molecular orientation which all strongly affected by the spinning, drawing and thermal setting process. Understanding the crystal and orientation structure formed during the deformation process is essential to make quantitative predictions about the properties of the final fiber such as mechanical property and thermal stability. Considerable work has been undertaken to study the effects of strain or stress on the induced crystallization of PET fiber during flow and heat-stretching process. Most of them emphasize the effect of draw rate, draw ratio and temperature on the strain-induced crystallization during the deformation process. In the study presented here, we focused on the effect of pre-orientation on the crystallization of PET fibers by using wide-angle X-ray diffraction (WAXD), Polarizing microscope and FTIR.

The glassy state PET fiber was prepared at low spinning speed and then stretched near the glass temperature of the PET(70°C) with different pre-draw ratio. The pre-oriented PET fibers at glassy state with various birefringence (Δn) were treated by uniaxial tensile at 116 °C with low tensile stress ($\leq 3\text{cN}$) as the strain-induced crystallization could be ignored. The tensile rate was controlled to change the crystallization time and the fibers with different crystallinity were obtained.

From the results of WAXD and FTIR of the PET fibers, there is a remarkable growth of fibers' crystallization rate with the increase of the pre-orientation. The most interesting result is the aligning of the crystal plane. When the pre-orientation is low ($\Delta n \leq 0.0690$), the diffraction of (100) appears on the meridian line, which means the normal direction of the (100) is perpendicular to the drawing direction. In other words, the macromolecular chain of PET is aligned perpendicular to the drawing axis. When the birefringence $\Delta n \geq 0.1475$, the diffraction of (100) appears on the equator line and the macromolecular chain of PET would be oriented along the axial of fibers. Furthermore, the FTIR spectrum analysis shows that the pre-orientation has a significant effect on the amount of trans conformation in PET fibers.

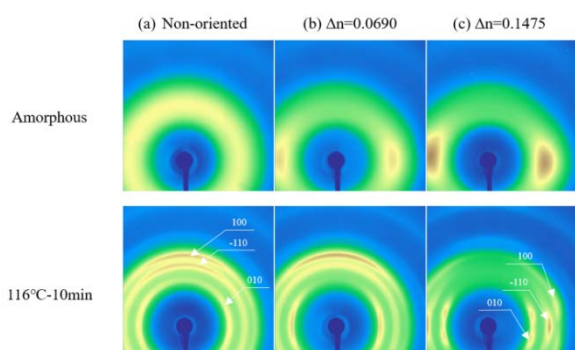


Figure 1. WAXD patterns of PET fibers with different pre-orientation.

ACKNOWLEDGMENT

This work was financially supported by the National Key Research and Development Program of China (2016YFB0303004) and Shanghai Synchrotron Radiation Facility (SSRF).

Innovative Conjugate Spinning Technology NANODESIGN[®]

Masato Masuda, Tomohiko Matsuura, Hirofumi Yamanaka, Yoshitaka Aranishi

Fibers & Textiles Research Laboratories, Toray Industries, Inc., Japan

Masato_Masuda@nts.toray.co.jp

INTRODUCTION

The fiber is processed into a wide variety of products with their useful thin and long shapes. Especially, pursuing the fineness of the fiber is one of the most important subjects both academically and industrially. Nanofibers show nano-size effects not emerging in conventional fibers because of high specific surface area, nanoscale spaces between the fibers etc.

The sea-islands conjugate spinning is one of the nanofiber production methods. Toray established this technology in 1970's for producing filament type ultrafine fibers. Ultrafine fibers derived from the islands are produced by removing the sea component of the sea-islands conjugate fibers (Figure 1).

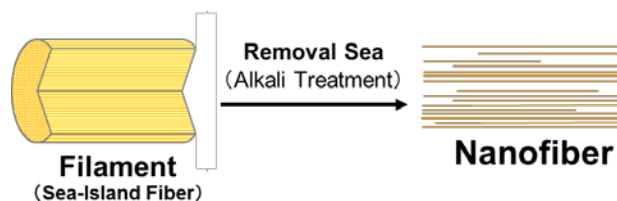


Figure 1. The image of nanofiber production methods from the sea-island conjugate fibers.

TECHNICAL BREAKTHROUGH

In order to pursue the fineness of nanofibers by the sea-islands conjugate spinning, we had to arrange the number of the islands as large as possible. However, this problem was extremely difficult due to spinneret process limitation and control of minute polymer flows divided in a spinneret. We promoted the extension of the research on the sea-islands conjugate spinning and pursued the precise control of minute polymer flows to overcome this technical issue. Finally, we led to the creation of innovative conjugate spinning technology NANODESIGN[®], which can design the cross-section shapes of conjugate fibers on nano-scale.

In the result, we succeeded in producing filament type nanofibers which have 150 nm fiber diameter and homogeneous round cross section. Furthermore, we got to be able to control various cross-section shapes shown in Figure 2, e.g., polygon, Y-shape, side-by-side etc. Therefore, we succeeded in the world's first production of modified cross-section nanofibers.

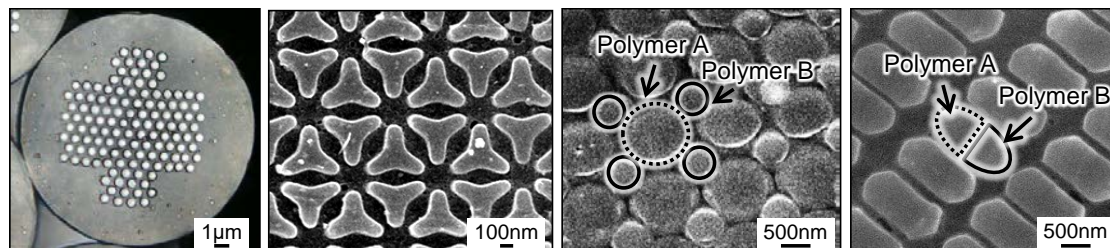


Figure 2. Cross-section shapes of highly precise conjugate fibers via NANODESIGN[®].

CONCLUSIONS

NANODESIGN[®] can design the cross-section shapes of conjugate fibers on a scale of under 1000 nm. This precise control of the polymer flows can be applied to not only the nanofiber production but also the developments of a wide variety of fiber materials. We are advancing the development of highly functional apparel fabrics and high performance industrial products by this cutting-edge technology. In the poster session, we are going to report the characteristics of fiber materials made by NANODESIGN[®].

Dyeing Wool Fibre in a Lower Temperature Condition

Chi-wai Kan

Institute of Textiles and Clothing, The Hong Kong Polytechnic University
Hung Hom, Kowloon, Hong Kong

tccwk@polyu.edu.hk

In this study, reactive dye encapsulated in reverse micelle in octane using non-ionic surfactant was used as an environmental friendly for sustainable textile coloration of wool fabric with primary emphasis on highly reduction of water usage for the solubilization of reactive dyes. The working temperature of reverse micellar dyeing is 88°C, which is 10 degrees lower than in conventional water-dyeing process in terms of energy saving aspect. Dyeability of wool fibre with reactive dye from the reverse micellar solution was improved without incorporation of textile auxillaries such as electrolytes and chemicals such as acetic acid or sodium bicarbonate for pH adjustment (Figure 1). The obtained color strength of reverse micellar dyed wool fibre is better than that in conventional aqueous dyeing (Figure 2).

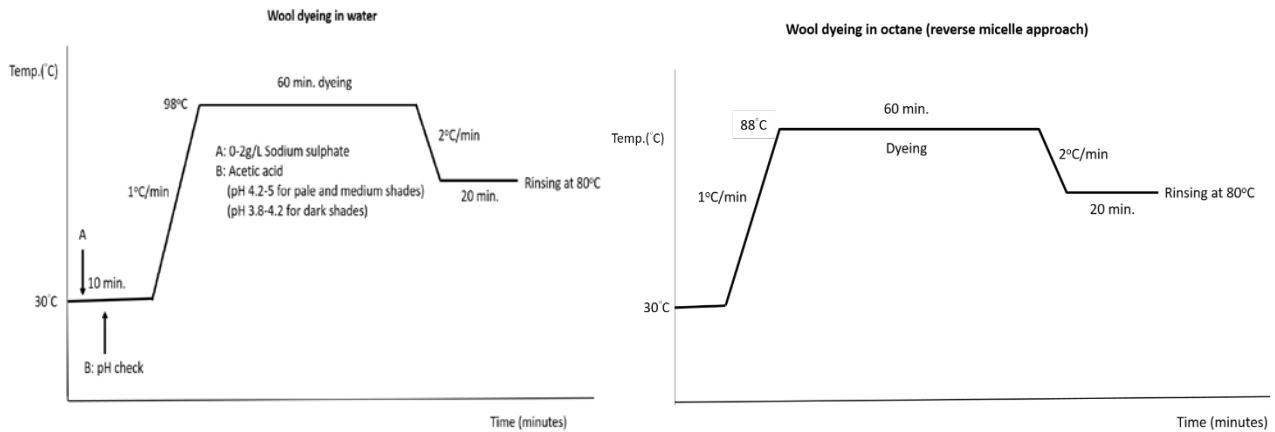


Figure 1. The workflow of wool dyeing using water (left) and wool dyeing using reverse micelle (right).

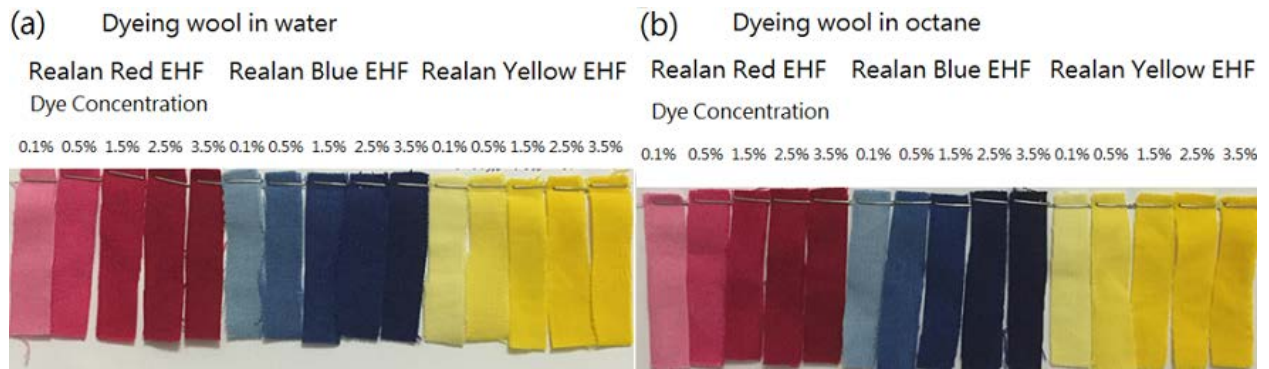


Figure 2. Dyed wool sample in (a) water and (b) reverse micelle.

ACKNOWLEDGMENT

This is a research project funded by Innovation and Technology Fund (ITF) with title “Novel Non-aqueous Wool Fibre Dyeing Process Using Nonionic Surfactant as Reactive Dye Carrier” (ITS/279/16). Author would like to thank the financial support by ITF.

Preparation of Colored Antibacterial Functional Acrylic Fibers by Gel Adsorption Method

Dejun Feng, Kaijian Wu, Jinchao Yu, Yumei Zhang, Huaping Wang

State Key Laboratory for Modification of Chemical Fibers and Polymer Materials,
College of Materials Science and Engineering, Donghua University, Shanghai, China

454728401@qq.com

Nowadays, the colored and antibacterial functional acrylic fibers are widely used in the textile industry, most of the fibers have been successfully developed by the methods of post-treatment and incorporation of dye and antibacterial in the spinning dope. However, these methods have many deficiencies including the high energy consumption and poor laundering durability. Thus, in order to prepare acrylic fibers with high color fastness, excellent antibacterial and laundering durability, the colored and antibacterial functional acrylic fibers were prepared by gel adsorption method after the pre-drawing and washing process. In this stage, the PAN gel fibers showed a loose structure with a large specific surface area, which contributed to the adsorption of cationic dyes and antibacterial agents. In the following heat stretching and heat setting process, the structure of PAN fibers became much denser and the ionic bond formed between the dyes, antibacterial agents and sulphonate group on the PAN molecules leading to a higher laundering durability.

In our present work, the PAN gel fibers were treated at different conditions, such as the concentration of dyes and antibacterial agent, bath ratio, adsorption time and adsorption temperature. The color fastness, antibacterial properties as well as mechanical performance were also evaluated. The optimized technological conditions were screened out. It was found that when the bath ratio is 1:10, dyes and antibacterial agent concentrations were 5wt% and 30wt%, respectively, the acrylic fibers adsorbed the dyes and antibacterial agent for 20 seconds at 50°C, the acrylic fibers showed excellent antibacterial properties and laundering durability, still over 99% bacteria reduction remained after 10 laundering times. The color fastness to washing of the PAN fiber could also reach 4-5 grade. More importantly, the dyeing and antibacterial treatment have little adverse effect on the mechanical performance of PAN fibers.

In brief, this work provides an effective way to prepare colored antibacterial functional acrylic fibers with high color fastness, excellent antibacterial properties and laundering durability, and meets the basic mechanical properties requirements of the acrylic fibers.

ACKNOWLEDGMENT

This work was financially supported by the Sinopec Shanghai Petrochemical Company Limited.

A Consciousness Survey on Kurashiki Canvas and Design Proposal

Manami Fukumura^{1,2}, Ikuko Turo¹, Kunio Kimura²

¹Kurashiki City College; ²Okayama University

fukumura@kurashiki-cu.ac.jp; polykim@okayama-u.ac.jp

While, Kurashiki canvas followed a course of decline because of the import of low price fabrics from overseas, it had been meeting the requirements of consumers by the increase in the type of products and the improvement of its functionality. The consciousness survey on Kurashiki canvas of the consumers and the producers was conducted to analyze the recognition and images of Kurashiki canvas and to find the answer to what kind of canvas products was required. In this study, we consider the characteristic and attraction of Kurashiki canvas, and propose the new design acceptable to wider consumers leading to the sales promotion. The contents of a questionnaire are about the awareness of the storage charge sailcloth, evaluation, an image, the color and the pattern.

The survey lead to the following six results:

1. Although the recognition ratio of Kurashiki canvas is averagely high, that of the students of teens and twenties is comparatively low.
2. The ratio of the people who want to purchase is totally high, but those of the students and the office workers are lower than that of the customers of Kurashiki canvas.
3. The people who did not see the Kurashiki canvas tends not to purchase Kurashiki canvas goods in future even though they recognize their high quality.
4. High quality and strength of Kurashiki canvas are well perceived.
5. Image of Kurashiki canvas is simple, casual and natural.
6. Favorable color is red, white and blue, respectively.



Fig. 1. School uniform and rucksack of Kurashiki canvas.

On the basis of this evaluation, the rucksack was designed and produced as shown in Fig. 1. The school uniforms are thriving as a local apparel industry. These analysis results concluded that Kurashiki canvas was a valuable traditional material and the satisfaction level of people who actually used Kurashiki canvas was quite high.

ACKNOWLEDGMENT

The authors would like to express special thanks to Mr. A. Takeyari of Baiston Co., Ltd. and Mr. K. Honbo of Marushin Industry Co., Ltd. for their support for the survey and the planning department of Kojima Co., Ltd., Ms. N. Kajitani of Kurashiki City College for their support for production of the work.

Fabrication of High-resolution Conductive Patterns on the Thermal Imprinted Polyetherimide Film by Capillary Flow of Conductive Ink

Takashi Kurose, Keita Shishido, Akihiko Nemoto, Hiroshi Ito

Graduate School of Organic Material Science, Yamagata University, Japan

takashi.kurose@yz.yamagata-u.ac.jp; ihiroshi@yz.yamagata-u.ac.jp

A flexible printed circuits (FPC) with fine pitch (e.g. line & space:10 μ m &10 μ m) to connect to a high resolution display such as smart phones will be highly demanded near future. High resolution conductive patterns were fabricated on thermal imprinted Polyetherimide (PEI) film by applying capillary flow of conductive silver nanoparticles ink. Line & space structures having pitch distance 20 μ m, depth 10 μ m, and length 9mm were imprinted on a PEI film (film thickness: 115 μ m, SUPERIOTM UT, Mitsubishi chemical holding group) at temperature 285 $^{\circ}$ C by the surface structured metal mold. The selected imprinting temperature is higher than the glass transition temperature ($T_g = 225^{\circ}$ C) of the PEI film.

Figure 1 shows the surface structure after thermal imprinting observed by 3D leaser microscope (Lext OLS4000, Olympus). It was confirmed that line & space structures were successfully imprinted and the replication ratio was almost 100%. Silver nanoparticle ink (particle concentration: 55wt%, average particle size: 5nm, NPS-JL, Harima chemical group) was dropped on the edge of the line & space structures. The ink flew along the grooves and 9mm grooves were covered by silver ink, and conductive patterns with silver particles were formed. The film was heated up at 180 $^{\circ}$ C to sinter silver particles and to increase adhesion between silver patterns and the PEI film. Figure 2 shows a cross sectional image of the patterned PEI films after sintering, which was observed by SEM (JSM-6510, JOEL). It was clearly observed that only grooves area were filled by silver and there was no residual silver layer on the top surface of PEI film. Four electrodes by applying conductive paste across all the grooves were created and the electrical conduction of these silver patterns was confirmed by four terminal method. The average electrical resistivity of these silver patterns will be estimated and reported in detail in the presentation.

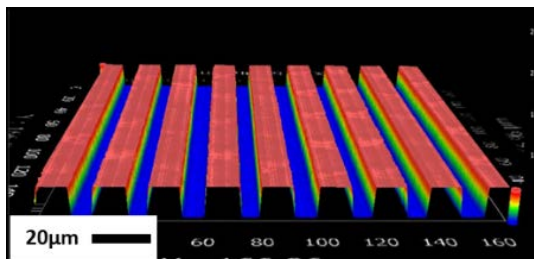


Figure 1. Surface structural image after the thermal imprinting at 285 $^{\circ}$ C observed by 3D leaser microscope.

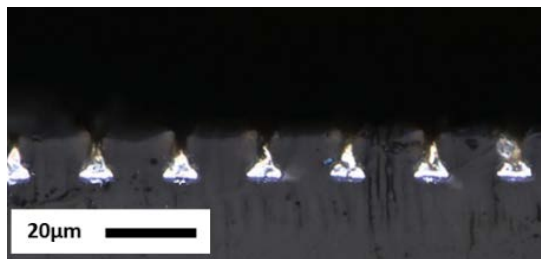


Figure 2. SEM cross sectional image of the conductive patterned PEI films after sintering.

Fabrication of Piezoelectric PLLA/BaTiO₃ Filaments for Smart Sensors and Their Applications

Do-Kun Kim, Hyun Ju Oh, Bo-Seok Song, Byeong Jin Yeang

Technical Textile R&D Group, Korea Institute of Industrial Technology (KITECH), Ansan, Republic of Korea

dogun419@kitech.re.kr

Poly-L-lactic acid (PLLA) has been an attention as a substitute for conventional piezoelectric materials. It exhibits a specific piezoelectric behavior having a net dipole moment when the C=O dipole groups along the main chain are oriented. However, PLLA has a weaker piezoelectric property than commercial PVDF, many studies have been made to improve the piezoelectric property by transforming from the α -form to β -form crystal with high drawing ratios at high temperatures. In this study, the PLLA filament fiber reinforced with barium titanate (BaTiO₃) was fabricated by high speed melt-spinning. The effect of an amount of reinforcement contents and the drawing ratio on the piezoelectric property of PLLA filament fiber was investigated. The change of β -phase crystal formation on PLLA filament fibers at each conditions was characterized by SAXS, DSC, D_{33} meter. From those results, it shows that the piezoelectric performance of PLLA filaments could be enhanced by the drawing process and the reinforcement in high speed melt-spinning process.

Electrical Percolation Behavior of Carbon Black/Polymer Composites

Hyun-Jung Choi, Moo Sung Kim, Damiro Ahn, Sang Young Yeo

Technical Textile R&D Group, Korea Institute of Industrial Technology (KITECH), Korea

miracle@kitech.re.kr; hjchoi@kitech.re.kr

The demand for smart devices has grown exponentially in recent years. Flexibility and elasticity of electrical devices need to meet the required standards of the next-generation wearable electronics. Carbon is used the most as a plastic material conductive additive. In this study, carbon black (CB)/polymer composites were prepared by melt-spinning method using three kinds of polymer resins (Polypropylene; PP, Polyethylene terephthalate; PET and Polyamide; Nylon) as a matrix and CB as a conductive additive. Through an analysis of the contact angle, the polarity of the polymer matrix was confirmed, and the electric conductivity of the CB/polymer composite based on the polarity was checked. As a result, it was confirmed that the CB/PET composite showed a low percolation threshold value of 0.58 wt% with the best electrical conductivity. It was confirmed that the volume electrical conductivity of the CB/PET composite well matched with the percolation scaling law ($\sigma = \sigma_0(v - v_c)^t$). Through SEM analysis, the dispersion and morphology of the carbon black inside the polymer resin were confirmed. The CB/PET composites showed the well dispersion of CB in PET matrix. The lowest percolation threshold of CB/PET composite was caused by the formation of a contact surface due to the surface area increase due to the even dispersion. By using knitted CB/PET composite fabric, it can be used to antistatic fibers.

Influence of Electrolyte on the Self-organization of Liquid Silk

Yutaka Kawahara, Ayumi Sato

Division of Environmental Engineering Science, Gunma University, Kiryu, Japan
kawahara@gunma-u.ac.jp

In the cocooning of domesticated silkworms, it has been reported that Ca^{++} , K^+ play an important role in the transition from gel to sol for the liquid silk to reduce its viscosity and to enhance the spinnability. In this presentation, the influence of the electrolyte on the self-organization of liquid silk was investigated.

We collected gel-like liquid silk samples from the middle division of the middle silk gland. The samples were then kept in distilled water. Fibroin molecules gradually dissolved into water during 2 days in a refrigerator. The concentration prepared was ca. 3.0 wt%. The electrolyte aqueous solution were dropped into the liquid silk solution in flow state controlled by a stirrer at room temperature. The coagulums obtained were observed with a polarization microscope.

Fig. 1 shows a polarization microscope image for the coagulum obtained by dropping the liquid silk solution to the mixture of KCl and CaCl_2 solution. The fine fibrous texture could be seen in the isotropic films.

In the case of KCl, however, both films and fibers were obtained. The polarization microscope image revealed that the fibrous materials with the molecular orientation along the fiber axis were randomly embedded in the isotropic films (see Fig. 2).

It seems difficult to dissociate the chelate bonding by Ca^{++} in liquid silk only by adding K^+ . K^+ tends to coagulate fibroin and/or sericin instead of the dissociation of the chelate bonding by Ca^{++} .

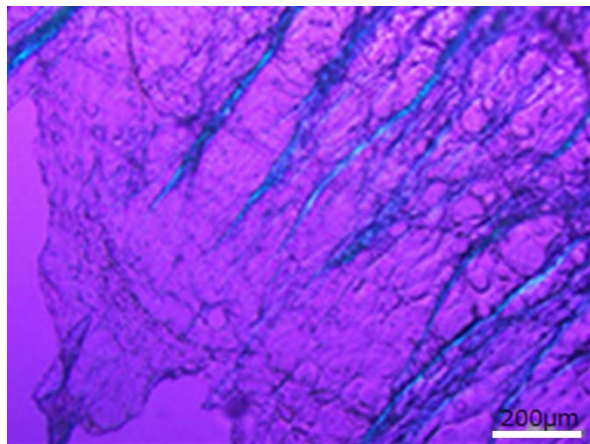


Fig. 1. Polarization microscope image for the coagulum obtained by dropping the liquid silk solution into the mixture of KCl and CaCl_2 solution. The mixture of KCl and CaCl_2 (mass ration=1:2) solution of 10% was prepared and its pH was controlled at around 5.2 by adding 0.05 M acetic acid solution. Then the solution was diluted to 10 times. The diluted solution was stirred at 100 rpm, and 1 mL of the liquid silk solution of 0.3 % was dropped three times taking the interval of 10 min.

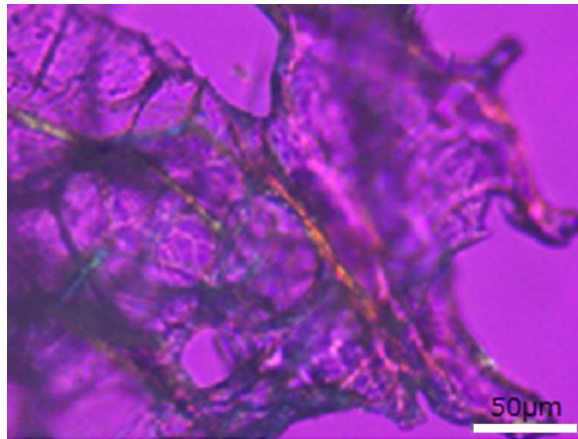


Fig. 2. Polarization microscope image for the coagulum obtained by adding KCl to the liquid silk solution. The liquid silk solution of ca. 3% was stirred at 100 rpm, and the KCl solution of 10 % was dropped into the liquid silk solution to the amount of 0.9 ml so that the mass of KCl against the liquid silk was controlled to be 20 %owf.

Fabrication and Characterization of Anti-yellowing Silk with TiO₂ Coating on Zirconium Phosphate Undercoat

Meguru Yokoyama, Hisanao Usami

Department of Chemistry and Materials, Faculty of Textile Science and Technology, Shinshu University, Japan

hisayan@shinshu-u.ac.jp

Anti-yellowing silk fibers with smooth nano-coating of TiO₂ on γ -zirconium phosphate (ZrP) undercoat was fabricated using wet process under mild condition. Surface morphology of the modified silk with slightly wrinkled thin layer was observed by a SEM. Presence of Ti and Zr was confirmed by an EDX analysis. Diffuse reflectance absorption spectra of the silk taffeta coated with the TiO₂-ZrP layer showed significant absorption in 300 - 400 nm wavelength region, which is contrasted with small absorption for pristine silk taffeta without the coating. Irradiation with uv-light using 500 W Hg lamp caused a significant yellowing to the pristine silk. However, yellowing of the TiO₂-ZrP coated silk taffeta was suppressed according to the strong uv-absorption of the TiO₂ layer.

Silk has been used as a high-class material for formal dress due to its unique gloss, fine texture and humidity conditioning, etc. However, the silk is sensitive to ultraviolet irradiation to be yellowed and brittle mainly due to disadvantageous oxidation of fibroin proteins. Many studies to overcome the drawbacks have been carried out, such as blocking of OH groups in the peptides or uv-light absorbing dye bound on the surface of silk fibers. However organic dyes showed insufficient absorption and low wash toughness. Inorganic coatings with CeO₂ or TiO₂-clay hybrid were reported as uv-protecting layer for silk. Direct coating of TiO₂ by several hundreds of sol-gel cycle showed good uv-protection effect on tensile strength. However, binding strength and washing toughness of the layer have not been reported.

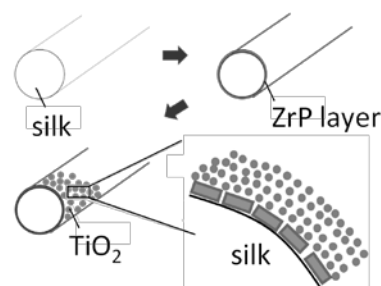


Fig. 1. Layering process of inorganic coating on silk fiber.

In this paper, we developed novel strategy on anti-yellowing of silk fibers using inorganic uv-absorbing material, titanium oxide nano-particles, deposited on γ -zirconium phosphate (ZrP) undercoat layer covered on the original silk fibers.

Silk taffeta was washed with nonionic detergent solution and dried under air, then dipped in aqueous dispersion of ZrP to cover the silk fiber, washed with distilled water and dried in air. The ZrP coated silk taffeta was immersed in a dispersion of TiO₂ nano-particles, which was deposited on the ZrP layer. ZrP serves as binder to the silk surface, according to electrostatic interaction between permanent anionic charges on the ZrP and cationic charges on silk fibers, and also serves as binder of TiO₂ nano-particles due to strong affinity of phosphate group to the TiO₂ particle. Diffuse reflectance absorption spectra of the TiO₂-ZrP modified silk taffeta showed significant absorption band in the uv-region, in contrast to the small absorption of the pristine silk taffeta. Titanium oxide has strong absorption band restricted in the uv-region and has no absorption in the visible region, which shows significant advantage on uv-protection without yellowing.

Uv-toughness was measured by irradiation using 500 W high pressure Hg lamp. Irradiance power of the lamp was 21 mW/cm², which is estimated as 54 times stronger than that in the solar spectrum. After irradiation for 3 h, the absorbance of the pristine silk taffeta at 400 nm increased up to 0.16, in contrast the increase in the TiO₂-ZrP coated silk was suppressed to 0.05 due to the protection layer. The difference in the absorbance was reflected to the yellowing, which was almost negligible in TiO₂-ZrP modified silk compared with the uncoated one. The uv-damage was also estimated by fluorescence spectroscopy.

ACKNOWLEDGMENT

The authors thanks to professor Zenta Kajiura in Shinshu University for supplying the silk taffeta.

Construction of a Cell Adhesive Silk Fibroin Material by Mixing with Peptides

Chikako T. Nakazawa, Ryoichi Takahashi, Momoko Sonoda, Atsushi Asano

National Defense Academy, Japan

chikakot@nda.ac.jp

INTRODUCTION

Silk fibroin is one of the powerful candidate polymers to create new bioabsorbable tissue engineering materials because of the strength, the workability and the fact that it is a protein from an insect, *Bombyx mori*. The most remarkable property is that water-insoluble materials are made by the aqueous solution. It is achieved by the conformational change of the crystalline induced by simple treatments like exposing to ethanol or high humidity. However, fibroin does not have any physiological activity. Therefore, functionalization is necessary to use as biomaterials. In this presentation, we will report a simple functionalization method for fibroin using peptides, which consist of two parts, one is homological with fibroin crystalline regions and the other is cell adhesive sequences.

EXPERIMENTS

Peptides were synthesized by using peptide synthesizer. Fibroin sponges were prepared by freeze-drying from the aqueous solution after dialyzing of the degummed cocoon fiber dissolved in 9M LiBr aq. The peptides and sponges were dissolved in 9M LiBr aq. each, and then, mixed them in various proportions. After dialyzing of the mixture, obtained aqueous solutions were cast to 96 well plates. Human dermal fibroblasts were seeded on the films at 8,000 cells/well, the number of adhered cells was counted after an hour of seeding by using WST-8.

RESULTS AND DISCUSSIONS

Relative cell adhesive activities of fibroin films including 5 or 10 % of peptides, (AGSGAG)₄GTGRGDSAG (shown as RGD) or (AGSGAG)₄GTGAGDSPAG (shown as AGD), were shown in Figure 1 by using the number of adhesive cells on pure fibroin film as a standard. The films including RGD peptides indicated a higher adhesion although AGD peptides were not. It suggests that RGD sequence assuming a cell adhesion activity is successfully workable in the fibroin films. However, the film containing 10 % of RGD peptides indicated lower activity than that of 5 % one. It seems that the increase of hydrophobicity by adding the peptides affects in an adverse way. We will show the additional results using other cell adhesive peptides and will discuss about positive and negative effects of the mixing of peptides with fibroin for the functionalization in the presentation.

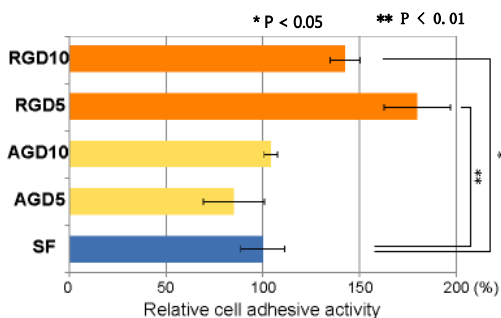


Figure 1. Cell adhesive activity of SF films RGD10 and AGD10 mean 10 % of RGD peptide or ADG peptide, respectively.

Characteristics of the Cellulose Nanofiber Coatings on TEMPO-treated Fabrics

Natsuki Shirai, Nao Kamatsuka, Haruka Kijima, Miki Nakano, Hitomi Hamada

Tokyo Kasei University, Tokyo, Japan

shirai-n@tokyo-kasei.ac.jp

OBJECTIVE

To investigate the effect of cellulose nanofiber (CNF) as a coating agent on fabrics, we studied the characteristics of the CNF coating on chemically surface-treated ramie and cuprammonium rayon fabrics.

METHOD

The chemical treatment with TEMPO (2, 2, 6, 6, -tetramethylpiperidine-1-oxy radical)-mediated oxidation was applied for ramie and cuprammonium rayon fabrics after the pretreatment to remove oil and resin on the fabric surface. The CNFs used in this study (CNF-1, BB-A supplied by Chuetsu Pulp & Paper Co., Ltd., Japan) were derived from bamboo bleached kraft pulp and prepared by the aqueous counter collision method as a suspension of approximately 0.5 wt.%. CNF suspension was coated onto the pretreated fabrics before and after the TEMPO treatment with wire bars using a coater. The coated samples were dried by a hot-air dryer for three minutes. The samples surfaces were observed by a digital microscope. The texture and physical properties of the samples were evaluated by the Kawabata Evaluation System. The water absorbency, the hygroscopic property, and the washing durability were examined according to instructions of the Japanese Industrial Standards test methods (JIS).

RESULTS AND DISCUSSION

The average frictional coefficient (MIU) of the fabric surfaces were slightly decreased after the CNF coating, which means the fabric surfaces became smooth by coating CNFs. The resistance to air permeation were slightly increased by the TEMPO-pretreatment and was extremely increased after the CNF coating. The thermal conductivity was increased after the CNF coating. CNF coatings may fill in pores with poor thermal conductivity in the substrates, which prevent air permeation and increase thermal conductivity. The water absorbency of ramie and cuprammonium rayon fabrics increased by the TEMPO-treatment. This should be attributed to the more hydrophilic nature of the surface of the TEMPO-treated fabrics. But, it slightly decreased after the CNF coating. It is considered that the capillaries to absorb water in the substrates were filled with the coated CNFs. About the washing durability of the CNF coating, the weight decrease of the coated CNFs was small especially after the TEMPO-treatment. The TEMPO-treatment on the substrates may help to improve the durability of the CNF coating.

ACKNOWLEDGMENT

We gratefully appreciate the financial support of JSPS KAKENHI under Grant Number 15K12318.

Production of Cellulose Nanofibers from Oil Palm Residue

Yoko Okahisa¹, Yuma Furukawa², Kiyooki Ishimoto³, Kamthorn Intharapichai²

¹Institute for the Promotion of University Strategy, Kyoto Institute of Technology, Kyoto, Japan; ²Department of Fibre Science Engineering, Kyoto Institute of Technology, Kyoto, Japan; ³Department of Materials and Metallurgical Engineering, Rajamangala University of Technology, Thanyaburi, Thailand

okahisa@kit.ac.jp

INTRODUCTION

The production of cellulose nanofibers and their application in composite materials has gained significant interest due to their high Young's modulus, high strength, and a low coefficient of thermal expansion combine with low weight, biodegradability, and renewability. Cellulose is synthesized by all plant materials. In southeast Asia countries, there is abundant locally produced biomass source. During the last century, large scale oil palm plantation developed in these countries. They have the advantage that they can be harvested throughout the year, however, also have a serious problem about waste handling. After the oil production, Meso carp, Empty Fruit Bunch (FFB), and Palm Kernel Shell (PKS) were produced as waste materials. The production of cellulose nanofibers should be effective utilization of these wastes. They have different cell wall structures and chemical components each other [1], whereas they grown out of same plants. It could be that the performances of cellulose nanofibers differ depend on which part of plants used as raw material. Here, we produced the cellulose nanofibers from three different oil palm residues and compared the properties with the cellulose nanofibers obtained from trunk of oil palm tree.

MATERIAL AND METHODS

Extractive of Meso carp, FFB, PKS and trunk powder (Fig.1) were removed using methanol/toluene solution (v/v=1:2) for 12h in a Soxhlet apparatus. The sample was cyclically treated using an acidified sodium chlorite (NaClO₂) solution at 70 °C for an hour until the product became white to leach lignin. To leach hemicelluloses, the sample was treated in a 5wt.% sodium hydroxide over night at room temperature and then at 80 °C for 2 h, and the process was repeated until α -cellulose content of the sample is over 85 %. Afterwards, the slurry of 1 wt.% of these purified samples were passed once through the grinder (Masuko Corp., Japan) at 1500 rpm with the grinding stones (NKG6-80) pressed closely together. Nanofiber sheets, 90 mm in a diameter, were obtained from each portion of fibrillated slurry at a fiber content of 0.2 wt.% by filtration and dried at 120 °C for 20 min.

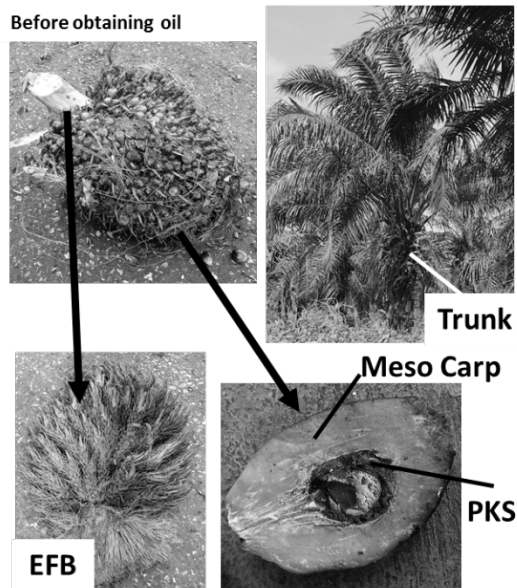


Fig.1. Sample information

RESULTS AND DISCUSSION

The lignin contents of Meso carp was 29.0 %, EFB was 23.2 %, PKS was 36.9 %, and trunk was 22.0 %. FTIR analysis shown that the cellulose purification was succeeded with chemical treatment from all samples. X-ray diffraction patterns of all purified cellulose were the typical Cellulose I pattern. Cellulose nanofiber sheets was also obtained from all samples, however, only from Meso carp was not transparent. The sheets were tested in a tensile test, and stress-strain curves were calculated. There was a clear difference in the stress-strain behavior depending on the samples, and trunk sheet had a highest strength and highest strain. The morphology and properties of cellulose nanofibers from different parts of plants might be different.

ACKNOWLEDGMENT

This work was supported by Center for Fiber and Textile Science, Kyoto Institute of Technology.

Preparation of Porous Cellulose Acetate-Titanium Dioxide Composite Fiber and Its Characterization

Kosuke Iriyama, Hanako Asai, Koji Nakane

University of Fukui, Japan

h_asai@u-fukui.ac.jp; est.1c5@softbank.ne.jp

INTRODUCTION

TiO₂ is known as a photocatalyst under UV irradiation. However, most of the TiO₂ studies are related to the crystalline TiO₂, and there are few studies about amorphous one. On the other hand, Wang et al. recently reported that amorphous TiO₂ can decompose dyes and reduce toxic Cr(VI), simultaneously under visible light.

Here, we have been studying a cellulose acetate (CA) fiber crosslinked by amorphous TiO₂, i.e. CA-TiO₂ fiber. Then in this study, we tried to apply the fiber to remove dye and Cr(VI). We investigated a method to add pores on the fiber surface to enlarge the surface area for more rapid processing speed.

EXPERIMENT

We fabricated the sample fibers as follows: First, we prepared a spinning solution consisting of 15wt% of cellulose acetate and 85wt% of acetone. Then, various amount of NaCl powder was added to the spinning solution. Thus obtained spinning solution was ejected from a syringe to a coagulating liquid, which consisting of 0.8g titanium tetraisopropoxide and 15.2g dehydrated acetone. After washing the sample, it was completely dried. We refer to this sample as CA-TiO₂S.

RESULTS

Fig.1 shows the SEM image of the obtained sample. As shown in this figure, many holes were seen on the fiber surface. These pores were prepared by removing NaCl powder from CA-TiO₂S fiber in the preparation process. We immersed the fiber in a test solution, which contained methylene blue (MB) and Cr(VI). After sufficient adsorption, we irradiated visible light to the system, and evaluated the MB decomposition ability of the fiber. Fig.2 shows the result of decomposition of MB as a function of the immersing time. As shown in the figure, the CA-TiO₂S fiber could decompose MB more rapidly than the case of CA-TiO₂ fiber, which did not have any pores on the fiber surface. We will discuss more detail including the result of Cr(VI) at the presentation.

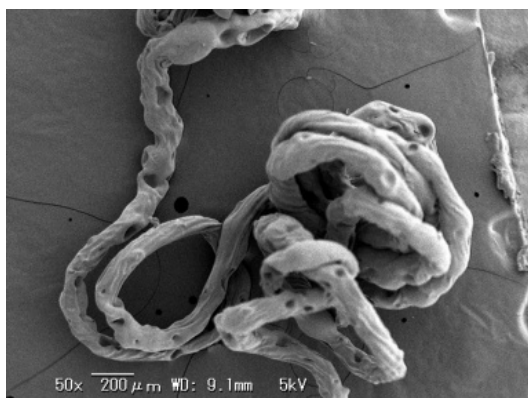


Fig.1. SEM image of CA-TiO₂S fiber.

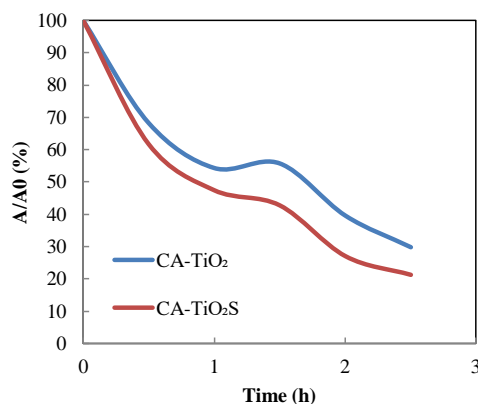


Fig. 2. Variation of absorbance for MB as a function of time.

Design and Characterization of Micro- and Nano-hybrid Mats with High-filtration Efficiency

Lingli Deng¹, Ruitian Zhu², Peng Zhang², Zhiming Qiu¹, Yurong Yan¹

¹School of Materials Science and Engineering, South China University of Technology, Guangzhou, China;

²Guangzhou Inspection Testing and Certification Group Co., Ltd., Guangzhou, China; ³Guangzhou Fibre Product Testing and Research Institute, Guangzhou, China

yryan@scut.edu.cn; railteen@163.com; dll93521@163.com

Nanofiber shows an advantage in high-efficiency air filtrator because it features by a higher specific surface area and a thinner fiber diameter comparing with micro- scale fibers, but a sacrifice is the noticeable increase on the filtration pressure. Nanofiber cannot be used directly without supporting materials because of its low mechanical properties, while this provide the choice to design a special multi-scaled structures in filtration materials with high filtration efficiency and low filtration pressure. Meltblown and needle-punched nonwovens were always considered, but little research on the texture and shape of supporting fibers themselves was reported.

In this study, a hybrid structure combined of micro- and nano- scale fibers is an ideal material to meet these requirements. Hybrid recycled polyester fiber mats with special 3D structure were prepared by electrospinning PLA porous fibers onto carded PET fiber mats. Systematic study on electrospinning parameters of the nanofiber mat as well as the fineness, cross-section and crimp of the PET microfibers were fulfilled. An optimize result with a filtration efficiency of 99.99% and a pressure drop of 177.8 Pa was achieved in a micro- and nano-hybrid filtration material. Results showed that a fluffy support matrix contributed the low pressure of filtration materials.

Reactive Fibers for Air Filtration in Wastewater Treatment Plants

Lukasz Debicki¹, Inga Noll¹, Thomas Gries¹, Andreas Obermayer², Frank Magdeburg²

¹Institut für Textiltechnik der RWTH Aachen University, Aachen, Germany

²UNITECHNICS KG, Schwerin, Germany

lukasz.debicki@ita.rwth-aachen.de; inga.noll@ita.rwth-aachen.de

For reasons of health, hydrogen sulfide (H₂S) which is released during waste water treatment must be filtered from exhaust air. The disadvantage of the currently used bio-filter system is its huge volume (10 m³). As a result, difficult handling is required for maintenance leading to enormous costs for the operator.

Nonwovens have so far not been used for exhaust air filtration in waste water treatment plants. Especially for reactive filtration, nonwovens are very suitable because of their high volume specific surface. Within the project “Reaktivfilter” the Institut für Textiltechnik in cooperation with UNITECHNICS KG is developing a controllable, compact (1 m³) filter system which will be used to remove H₂S from exhaust air.

The approach is to attach a reactive substance to a carrier material. While in contact with exhaust air toxins will get neutralised. For this purpose, different filter media are developed and the most effective one will be chosen. Therefore, a test stand is prepared to measure the filters’ efficiency and resistance.

As first approach a nonwoven filter medium is developed from fibres made of polylactide acid (PLA). The filter effect results from decomposition of the used carrier material. When PLA meets H₂S and water, it releases the reactive substance continuously. To implement this filter medium, a melt spinning process for filament yarn from PLA and compounded reactive particles is developed. In addition to the insertion of reactive particles into the polymer, activation by coating of the carrier material is examined as second approach. For this purpose, a nonwoven fabric made from polyester passes through an immersion bath from a dispersion of the reactive substance in a so called padding process.

The aim of the project is to develop a new filter system that is inexpensive and highly effective.

ACKNOWLEDGMENT

The project “Reaktivfilter” is supported by the Federal Ministry of Economics and Energy in Germany as a part of the central innovation program for medium-sized companies (ZIM).

Influence of Non-cellulosic Components Removal on the Wet-Dry Cycling Durability of Flax Textile-reinforced Cement Composites

Laura González¹, Heura Ventura¹, Josep Claramunt², Mònica Ardanuy¹

¹Departament de Ciència dels Materials i Eng. Metal·lúrgica, Secció Eng. Tèxtil. Universitat Politècnica de Catalunya

²Departament d'Eng. Agroalimentària i Biotecnologia, Universitat Politècnica de Catalunya

monica.ardanuy@upc.edu

During the last decades there has been a considerable interest in the development of biocomposites reinforced with natural fibers mainly for commercial applications in automotive sector or sports equipment. More recently, the building industry application segment has also increased attention on biocomposites as lightweight materials with good mechanical performance and lower environmental impact. In this sense lots of interesting works have been published describing the mechanical performance of cement-based composites reinforced with a wide variety of cellulosic fibers, such as sisal, flax, jute, fique or hemp, among others [1]. In the majority of these composites the reinforcement is randomly dispersed on the matrix (fiber reinforced composites -FRC) and only few studies describe the performance of composites with these natural fibers in the form of textile structures (textile reinforced composites-TRC). The incorporation of these textile structures made of vegetable fibers on cement-based matrix lead to new sustainable construction materials with high strength under flexural and tension forces. Moreover, the hydrophilic behavior of cement-based materials leads to the formation of composites with very good fiber-matrix adhesion. However, one of the main downside of cellulose fibers for cement-based composite reinforcement is their high level of moisture absorption-desorption since changes in environmental moisture diffuse through the hydrophilic matrix, leading to materials with low durability to wet/dry cycling.

One possible treatment of bast fibers to decrease the moisture absorption is the removal of non-cellulosic components. Although this effect is very well known and analyzed in previous works, the influence on the durability of cement-based composites is less studied.

In this work, the influence of the removal of non-cellulosic components on flax's nonwoven fabrics as textile reinforcement on the durability of calcium aluminate-based cement composites is experimentally evaluated. For this purpose, needle-punched nonwoven fabrics specifically designed as reinforcements for cement-based matrix, have been subjected to different chemical treatments to reduce the non-cellulosic components. The effect of these treatments on the durability of calcium aluminate cement-based composites has been assessed through the analysis of their flexural performance before and after a wet-dry cycling accelerated process.

REFERENCES

1. Ardanuy, M., Claramunt, J., Toledo Filho, R.D. *Constr. Build. Mater.*, 79, 2015: 115-28.